DIFFERENTIAL DERMAL POTENTIAL: ACQUISITION, VALIDATION AND APPLICATIONS

A dissertation submitted to the
Jadavpur University, Kolkata
for the award of the degree of
Doctor of Philosophy
in
Engineering

Submitted by
Arindam Sarkar

Supervised by
Prof. Ratna Ghosh
&
Prof. (Retired) Bhaswati Goswami

Department of Instrumentation and Electronics Engineering
Jadavpur University
West Bengal, India
September 20, 2023

JADAVPUR UNIVERSITY
KOLKATA - 700 032, INDIA

1. Title of the Thesis:

DIFFERENTIAL DERMAL POTENTIAL: ACQUISITION, VALIDATION AND APPLICATIONS.

2. Name, Designation & Affiliation of the Supervisors

Supervisor 1: Dr. Ratna Ghosh

Professor
Instrumentation and Electronics Engineering Department
Jadavpur University
Salt Lake Campus
Kolkata - 700 106
West Bengal, India

Supervisor 2: Dr. Bhaswati Goswami

Former Professor
Instrumentation and Electronics Engineering Department
Jadavpur University
Salt Lake Campus
Kolkata - 700 106
West Bengal, India

3. List of Publications:

a. Peer reviewed journals:

A. Sarkar, B. Goswami, and R. Ghosh, "Validating Differential Dermal Potentials for use in Real-time Human Condition Monitoring," *IEEE Transactions on Instrumentation and Measurement*, vol. 71, pp. 1–9, 2022, *doi.https* : *//doi.org*/10.1109/TIM.2022.3141145

b. International conferences:

1. A. Sarkar, A. Bhattacharya, R. Ghosh, and B. Goswami, "A Comparative Study of Biopotentials Acquired from Left and Right Hands of Human Subjects," in *Advanced Computational and Communication Paradigms*. Springer, 2018, pp. 110–117., doi. $https://doi.org/10.1007/978-981-10-8240-5\_12$
2. A. Sarkar, S. Biswas, G. Datwal, S. Debnath, B. Goswami, and R. Ghosh, "Design and calibration of a multi-channel low voltage data acquisition system," in *2018 IEEE Applied Signal Processing Conference (ASPCON)*, 2018, pp. 119–123. $doi.https://doi.org/10.1109/ASPCON.2018.8748769$

4. Patent:

R. Ghosh, B. Goswami, A. Bhattacharya, D. Mondal, S. Biswas, S. Nandy, and A. Sarkar, "An expert system to determine the human condition using bilateral endosomatic eda and the method thereof," Indian patent IN201931038304, Oct. 23, 2022, grant No. 402187. [Online]. Available: $https://patentscope.wipo.int/search/en/detail.jsf?docId=IN309729256\&_cid=P10-L776DE-43223-1$

5. List of Presentations in National/International/Conferences/Workshops:

1. A. Sarkar, A. Bhattacharya, R. Ghosh, and B. Goswami, "A Comparative Study of Biopotentials Acquired from Left and Right Hands of Human Subjects," in *Advanced Computational and Communication Paradigms*. Springer, 2018, pp. 110–117., doi. $https://doi.org/10.1007/978-981-10-8240-5\_12$
2. A. Sarkar, S. Biswas, G. Datwal, S. Debnath, B. Goswami, and R. Ghosh, "Design and calibration of a multi-channel low voltage data acquisition system," in *2018 IEEE Applied Signal Processing Conference (ASPCON)*, 2018, pp. 119–123. $doi.https://doi.org/10.1109/ASPCON.2018.8748769$

PROFORMA - 1

"Statement of Originality"

I, **Arindam Sarkar**, do hereby declare that this thesis entitled "**STUDY AND CHARACTERIZATION OF THE RELATIONAL ASPECTS OF HUMAN BIOPOTENTIALS EXTERNALLY ACQUIRED FROM MULTIPLE LOCATIONS**" contains literature survey and original research work done by the undersigned candidate as part of Doctoral studies.

All information in this thesis have been obtained and presented in accordance with existing academic rules and ethical conduct. I declare that, as required by these rules and conduct, I have fully cited and referred all materials and results that are not original to this work.

I also declare that I have checked this thesis as per the "Policy on Anti Plagiarism, Jadavpur University, 2019", and the level of similarity as checked by iThenticate software is 7%.

Signature of Candidate:

Date :

Certified by Supervisor(s):
(Signature with date, seal)

(Dr. Ratna Ghosh)
Professor
Dept. of Instrumentation &
Electronics Engineering
Jadavpur University
Kolkata 700106, India

(Dr. Bhaswati Goswami)
Former Professor
Dept. of Instrumentation &
Electronics Engineering
Jadavpur University
Kolkata 700106, India

PROFORMA - 2

Certificate from the Supervisors

This is to certify that the thesis entitled **STUDY AND CHARACTERIZATION OF THE RELATIONAL ASPECTS OF HUMAN BIOPOTENTIALS EXTERNALLY ACQUIRED FROM MULTIPLE LOCATIONS** submitted by **Mr. Arindam Sarkar**, who got his name registered on February 02, 2017 for the award of Ph.D.(Engg.) degree of Jadavpur University, is absolutely based upon his own work done under the supervision of Prof. Ratna Ghosh and Former Prof. Bhaswati Goswami and that neither his thesis nor any part of the thesis has been submitted for any degree/ diploma or any other academic award anywhere before.

(Dr. Ratna Ghosh)
Professor
Dept. of Instrumentation &
Electronics Engineering
Jadavpur University
Kolkata 700106, India

(Dr. Bhaswati Goswami)
Former Professor
Dept. of Instrumentation &
Electronics Engineering
Jadavpur University
Kolkata 700106, India

ACKNOWLEDGEMENT

I would like to acknowledge and give my gratitude to my supervisors, Prof. Ratna Ghosh and Prof. Bhaswati Goswami, Dept. of Instrumentation and Electronics Engineering, Jadavpur University, who made this work possible. Their guidance, encouragement and constant support helped me to build my knowledge and understanding of the research problem and deliver the outcome. They were always available for problem discussions. Whenever I stumbled, they backed me to stand up again and go ahead in research as well as in life. In short, I was very lucky to get the opportunity to do my doctoral work under their guidance.

I would also like to thank my parents, my wife and the whole family for their constant support while undertaking my research work, specially my wife Mrs. Rijhi Dey, who always stood by me as my strongest support and always kept me focussed on my goal.

I also like to thank my lab mates, specially Dr. Aditi Bhattacharya for introducing me to the research domain and encouraging me as an elder sister, Mr. Somen Biswas for the support in the hardware section of my work and Mrs. Somali Nandy for her cooperation. I am also thankful for the support rendered by Mr. Radhakrishna Khatua, Mr. Sandeep Koley and Mr. Sunil Dutta in the implementation of the hardware portion of my research. Along with that, thanks to all the participating volunteers for their immense contribution in my research work.

I am very grateful to all teachers and staff of the IEE Department and allied facilities of Jadavpur University for giving me the opportunity to conduct my research by providing a beautiful laboratory, high end equipments and top class facilities. I specially thank the Institutional Review Board (IRB), Jadavpur University for providing me necessary clearance to work with human subjects, which allowed me to do the work successfully.

I owe it all to Almighty God for granting me the wisdom, health and strength to undertake this research task and enabling me to complete it.

September 20, 2023 (Arindam Sarkar)

Abstract

Electrodermal Activity or simply EDA is the bio-electrical activity observed on the human dermal surface. The activity is recorded in the form of responses due to electrical stimulus, known as exosomatic EDA or in the form of potential differences without any electrical stimulus, known as endosomatic EDA. Exosomatic EDA signals are mostly recorded for psychophysiological assessments of human being, though physiological information can be captured more accurately using endosomatic EDA.

Differential dermal potential or DDP signal is a specific type of endosomatic EDA that has been proposed recently and is finding uses in various applications. The DDP is the potential difference between two adjacent active sites on the skin surface without any electrical stimuli, typically the intermediate phalanges of the index and middle fingers of hands and feet. This signal has initially been acquired using the commercially available RISH Multi 18S multimeter based data acquisition system (DAS). This DAS is capable of acquiring low voltage signals (in order of 10μV) from multiple locations simultaneously with moderate speed, good accuracy and acceptable precision. It also has optical isolation to provide electrical safety. However, its major limitations are the lack of compatibility of its computer interface software Rishcom 100 with Windows 7 onwards updated OS platforms and its lack of portability, specially when the number of channels are more.

In view of this, two other advanced acquisition systems (Advantech USB-4704 and Keysight LXI) have been tested in this study but these did not perform as expected. Advantech USB-4704 lacks the required accuracy as well as precision, while the Keysight LXI lacks in portability and consumes much power. Along with that, it is unable to acquire data with required sampling speed in high resolution.

The limitations of the RISH Multi 18S based system and the unsuitability of the other two systems tested led to the calibration and testing of a dedicated 4-channel data acquisition system that was designed and developed indigenously by Somen Biswas, a co-author in [1], in the same research laboratory in which the present study is done.

A standard protocol has been developed in this work for balancing and calibrating the 4-channel DAS. This starts with a preliminary static calibra-

tion of the 4-channel DAS to estimate its nominal performance. Thereafter, for the balancing of the 4 channels, the addition of error curve method is employed after comparing its performance with those of the inverse slope multiplication and spline fitting methods. A comparison of the calibration results of the RISH Multi 18S and the balanced and standardized 4-channel DAS show that both these systems exhibit comparable performances. Thus, while both these systems have been used in the present work, the preferred system is the 4-channel DAS due to its enhanced portability and updated interfacing abilities.

In order to fulfill the multiple objectives of this present study, four (4) specific experiments have been designed and conducted to acquire 4 different data sets for 6 applications in total as listed hereafter. The data sets collected from these experiments are labelled henceforth as DS1, DS2, DS3 and DS4, while the terms LH, RH, LL and RL denote left hand, right hand, left leg and right leg respectively.

Experiments : DS1: DDP signals are acquired from only LH for 20 minutes which include 2 minutes in sitting posture, then 2 minutes during change in posture from sitting to supine and last 16 minutes in supine posture

DS2: DDP signals are acquired from LH and RH of supine subjects for 10 minutes

DS3: DDP signals are acquired from LH, RH of subjects for a specific set sequence: supine for 4 minutes, then sitting and then standing for 2 minutes each. This is followed by a no recording 1 minute activity session. Then subject sits again and DDP signals are acquired till a specified condition is met.

DS4: DDP signals acquired continuously from LH, RH, LL and RL of supine subjects for 10 minutes

Applications : Application1: Validation of the DDP signal by comparing it with standard recommended endosomatic EDA signals (golden reference) using DS1 dataset

Application2: Study unilateral characteristics of DDP signals using DS2, DS3 and DS4 data sets

Application3: Study bilateral characteristics of DDP signals using DS4 data set

Application4: Classification of hypertensive and normotensive subjects using LH and RH of DS2

Application5: Classification of different postures using LH of DS1 and both LH and RH data of DS3

Application6: Determination of the effective duration of rest in supine posture from LH of DS1, both hands data (LH and RH) of DS2 and all 4 channel data (LH, RH, LL and RL) of DS4 data sets and in sitting posture from both hands data (LH and RH) of DS3 data set

In Application1, the DDP signals have been validated by establishing the physiological basis and comparison with 2 standard endosomatic EDA signals as well as their difference signal. Since this signal is recorded in the DC mode, hence it is inferred from the standard RC model of the skin that this signal primarily records the differential information communicated by the nerve endings or the capillaries in the dermis and hypodermis, rather than the sweat gland activity recorded in usual EDA signals. The autocorrelation functions (ACF) of these differential signals confirmed that these signals are non-random signals originating from inherent time-varying processes. It is further verified that these signals are stable with settling times typically within 2 minutes, thus validating their usability in real-time applications.

Application2 deals with the unilateral characterization of these signals for which all the LH, RH, LL and RL signals from the DS2, DS3 and DS4 data sets have been clubbed together into their respective classes. The characteristics of these 4 classes of acquired signals were studied, followed by a study of their mean values and then the study of the (mean subtracted) debiased signals. The aspects studied include their polarities, trends, statistical, linear regression and spectral characteristics. A significant finding is that the spectral moment SM1, which can be considered as the gain-bandwidth product (GBP), are almost identical indicating that a constant GBP is maintained in the system.

Application3 deals with the study of the bilateral characteristics of the hand and feet signals using the DS4 data set. The aspects studied include the trends of signal pairs, study of the derived bilateral signals, Gap and Pair Sum (PS), as well as the interdependence of both the hand signals and both the feet signals.

Based on the characteristics studied, two bias parameters have been proposed in this study, namely differential bias μ_{diff} and common mode bias μ_{cb}, to quantify the hemispheric dominance between the bias of acquired signals. Furthermore, 4 other bilateral parameters using the debiased signals have also been proposed in this study, namely the ratios of the zero crossing instants (ZCI_{ratio}), the ratios of the slopes (m_{ratio}), the debias ratio (DR_k) to represent the instantaneous behaviours of the debiased pair of signals and

the log SD ratio (ξ_{sd}). All these proposed parameters have been statistically characterized for hands as well as for feet signals.

Finally, three different human condition monitoring applications have been presented in detail. Application4 pertains to hypertensive and normotensive subject classification, Application5 to different posture classification and Application6 to the estimation of the effective duration of rest. In Application4 and Application5, the attribute selection and classification have been done in WEKA version 3.9.4 using the random forest (RF) classifier using all the unilateral as well as the bilateral parameters studied in Application2 and Application3 along with two additional derived features, namely normalized variance and normalized kurtosis. However, mainly spectral characteristics have been studied for the assessment of rest duration in Application6.

In Application4, DS3 data has been used for classification of hypertensive and normotensive subjects. Attribute selection filter selected only 5 attributes among all, of which 4 are bilateral parameters. However, the most preferred attribute for differentiating hypertension is the SD of the left hand. It is to be noted that while the SD is indicative of the random variations in the signal, the LH signal is from a location that is physically closer to the heart than the RH signal. Although the classification results are significantly low at 75% in comparison to existing methods based on ECG, which can differentiate these classes with accuracies well above 90%, yet the minimal subject discomfort during its acquisition using the simple 10 minutes rest protocol and the simplicity of the protocol that allows even nominally skilled health workers to handle this procedure can be useful for primary monitoring and screening purposes.

In Application5, sitting and supine postures have been classified almost flawlessly using the relevant 2 minute subsets of the LH signals in the DS1 data sets, while a 3-level classification of supine, sitting and standing postures have also been done fairly accurately at 80% using the relevant subsets of the DS3 data sets. In both cases, the mean, ZCI and slope m of the signals are the major chosen attributes.

In Application6, the *effective* duration of rest of no-nap supine subjects has been estimated using all three data sets DS1, DS2 and DS4 based on the maxima of the system entropy. It is inferred from this study that if a subject maintains a supine posture typically for 4 to 6 minutes, it provides effective rest to the system. This result differs significantly from the other results of effective duration of rest, which are typically based on short nap condition. The same study done on subjects in sitting posture in the DS3 experiment show trends but are not conclusive, possibly since the acquisition was not continuous but was stopped after every 2 minutes.

Thus it can be concluded that the differential dermal potential is an unique signal, which is similar but not identical to the difference between respective endosomatic EDA signals. These can be acquired reliably using both RISH Multi 18S ans and 4 channel DAS in well designed, yet simple experimental protocols. It is further validated that their various statistical, spectral, linear regression and other characteristics are useful in screening hypertensive and normotensive subjects, classifying posture changes as well as estimating effective duration of rest.

List of Abbreviations

10FCV	10 fold cross validation
ACF	Auto-Correlation Function
ADC	Analog to Digital Converter
Ag-AgCl	Silver-Silver Chloride
ANS	Autonomic Nervous System
AUC	Area Under Curve
BCB	Borland C++ Builder
BP	Blood Pressure
CDF	Cumulative Distribution Function
CMIV	Common Mode Interference Voltage
CMRR	Common Mode Rejection Ratio
dB	Decibel
DAS	Data Acquisition System
debiased	Mean subtracted
ECG	Eleccardiogram
EDA	Electro-Dermal Activity
EDL	Electro-Dermal Level
EDR	Electro-Dermal Response
EEG	Electroencephalogram
EMG	Electromyogram
EOG	Electroocoulogram
ERG	Electrratinogram
FSR	Full Scale Reading
FPR	False positive rate
GapH	Difference signal between LH and RH
GapL	Difference signal between LL and RL
GBP	Gain Bandwidth Product
HRV	Heart Rate Variability
I2C	Inter-Integrated Circuit

IMU Inertial Measurement Unit

IQR Inter-Quartile Range

k-NN k-Nearest Neighbour

LH Left Hand signal

LL Left Leg signal

LOOCV Leave One Out Cross Validation

LOSOCV Leave One Subject Out Cross Validation

MFC Microsoft Foundation Class

MV Measured Value

OS Operation System

PC Personal Computer

PPV Positive Predictive Value

PR Pulse Rate

PRC Precision-Recall Curve

PSD Power Spectral Density

PSH Pair of LH and RH

PSL Pair of LL and RL

QQ Quantile-Quantile plot

RA Relative Accuracy, defined as $(1 - RE) \times 100\%$

RE Relative Error, defined as $\frac{TV-MV}{TV}$

RF Randm Forest

RH Right Hand signal

RL Right Leg signal

RMS Root Mean Square

RMSE Root Mean Square Error

ROC Receiver Operating Characteristic

SE Static Error

SNR Signal to Noise Ratio

SPL Skin Potential Level

SPR Skin Potential Response

SpO2 Saturation of Peripheral Oxygen

SSE	Sum of Square Error
SVM	Support Vector Machine
TNR	True negative rate
TPR	True positive rate
TV	True Value
USB	Universal Serial Bus
USG	Ultrasonogram
VB	Visual Basic
WA	Weighted Average
ZCL	Zero-Crossing Lag

List of symbols and variables

$Diff_{MLIL}$	Difference between ML_{Ref} and IL_{Ref}
ΔMV	Change in measured value
DR_k	Ratio of the debiased left sided and debiased right sided signal
ΔTV	Change in true value
E	Spectral entropy, defined as $-\sum_{k=1}^{N} P(k) log_2 P(k)$
IL_{Ref}	Potential difference between the intermediate phalanx of the index finger and the forearm of the left hand
LC1	Lateralisation coefficient 1, defined as $\frac{EDR_{right}-EDR_{left}}{EDR_{max}}$
LC2	Lateralisation coefficient 1, defined as $\frac{EDR_{right}-EDR_{left}}{EDR_{right}+EDR_{left}}$
m_{ratio}	$\frac{m(Left)}{m(Right)}$
ML_{Ref}	Potential difference between the intermediate phalanx of the middle finger and the forearm of the left hand
μ	Mean value of a data set
μ_{cb}	Sum of the mean of the left sided signal and right sided signal
μ_{diff}	Difference between mean of the left sided signal and right sided signal
MDF	Median Frequency
MNF	Mean Frequency
PKF	Peak Frequency
P_{MNF}	Power at the mean frequency
P_{MDF}	Power at the median frequency
P_{PKF}	Power at the peak frequency
SD	Standard deviation value of a data set.
σ	Standard deviation value of a data set.
SM1	First spectral moment, defined as $\sum_{k=1}^{N} f_k P_k$
SM2	Second spectral moment, defined as $\sum_{k=1}^{N} f_k^2 P_k$
SM3	Third spectral moment, defined as $\sum_{k=1}^{N} f_k^3 P_k$
ξ_{sd}	$log_{10} \frac{sd(left)}{sd(right)}$
ZCI	Zero Crossing Instant
ZCI_{ratio}	$\frac{ZCI(Left)}{ZCI(Right)}$

Contents

List of Figures

List of Tables

CHAPTER 1

Introduction

Healthy living has become the prime focus for humans in this fast, dynamic and hostile world. For this reason, human condition monitoring has become a major topic of research nowadays. This vast field of research incorporates the measurement and analysis of various physiological parameters, which often makes the overall system heavy and/or expensive.

Biopotentials can provide a possible solution to these issues and are thus being explored presently in various condition monitoring studies. These signals owe their origin to the electrochemical activity of the excitable cells that are present in the nervous, muscular and glandular systems in the body [8]. Some of the common clinical methods for capturing these bioelectric signals are tabulated in Table 1.1.

Table 1.1: Some Typical Bioelectric Signals [5, 8]

Bioelectric Signal	Abbreviation	Biologic Source	Frequency range(Hz)	Dynamic range
Electrocardiogram	ECG	Heart surface	0.05 to 100	1 to 10 mV
Electromyogram	EMG	Muscle	500 to 10000	1 to 10μV
Electroencephalogram	EEG	Brain surface	0.5 to 100	2 to 100μV
Electrooculogram	EOG	Eye-dipole field	dc to 100	10μV to 5mV
Electroretinogram	ERG	Eye retina	0.2 to 200	0:5μV to 1mV
Skin Potential	EDA	Skin Level	0 to 3	10mV to (-70)mV
Action Potential	-	Nerve or muscle	100 to 2000	10μV to 100mV

Electrocardiogram or ECG records different electrical potentials of the heart [9]. It is the most common biopotential signal that is acquired for clinical or research purposes. In recent studies, this has been used for arrhythmia detection [10] and to assess the possible risk factors due to heart abnormalities [11]. In Electroencephalography or EEG, voltage fluctuations due to ionic current within the brain neurons are recorded [12]. EEG signals are used for epilepsy detection [13], sleep disorder detection [14], measuring depth of anaesthesia [15], prime indicator of brain death [16] and stroke [17]

etc. The other bioelectric signals are sparingly used in clinical or research applications. EMG that is recorded from the muscles is mostly used in biomechanics applications [18, 19] while EOG and ERG, both recorded from the eyes, are used for eye movement detection [20, 21] and optical disorder detection.

In recent studies, some of these signals have been used for other diverse applications too. It is well established from several studies that posture and cardiac activity are dependent on each other [22] in terms of cardiac output [23], heart rate or R-R interval [24] or even systolic blood pressure [25]. For this reason, posture estimation has reliably been performed from cardiac monitoring also [26, 27]. Machine learning approach is typically used for this approach in which the data for different postures are considered as different classes for the classification [26–28].

Another research area that uses biopotential signals is the study of rest, sleep, alertness or wakefulness. Sometimes short nap is used synonymously to rest. There are various studies where researchers observed the effect of short rest during various experiments like effect of 15 minute nap after a short night sleep [29], short rest [30] and ultra short term rest [31] after noctural sleep restriction, effect of 20 minute nap at noon [32] and afternoon [33] to name a few. ECG and EEG signals have been used to study day time short nap [34]. The effect of coffee, placebo [35], face wash and strong light [36] have also been studied using ECG and EEG signals.

However, the most relevant application of ECG signals is in hypertension studies. In a research article, the author presented a hypertension assessment method using ECG and photoplethysmograph (PPG) signals [37]. Assessment of pulmonary hypertension was also reported using ECG and some other simple non-invasive techniques. Several indices have also been proposed for hypertension detection using ECG signals [38, 39]. Some recent AI and machine learning based ECG studies focussed on detection of severity of hypertension in human subjects [40], blood pressure classification [41], pulmonary hypertension detection [42] and automated classification based on HRV analysis [43].

As is evident, all these signals provide mostly either physiological or psychological information. On the other hand, electrodermal activity (EDA) signals provide both physiological as well as psychological information of the human subject. Very recently, a special type of EDA signals termed as differential dermal potentials (DDP) are being studied successfully for assessing the human condition and its bilaterality.

Being relatively new, a systematic validation of the DDP signal as well as studies of its various characteristics and further applications are yet to be performed. Detailed analysis may lead to find out some characteristic

features and propose some parameters, which can be used further along with other unilateral parameters in various applications.

The aim of this research is to acquire the differential dermal potential (DDP) reliably using a suitable data acquisition system, validate it systematically, characterize and determine some specific features that can be used for specific human condition monitoring applications.

1.1 Literature review

This section contains the literature survey of the different aspects of this research including the EDA signal, their applications as well as limitations, evolution of DDP signals and their applications. A survey of different acquisition systems and different validation techniques used for biopotentials is also provided.

1.1.1 Electrodermal activity (EDA)

Electrical activity observed on human skin is called electrodermal activity or EDA [3, 44]. Changes in human psychophysiology stimulate the autonomic nervous system (ANS). This often causes change in the electrical activity captured on the skin and can be recorded as either potential, resistance, conductance, impedance or admittance [3].

Exosomatic and endosomatic EDA

There are 2 techniques by which EDA signals can be acquired and thereby they are named as endosomatic or exosomatic EDA. Exosomatic EDA is acquired while constant DC or AC stimulus is applied to the skin in the form of resistance, conductance, impedance or admittance. This type of EDA is significantly related to changes in sweat gland activity. In standard recommended endosomatic recording, skin potential difference is recorded between two sites (one active and one inactive), without applying any electrical stimuli [45, 46].

Choice of sites

Christie and Venables [47] characterized 8 palmar sites of both hands for acquiring the EDA signals. Thereafter, a number of other sites were also tested for acquisition of different parameters of EDA signals [47–50]. Finally it was recommended [45, 46] to acquire EDA signals from the intermediate phalanges of index and middle finger due to a number of advantages [2].

Sites suitable for acquisition of EDA signals of both hand and feet are shown in Figure 1.1 and Figure 1.2 respectively. As shown in the figures, it is recommended in all these studies that exosomatic EDA should be recorded in differential mode across two active sites while endosomatic EDA should be acquired in referenced mode across an active and an inactive site.

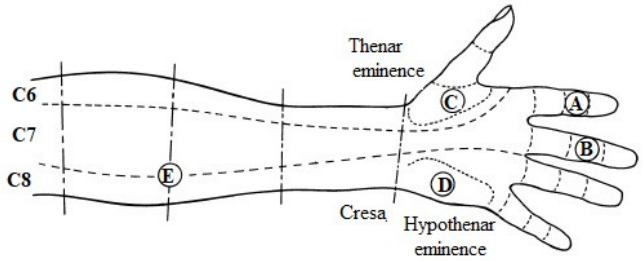

Figure 1.1: Preferred palmar or volar electrode sites (A-D), recommended position for the inactive electrode (E) used in endosomatic recording, and their relationship to dermatomes (C6-C8) [2]

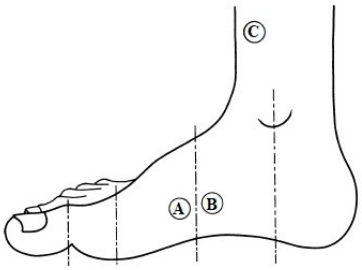

Figure 1.2: Medial side of the right foot with the recommended recording sites A and B for exosomatic recording, and position C of the inactive electrode for endosomatic recording [3]

Acquisition systems

Since the EDA signals are typically of the order of hundreds of mV, so special acquisition systems are used for recording these signals reliably. It is recommended that the input impedance of the amplifier for endosomatic recording should be 1MΩ to 5 MΩ for suitable acquisition and amplification [51]. The amplifiers used for recording skin potentials are not ordinary ones since they record such low voltage skin potential level SPL and/or skin potential responses SPR. Special *backing-off* circuits are recommended for accurate recording of very low amplitude SPR [52, 53].

Nowadays, portable, specially wearable systems or devices are in high demand for acquisition of EDA signals also [54]. Accordingly, an elaborate human condition monitoring system has been designed and described in a patent by Stoller [55]. In this, skin potential is acquired from 22 dermal surfaces of both hands and feet using multi-point differential probes. Researchers have also designed several other wearable electrodermal signal acquisition systems for real-time applications [54, 56].

Tonic and phasic components

Electrodermal signals consist of two parts, termed as tonic and phasic components. Tonic signifies the slow changing or quasi-static electrodermal level EDL of the acquired signal. The low basal skin potential level SPL is one EDL based score proposed by Christie and Venables [57]. Lykken et al. observed inter-individual differences for the minimum SPL even in fully relaxed individuals [58]. One of the typical use of tonic level is in monitoring the effect of habituation.

The phasic part of the EDA signal is called electrodermal response EDR, although it is not always necessary to have a distinct relationship between a stimulus and an EDR. Study of EDR is mostly done by analyzing latency time, window, amplitude and shape of response [3]. Depending on the amplitude, EDA signals can be either monophasic, biphasic or even triphasic. Exosomatic EDA signal responses are monophasic in nature, but all three types of responses can be seen in case of endosomatic signals, which makes it hard to interpret. Reason for these different responses have also been studied [2, 59, 60].

Applications of EDA signals

Exosomatic EDA signals are popularly used to research psycho-sociological states since long. Non-electrical stimuli like audio, visual even different odorant stimuli are also used along with the electrical stimuli in some of these studies [61–64]. Arousal assessment by measuring tonic EDA signals [65], multiple arousal studies based on daily life EDA asymmetry [66], habituation [67] and dishabituation [68] studies are some such examples. EDA studies for assessing emotional states and stress (by applying different stressful stimuli) [54,69,70], anxiety disorder [71–73] and depression [74] confirmed that both specific and non-specific responses are useful for the assessment of stress. It was seen that SCL and NS.SCR (non-specific skin conductance response) frequency is higher in case of patients with anxiety disorder while SCL (skin conductance level), SCR (skin conductance response) and NS.SCR

frequency are considered to be very useful for depression identification [75,76]. Subjects with some phobia, like spider phobia, have been identified by recording SC (skin conductance) and fMRI (Functional magnetic resonance imaging) together [77]. In the field of physiological research also, tests have been conducted to understand behavior [78], gender and hemispheric dominance using mirror image stimulus morphometry [79, 80].

As mentioned, all of these studies use exosomatic EDA data acquisition technique. However, the endosomatic EDA acquisition technique, which does not require electrical stimuli, is known to contain more physiological information [81] but it is not popular due to its unstable and irregular response characteristics [3]. One of the old studies using endosomatic EDA signals was detection of alertness [82]. In present days, wearable monitoring devices are being developed by a group of researchers [83, 84]. These are also used for drivers stress level detection at driving [85].

In almost all these studies, electrical and/or non-electrical stimuli have been used. So these techniques are more representative of the system response to the stimuli than the inherent characteristics of the human system. The probable solution would be to acquire the recommended standard endosomatic EDA signals as mentioned in [46] without any electrical or non-electrical stimuli but as mentioned earlier, these signals are very hard to interpret [3].

Therefore, there is a need for a suitable endosomatic signal and associated acquisition system that can capture the inherent physiological information in a more interpretable and reliable form.

1.1.2 Differential dermal potential (DDP)

Differential dermal potentials are a specific type of endosomatic EDA signals that are acquired in the *differential mode* across *two active sites* in contravention to the standard recommendations for endosomatic EDA signals. The sites and mode of acquisition of this signal is similar to that of exosomatic EDA signals but *without any applied stimuli*. These signals were first studied by Bhattacharya et al. [86] in the same research lab as this present study as generic biopotential signals representative of the global homeostasis of the human system. Later, this signal was named as differential dermal potential or *DDP* signal.

DDP acquisition

The schematic of the instrumentation system used to acquire the DDP signals is shown in Figure 3.1. In this, a pair of bipolar, surface electrodes made

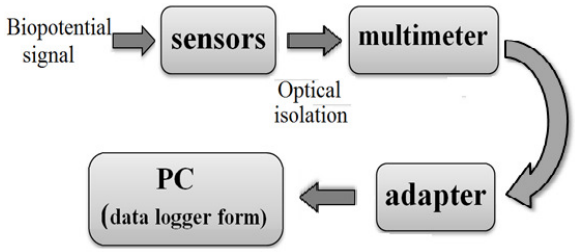

Figure 1.3: Schematic diagram

of Ag-AgCl are used as sensors to collect the signals from the intermediate phalanges of the index and the middle finger of both the hands of human subjects. The following reasons are given by Bhattacharya et al. [86] and Venables and Christie [2] in support of the site selection.

1. Since the fingers are situated far away from the major biopotential generating organs like heart, brain etc., so they would not reflect the information of any specific organ.

2. The middle phalanges of index and middle fingers are less prone to scars and to the movement effect than other phalanges of the same fingers, as well as the middle phalanges of other fingers.

3. The electrodes can be fixed easily since there is enough space to connect them.

The DDP signals were initially acquired using the Rish Multi 18S [4] multimeter and Rish Multi SI232 [87] adapter assembly [86]. A differential amplifier based signal conditioning circuit was proposed by Bhattacharya et al. [88] for this system to amplify the very low voltage acquired signals. But this was later discontinued due to its non-linear input/output characteristics and the distortions in the amplified characteristics, specially in the negative voltage region. The Rish Multi 18S based system, being bulky, is also not very portable and its interfacing Rishcom 100 software is not compatible with the updated operating systems.

Therefore, some other existing advanced data acquisition systems need to be tested for possible use in DDP data acquisition.

In a further development, an indigenous 4-channel data acquisition system to acquire DDP signals was designed and developed by S. Biswas, a co-author of [1]. This system is capable of acquiring DDP signals simultaneously from a maximum of 4 locations and send these to the PC or laptop for monitoring and storage purposes. This system is named henceforth as the 4-channel data acquisition system or DAS.

It is necessary to standardize the channels of the 4-channel DAS and for this, proper calibration and tuning procedures need to be developed.

Comparison with standard signals

Some recent validation studies have been reported in the field of biopotential research by applying various stimuli and comparing the responses with other established methods. An open source EDA acquisition device Obimon has been validated using another established EDA acquisition system NeXus 10 MKII [89]. Another EDA based wrist worn person specific stressor detection system has been validated by applying different stressors and comparing with established palm based skin conductance response (SCR) and skin conductance level (SCL) measurements [90]. In another article, authors have validated a wearable system for distress detection for visual image stimuli using a self assessment scoring system [91].

In a similar fashion, it is necessary to validate the DDP signals acquired using the tuned and calibrated DAS by comparing them with respect to some standard recommended signals.

DDP signal characterization

Various time domain characteristics of the DDP signals acquired from both hands has been reported by Bhattacharya in [5]. This includes the study of the polarity and trends of the individual signals and detailed statistical characterization of the signals. Thereafter the bilateral characteristics of the signals have also been studied in terms of their interaction trends as well as two proposed derived signals, termed as Gap and Pair Sum (**PS!**) signals.

A linear model of the (mean subtracted) deviation signals and certain model parameters like zero crossing instant (ZCI) have also been proposed in this study since the signals vary characteristically about a mean value. A composition of the DDP signals in terms of these various parameters was also developed in this study. In a different study, another linear model was proposed by Nandy [92] that depends upon the first order zero crossing lag (ZCL) of the signal autocorrelation function (ACF).

Therefore, there is a scope to characterize the feet signals also along with the hand signals. Along with that, bilateral and other interdependencies also need to be studied.

1.1.3 Bilaterality studies on biopotential signals

Studies of bilateral relationship of various biopotential signals, including the EDA and in particular the DDP signals, have been performed with different objectives as discussed hereafter.

Bilaterality in biopotential signals

Studies in bilateral similarity and dissimilarity were conducted to understand behaviour [78], gender, left and right handedness using mirror image stimulus discrimination or morphometry [79, 80], performance of athletes [93, 94] by studying their degree of lower body symmetry, infirmities like scoliosis and spinal pain [95] using physical traits, as well as stroke patients identification [96, 97] using Brain Symmetry Index (BSI) or Bilateral BSI (BBSI). In another study, bilaterality of the brain EEG signals were analyzed for identification and localization of brain generators [98]. Bilaterality of EMG signals were also studied for gait phase classification [99] with 96% classification accuracy, chronic pain diagnosis [100], studying aspects of neural synchronization [101] etc. Bilateral EOG signals have been studied in sleep analysis [102].

Bilaterality of exosomatic EDA

Bilaterality studies were performed on exosomatic EDA signals to investigate the physiological aspects of human beings. Analysis of bilateral EDA measured by applying DC stimuli to specific intracerebral sites have shown that the human body shows strong ipsilateral control to limbic structure stimulation [103]. Bilateral responses of these signals to various non-electrical stimuli like audio, visual even odorant stimuli have also been studied. It has been seen that strong acoustic stimuli cause noticeable bilateral differences within the ratio of 1:1.5 [61] [62] and also that this is moderated due to the habituation to such stimulus, as measured using SCR (Skin Conductance Response) [63]. Importance of the stimulus intensity has been studied using odorant stimuli [104].

The correlation between cardiovascular and electrodermal responses have also been tested using adverse and non-adverse visual stimuli [64]. Bilateral asymmetry of these signals has been observed to be correlated with Autonomic Nervous System (ANS) activity [105] and subsequent studies on bilaterality have been performed to understand depression and schizophrenia [106] [107]. Skin conductance level (SCL) and eye movement have been used as indicators of bilaterality and these have been used to identify depressive patients from normal subjects as well as to understand responses to

different stimuli [108]. However, in a review of more than 50 papers [81], it has been stated that the assumption that bilateral EDA recordings are related to hemispheric asymmetry is ambiguous. These results are often contradictory to each other, possibly since this signal is a response to the applied stimuli and hence is significantly dependent on optimal experimental conditions.

Endosomatic EDA signals

Studies on bilateral endosomatic EDA signals are very few, although it is known that endosomatic recording does not depend on contact area. Hence NS.EDR (Non-specific electrodermal response) may be more sensitive in endosomatic recording than exosomatic recording [109]. In a patented study, Stoller et al. [55] have collected bilateral DC bioelectric potentials from all fingers of both hands, with respect to two reference sites at the palm of both hands. This DC bioelectric potential is very similar to endosomatic EDA signals. From the collected data, it has been shown that bilateral variance of diseased subjects is much higher than that of healthy subjects. Bilateral endosomatic EDA signals have also been studied by Wyatt to show that the SPL of right hand is much higher than that of the left hand, irrespective of left or right handed subject [110]. In a recent study by Hyatt et al. [111], a comparison of SPL of 12 left handed and 12 right handed male subjects shows higher SPL for right hand for both classes. It is observed in this study that external stimuli also shows same result.

DDP signals

So far there is only few studies available on the bilateral asymmetry of DDP signals. As mentioned earlier, Bhattacharya [5] has characterized the bilateral asymmetry of hand signals by studying the gap and pairsum derived signals, which are the difference between and sum of the simultaneously acquired hand signals. In Bhattacharya et al. [86], the signals have been analyzed statistically to ascertain parameters for health. In a very recent study by Jaiswal et al. [112], cognitive load assessment was performed using features of the DDP signals with an achieved F1 score of 89%. In this study, signals were acquired from both hands as well as both feet. This study indicates that feet signals have also significant characteristics to contribute in the DDP signal based application studies.

Thus there is scope for a more detailed study of the characteristics of the DDP signals acquired under various conditions and to study their applicability in human condition monitoring.

1.2 Aim and organization of the thesis

The aim of this work, as stated at the outset, is to acquire Differential Dermal Potentials (DDP) reliably from multiple locations, validate the signals in terms of standard endosomatic EDA signals, study their unilateral and bilateral characteristics and use these features for practical human condition monitoring.

For this purpose, the work has been subdivided into multiple objectives. In the first stage, several existing advanced data acquisition systems have been tested for use in DDP acquisition. Thereafter, the task of calibrating and tuning the 4-channel DAS developed earlier in the research laboratory has been taken up. Subsequently, 4 sets of experiments were designed and data was accordingly collected from human subjects. The collected data were used for validation in terms of standard endosomatic EDA, characterization studies as well as for human condition assessment applications. These have been presented hereafter in some detail.

1.2.1 Organization of the thesis

The thesis is organized as follows:

Chapter 1 is the introduction of this thesis. It contains the review of existing literature, followed by aim and organization of this thesis and list of contributions.

In Chapter 2, three prevalent data acquisition systems, namely the Rish Multi 18S multimeter and its associated adapter assembly, the Advantech USB 4704 system and the Keysight LXI data acquisition/switching unit, have been studied in terms of their features as well as their limitations. The Rish Multi 18S and associated adapter assembly is discussed in Section 2.2. This system is still in use in the laboratory conditions in a limited manner. Thereafter, the Advantech USB 4704 system and the Keysight LXI data acquisition systems were studied in Section 2.3 and Section 2.4 respectively with the objective of testing their possible use for DDP signal acquisition. Other peripheral components and measurements required for the actual experimentation are discussed in Section 2.4.5. The overall findings are discussed in Section 2.5.

Chapter 3 deals with the complete calibration, tuning and channel balancing of a dedicated 4-channel data acquisition system, henceforth referred to as the DAS. This DAS was designed and developed by Biswas, a co-author in [1], in the same research laboratory in which the present work has been done. Its major characteristics and working principle are stated in Section

3.1. The static calibration details of this DAS is presented in Section 3.2. Different tuning methods that were tested to balance the performances of all the channels of the DAS are presented in Section 3.3. This is followed by a detailed static calibration of this balanced DAS in Section 3.4. Section 3.5 contains a study of the common-mode voltage characteristics. Thereafter, a comparison of the static characteristics of the Rish Multi 18S based system and the 4-channel DAS is provided in Section 3.6. The overall discussions is presented in Section 3.7.

Chapter 4 includes the details of four experiments designed and conducted to acquire DDP signals. General conditions of all 4 experiments are discussed in Section 4.1. It contains the ethical committee details, criterion for subject selection, material and methods used for the experiments. The 4 experiments designed to collect the data for the various applications in this thesis are detailed in Section 4.2. The common steps followed in all 4 experiments are discussed in Section 4.2.1. Thereafter, all 4 experiments are detailed out in subsequent subsections. The overview of all 4 experiments and the use of the particular data set(s) in the various applications discussed in subsequent Chapters is stated in Section 4.3.

Chapter 5 deals with the validation of the DDP signal in terms of standard endosomatic EDA signals as well as their unilateral and bilateral characterization. The physiological basis of this DDP signals is presented in Section 5.1. This is followed in Section 5.2 by the validation of this DDP signal by comparing it with the simultaneously acquired standard endosomatic EDA signals. Section 5.3 and Section 5.4 contain the characterization of the DDP signals acquired from all 4 locations during all 4 experiments stated in Chapter 3. The unilateral characteristics are discussed in detail in Section 5.3. The bilateral characteristics, both existing and some proposed, are discussed in detail in Section 5.4. Section 5.5 contains the overall discussion of this chapter.

Chapter 6 deals with 3 particular application studies that have been conducted in this thesis. These are (1) classification of hypertensive and normotensive subjects, (2) 2-level classification of sitting and supine postures and 3-level classification of supine, sitting and standing postures and (3) determination of the effective duration of rest in supine (or sitting) posture. Section 6.1 contains the details of the preprocessing of the data for the applications stated. The details of the classification technique used in the first two application studies are stated in Section 6.2. The classification studies were done using random forest (RF) classifier. This was applied upon all the relevant time domain and spectral characteristics of the signals described and/or developed in Chapter 5. Thereafter, Section 6.3 to Section 6.5 contain the details and results of the 3 aforementioned application studies. The overall

discussion is presented in Section 6.6

The overall conclusion and scope for future work is presented in Chapter 7.

1.3 List of contributions

The list of contributions of this study presented chapter-wise are as follows:

1. Chapter 3: Setting up calibration, tuning and channel balancing procedures for the 4-channel Data Acquisition System (DAS) developed erstwhile in the research laboratory. This ensures interchangeability of the DAS devices for experimentation purposes.

2. Chapter 4: Design and implementation of 4 specific experiments in order to achieve the various objectives of the present work.

3. Chapter 5: Systematic validation of the DDP signal in terms of standardly accepted endosomatic EDA signals. This study establishes the independence of the DDP signals from dermal sweat gland activity as in standard endosomatic and/or exosomatic EDA.

4. Chapter 5: Proposed new bilateral characteristics of DDP signals. This follows the detailed unilateral and bilateral characterization of single channel, dual channel (from both hands) as well as 4-channel (from both hands and both feet) DDP signals using available characteristics.

5. Chapter 6: Human condition monitoring studies on

   (a) Classification of hypertensive and normotensive subjects

   (b) 2-level classification of sitting and supine postures and 3-level classification of supine, sitting and standing postures

   (c) Determination of the effective duration of rest in supine posture

CHAPTER 2

Testing available data acquisition systems for acquiring DDP signals

This chapter deals with the testing of the suitability of 3 available data acquisition systems for acquiring the low voltage DDP signals reliably. As mentioned earlier, these are the RISH Multi 18S and associated adapter assembly, the Advantech USB 4704 and the Keysight LXI data acquisition/switching unit.

The RISH Multi 18S based system consisting of the multimeters, the adapters, electrodes, connectors and other peripheral components have been used successfully in acquiring the DDP signals [5]. However, further studies require the portability as well as improvements in the compatibility, efficiency and performance of the existing system. Consequently, this system as well as two other comparable systems have been compared on the basis of their accuracy, precision, resolution, portability, electrical safety, input impedance, compatibility, cost and user friendliness.

2.1 RISH Multi 18S based system

The RISH Multi 18S based system [5, 113] consists of a battery powered precise multimeter along with a battery powered optically isolated adapter for each data channel being acquired, adequate number of Ag-AgCl snap type EDA electrodes and single core coaxial snap type connectors and a PC/Laptop for recording and display purposes. The overall instrumentation system is described along with its features hereafter.

2.1.1 Instrumentation system

The block diagram of the RISH Multi 18S based system including the RISH Multi SI232 adapter assembly and the Rishcom 100 software is given in Figure

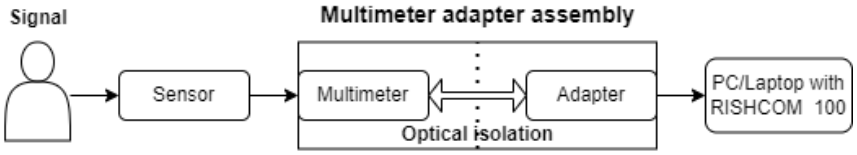

Figure 2.1: Block diagram of the RISH Multi 18S based data acquisition system [4]

(a) (b) (c)

Figure 2.2: (a)Snap type Ag/AgCl electrodes , (b) Electrode connectors and (c) RISH Multi 18S multimeter and RISH Multi SI232 adapter assembly.

2.1. The electrodes, connectors and multimeter-adapter assembly that are actually used are shown in Figure 2.2. The experimental setup with the data acquisition system [5] is shown in Figure 2.3.

Biopotential signals are acquired using Ag-AgCl snap type 8mm electrodes (Make: Shimmer Sensing) from the respective skin surfaces (intermediate phalanges of index and middle fingers of hand and/or feet) and fed to the multimeter-adapter assembly. The electrodes are connected to the skin surface using aqueous ultrasound gel to provide skin-electrode interface. The multimeter-adapter assembly consists of a $4\frac{3}{4}$ digit digital multimeter (Make: Rishabh Instruments, model: RISH Multi 18S) [4] and an optically isolated adapter (Make: Rishabh Instruments, model: RISH Multi SI232) [87] module. Acquired data is then sent to the PC or laptop via serial cable. The PC/laptop has a software installed in it (Make: Rishabh Instruments, model: Rishcom 100) to interface with the multimeter-adapter assembly. It is used to set up the multimeter, display the acquired signals in form of voltage data log or graphical representation and store these into a data logger format.

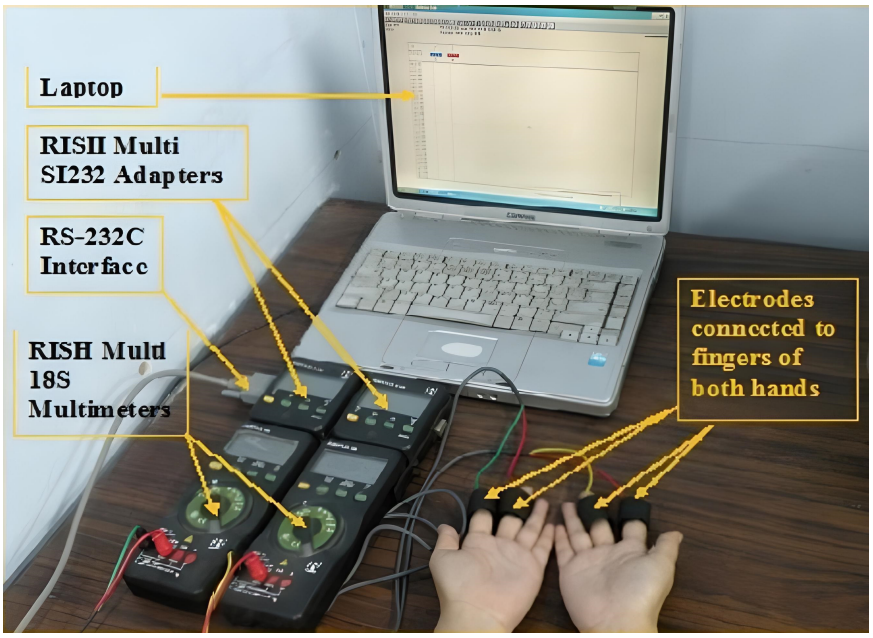

Figure 2.3: Experimental setup with RISH Multi 18S and RISH Multi SI232 adapter assembly [5]

2.1.2 Key features

The key properties of this data acquisition system are given hereafter.

- It is a $4\frac{3}{4}$ digit display multimeter with four digits with 0-9 display capability and one digit with 0-2 display capability.
- It is a precise multimeter with resolution of 10 μV within $\pm$300mV range. Beyond this, the resolution is 100 μV upto $\pm$ 3V.
- Within $\pm$300mV, the input impedance is >10GΩ and beyond that, it is around 11MΩ upto 3V.
- Up to 6 multimeters can be connected together to acquire signals from 6 different locations simultaneously. However, the sampling speed is compromised as more channels are added.
- A software, name: Rishcom 100, is required for communication with PC for storage and display purposes.
- No additional filter is used in order to keep all the information as intact as possible.

Three very important features of this multimeter adapter assembly that justify its use for DDP signal acquisition are:

(i) These multimeters have a resolution of $10\mu V$, which is known to be the typical minimum value of biopotentials [114].

(ii) The typical bandwidth of the EDA signals is 0-3Hz [3]. In this present study, the sampling frequency has been set to 20 samples/second to ensure adequate sampling rate for capturing the DDP system dynamics. in accordance with Shannon's sampling theorem.

(iii) It is known that if more than $5mA$ of current passes through the heart of an human beings, it may cause the person to die [115]. There is an in-built optical isolation between the multimeter and the adapter, which provides safety to the human body from any electrical hazard during data recording.

Static Characteristics

A detailed analysis of the static characteristics of RISH Multi 18S multimeters has been done by Bhattacharya [5]. The main outcomes of this study are given hereafter.

- Maximum range of the static error lies within $\pm 0.07\%$ of the measured value.
- Standard deviation of the potential signal within $\pm$ 300mV range is 0.01mV, which equals the rated resolution.
- Sensitivity is 0.999, which is very close to 1.
- The system tested has an offset of 0.02mV.
- The sum of square error (SSE) is found to be 0.151mV, whereas the root mean square error (RMSE) is 0.075mV.
- It follows a linear input/output characteristics.

Drawbacks

Some of the major drawbacks and limitations of this system are stated hereafter.

- The Rishcom 100 runs only on Windows XP platform, which does not support the modern day PC configurations.

- In case more than one channel of data has to be acquired, the system becomes unwieldy and loses portability due to the multiple sets of multimeter-adapter assemblies required.
- Any signal lower than 10μV can not be acquired using this data acquisition system.

2.2 Advantech USB-4704

The Advantech USB-4704 is a low-cost, modern, adaptable data acquisition module from Advantech Co. Ltd with high end features. This has been tested as a possible improvement or replacement of the RISH Multi 18S based data acquisition system.

2.2.1 Key features

The key features of the Advantech USB-4704 system are listed hereafter.

- It has 8 input/output ports those can be used as 8 single ended or 4 differential ended terminals.
- It can be connected to PC via USB 2.0 module.
- It draws all its required power from the USB port. So no external power, neither battery nor power adapter, is required. Power rating of this instrument is 5V, 360mA to 5V, 450mA.
- It can be interfaced using many softwares like C#, C++, LabVIEW, VB.Net, BCB, MFC, VB6, Delphi, Java, Matlab and Qt.
- It works well with the updated operating systems like 32-bit/64-bit Windows 7/8/10 and Linux.
- For analog inputs, its sampling speed is 48 Ksamples/second, which is very high compared to the RISH Multi 18S multimeter.
- It has a resolution of 14 bits or approximately 61 μV.
- The input impedance of this acquisition system is 127kΩ. However, this is quite low compared to the recommended input impedance of minimum 5MΩ for acquiring the potential signals [51].
- It is easy to use and rugged enough for industrial applications as well as scientific experiments.

2.2.2 Static characteristics

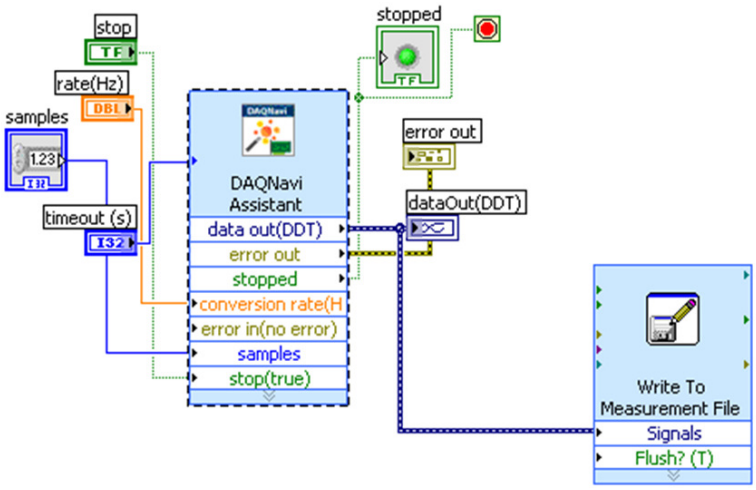

Figure 2.4: LABView virtual instrumentation system

The static input-output characteristics of this instrument was tested using the LABView virtual instrumentation system. The designed virtual instrumentation (VI) system is shown in Figure 2.4. The measuring range was set to ±1V in differential input measuring mode.

The true values (TV) were generated using Libratherm LC-05 millivolt calibrator and the measured values (MV) were displayed in VI and stored in an excel file for calculation. Predetermined TVs were set within ±300mV as it was seen in [5] that DDP signals lie within this range. For the calibration, the TVs were varied 10 times in ascending and descending order. The TVs, MVs and mean of MVs are tabulated in Table 2.1 while the calibration curve for mean of MV vs. TV is plotted in Figure 2.5.

From Figure 2.5 and Table 2.1, it is clear that MV vs. TV shows a linear characteristics. Relative error ($RE = \frac{TV-MV}{TV}$) and relative accuracy ($RA = (1 - RE) \times 100\%$) have also been calculated and tabulated in Table 2.1. It is observed that both RE and RA are good at higher TVs but the performance degrades markedly for lower TVs. Sensitivity of this instrument was calculated to be 0.99 but it has an offset of -6.7mV. This is a high value when compared to the low voltage DDP signals.

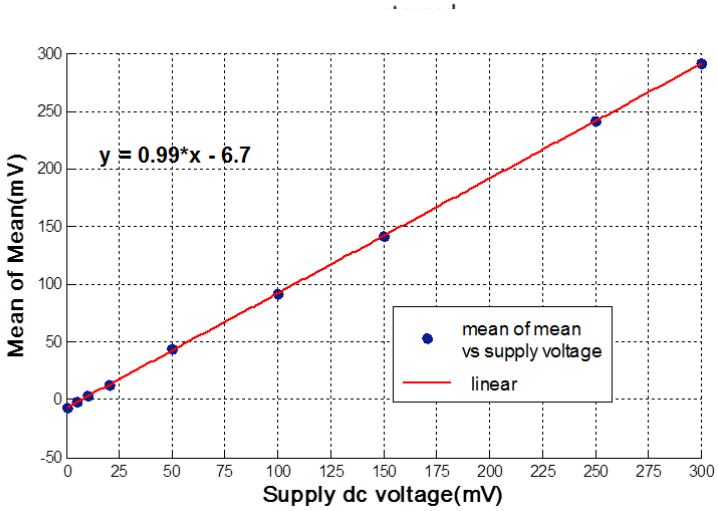

Figure 2.5: Calibration curve of Advantech USB-4704 data acquisition system

Table 2.1: Calibration table of Advantech USB-4704 data acquisition system

True value	Measured value (MV) in mV										Mean of the	Relative	Relative
(TV) in mV	1	2	3	4	5	6	7	8	9	10	MV in mV	error	Accuracy
300.00	290.47	290.50	290.27	290.36	290.47	290.21	290.56	290.56	290.30	290.01	290.37	0.03	96.79
250.00	240.94	240.56	240.99	241.04	240.85	240.66	240.58	240.56	240.61	240.97	240.78	0.04	96.31
150.00	141.77	141.66	141.79	141.69	141.89	141.89	141.73	141.70	141.69	141.80	141.76	0.05	94.51
100.00	92.22	92.22	92.30	92.21	92.36	92.35	92.39	92.29	92.37	92.27	92.30	0.08	92.30
50.00	42.81	42.78	42.80	42.83	42.76	42.78	42.83	42.80	42.81	42.77	42.80	0.14	85.60
20.00	13.09	13.09	13.09	13.09	13.09	13.10	13.10	13.09	13.09	13.10	13.09	0.35	65.45
10.00	3.20	3.20	3.20	3.20	3.20	3.20	3.20	3.20	3.20	3.20	3.20	0.68	32.00
5.00	-1.75	-1.75	-1.75	-1.75	-1.75	-1.75	-1.75	-1.75	-1.75	-1.75	-1.75	1.35	-35.00
1.00	-5.71	-5.71	-5.71	-5.71	-5.72	-5.70	-5.71	-5.71	-5.71	-5.70	-5.71	6.71	-571.00
0.50	-6.21	-6.21	-6.20	-6.21	-6.21	-6.21	-6.20	-6.20	-6.21	-6.20	-6.21	13.42	-1242.00
0.20	-6.51	-6.50	-6.51	-6.50	-6.50	-6.50	-6.50	-6.50	-6.50	-6.50	-6.50	33.50	-3250.00
0.10	-6.61	-6.60	-6.60	-6.60	-6.60	-6.60	-6.59	-6.61	-6.60	-6.60	-6.60	67.00	-6600.00
0.05	-6.64	-6.66	-6.66	-6.65	-6.65	-6.65	-6.65	-6.65	-6.65	-6.65	-6.65	134.00	-13300.00
0.02	-6.68	-6.68	-6.69	-6.68	-6.69	-6.68	-6.68	-6.68	-6.69	-6.69	-6.68	335.00	-33400.00
0.01	-6.69	-6.68	-6.68	-6.69	-6.69	-6.69	-6.70	-6.68	-6.69	-6.69	-6.69	670.00	-66900.00
0.00	-6.70	-6.70	-6.70	-6.70	-6.70	-6.70	-6.70	-6.70	-6.69	-6.69	-6.70	Inf	-Inf
-0.01	-6.71	-6.71	-6.72	-6.71	-6.70	-6.71	-6.71	-6.71	-6.71	-6.71	-6.71	-670.00	67100.00
-0.02	-6.72	-6.72	-6.72	-6.71	-6.73	-6.72	-6.72	-6.72	-6.72	-6.73	-6.72	-335.00	33600.00
-0.05	-6.75	-6.75	-6.75	-6.75	-6.74	-6.75	-6.75	-6.75	-6.75	-6.75	-6.75	-134.00	13500.00
-0.10	-6.80	-6.80	-6.80	-6.80	-6.80	-6.80	-6.80	-6.79	-6.80	-6.79	-6.80	-67.00	6800.00
-0.20	-6.90	-6.90	-6.89	-6.90	-6.90	-6.89	-6.90	-6.90	-6.89	-6.89	-6.90	-33.50	3450.00
-0.50	-7.20	-7.19	-7.20	-7.20	-7.20	-7.19	-7.20	-7.20	-7.20	-7.19	-7.20	-13.40	1440.00
-1.00	-7.69	-7.70	-7.69	-7.68	-7.68	-7.69	-7.70	-7.68	-7.69	-7.69	-7.69	-6.69	769.00
-5.00	-11.65	-11.64	-11.65	-11.66	-11.64	-11.64	-11.66	-11.66	-11.66	-11.65	-11.65	-1.33	233.00
-10.00	-16.61	-16.59	-16.61	-16.58	-16.61	-16.60	-16.60	-16.61	-16.61	-16.61	-16.60	-0.66	166.00
-20.00	-26.49	-26.50	-26.51	-26.52	-26.52	-26.52	-26.53	-26.48	-26.52	-26.51	-26.51	-0.33	132.55
-50.00	-56.21	-56.21	-56.21	-56.24	-56.14	-56.23	-56.24	-56.15	-56.22	-56.21	-56.21	-0.12	112.42
-100.00	-105.78	-105.78	-105.69	-105.60	-105.75	-105.74	-105.81	-105.69	-105.75	-105.73	-105.73	-0.06	105.73
-150.00	-155.31	-155.18	-155.12	-155.22	-155.36	-155.36	-155.25	-155.31	-155.32	-155.32	-155.27	-0.04	103.51
-250.00	-254.40	-254.17	-254.17	-254.43	-254.12	-254.35	-254.12	-254.17	-253.97	-254.28	-254.22	-0.02	101.69
-300.00	-303.97	-303.85	-303.40	-303.58	-303.79	-303.76	-303.70	-303.64	-303.61	-303.94	-303.72	-0.01	101.24

2.2.3 Drawbacks

Some major drawbacks of the system are thus:

- The system has a large offset voltage of -6.7mV, particularly when compared to mV and μV level DDP signals.
- Its resolution is limited to approx. 60 μV hence it is unusable for the DDP signals which have dynamics in the order of μVs.
- Its low input impedance makes it unsuited for potential signal acquisitions.
- Its absolute accuracy is 0.1% of the full scale reading (FSR) of 1mV. This is very high in comparison to the DDP signals.
- There is no provision for electrical safety in this device.

This system is thus unsuitable for acquiring DDP signals.

2.3 Keysight LXI Data Acquisition/Switch Unit

Another data acquisition system (make: Keysight Technologies, name: Keysight LXI Data Acquisition/Switch Unit, model: 34972A) with multiplexor module Module-34901A has also been tested for usability in DDP signal acquisition.

2.3.1 Key features

Some key properties of this system are:

- It is a multiplexor unit that can acquire upto 60 differential channels.
- It has a selectable resolution of $4\frac{1}{2}$ digit, $5\frac{1}{2}$ digit and $6\frac{1}{2}$ digit. However, the speed of acquisition decreases as the resolution is increased.
- It has selectable input impedance from a nominal value of 10 MΩ to $>$ 10,000 MΩ for the $\pm$1V range.
- Common mode rejection ratio (CMRR) for dc measurement is 140 dB.
- This acquisition system is ac powered and weighs around 3.6kg.
- It has USB interface with PC or laptop and a dedicated software name BenchView that is used for device set up, data display, control and storage purposes.

Table 2.2: Trial readings of Keysight LXI Data Acquisition/Switch Unit

Resolution in digit	Time interval in ms	Number of samples in 2 minutes	
		Theoretical	Actual
6.5	1	120	120
	900	133	134
	800	150	150
	700	171	171
	600	200	200
	500	240	239
	400	300	298
	340	353	300
5.5	340	353	352
	300	400	402
	200	600	597
	150	800	798
	100	1200	1193
	75	1600	1696
	50	2400	2402
	40	3000	2810
4.5	40	3000	3002
	30	4000	4003
	20	6000	5998
	10	12000	12001
	5	24000	24005

2.3.2 Static Calibration

In the first test, an arbitrary constant input of 0.1mV was supplied to a single channel of the data acquisition system and the number of samples recorded in the system in 2 minutes duration was noted for the different system resolution settings. Table 2.2 provides the record of the set system resolution vs. the number of data samples acquired in 2 minutes using the system.

From the stated characteristics, it is noted that at resolution settings of 6.5, 5.5 and 4.5, signals upto 10 nV, 1μV and 100μV respectively can be acquired. But, as stated in the system manual, it is observed that even for the constant dc input, the speed of acquisition decreases as the resolution increases.

The plot of the acquired data is shown in Fig. 2.6. It can be seen from the plot that the mean value of the acquired signal is 0.1054mV for the input

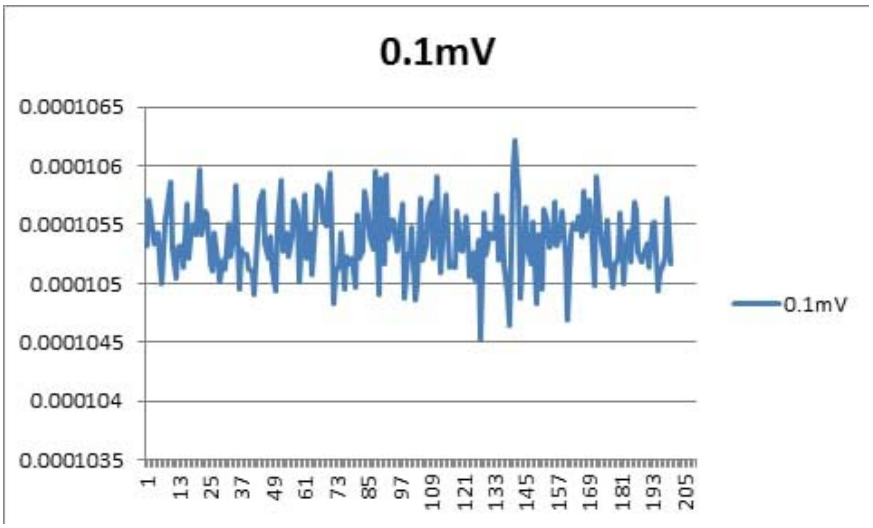

Figure 2.6: Output of Keysight LXI Data Acquisition/Switch Unit for a constant dc supply of 0.1mV

voltage of 0.1mV. Therefore, the % error is calculated to be 5.4% which is on the higher side.

2.3.3 Drawbacks

The major drawbacks of this system are:

- The system is not portable due to its direct ac power requirement as well as its weight.
- It does not provide isolation from electrical safety.
- Resolution and speed can not be achieved simultaneously in this device. As a result, the minimum sampling speed required for capturing the DDP dynamics cannot be achieved with the required system resolution using this system.
- Use of multiple channels will decrease the speed proportionately. In $6\frac{1}{2}$ digit, its acquisition speed is 6 channels/sec. For $5\frac{1}{2}$ and $4\frac{1}{2}$ digit, the acquisition speed are 54 channels/sec and 500 channels/sec respectively.

This system is also thus unsuitable for acquiring DDP signals.

2.4 Peripheral components and measurements

Apart from the basic data acquisition system, there are several other components that are necessary for the experimental setup and certain measurements that are needed for conducting the experiments.

2.4.1 Electrodes and connectors

The description of electrodes and connectors used in the data acquisition using RISH Multi acquisition system has already been stated in 2.2.1. The same electrodes and connectors were used for testing Advantech USB-4704 and Keysight LXI data acquisition systems. For static calibration, supply was given directly to the electrodes from voltage calibrator (Model: LC-05, Make: Libratherm Instruments Pvt. ltd.). However, the terminals connecting the acquisition systems of the connecting cable were modified accordingly.

2.4.2 Gel

When experimenting with human subjects, aqueous ultrasound (USG) gel was used at the electrode-skin interface for acquiring the human skin potentials since it provides good transfer of ions between electrode and skin. For static calibration, gel was not used.

2.4.3 Power supply

RISH Multi 18S multimeter is a 9V battery powered system and the RISH Multi SI232 adapter is a 2×1.5V battery powered device. The Advantech USB-4704 takes power using the connected USB cable from the connected PC. On the other hand, Keysight LXI acquisition system takes power directly from the household power supply of 220V ac.

2.4.4 USB connector

The RISH Multi 18S based system is connected to PC via serial cable, whereas both the Advantech USB 4704 and Keysight LXI are USB connected devices. Advantages of USB over the serial communication have been listed below.

- **Speed:** Data transfer rate using serial communication is 1 Mbps to 10 Mbps while the data transfer speed in USB communication is up to

Table 2.3: Instruments used for health parameter measurements

Parameter	Instrument	Model	Make
BP	Digital BP Monitor	HEM-7201	Omron Healthcare
	Analog BP monitor	GB101 (Sphygmomanometer)	Rossmax
		MDF 747 Dual Head Stethoscope	MDF Instruments USA
Pulse rate	Digital BP Monitor	HEM-7201	Omron Healthcare
	Manual	Using a stop watch for 1 minute duration	
SpO2	Pulse Oximeter	CMS50D	CONTEC

10,000 Mbps, which is at least 1000 times faster compared to the serial communication.

- **Power:** USB is much more capable to power the system compared to serial communication as it delivers 5V with upto 900mA current.
- **Compatibility:** Nowadays, USBs are compatible with every PC or laptop while serial connectors are rarely available.

2.4.5 Health parameters

Since the experiments involve human subjects so it is necessary to record some physiological parameters to ensure the normalcy of the subjects. These health parameters are: blood pressure (BP), pulse rate and oxygen saturation level (SpO2). Instruments used for these measurements are tabulated in Table 2.3. These parameters were recorded from the subjects both before and after the data acquisition.

2.5 Discussions

It is observed that the RISH Multi 18S based present data acquisition system is capable of acquiring the low voltage DDP signals from multiple locations simultaneously with moderate speed. This system provides good accuracy and acceptable precision. It also has optical isolation to provide electrical safety. However, its major limitations are its lack of compatibility with updated OS platforms and its lack of portability, specially when the number of channels are more.

In view of these limitations, two other data acquisition systems were tested. The Advantech USB-4704 is a low powered compact, portable device that can provide high speed data acquisition. But it lacks the accuracy and precision required for DDP signal acquisition. The Keysight LXI Data Acquisition/Switch Unit, on the other hand, is not portable and consumes relatively high power but it is accurate, precise and updated. It acquires data with good speed in low resolution but as the resolution increases, its speed decreases. Furthermore, the acquisition speed also decreases proportionately with increase in the number of acquiring channels.

A table has been provided comparing these 3 data acquisition systems on the basis of the required characteristics in Table 2.4. Comparing all the characteristics, it can be said that while the RISH Multi 18S based system has certain limitations, it is still a reliable system but the other two systems tested are not suitable for use as a reliable and portable acquisition system for DDP signals.

Table 2.4: Comparison of the available data acquisition systems

Properties	**Requirement**	**Data acquisition systems**		
		RISH Multi 18S	**Advantech USB 4704**	**Keysight LXI switching unit**
Accuracy	High	Relative accuracy 100 ± 0.07%	Relative error very high in low voltage range	Relative error also high, 5.4% for 0.1mV
Resolution	Typically 0.01mV or better	0.01mV for ±300mV	0.12mV within ± 1V	Resolution is good but acquisition speed need to be sacrificed.
Precision	SD should lie in the order of resolution, typically 0.01mV	0.01mV	Precision is low	The system is precise.
Portability	Must be small, light weight and battery powered	Not portable, containing many parts	small, light weight and USB powered	Very heavy, ac 220V supply required, not portable.
Electrical safety	Some isolation between input and output for electrical safety	Optical isolation for safety	No isolation	No isolation
Input impedance	Typically greater than 10MΩ	>10GΩ	127kΩ, which is very low	10 MΩ or > 10,000 MΩ, satisfactory

Table 2.4 – continued from previous page

Properties	Requirement	Data acquisition systems		
		RISH Multi 18S	**Advantech USB 4704**	**Keysight LXI switching unit**
Communication	USB communication for speed and availability	Serial communication	USB communication	USB communication
Compatibility	Must be compatible with the updated OS as well as the PC/Laptop hardware	Not compatible as the software does not work of windows 7,8 or 10	Work on a number of softwares and all these are compatible with the modern systems	BenchView is compatible with windows 10 also.
Cost	Should not be cost too high	This system is expensive	Low cost	Expensive
User friendliness	Should be user friendly	Not too user friendly	Expertise required on a software like labView, Matlab, Python etc.	User friendly, BenchView is very simple lo understand

CHAPTER 3

Calibration of 4 channel DAS

The limitations of the RISH Multi 18S based system and the unsuitability of the other two systems tested led to the necessity for developing a reliable and portable acquisition system for DDP signals. So a dedicated 4-channel data acquisition system was designed and developed indigenously by Somen Biswas, a co-author in [1], in the same research laboratory in which the present study is done.

This chapter deals with the standardization of this 4-channel data acquisition system (DAS). The characteristics of the 4-channel DAS and its working principle have been stated at the outset. Thereafter, details of a preliminary calibration performed to estimate its performance have been stated. Based on the calibration results, procedures for tuning and balancing the channels of this DAS have been tested. Thereafter, the complete static calibration of the balanced 4-channel DAS has been stated. A study of the common mode interference voltage of this DAS has also been presented. Finally, a comparison with the RISH Multi 18S based system is provided.

3.1 Major characteristics

The 4-channel DAS can acquire differential potentials from maximum 4 locations. It is a battery operated micro-controller based system that is specifically designed to acquire the potential differences in the order of DDP signals. The major characteristics of this acquisition system that make it ideal for DDP signal acquisition have been stated hereafter.

Differential dermal signal acquisition: The DDP signals typically lie within ±500mV. So, a silicon zener diode has been used to supply the reference voltage close to that range as it has a forward voltage cutoff of 0.7V.

Accuracy, resolution and precision: To achieve the resolution of 0.01mV

for this reference voltage, an ADC with at least 17 bits is needed. Hence, a high speed 22 bit ADC has been used in each channel.

Simultaneous acquisition: Individual sample/hold circuits have been used in each channel with a common pulse for simultaneous acquisition from different locations.

Portability: The system is powered with rechargeable batteries.

Electrical safety: Opto-couplers have been used to provide isolation to the communication section as it is connected to the USB of a PC/laptop. The PC is connected to the electric AC supply. Under normal working conditions, USB output does not cause any electrical hazard. But in some rare situations, malfunctions of USB may cause electrical hazard. For this reason, opto-couplers have been provides in the communication (Tx and Rx) section. However, the acquisition system is battery powered with 3 Li-ion batteries (18650 Li-ion battery, nominal voltage 3.7V) connected in series to obtain 11.10V power supply.

Communication: The I2C protocol has been used for better communication speed.

Figure 3.1 represents the schematic diagram of the 4-channel DAS. The DAS consists of 4 terminal units and 1 main unit. These terminal units have a 22 bit ADCs each to acquire the DDP signals between two input terminals. Silicon zener diodes are used in these terminal units to provide the reference voltage of 0.650mV. All the terminals units are connected to the main unit using input units. The main unit consists of a microcontroller block for controlling all its operations, a multiplexor block for sequentially data processing, a battery powered power supply block to provide portability and a communication block for communicating with the PC or laptop via USB. The communication block has been provided with optical isolation for the electrical safety. An actual 4-channel DAS has been shown in Figure 3.2.

3.1.1 Working principle

The flowchart for the working of the DAS is shown in Figure 3.3. The working principle is outlined hereafter.

1. The micro-controller in the main unit initializes all parameters with default or user provided values when the acquisition system has been switched on or reset. It also sets all the counters to zero at this point of time and is ready to send the signal for starting the program.

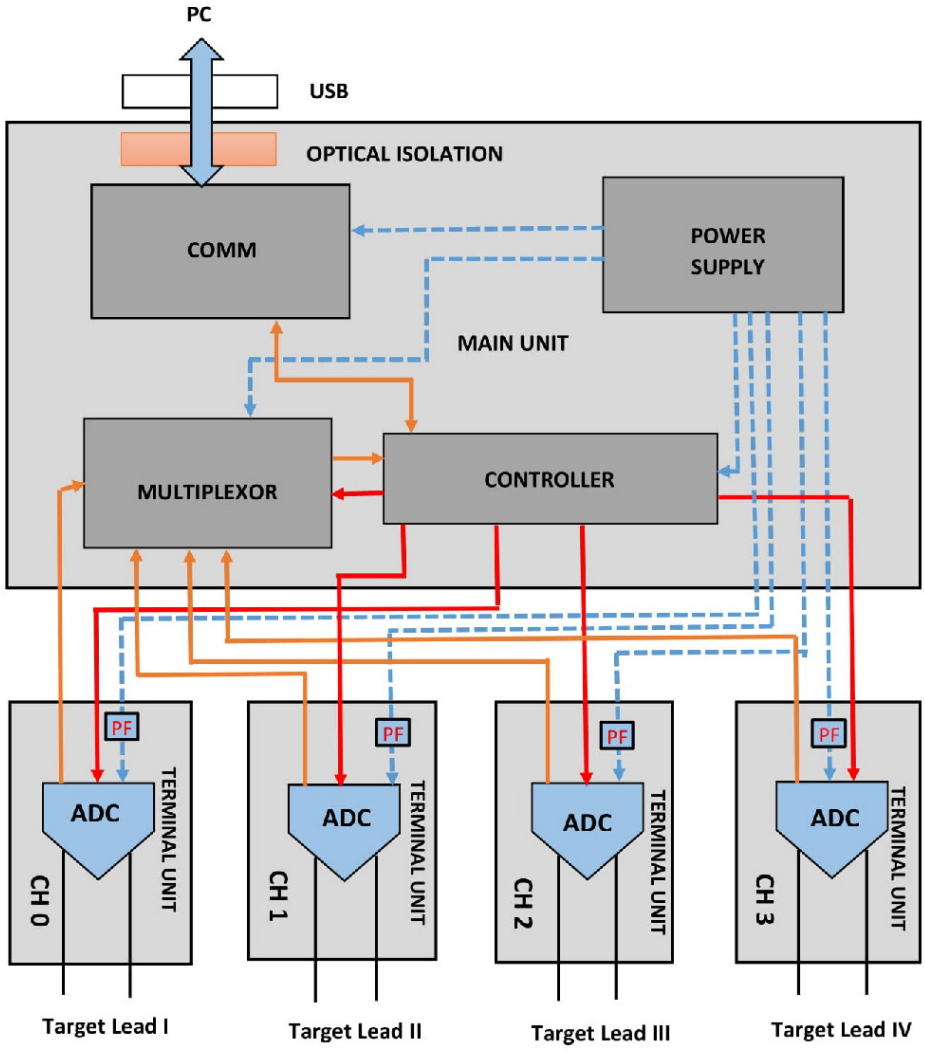

Figure 3.1: Schematic diagram of the 4-channel DAS.

2. After getting the software or hardware 'START' signal, the ADCs of the terminal units start sampling the data simultaneously and then hold them for conversion.

3. The micro-controller then selects the first channel number that is set using the multiplexer, checks the end of conversion bit, waits and then reads the data after end of conversion. Next, the micro-controller stores the data in its temporary memory.

4. The micro-controller then selects the next channel and follows the same

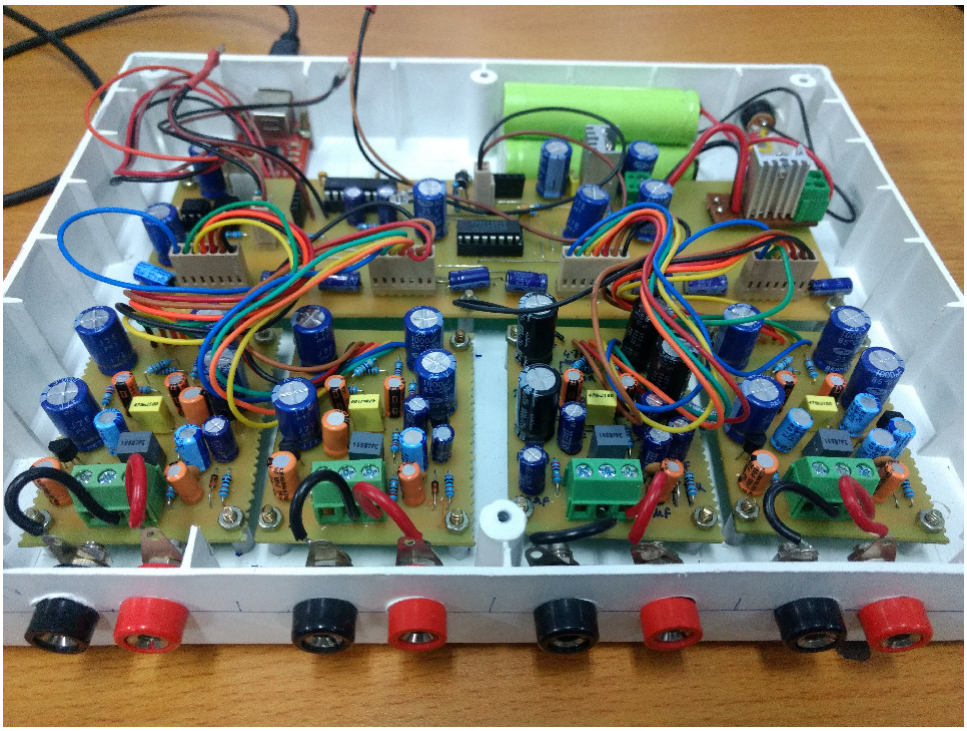

Figure 3.2: A typical 4-channel DAS.

procedure as in step 3. This is repeated until it acquires the data from all channels.

5. After storing the data of all the selected channels for a particular instant in its temporary memory, the main unit processes the stored data and sends it for display and/or storage through an UART to USB converter module.

6. The process in steps 1 till 5 is repeated for a predetermined period till the total number of samples of data to be recorded from all the selected channels are acquired and stored.

7. After completing the total task of acquiring the data, the DAS goes into sleep mode. A software or hardware reset is needed to bring it out from the sleep mode.

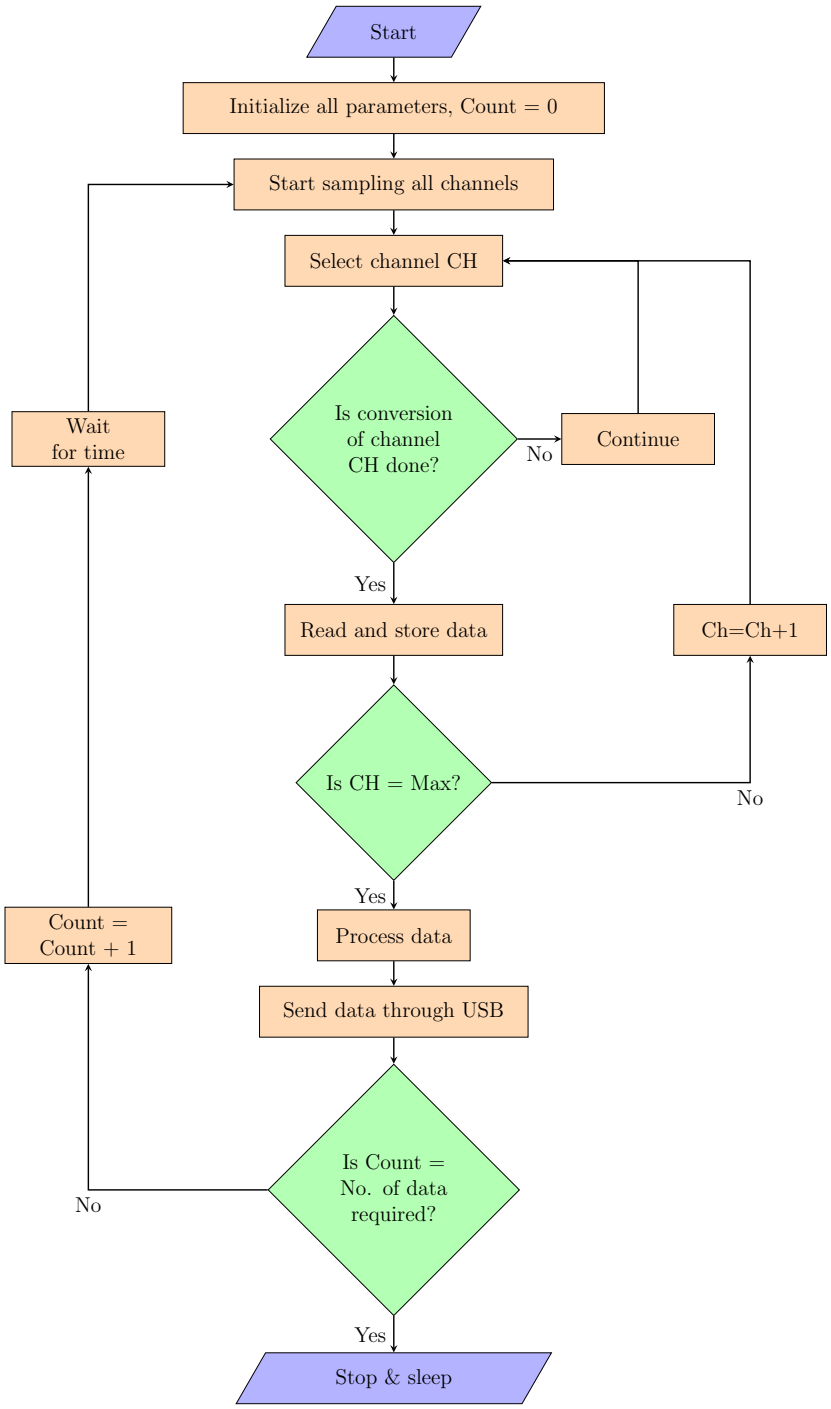

Figure 3.3: Flowchart of the working principle of the 4-channel DAS

3.2 Calibration of the DAS

The DAS was calibrated systematically for determining its accuracy, precision, linearity and sensitivity. This 4 channel DAS was designed to acquire low voltage signals within $\pm 500mV$, which covers the range of observed DDP signals. So for its calibration, DC signals of different input voltages within $\pm 500mV$ were acquired and recorded. At every input voltage, 2400 samples of data were acquired at a sampling rate of 20 samples/s for every individual channel. The standard input voltages were considered here as true values (TV) and the acquired voltages were considered as measured values (MV). The same calibration procedure was followed for every input voltage value and for all 4 channels individually.

The calibration was done in two phases. At first, a basic calibration was performed to get the input vs. output calibration curve. From this the accuracy, precision, linearity and sensitivity of the DAS was determined. After that, this calibration curve was subtracted from the ideal calibration curve (TV vs. expected reading) to get the error curve, which was then added to the calibration curve to get the corrected calibration curve. This was done for all 4 channels individually. Finally, this new system was studied systematically to find all the static parameters.

The input vs. output calibration curve was obtained as the plot of the mean of the MV with respect to the TV as shown in Figure 3.4. It is observed from the figure that the input-output relationships of all 4 channels are almost identical. To ascertain the characteristics furthermore, few static performance characteristics have been calculated.

3.2.1 Accuracy

Static error (SE) is defined as the difference between TV and MV [116, 117], while the corresponding terms, relative error and % relative accuracy are defined as [118]
Relative Error $(RE) = \frac{SE}{TV} = \frac{TV-MV}{TV}$
and % Relative Accuracy $\%(RA) = (1 - RE) \times 100\%$.

For each input voltage, the static errors were calculated for all the 2400 samples. Their maximum and minimum values are tabulated in Table 3.1and the corresponding % RA values are tabulated in Table 3.2. From Table 3.1, it is observed that the SE is lesser for smaller input voltages than the larger inputs, as is to be expected. This is supported by the results in Table 3.2, where it is observed that the overall % RA of all the channels for all the inputs lies within 100±5%, except in a few instances. The RA of 100±5%

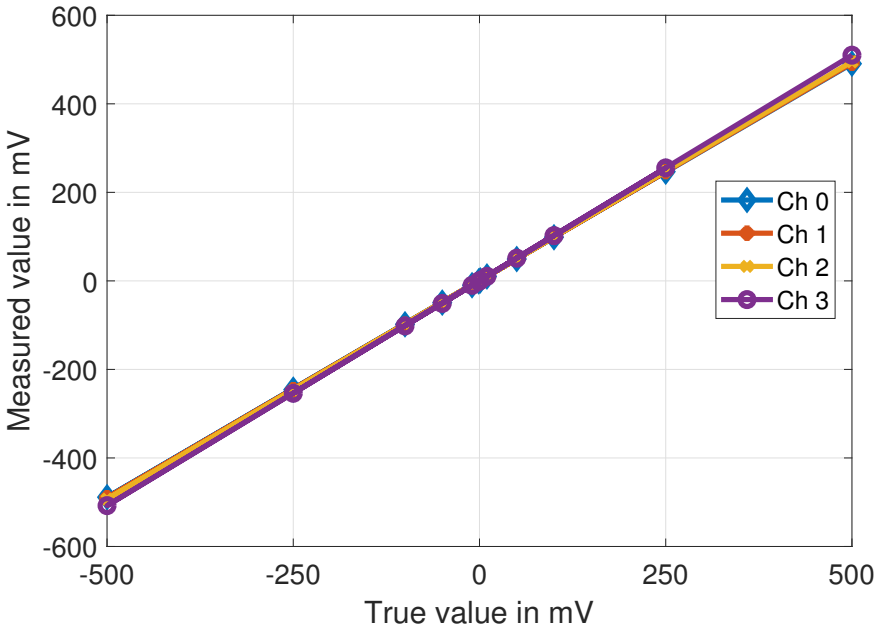

Figure 3.4: Plot of measured value vs. true value for all 4 channels

is not adequate for an accurate data acquisition system. Therefore, further tuning is required to improve the accuracy. This is discussed in Section 3.3.

3.2.2 Precision

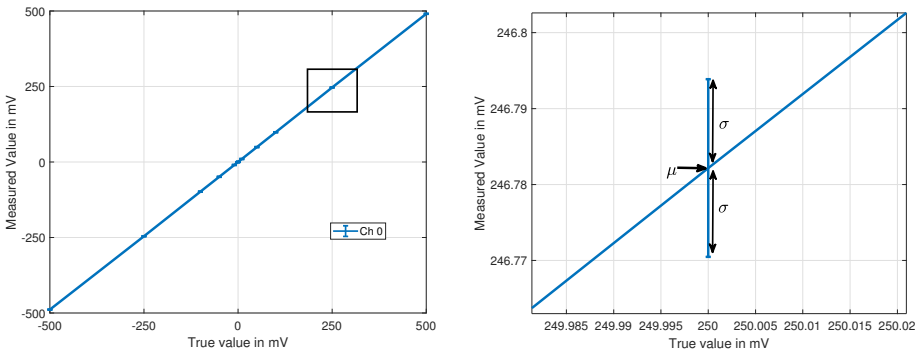

(a) (b)

Figure 3.5: (a)Output voltage vs input voltage of a single channel with $\mu \pm 1\sigma$ ranges at all test points (b)Enlarged view of $\mu \pm 1\sigma$ range of the highlighted test point.

Table 3.1: Maximum and minimum values of Static Error (SE) for different input voltages for all 4 channels.

True value in mV	Static error			
	Channel 0	Channel 1	Channel 2	Channel 3
	Min, Max in mV	Min, Max in mV	Min, Max in mV	Min, Max in mV
500	9.10, 9.64	8.05, 8.29	4.67, 5.10	-9.91, -9.81
250	3.17, 3.25	2.96, 3.03	1.30, 1.39	-5.31, -5.05
100	1.44, 1.53	1.24, 1.33	0.55, 0.65	-2.31, -2.22
50	0.65, 0.71	0.47, 0.50	0.14, 2.89	-1.25, -1.19
10	0.06, 0.10	0.06, 0.09	-0.01, 0.03	-0.29, -0.24
1	-0.04, 0.01	-0.05, -0.01	-0.05, -0.02	-0.08, -0.04
-1	-0.05, -0.01	-0.06, -0.02	-0.05, -0.01	-0.13, 0.02
-10	-0.19, -0.15	-0.06, -0.02	-0.13, -0.09	-0.64, 0.19
-50	-0.95, -0.89	-0.76, -0.72	-0.44, -0.40	0.93, 0.99
-100	-1.98, -1.82	-1.76, -1.70	-1.13, -1.03	1.76, 1.84
-250	-4.23, -4.14	-5.48, -3.95	-2.37, -2.28	3.68, 4.09
-500	-10.92, -11.84	-10.29, -9.86	-6.94, -6.69	7.61, 7.82

Precision is determined in terms of two statistical parameters, namely mean (μ) and standard deviation (σ), also denoted as SD. The mean and SD of the measured value were calculated for every true value (input) for all 4 channels and tabulated in Table 3.3 and $\mu \pm 1\sigma$ was indicated over an input-output relation plot for a single channel in Figure 3.5. From Table 3.3 and Figure 3.5, it may be said that the instrument is precise, with very small deviations that are well within limits.

3.2.3 Linearity and Sensitivity

Figure 3.4 shown at the outset contains the plot of the mean (μ) of the measured values with respect to the corresponding inputs for all 4 channels. From this figure, it can be said that the input and output follow a linear relationship. So, a curve fitting algorithm of MATLAB software is used to find the functional form of the best fit line. The goodness of fit (R^2) and

Table 3.2: Maximum and minimum % Relative Accuracy for different input voltages for all 4 channels.

True value in mV	% Relative Accuracy			
	Channel 0	Channel 1	Channel 2	Channel 3
	Min, Max	Min, Max	Min, Max	Min, Max
500	98.07, 98.17	98.34, 98.39	98.98, 99.07	101.96, 101.98
250	98.69, 98.73	98.78, 98.81	99.45, 99.48	102.02, 102.12
100	98.46, 98.56	98.66, 98.76	99.35, 99.45	102.22, 102.31
50	98.57, 98.70	98.99, 99.07	94.22, 99.72	102.39, 102.49
10	98.96, 99.37	99.13, 99.44	99.72, 100.14	102.43, 102.93
1	99.40, 103.90	101.20, 104.80	101.50, 105.30	103.90, 108.30
-1	95.00, 98.90	94.30, 97.70	95.20, 98.90	87.50, 101.90
-10	98.05, 98.47	98.07, 98.38	98.74, 99.10	93.58, 101.88
-50	98.10, 98.21	98.48, 98.55	99.13, 99.20	101.86, 101.97
-100	98.02, 98.17	98.24, 98.30	98.87, 98.97	101.76, 101.84
-250	98.30, 98.34	97.80, 98.42	99.05, 99.09	101.47, 101.64
-500	97.61, 97.83	97.94, 98.03	98.61, 98.66	101.52, 101.56

RMSE of all 4 channels were calculated and tabulated in Table 3.4. It is evident from the plots in Figure 3.4 and the R^2 of 1 for all channels with corresponding significantly low values of RMSE that linearity of response is established for all 4 channels of the DAS.

Sensitivity, which indicates the smallest amount of change that can be detected due to the change of input of unit amount, is standardly defined as

Sensitivity (S)= $\frac{\Delta MV}{\Delta TV}$, where ΔTV is the change in measured value and ΔMV is the change in true value. The sensitivity of the DAS channels have been determined as stated in Table 3.4. It is observed that the values of sensitivity are close to the ideal value of 1 for all 4 channels. It is to be mentioned that since the input vs. output characteristics is linear, therefore slope of the best fit line and sensitivity are synonymous in this case.

Table 3.3: Mean and SD of Measured Values for different inputs for all 4 channels.

True value in mV	Measured value							
	Channel 0		Channel 1		Channel 2		Channel 3	
	μ in mV	σ in mV	μ in mV	σ in mV	μ in mV	σ in mV	μ in mV	σ in mV
500	490.65	0.14	491.84	0.05	495.09	0.14	509.86	0.02
250	246.78	0.01	247.00	0.01	248.66	0.01	255.19	0.06
100	98.51	0.02	98.70	0.01	99.40	0.02	102.26	0.02
50	49.32	0.01	49.52	0.01	49.84	0.06	51.22	0.01
10	9.92	0.01	9.93	0.01	9.99	0.01	10.27	0.01
1	1.02	0.01	1.03	0.01	1.03	0.01	1.06	0.01
-1	-0.97	0.01	-0.96	0	-0.97	0.01	-1	0.01
-10	-9.83	0.01	-9.82	0.01	-9.89	0.01	-10.16	0.02
-50	-49.08	0.01	-49.26	0.01	-49.58	0.01	-50.96	0.01
-100	-98.11	0.05	-98.27	0.01	-98.93	0.01	-101.80	0.01
-250	-245.81	0.01	-246.00	0.02	-247.67	0.01	-253.90	0.10
-500	-488.70	0.40	-490.00	0.07	-493.18	0.05	-507.72	0.04

Table 3.4: Table for the R^2 and RMSE for different input voltages for all 4 channels.

Parameter	Channel 0	Channel 1	Channel 2	Channel 3
R^2	1	1	1	1
RMSE in mV	0.7019	0.5608	0.5872	0.4422
Sensitivity	0.9806	0.9828	0.9893	1.018

3.3 DAS tuning and channel balancing

In Figure 3.4, it can be seen that the calibration curves for all 4 channels of the DAS are similar but not exactly identical to each other. As expected, this phenomena is observed for the various channels in different data acquisition systems also. Furthermore, it was seen from the basic calibration that since

static error is larger for large input voltages, so this causes a decrease in accuracy for such inputs.

This necessitates putting in place a procedure to configure the calibration curves for each channel of a particular DAS and achieve channel balancing. 3 different approaches have been tested and these procedures are illustrated henceforth for one specific DAS. In all cases, the modifications have been performed stage-wise in order to correct for the remnant inaccuracy in the previous stage.

3.3.1 Multiplying inverse slope

The first method attempts to correct the calibration curve by multiplying the inverse of the calculated sensitivity, henceforth also referred to as slope, to the existing output. The objective is to achieve the ideal accuracy of 100% and the corresponding ideal slope of the input/output calibration curve as 1. This technique is very easy to implement at the programming level in the microcontroller and takes very less time to execute. Details of the method are stated below.

Method

Consider the initial input-output relationship

$$y_i = m \times x_i + c \tag{3.1}$$

where x_i and y_i are the input and output variables at i^{th} instant, while m and c are the slope and intercept of the input-output curve. For calibration purposes, TV is considered to be an almost constant DC input voltage supplied from a standard function generator (make and model: Keysight 33500B). The instantaneous value of this voltage is considered as x_i. Since the values of c at various input voltage levels are negligibly small, so it was neglected. Hence, the corrected output, y_c, which is expected to match the TV x_i, is obtained as $y_c = 1/m \times y_i$.

Result

A comparison of the accuracy and precision before and after slope correction in Channel 1 of the DAS is shown in Table 3.5.

It is observed that while the accuracy increases, yet the SD increases leading to a decrease in precision. Correspondingly, the uncertainty and % error of readings also increase. This observation indicates that while the value of the intercept is small, yet it is significant in maintaining the SD at

Table 3.5: Comparison of accuracy and precision before and after inverse of slope correction

True value in	mean in mV		SD in mV	
	Before correction	After correction	Before correction	After correction
500	490.65	497.52	0.14	0.19
250	246.78	248.38	0.01	0.02
100	98.51	98.95	0.02	0.02
50	49.32	49.56	0.01	0.02
10	9.92	9.94	0.01	0.01
1	1.02	1.01	0.01	0.01
-1	-0.97	-0.98	0.01	0.01
-10	-9.83	-9.89	0.01	0.02
-50	-49.08	-49.48	0.01	0.01
-100	-98.11	-98.91	0.05	0.02
-250	-245.81	-248.55	0.01	0.02
-500	-488.70	-496.23	0.40	0.42

lower values. Hence, a scheme accounting for the local changes in slopes and intercepts needs to be explored for improving the performance.

3.3.2 Spline fitting

The second approach for error correction is that of fitting multiple straight lines or splines. It was seen that % RA within the range $\pm 10mV$ is very high as compared to that for the range beyond. It is to be noted that the DAS has been calibrated using a calibrator (Model: LC05, Make: Libratherm Instruments Private Limited) which has 3 distinct ranges: a) within ±10mV and b) 2 ranges of opposing signs for magnitudes beyond 10mV. This difference in the slopes of the calibrator output can be expected to affect the DAS performance also in the similar ranges. Hence, the resultant calibration curve contains 3 parts but with two effective slopes as follows.

For $10mV < |x_i| \leq 650mV$, the resultant calibration curve slope is m_1.

For $-10mV \leq x_i \leq 10mV$, the resultant calibration curve slope is m_2.

Result

A comparison of the accuracy and precision obtained using the earlier stated linear fit and using this spline fit were tabulated in Table 3.6.

Table 3.6: Comparison of accuracy and precision after spline fitting for error correction

True value in	mean in mV		standard deviation in mV		% relative accuracy	
	Before correction	After correction	Before correction	After correction	Before correction	After correction
500.00	499.76	499.76	0.14	0.24	99.95	99.95
250.00	251.21	251.21	0.01	0.05	100.49	100.49
100.00	100.11	100.11	0.02	0.02	100.11	100.11
50.00	50.18	50.18	0.01	0.02	100.35	100.35
10.00	9.82	10.01	0.01	0.02	98.21	100.08
1.00	0.75	1.00	0.01	0.01	75.29	99.71
-1.00	-1.27	-1.02	0.01	0.01	127.27	101.57
-10.00	-10.30	-9.99	0.01	0.02	103.02	99.88
-50.00	-50.48	-50.48	0.01	0.02	100.97	100.97
-100.00	-100.30	-100.30	0.02	0.02	100.30	100.30
-250.00	-250.79	-250.79	0.01	0.05	100.32	100.32
-500.00	-498.62	-498.62	0.14	0.24	99.72	99.72

It is observed that the correction has improved the accuracy in the region $-10mV \leq x \leq 10mV$ without hampering the precision. This is as expected since the correction essentially applies only to the region $-10mV \leq x \leq 10mV$, for which the slope has changed to m_2. It is to be noted that the slope m_1 is identical to the slope m determined in the first method for the overall range of voltages.

As a result of this spline fit, the mean of the measured value is now closer to the corresponding true value for the overall range, including the region $-10mV \leq x \leq 10mV$. The overall % RA is also closer to 100 %.

Static error using the spline fit calibration curve has also been calculated and is plotted with error bars in Figure 3.6. It is observed that the static error in the region $-10mV \leq x \leq 10mV$ has reduced after spline fitting.

Despite the improvement in the region $-10mV < x < 10mV$, this technique has a major drawback that the measured value jumps between two calibration curves at $\pm 10mV$. For this reason, the SD at $\pm 10mV$ increases

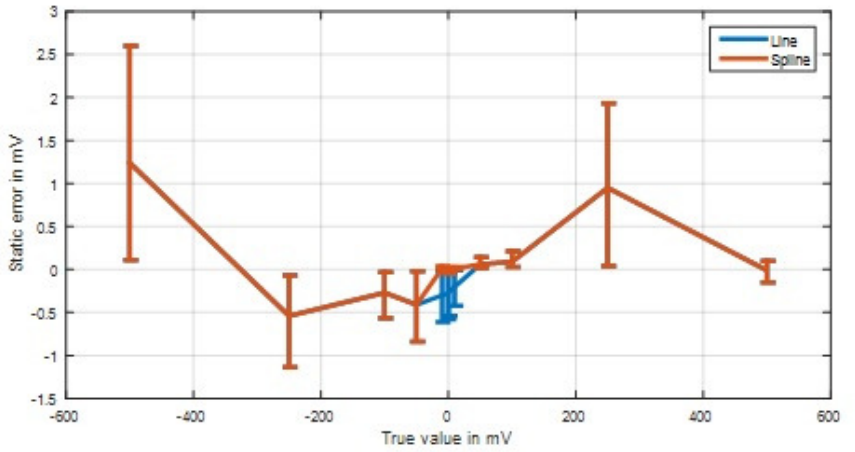

Figure 3.6: Error bar plot for the static error for the line and spline fitting.

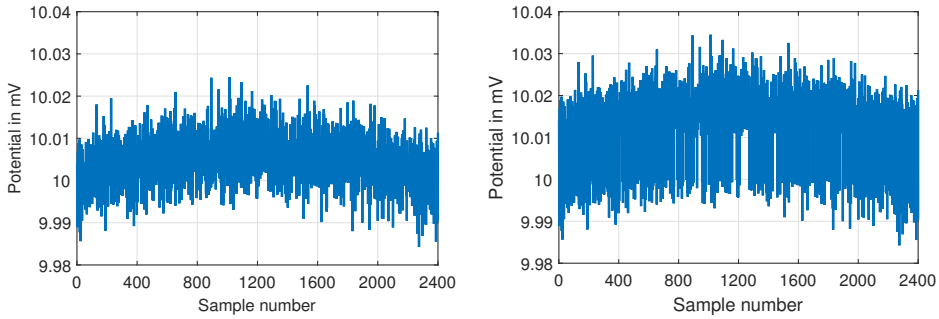

(a) (b)

Figure 3.7: Plot of the measured value at 10mV input voltage (a) for line calibration curve (b) for spline calibration curve.

significantly. Therefore, the precision of this instrument at $\pm 10mV$ decreases. As a result, the overall performance loses its continuity at ±10mV. The outputs at +10mV for line fit and spline fit calibration curves are plotted in Figure 3.7a and Figure 3.7b respectively. It is clearly observed that the precision has decreased due to spline fitting. Furthermore, spline fit also introduces nonlinearity into the system. Hence an alternative method has to be determined that overcomes this problem.

3.3.3 Addition of error curve

The third and the most effective method that was finally used for obtaining the final calibration curve is that of adding an error curve to the actual curve. The previous two methods led to increase in accuracy at the cost of precision, but loss of precision makes an instrument unreliable. For this reason, the previous two methods have not been used although they are easily implementable at the microcontroller programming level, while the error correction method is cumbersome. This disadvantage of the present method is offset by implementing it at the software level.

Method

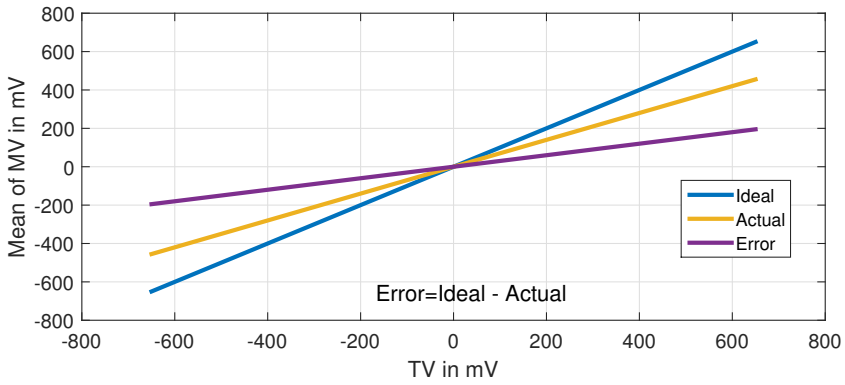

Figure 3.8: Error curve generation.

In the proposed method, the error curve for a particular channel of a DAS was obtained by subtracting the ideal curve from the linear fit of the actual channel input-output response.

The linear fit for the actual response of a DAS channel is denoted as $y_i = m \times x_i + c$ as stated in Section 3.3.1. Since the output follows the input exactly, the corresponding ideal response can be represented as $Y_i = x_i$, where Y_i denotes the ideal output. The proposed error is thus obtained as $e_i = Y_i - y_i = (1 - m) \times x_i - c$. The actual linear fit, the ideal response and the error curve are shown in Figure 3.8 for Channel 1 of the DAS. The error curve for each individual channel was saved in the microcontroller as a table and corrections were applied accordingly to the measured values for the respective channels.

The comparative calibration curves for all 4 channels of a DAS for linear fits and error curve fits shown in Figure 3.9. Although this process is time consuming, but the results show almost ideal input-output characteristics for

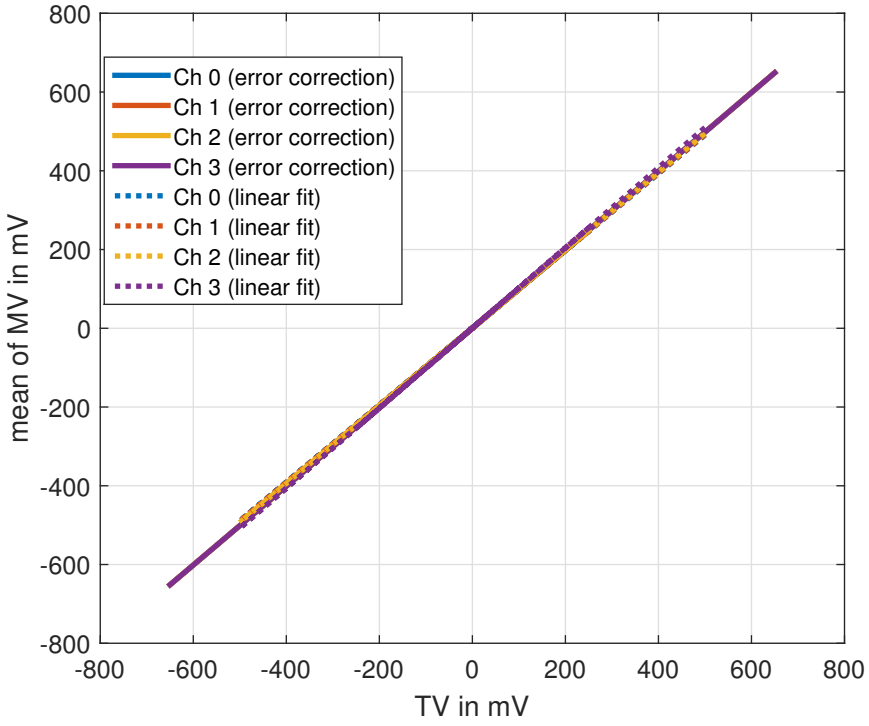

Figure 3.9: Line plot for TV vs. mean of MV for all 4 channels using linear fit and error correction.

all the channels. Also, all 4 channels of the DAS exhibit similar balanced performances. This has been validated hereafter by calibrating the tuned DAS.

3.4 Calibration after DAS tuning

The overall performance of the DAS channels tuned using their respective error correction curves has been validated by determining the static parameters stated in Section 3.2. These were calculated again for all the 4 channels in the input range [-650mV, 650mV].

3.4.1 Accuracy

Table 3.7: Maximum and minimum values of Static Error (SE) for different input voltages for all 4 error corrected channels

True value in mV	Static error			
	Channel 0	Channel 1	Channel 2	Channel 3
	Min, Max in mV	Min, Max in mV	Min, Max in mV	Min, Max in mV
650.00	0.65, 1.40	0.57, 1.47	0.58, 1.48	0.57, 1.49
500.00	1.59, 2.37	1.52, 2.44	1.51, 2.44	1.51, 2.46
300.00	1.12, 1.51	1.04, 1.60	1.04, 1.58	1.03, 1.59
100.00	0.07, 0.26	-0.01, 0.34	-0.02, 0.35	-0.01, 0.34
50.00	-0.38, -0.34	-0.47, -0.25	-0.47, -0.24	-0.47, -0.25
25.00	-0.32, -0.28	-0.41, -0.19	-0.41, -0.19	-0.41, -0.19
20.00	-0.31, -0.27	-0.40, -0.17	-0.40, -0.17	-0.40, -0.18
15.00	-0.31, -0.27	-0.40, -0.18	-0.40, -0.17	-0.40, -0.17
10.00	-0.30, -0.24	-0.39, -0.17	-0.39, -0.17	-0.39, -0.17
5.00	-0.27, -0.24	-0.37, -0.15	-0.37, -0.14	-0.37, -0.14
2.00	-0.28, -0.24	-0.36, -0.15	-0.37, -0.15	-0.37, -0.15
1.00	-0.27, -0.23	-0.36, -0.14	-0.36, -0.14	-0.36, -0.14
0.50	-0.26, -0.23	-0.36, -0.14	-0.36, -0.14	-0.36, -0.14
0.20	-0.27, -0.24	-0.37, -0.15	-0.37, -0.15	-0.37, -0.15
0.01	-0.38, -0.32	-0.46, -0.23	-0.46, -0.24	-0.46, -0.24
0.05	-0.29, -0.23	-0.37, -0.15	-0.38, -0.15	-0.38, -0.15
0.02	-0.28, -0.24	-0.37, -0.15	-0.37, -0.15	-0.38, -0.15
0.01	-0.29, -0.25	-0.38, -0.15	-0.37, -0.15	-0.38, -0.16
0.00	-0.28, -0.24	-0.37, -0.15	-0.37, -0.15	-0.37, -0.15
0.00	-0.28, -0.24	-0.37, -0.15	-0.37, -0.15	-0.37, -0.15
-0.01	-0.27, -0.23	-0.36, -0.14	-0.36, -0.14	-0.37, -0.14
-0.02	-0.27, -0.24	-0.37, -0.14	-0.36, -0.14	-0.37, -0.14
-0.05	-0.27, -0.24	-0.37, -0.15	-0.37, -0.14	-0.36, -0.14
-0.10	-0.28, -0.24	-0.37, -0.15	-0.36, -0.15	-0.37, -0.15
-0.20	-0.28, -0.24	-0.37, -0.15	-0.37, -0.15	-0.37, -0.15
-0.50	-0.27, -0.24	-0.36, -0.14	-0.36, -0.15	-0.36, -0.14
-1.00	-0.29, -0.25	-0.38, -0.15	-0.38, -0.16	-0.38, -0.16
-2.00	-0.28, -0.24	-0.37, -0.14	-0.37, -0.15	-0.37, -0.15
-5.00	-0.28, -0.24	-0.37, -0.15	-0.37, -0.15	-0.37, -0.14
-10.00	-0.26, -0.22	-0.35, -0.13	-0.35, -0.13	-0.35, -0.13
-15.00	-0.25, -0.21	-0.34, -0.12	-0.34, -0.12	-0.34, -0.12
-20.00	-0.23, -0.17	-0.32, -0.09	-0.32, -0.11	-0.32, -0.10
-25.00	-0.22, -0.18	-0.31, -0.09	-0.31, -0.09	-0.31, -0.09

Table 3.7 – continued from previous page

True value in mV	Static error			
	Channel 0	Channel 1	Channel 2	Channel 3
	Min, Max in mV	Min, Max in mV	Min, Max in mV	Min, Max in mV
-50.00	-0.15, -0.11	-0.24, -0.02	-0.25, -0.02	-0.23, -0.02
-100.00	0.08, 0.15	-0.01, 0.24	-0.01, 0.23	-0.01, 0.23
-300.00	0.74, 0.83	0.65, 0.92	0.67, 0.92	0.66, 0.92
-500.00	1.11, 1.26	1.02, 1.34	1.02, 1.34	1.05, 1.35
-650.00	1.29, 1.63	1.21, 1.69	1.21, 1.71	1.20, 1.70

As in the previous case, Static Errors (SE) were calculated for all TVs of all 4 channels and are tabulated in Table 3.7. Comparing these results with that of Table 3.1 for the linear fit, it can be seen that SE in this case is much smaller than the previous case. Without error correction, the maximum amplitude of SE for all inputs and all channels was $11.84mV$ but this reduces to $2.37mV$ using error correction method.

% Relative Accuracy (% RA) has been calculated at various input voltage levels for all 4 channels and the maximum and the minimum values are tabulated in Table 3.8. It is observed that even using the error correction method, the % RA at very low input values, typically within ±1mV, is poor. This is evident in the results for SE also, where it is observed that the SE is larger than the TV for this range. However, comparing these results with those in Table 3.2 for the linear fit case, it can be said that with error correction the % RA has particularly improved in the range 10mV ¡ $|x_i|$ ¡ 500mV.

Thus, on the basis of SE and %RA, it can be said that the accuracy of this DAS has improved on using error correction.

3.4.2 Precision

As in the earlier case, the mean and SD of the acquired data were calculated and tabulated in Table 3.9 for each TV of all 4 channels as a measure of precision of the DAS. Comparing the results with those stated in Table 3.3 for the linear fit case, it can be said that while the mean values have changed, there is no significant change in the σ values. This is evident from the $\mu \pm 1\sigma$ error bar at a particular TV depicted in the magnified input-output relation plot for Channel 1 of the DAS as shown in Figure 3.10.

Table 3.8: Maximum and minimum values of % Relative Accuracy (% RA) for different input voltages for all 4 error corrected channels

True value in mV	Relative accuracy in %			
	Channel 0	Channel 1	Channel 2	Channel 3
	Min, Max	Min, Max	Min, Max	Min, Max
650.00	99.78, 99.90	99.77, 99.91	99.77, 99.91	99.77, 99.91
500.00	99.53, 99.68	99.51, 99.7	99.51, 99.7	99.51, 99.70
300.00	99.5, 99.63	99.47, 99.65	99.47, 99.65	99.47, 99.66
100.00	99.74, 99.93	99.66, 100.01	99.65, 100.02	99.66, 100.01
50.00	100.67, 100.75	100.49, 100.93	100.49, 100.94	100.49, 100.93
25.00	101.14, 101.28	100.76, 101.65	100.76, 101.65	100.77, 101.65
20.00	101.33, 101.53	100.85, 102.00	100.87, 102.02	100.90, 102.00
15.00	101.80, 102.04	101.18, 102.65	101.15, 102.64	101.14, 102.68
10.00	102.45, 103.01	101.70, 103.93	101.72, 103.92	101.75, 103.94
5.00	104.7, 105.49	102.93, 107.37	102.90, 107.32	102.80, 107.39
2.00	112.04, 113.84	107.32, 118.22	107.33, 118.29	107.46, 118.32
1.00	123.07, 126.53	113.56, 136.23	113.63, 135.84	113.74, 136.36
0.50	145.79, 152.50	127.23, 171.28	127.43, 171.73	127.77, 172.01
0.20	219.33, 236.98	173.43, 283.45	173.07, 285.06	173.18, 283.77
0.01	3302.43, 3865.91	2389.49, 4726.75	2508.57, 4741.08	2498.57, 4724.65
0.05	555.63, 679.03	406.99, 846.22	409.56, 854.78	406.28, 852.33
0.02	1303.50, 1494.29	839.54, 1933.28	869.51, 1962.90	835.24, 1980.38
0.01	2567.76, 2956.49	1614.12, 3871.60	1610.56, 3829.5	1669.79, 3874.47
-0.01	-2614.12, -2211.13	-3492.87, -1256.09	-3528.53, -1268.19	-3553.50, -1345.95
-0.02	-1253.57, -1080.60	-1732.17, -619.83	-1711.12, -585.60	-1735.00, -596.65
-0.05	-445.08, -372.33	-635.23, -192.16	-636.52, -189.16	-627.09, -182.33
-0.10	-175.82, -141.23	-273.75, -49.00	-264.41, -46.22	-268.47, -45.08
-0.20	-39.41, -20.51	-84.66, 25.75	-85.16, 26.46	-85.59, 27.03
-0.50	45.93, 52.64	27.50, 72.14	27.28, 70.86	27.62, 71.83
-1.00	71.47, 75.29	62.28, 84.54	62.43, 84.41	61.88, 84.38
-2.00	85.91, 88.07	81.41, 92.78	81.34, 92.55	81.46, 92.49
-5.00	94.47, 95.26	92.66, 97.05	92.54, 97.05	92.58, 97.11
-10.00	97.39, 97.82	96.46, 98.74	96.53, 98.71	96.49, 98.72
-15.00	98.36, 98.59	97.74, 99.21	97.73, 99.22	97.74, 99.2
-20.00	98.83, 99.15	98.39, 99.55	98.38, 99.47	98.39, 99.49
-25.00	99.11, 99.27	98.76, 99.64	98.75, 99.62	98.76, 99.64
-50.00	99.7, 99.78	99.51, 99.97	99.51, 99.97	99.53, 99.97
-100.00	100.08, 100.15	99.99, 100.24	99.99, 100.23	99.99, 100.23
-300.00	100.25, 100.28	100.22, 100.31	100.22, 100.31	100.22, 100.31
-500.00	100.22, 100.25	100.2, 100.27	100.2 , 100.27	100.21, 100.27
-650.00	100.20, 100.25	100.19, 100.26	100.19, 100.26	100.19, 100.26

Table 3.9: Mean and SD of Measured Values for different input voltages for all 4 error corrected channels

True value in mV	Measured value							
	Channel 0		Channel 1		Channel 2		Channel 3	
	μ in mV	σ in mV	μ in mV	σ in mV	μ in mV	σ in mV	μ in mV	σ in mV
650.00	648.98	0.20	648.98	0.21	648.98	0.21	648.98	0.21
500.00	498.10	0.20	498.10	0.21	498.10	0.21	498.10	0.21
300.00	298.69	0.10	298.69	0.12	298.69	0.12	298.69	0.12
100.00	99.85	0.01	99.85	0.01	99.85	0.01	99.85	0.01
50.00	50.36	0.01	50.36	0.01	50.36	0.01	50.36	0.01
25.00	25.30	0.01	25.30	0.01	25.30	0.01	25.30	0.01
20.00	20.29	0.01	20.29	0.01	20.29	0.01	20.29	0.01
15.00	15.29	0.01	15.29	0.01	15.29	0.01	15.28	0.01
10.00	10.28	0.01	10.28	0.01	10.28	0.01	10.28	0.01
5.00	5.26	0.01	5.26	0.01	5.26	0.01	5.26	0.01
2.00	2.26	0.01	2.26	0.01	2.26	0.01	2.26	0.01
1.00	1.25	0.01	1.25	0.01	1.25	0.01	1.25	0.01
0.50	0.75	0.01	0.75	0.01	0.75	0.01	0.75	0.01
0.20	0.46	0.01	0.46	0.01	0.46	0.01	0.46	0.01
0.01	0.36	0.01	0.36	0.01	0.37	0.01	0.37	0.01
0.05	0.31	0.01	0.32	0.01	0.31	0.01	0.31	0.01
0.02	0.28	0.01	0.28	0.01	0.28	0.01	0.28	0.01
0.01	0.28	0.01	0.27	0.01	0.28	0.01	0.28	0.01
0.00	0.26	0.00	0.26	0.01	0.26	0.01	0.26	0.01
0.00	0.26	0.00	0.26	0.01	0.26	0.01	0.26	0.01
-0.01	0.24	0.01	0.24	0.01	0.24	0.01	0.24	0.01
-0.02	0.23	0.01	0.23	0.01	0.23	0.01	0.23	0.01
-0.05	0.21	0.01	0.20	0.01	0.21	0.01	0.21	0.01
-0.10	0.16	0.01	0.16	0.01	0.16	0.01	0.16	0.01
-0.20	0.01	0.01	0.01	0.01	0.01	0.01	0.01	0.01
-0.50	-0.25	0.01	-0.25	0.01	-0.25	0.01	-0.25	0.01
-1.00	-0.73	0.01	-0.73	0.01	-0.73	0.01	-0.73	0.01
-2.00	-1.74	0.01	-1.74	0.01	-1.74	0.01	-1.74	0.01
-5.00	-4.74	0.01	-4.75	0.01	-4.74	0.01	-4.74	0.01
-10.00	-9.76	0.01	-9.76	0.01	-9.76	0.01	-9.76	0.01
-15.00	-14.77	0.01	-14.77	0.01	-14.77	0.01	-14.77	0.01
-20.00	-19.79	0.01	-19.78	0.01	-19.78	0.01	-19.79	0.01
-25.00	-24.80	0.01	-24.80	0.01	-24.80	0.01	-24.80	0.01
-50.00	-49.87	0.01	-49.87	0.01	-49.87	0.01	-49.87	0.01
-100.00	-100.11	0.01	-100.11	0.01	-100.11	0.01	-100.11	0.01
-300.00	-300.79	0.01	-300.79	0.01	-300.79	0.01	-300.79	0.01
-500.00	-501.19	0.02	-501.19	0.01	-501.19	0.01	-501.19	0.01
-650.00	-651.47	0.07	-651.47	0.09	-651.47	0.09	-651.47	0.09

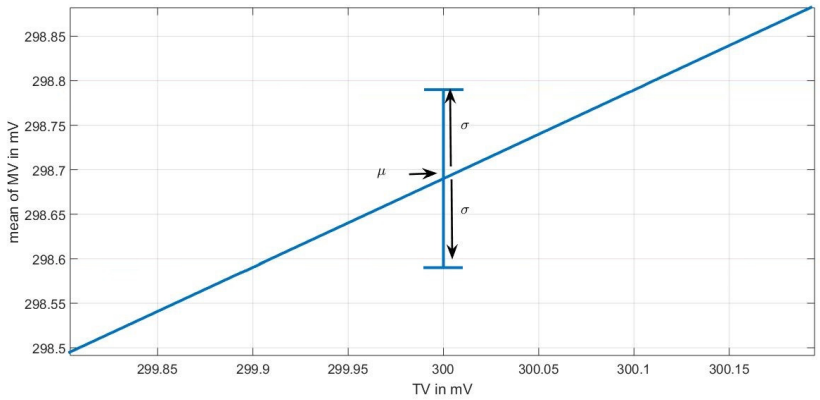

Figure 3.10: Magnified view of precision

3.4.3 Repeatability

From Table 3.7, it can be seen that the span of SEs are very small compared to the TVs in all cases with input magnitudes larger than 1mV. Furthermore, from Table 3.9, it is observed that corresponding σ values are very small. Thus, it can be said in this case also that repeatability of this DAS is very good.

3.4.4 Linearity and Sensitivity

The mean of the MVs were plotted with respect to the TVs in this case also and linear functions was fitted for interpreting the linearity and sensitivity. The overall goodness of fit coefficient R^2 is observed to be 1 in all cases as expected. The RMSE and sensitivity for the linear fit and the error correction fit cases were tabulated in Table 3.10.

It is observed that after error correction, all the channels exhibit a more balanced performance in terms of both linearity and sensitivity. Sensitivity has stabilized to 99.99% in all cases, which is very close to the ideal sensitivity of 1, while the overall RMSE has stabilized at a uniform acceptable value of 0.60mV for all 4 channels in place of the earlier range of [0.44mV,0.70mV].

3.4.5 Drift

To study the drift in the channels of the DAS, time series plots of 2400 samples, acquired for 2 minutes, were shown in Figure 3.11a and Figure 3.11b for input voltage levels of 100mV and 0.5mV respectively. It is observed that for high inputs, MV shows a small drift but for low input voltages, MV

Table 3.10: Table for the R^2 and RMSE for different input voltages for all 4 error corrected channels

Parameter		Channel 0	Channel 1	Channel 2	Channel 3
R^2		1	1	1	1
RMSE in mV	Before correction	0.7019	0.5608	0.5872	0.4422
	After correction	0.5993	0.5992	0.5996	0.5994
Sensitivity	Before correction	0.9806	0.9828	0.9893	1.018
	After correction	0.9999	0.9999	0.9999	0.9999

remains almost constant with time. However, further uses of this device with the DDP signals will require the study of its drift characteristics for longer durations.

3.4.6 Resolution

The resolution of a system is the smallest change of input that can be measured. The working range of the data acquisition system is $\pm 700mV$, hence the span is 1.4V. A 22 bit ADC was used in this case but due to noise, only 17 bits were considered for conversion. Therefore, the theoretical resolution of the data acquisition system is $\frac{1.4}{2^{17}} \approx 1\mu V$. However, the precision Keysight 33500B Function Generator that has been used to supply the input voltage for calibration has a resolution of $10\mu V$. So, it has not been possible to test the DAS below $10\mu V$.

3.4.7 Hysteresis

In order to test the hysteresis of the instrument, the input voltage was varied from maximum (+650mV) to minimum (-650mV) and then back to maximum again and this was repeated 5 times, but no hysteresis was observed in any of the channels.

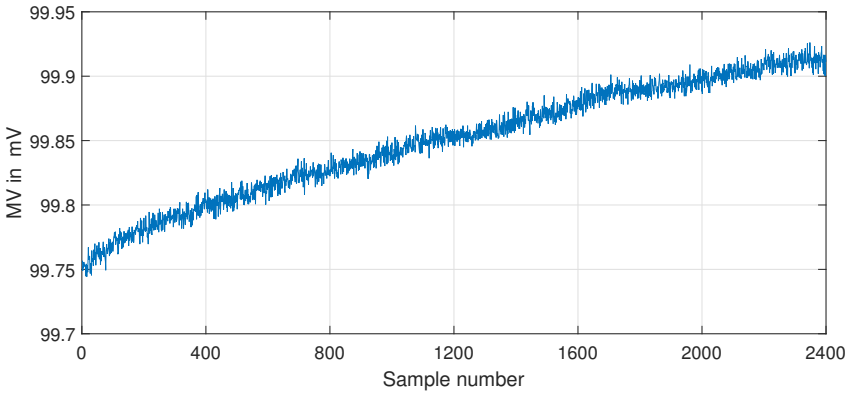

(a)

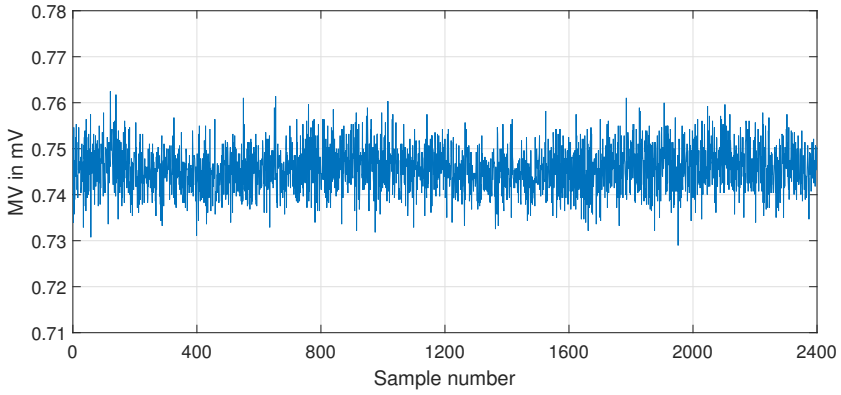

(b)

Figure 3.11: Time series plot for (a) a high input voltage of 100mV (b) a low input voltage of 0.5mV

3.5 Analysis of common-mode interference voltage

In the measurement of very low mV order signals, common mode interference voltage (CMIV), which is the voltage difference which is present at both input leads of an analog circuit with respect to analog ground, plays a very important role [119,120]. The source of common-mode noise is the difference in potential between two physically remote grounds. Figure 3.12 represents the source of common mode voltage.

Consider that Line 1 and Line 2 in Figure 3.12 are two sensor terminals connected with connector wires of the measuring system. In case of differential measurement, stray capacitances are generated between the reference

ground terminal (0V) and other two terminals if the reference terminal is not physically grounded. For this reason, separate potential differences are generated for two sensor terminals. In this figure these potential differences are considered as V1 and V2. If V1 $\neq$ V2, then a potential difference can be seen between V1 and V2 and this can be expressed as $V = V1 - V2$. This can easily be seen by shorting two terminals (Line 1 and Line 2) and observing the voltage.

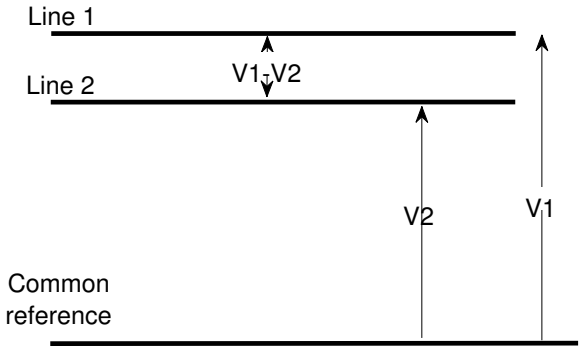

Figure 3.12: Common mode interference voltage

To study the effect of common mode interference voltage, 2 cases were considered.

1. Case 1: Terminals are shorted and no input voltage is applied
2. Case 2: A common voltage is applied to the shorted terminals

3.5.1 Case 1

In this experiment, Line 1 and and Line 2 were shorted for 2 minutes and the potential was recorded. In the ideal case, there is no common mode interference voltage and so the output voltage should be 0.00mV. But in this present experiment, it was seen that the short circuit potential varies from -7μV to 6μV as shown in Figure 3.13. It has already been mentioned that this device was calibrated for the resolution of 10μV, though it is designed to acquire a minimum of 1μV. Therefore, the CMIV lies below the resolution limit and so does not affect the accuracy of this instrument.

Furthermore, standard statistical quantities were also calculated for this common mode interference signal and tabulated in Table 3.11. It is observed from the table also that the CMIV lies well below the resolution with a mean value of 0.000 mV. Though skewness and kurtosis values lie close to normal distribution but the chi square goodness of fit test shows that the CMIV is not normally distributed.

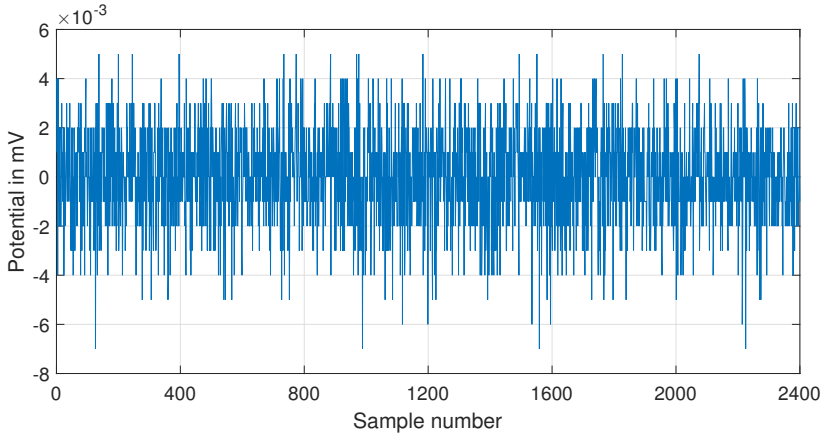

Figure 3.13: Common mode interference voltage with no input voltage

Table 3.11: Standard statistical parameters of Common Mode Interference Voltage (CMIV) for shorted terminals with no applied voltage

Parameter	Range in mV		μ in mV	SD in mV	Skew-ness	Kurt-osis
	Min	Max				
CMIV	-0.007	0.005	0.000	.002	-0.168	2.999

3.5.2 Case 2

For the next experiment, different input voltages were applied to the shorted terminals and output voltages were recorded for 2 minutes. In this experiment, the input voltages were varied from -500mV to +500mV and applied to both the positive and the negative terminals. The plots of the recorded voltages for a few input voltages is shown in Figure 3.14. Comparing Figure 3.14 with Figure 3.13, it is observed that the CMIV is higher for finite non-zero input voltages than that when no input voltage is applied. In this case, the overall output voltage lies within $\pm$0.08mV, which is much higher than the resolution of this instrument (0.01mV).

To study the common mode interference voltages for different input voltages, the root mean square (RMS) of output voltages were calculated for each individual input voltage and plotted with respect to the input voltages in Figure 3.15. It can be seen from the plot that the RMS value of output voltages increases as the magnitude of the input voltages increase. The RMS remains lower than the resolution of 0.01mV within an input voltage range of $\pm$100mV.

Standard statistical quantities of the output voltages measured for all the

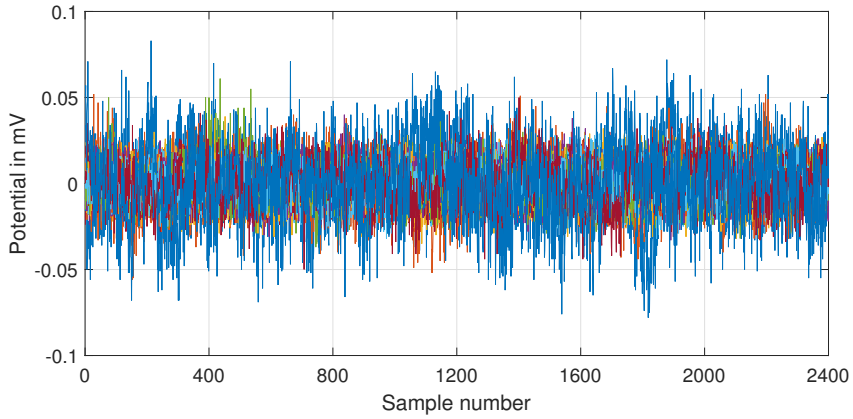

Figure 3.14: Common mode interference voltage with variable input voltages

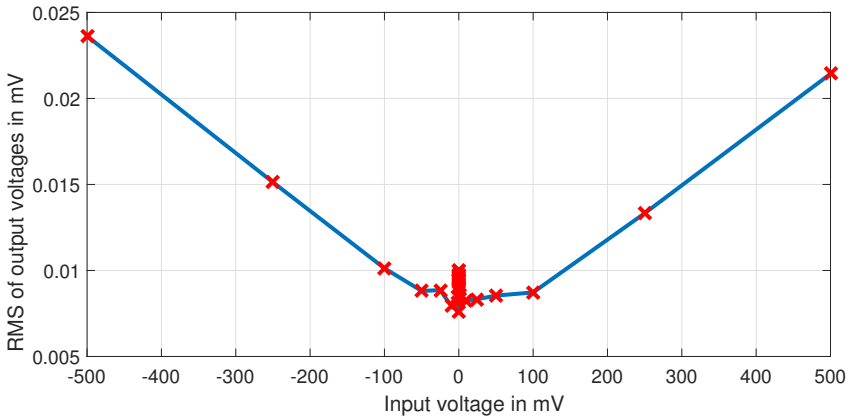

Figure 3.15: Plot of RMS voltages of Common Mode Interference Voltage for shorted terminals with variable input voltage applied

different input voltages applied were calculated and tabulated in Table 3.12. It can be seen from the table that when an input voltage is applied, common mode interference voltages become higher and exceeds the resolution of the DAS by a few times, although the mean value is 0.000 mV. SD is also higher for higher input voltages. As in the case of no applied voltage, the skewness and kurtosis values are close to normal distribution but none of these are normally distributed.

3.6 Comparison of DAS with RISH Multi 18S

Table 3.12: Standard statistical parameters of Common Mode Interference Voltage when different input voltages are applied

Input in mV	Range in mV		μ in mV	SD in mV	Skew-ness	Kurt-osis
	Min	Max				
Input in mV	Range in mV		μ in mV	SD in mV	Skew-ness	Kurt-osis
	Min	Max				
-500.00	-0.078	0.083	0.000	0.024	-0.006	2.961
-250.00	-0.056	0.052	0.000	0.015	-0.114	3.045
-100.00	-0.035	0.039	0.000	0.010	-0.041	2.986
-50.00	-0.030	0.026	0.000	0.009	0.044	2.871
-25.00	-0.029	0.050	0.000	0.009	0.098	3.353
-10.00	-0.024	0.026	0.000	0.008	0.073	3.005
-2.00	-0.028	0.029	0.000	0.008	-0.052	2.932
-1.00	-0.031	0.028	0.000	0.008	-0.089	2.958
-0.50	-0.035	0.034	0.000	0.010	0.019	2.839
-0.20	-0.031	0.032	0.000	0.009	0.057	2.906
-0.10	-0.031	0.038	0.000	0.009	0.015	2.936
-0.05	-0.032	0.030	0.000	0.009	0.042	2.786
-0.02	-0.032	0.031	0.000	0.010	-0.032	2.848
-0.01	-0.034	0.034	0.000	0.009	0.029	2.972
0.00	-0.025	0.032	0.000	0.008	0.063	3.094
0.01	-0.040	0.052	0.000	0.010	0.169	4.096
0.02	-0.031	0.030	0.000	0.010	-0.019	2.794
0.05	-0.033	0.040	0.000	0.009	0.107	3.212
0.10	-0.037	0.061	0.000	0.010	0.423	4.868
0.20	-0.030	0.031	0.000	0.009	0.051	3.006
0.50	-0.030	0.030	0.000	0.010	-0.005	2.883
1.00	-0.026	0.029	0.000	0.008	0.066	2.911
2.00	-0.028	0.035	0.000	0.009	0.020	2.934
10.00	-0.031	0.028	0.000	0.008	0.020	2.961
25.00	-0.026	0.027	0.000	0.008	0.066	2.945
50.00	-0.028	0.036	0.000	0.009	-0.007	3.075
100.00	-0.032	0.030	0.000	0.009	-0.010	2.944
250.00	-0.050	0.050	0.000	0.013	-0.085	3.132
500.00	-0.076	0.065	0.000	0.02 2	0.069	3.700

Table 3.13: Static Error and Relative Accuracy for different input voltages for RISH Multi 18S [5]

True value in mV	Measured value (mean) in mV	standard deviation in mV	Static error			Mean Relative Accuracy in %
			Min in mV	Max in mV	Mean in mV	
-300.00	-299.83	0.01	0.14	0.19	0.17	100.03
-200.00	-199.65	0.01	0.32	0.37	0.35	100.06
-100.00	-99.75	0.01	0.23	0.28	0.25	100.04
-50.00	-49.88	0.01	0.10	0.15	0.13	100.02
-25.00	-24.88	0.01	0.11	0.14	0.13	100.02
-10.00	-9.9	0.01	0.09	0.11	0.10	100.02
-2.00	-1.91	0.01	0.08	0.11	0.09	100.02
-1.00	-0.92	0.01	0.07	0.10	0.08	100.01
-0.50	-0.47	0.01	0.01	0.05	0.03	100.01
-0.20	-0.18	0.01	0.00	0.04	0.02	100.00
-0.10	-0.07	0.01	0.02	0.05	0.03	100.01
-0.05	-0.02	0.01	0.01	0.04	0.03	100.00
-0.02	0.00	0.01	0.00	0.05	0.02	100.00
-0.01	0.01	0.01	0.00	0.04	0.02	100.00
0.00	0.03	0.01	0.02	0.05	0.03	100.01
0.01	0.04	0.01	0.02	0.05	0.03	100.01
0.02	0.05	0.01	0.01	0.04	0.03	100.00
0.05	0.08	0.01	0.01	0.05	0.03	100.00
0.10	0.13	0.01	0.01	0.05	0.03	100.00
0.20	0.23	0.01	0.01	0.05	0.03	100.01
0.50	0.52	0.01	-0.01	0.04	0.02	100.00
1.00	1.08	0.01	0.06	0.09	0.08	100.01
2.00	2.07	0.01	0.05	0.08	0.07	100.01
10.00	10.04	0.01	0.02	0.06	0.04	100.01
25.00	25.00	0.01	-0.02	0.02	-0.00	100.00
50.00	49.97	0.01	-0.05	-0.01	-0.03	99.99
100.00	99.81	0.01	-0.22	-0.17	-0.19	99.97
200.00	199.55	0.01	-0.52	-0.42	-0.45	99.93
300.00	299.57	0.01	-0.47	-0.40	-0.43	99.93

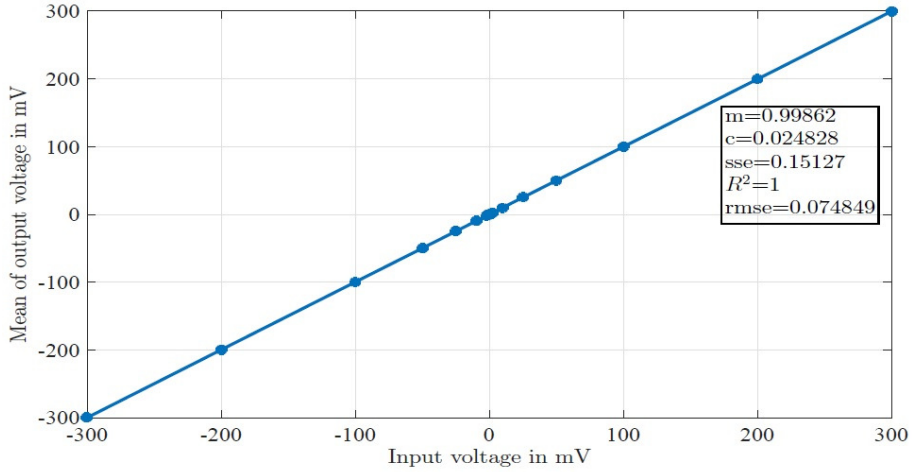

Figure 3.16: Plot of mean of measured voltages at different input voltages in the range $\pm 300mV$ for RISH Multi 18S [5]

Calibration results of the DAS were compared with those of the RISH Multi 18S multimeter as stated in Bhattacharya [5] in order to validate its performance in comparison with an existing measurement system for the DDP signals. In order to do so, mean and SD of MV, min, max and mean of SE and mean % RA for the output voltages measured using the RISH multimeter for standard input voltages have been reproduced in Table 3.13 from [5]. Figure 3.16 shows the plot of mean of measured voltages at different input voltages in the range $\pm 300mV$ for RISH Multi 18S, also from [5]. It is to be noted that the RISH multimeter was calibrated within $\pm 300mV$ since its resolution ($10\mu V$) changes beyond this range.

Comparing Table 3.13 with Table 3.7, it can be said that SE of DAS is little higher than RISH multimeter, though the span of SE are similar. The % RA for both RISH multimeter and DAS are almost similar for higher TV but for lower TVs, % RA is much better in the RISH multimeter than the DAS. Comparing Figure 3.16 with Figure 3.9, it is observed that both RISH multimeter and DAS show linear input-output relationship with similar goodness of fit. However, the RMSE of DAS is higher than that of RISH Multimeter. It has to be mentioned that no filter was used in DAS, whereas filters were used in RISH multimeter. Despite this, both the instruments have same SD, which signifies that precision of both these instruments are very close to each other.

The major advantage of this DAS is that it can acquire signals from 4 channels simultaneously and precisely and for very low input voltages, which is not possible using the RISH multimeter. This, along with the comparable

% RA, linearity and SD outweigh the slightly worse performances of the DAS in terms of the other parameters.

3.7 Discussions

This chapter deals with the tuning and calibration of the 4-channel DAS that was developed earlier in the research laboratory for the specific purpose of acquiring DDP signals.

The basic calibration of the device showed that RA is relatively high (100±5%), but precision and other static parameters are within acceptable limit. Therefore, the DAS has to be tuned to improve the accuracy without hampering other static parameters. It is also necessary to make the channel characteristics identical to each other. So, 3 tuning methods were tested and finally an error correction procedure has been proposed which can be implemented at the software level.

The subsequent calibration of a particular error corrected DAS established the improved and balanced performance of all channels of the DAS. Further analysis of its common mode interference voltage (CMIV) shows that these values are very low. Finally, a comparison of the results of the static calibration of the existing RISH Multi 18S system, as stated in [5], and the 4-channel DAS establish this system as a viable alternative for acquiring DDP signals.

CHAPTER 4

Experiments for acquiring DDP signals

In order to address the multiple objectives of this thesis, a total of 4 different experiments have been designed and conducted to acquire DDP signals for the subsequent validation, characterization and application studies. The details of these experiments, the protocol for data acquisition using RISH Multi 18S and/or DAS and the conditions maintained during these experiments are detailed in this chapter. DDP signals were accordingly collected from volunteers during various times as per the respective experiment protocols.

The data sets collected from these experiments are labelled henceforth as DS1, DS2, DS3 and DS4, while the terms LH, RH, LL and RL denote left hand, right hand, left leg and right leg respectively.

4.1 General conditions

The general conditions maintained for all the experiments are stated in this section. This contains the ethical committee clearance obtained for the study, the criteria used for subject selection and the materials and methods used for the signal acquisition and the experiments.

4.1.1 Ethical committee clearance

All the experiments performed in this study involve human subjects. The study, bearing approval number JU/IEC/2020/2312/01, was approved by the Institute Ethical Committee (IEC) of Jadavpur University, Kolkata, West Bengal, India.

In accordance with 1964 Helsinki Declaration and its later amendments or comparable ethical standards, all the participants were informed about the study briefly and consent forms were signed by each of the participants before participating in the study. A common overall questionnaire was filled up by each of the participants to record their general health condition. The

subjects also filled a daily questionnaire for recording their self assessment of their daily health. These consent form and the two sets of questionnaires are affixed as Annexures A, B and C respectively.

4.1.2 Subject selection criteria

Population: A total of 32 dextral subjects participated in this study. All the subjects were volunteers, either students, scholars or teaching and non-teaching staff members and associated with the Salt Lake campus of Jadavpur University.

Inclusion criterion: Subjects who are apparently healthy and gave their consent for participation.

Exclusion criterion All who did not give consent, cognitively impaired subjects, seriously ill patients, institutionalized persons, pregnant women, any person who consumes or has consumed anticholinergic drugs and/or any intoxicants (except cigarette/biri, jarda paan, tea and coffee) are excluded from the study.

Study characteristics The general characteristics of the selected subjects are:

Age : 24 to 58 years

Sex : both male and female

Weight : 55 to 105 kg

Height : 148 to 185 cm

Residence : Eastern India, both urban and rural localities in India

Education : Under graduate, post graduate, pursing Ph.D. or awarded.

Family : both nuclear and joint

Occupation : students, scholars, teachers or non-teaching staff members of a Department in the Jadavpur University Salt Lake campus

Addiction : Smoking cigarette/biri, jarda paan, tea and coffee. But consumption of alcohol and other intoxicating substances 72 hours prior to the participation was strongly discouraged.

Medical comorbidities allowed: Hypertension, diabetes mellitus, high cholesterol and/or thyroid problems

4.1.3 Materials and methods

Materials

Both the RISH Multi 18S with the RISH Multi SI232 assembly and the 4-channel DAS have been used for data acquisition. 8mm round Ag-AgCl velcro mounted snap type electrodes were used for connection along with single core coaxial cables as connectors and aqueous ultrasonic gel as the electrode-skin interface medium. Data were displayed and stored in a PC or a laptop.

Both the instrumentation systems contain 4 channels labelled as Ch0, Ch1, Ch2 and Ch3. These channels are used for collecting the signals from LH, RH, LL and RL locations respectively.

The BP and PR were measured in all the experiments. In case of the DS3 experiment, the oxygen saturation level (SpO2) was also recorded. The SpO2 and the systolic and diastolic BP were measured using a pulse oximeter (Make: CONTAC, Model: CMS50D) and a sphygmomanometer (Make: Rossmax , Model: GB101) respectively while the PR was measured manually using a stop watch.

Methods

Type of study Two types of studies were undertaken.

Observational analytical study: Analysis was done on the data collected from a number of subjects using suitable non-invasive, passive electrodes as mentioned earlier. Both cohort studies and case controlled studies are performed on these data.

Longitudinal study: For almost all the studies, data were collected from individual subjects repeatedly on same or different dates in different sessions.

Study Location: The study has been conducted in the Research Laboratory in the Instrumentation and Electronics Engineering Department, Jadavpur University, Salt Lake Campus, Kolkata, India. There is closed cubicle in the lab containing a bed aligned geographically North-South direction and a chair is placed just beside the bed for conducting all the experiments.

Environment: The light and sound levels of this closed cubicle were kept controlled. The temperature and relative humidity were also maintained constant at 25^oC and 50%RH respectively.

Subject sampling: Probability sampling method has been used for the subject sampling in this study. Based on the criterion, subjects are chosen randomly so that all the chosen subjects have equal opportunity.

Study tools: A structured protocol has been been sketched for each experiment on the basis of protocols for similar studies. On the basis of the preliminary trials, the protocol has been modified and finalized for the experiment. It includes consent, interviews/questionnaire, check-list and observational noting.

Study technique: Subjects were in supine posture on bed or sitting on a chair or the same bed or standing for the data acquisition, depending on the requirements of the experiment.

Sample size: A total number of 32 subjects participated in the 4 experiments. Each of the experiments were conducted for a period of 2 months or more. As a result, the total sample size for each experiment is suitably large, although it varies with respect to the experiment.

Methodology used: The methodology for data acquisition for each of the 4 experiments have been detailed in the subsequent Section.

4.2 Data acquisition

Each of the experiments contain some common protocol at the start where consent was given by the participants, different questionnaires were answered. These common protocols are explained first. The details of all 4 experiments, DS1 to DS4, are stated thereafter.

4.2.1 Preliminary steps

Before connecting the electrodes on the hands and/or feet of the subjects, a common protocol has been followed in all experiments as shown in Figure 4.1. The steps are elaborated hereafter.

Step 1: When a subject comes to participate in an experiment, it is checked whether the person is going to participate for the first time or not?

Step 2: If yes, the objectives and procedure of the study is briefed to them and they are asked to give their consent. The consent form has been

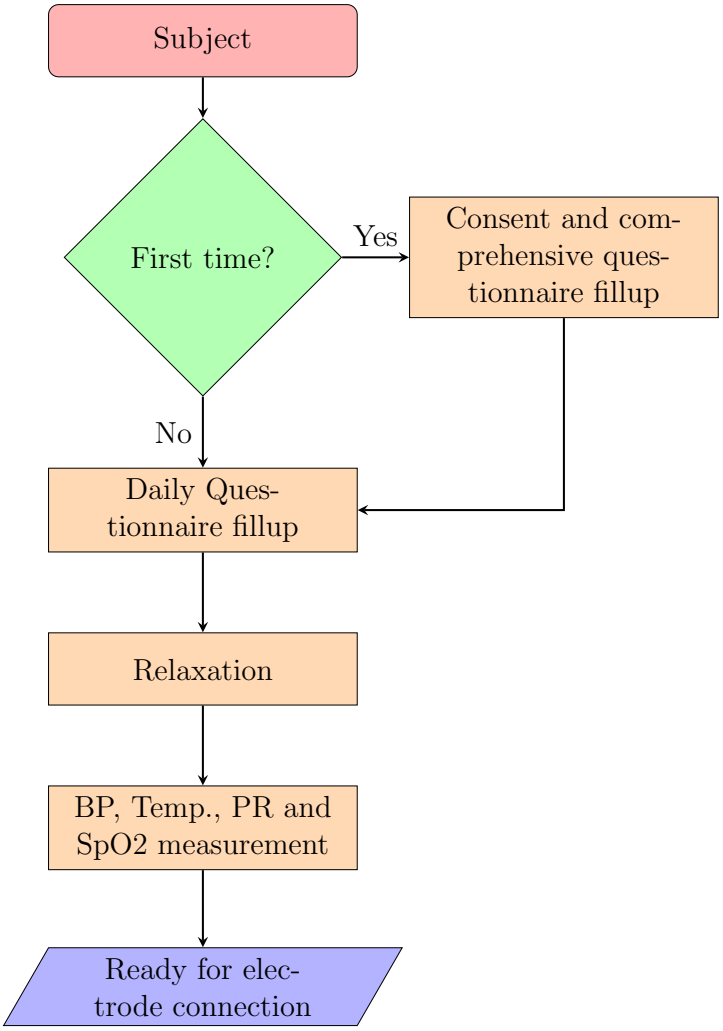

Figure 4.1: Common protocol followed prior to connecting the electrodes

shown in Appendix A.1. Once they give their consent, the comprehensive questionnaire given in Appendix A.1 for the overall health assessments and any medical record was filled up by the subject. If no, then we proceed to the next step.

Step 3: A set of daily questionnaires, as shown in Appendix A.3, Appendix A.4 and Appendix A.5, is provided to the subject regarding his physical and mental status on that day for filling up prior to the start of the experiment.

Step 4: Then the subject is asked to lie down on the experimental bed in supine posture and is allowed to relax typically for 10 minutes.

Step 5: After relaxation, the BP, temperature, PR and/or SpO2 of the subject are measured and recorded.

Step 6: Thereafter, the subjects are ready for connecting electrodes.

4.2.2 DS1: 20 minutes sitting to supine LH

In the DS1 experiment, DDP signals were acquired only from the left hand (LH) of individual subjects for 20 minutes in a predefined sequence as stated hereafter. The dataset was acquired for 2 minutes in sitting posture. The data recording continued in the next 2 minutes while subjects changed their posture from sitting to supine. In the subsequent 16 minutes, the acquisition continued while the subjects remained in supine posture.

As per standard recommendations, endosomatic signals should be acquired in referenced mode with one electrode placed at the active site and one on the inactive site [46]. In DS1, two such standard signals have been acquired simultaneously with the LH signal for comparison studies.

A total of 60 datasets of 20 minutes duration was acquired from 26 subjects within a period of 2 months.

Placement of electrodes

The DDP was acquired between the intermediate phalanges of the middle and the index fingers of the left hand, as shown in Figure 4.2(a). As mentioned, the golden reference in this study are standard recommended endosomatic EDA signals [46]. Two such signals were acquired simultaneously in this experiment, one each from the middle and the index fingers and sharing a common reference electrode that is affixed to the forearm. These reference signals are henceforth denoted as ML_{Ref} and IL_{Ref} respectively. Accordingly, 3 multimeter-adapter assemblies/ 3 channels of DAS named as CH1,

CH2 and CH3 have been used simultaneously to acquire the LH, ML_{Ref} and IL_{Ref} signals respectively. An image of the hand of a subject with the electrodes connected is shown in Figure 4.2(b).

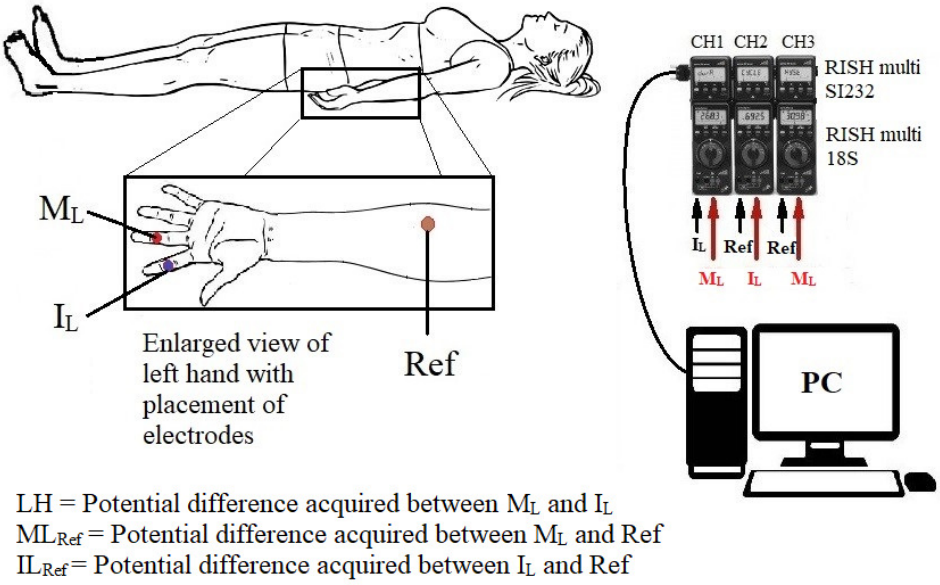

(a)

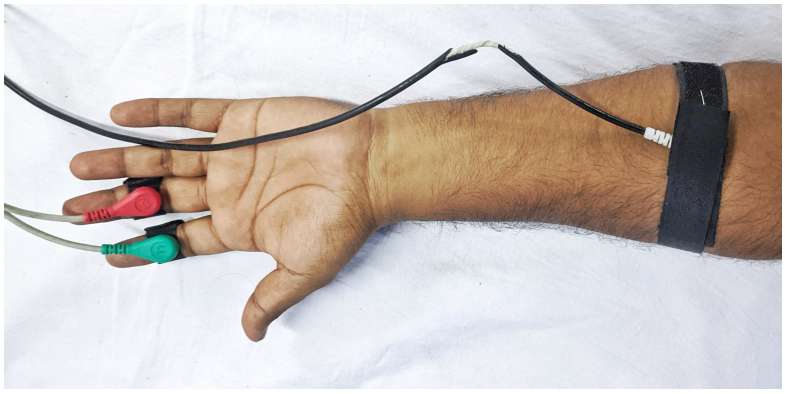

(b)

Figure 4.2: (a)Schematic diagram of experimental setup with details of electrodes and (b) Actual picture of hand with electrodes connected.

Data acquisition protocol

Figure 4.3 represents the flowchart for the data acquisition protocol for DS1. The overall algorithm has been elaborated hereafter.

Step 1: After completing all the steps shown in Figure 4.1, electrodes are connected to respective earmarked sites on the fingers and forearm of the left hand of the subject.

Step 2: The data recording of all three signals is begun simultaneously with the subject in a relaxed sitting posture for 2 minutes.

Step 3: After that, the subject is asked to lie down in the supine posture from the erstwhile sitting posture while the data acquisition continues. A duration of 2 minutes is allocated for this change of posture by the subject.

Step 4: Thereafter, the signal acquisition continues for another 16 minutes with the subject in the supine posture.

Step 5: Then the electrodes are disconnected and again BP, pulse rate and oxygen saturation level are recorded. Finally, the subject is asked to resume his/her normal work.

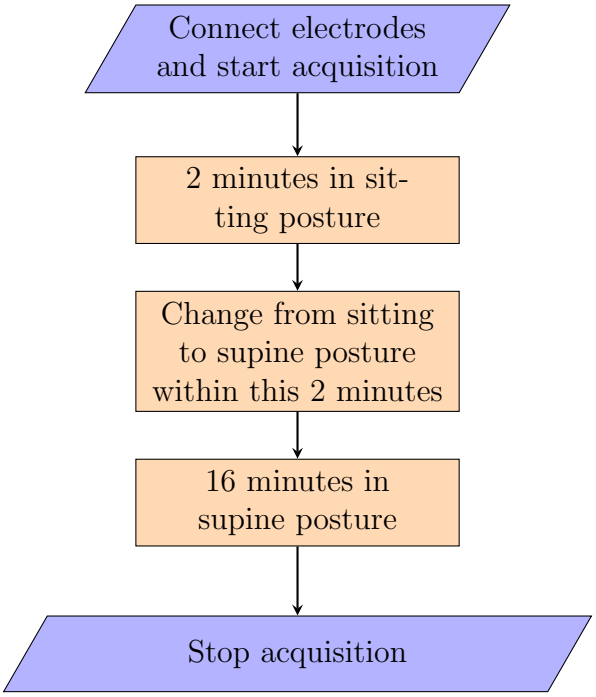

Figure 4.3: Data acquisition protocol for DS1 experiment.

4.2.3 DS2: 10 minutes supine LH and RH

In the DS2 experiment, DDP signals are acquired from both LH and RH of individual subjects for 10 continuous minutes while they relax in the sitting posture without any body movement.

A total number of 98 sessions of data were acquired from 16 subjects within 4 months duration for this experiment.

Placement of electrodes

Figure 4.4(a) shows the experimental setup with the subject in supine posture and the electrodes connected. The electrode connections on LH and RH are shown in Figure 4.4(b).

(a) (b)

Figure 4.4: (a) Subject in supine posture with electrode connections, (b) Connection of electrodes on the intermediate phalanges of both hands.

Data acquisition protocol

In this case also, all the prerequisite steps before connecting the electrodes are as given in Figure 4.1. Protocol for data acquisition in this dataset is shown in Figure 4.5. After the electrodes are connected, the acquisition is started and this continues for 10 minutes. After the acquisition is stopped, the BP and PR of the subject are recorded for normalcy checking. Then the subjects are asked to resume their regular work.

4.2.4 DS3: Long sequence of postures LH and RH

In the DS3 experiment also, the DDP signals are recorded from the LH and RH of subjects. However, the experimental protocol for this experiment involves a number of steps as detailed hereafter.

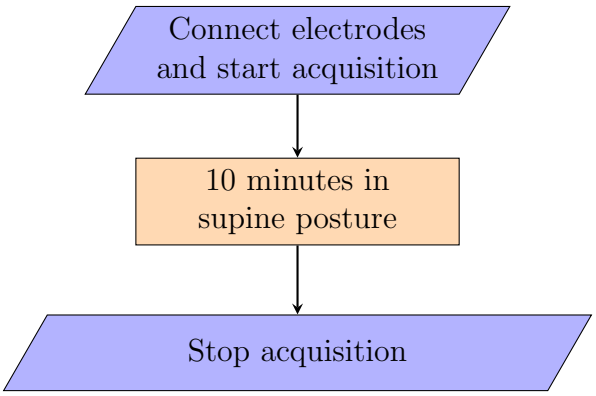

Figure 4.5: Protocol for data acquisition in DS2 experiment

The experimental set up (Figure 4.4(a)) and the electrode connections (Figure 4.4(b)) in DS3 are the same as in DS2. However, 2 pulse oximeters are used to record the SpO2 and PR throughout the experiment. In this experiment, BP and PR are additionally recorded after each 2 minutes of DDP signal (and SpO2) acquisition.

3 subjects participated in this experiment over a period of 3 months and a total of 66 datasets were recorded.

Data acquisition protocol

The data acquisition protocol followed for DS2 involves a number of steps as given in Figure 4.6. These steps for the data acquisition are also explained hereafter.

Step 1: Electrodes are connected to the intermediate phalanges of index and middle fingers of the left and the right hands of the supine subject using aqueous USG gel. 2 pre-configured pulse-oximeters are also connected to the thumbs of both hands. DDP signal acquisition and SpO2 recording are started simultaneously.

Acquisition in this supine posture is continued for 2 minutes.

Step 2: After completion of 2 minutes, the pulse oximeters are removed and BP and PR are recorded from both hands.

Step 3 After that, recording is resumed again for 2 minutes from both hands with the pulse oximeters connected to both the thumbs.

Step 4: Step 2 is repeated again after completion of this 2 minutes recording.

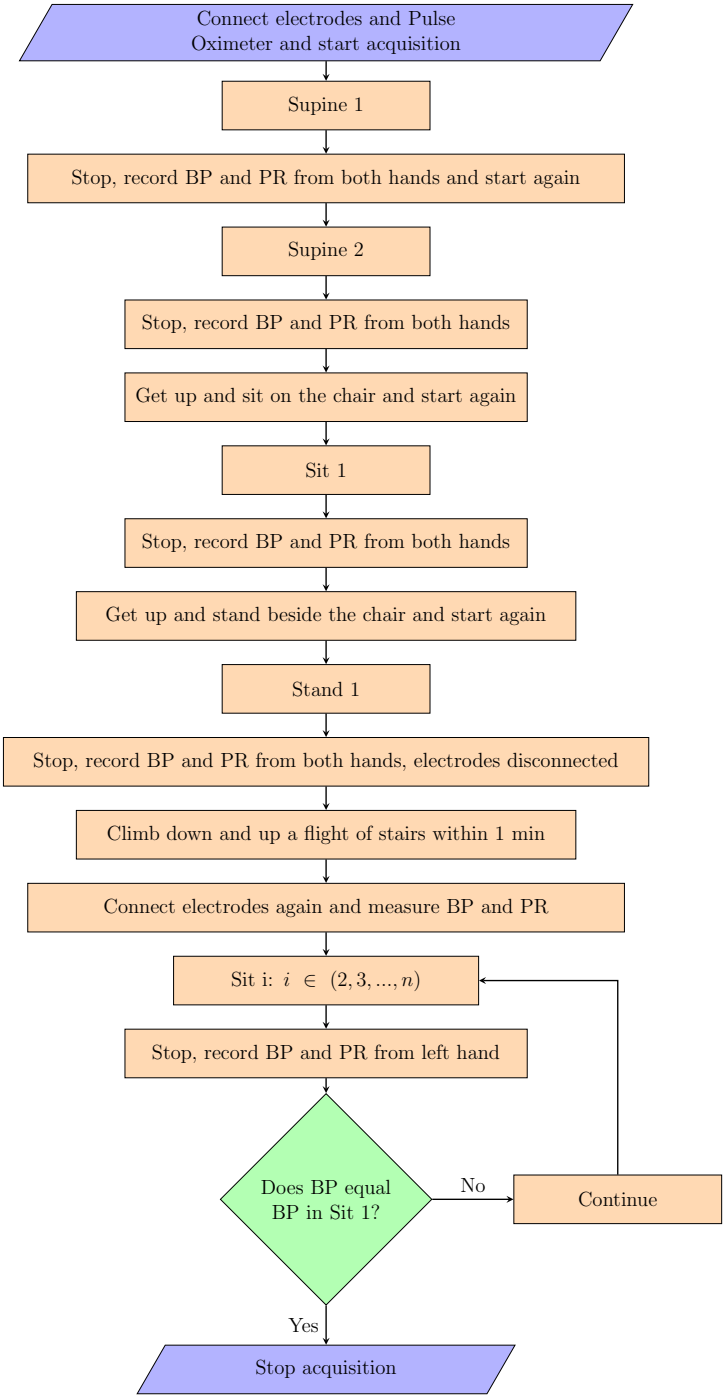

Figure 4.6: Protocol for data acquisition in DS3

Step 5: Then the subject is asked to get up from the supine position on bed and move to a sitting posture on the chair beside the bed and relax without any body movement.

After sitting on the chair, the DDP signal and SpO2 recordings are started again as in Step 3.

Step 6: Step 2 is repeated again after completion of this 2 minutes recording.

Step 7: Subject is now asked to get up and stand beside the chair. With the subject in this standing posture, the DDP signal and SpO2 recordings are started again as in Step 3.

Step 8: Step 2 is repeated again after completion of 2 minutes recording. Then the electrodes are disconnected.

Step 9: Then the subjects are asked to go out, climb down a fixed flight of stairs to the lower floor, climb back up the same way and return to the cubicle, all within 1 minute.

Step 10: After that, the subject is asked to sit in the chair while the electrodes and pulse oximeters are reconnected. Then the recording is restarted with the subject in sitting posture.

Step 11: After 2 minutes, BP is measured from the left hand only and compared with that recorded in Step 6.

If these are similar, then the acquisition is stopped.

Else the data recording in sitting posture is resumed again for 2 minutes followed by the BP check for the left hand until the condition is met.

Step 12: After the acquisition is finally stopped, the electrodes are disconnected, all the records are saved and subjects are asked to resume their regular work.

From the aforementioned sequence, it is evident that the dataset recorded in this experiment can be categorized into different states as tabulated in Table 4.1. The various measurements recorded for each state and the experimental conditions are also mentioned in the Table.

4.2.5 DS4: 10 minutes supine continuous 4 locations

In the DS4 experiment, DDP signals are recorded continuously for 10 minutes from all 4 locations, namely LH, RH, LL and RL, of a subject in supine posture.

Table 4.1: Different states of the DS3 data with their details

State no.	Posture	Name	Condition
1	Supine	Sup 1	Left and Right BP, then DDP+PR+SpO2.
2		Sup 2	DDP+PR+SpO2, then Left and Right BP.
3	Sitting	Sit 1	Left BP and PR, then DDP+PR+SpO2.
4	Standing	Stand 1	Left BP and PR, then DDP+PR+SpO2.
5	Climb down and up a flight of stairs in 1 min		
6	Sitting	Sit i, i∈(2,3,...,n)	DDP+PR+SpO2, then Left BP and PR. Repeat for every 2 minutes until BP matches that in state 3 (Sit 1).

A total of 66 datasets of 10 minutes duration were acquired from 12 subjects in a duration of 2 months.

Placement of electrodes

The experimental setup is similar to that in DS2 except that the signals are acquired in this case from all 4 locations as shown in Figure 4.7. Here "+" and "-" represent the earmarked positive and negative terminals of the corresponding channel in the DAS.

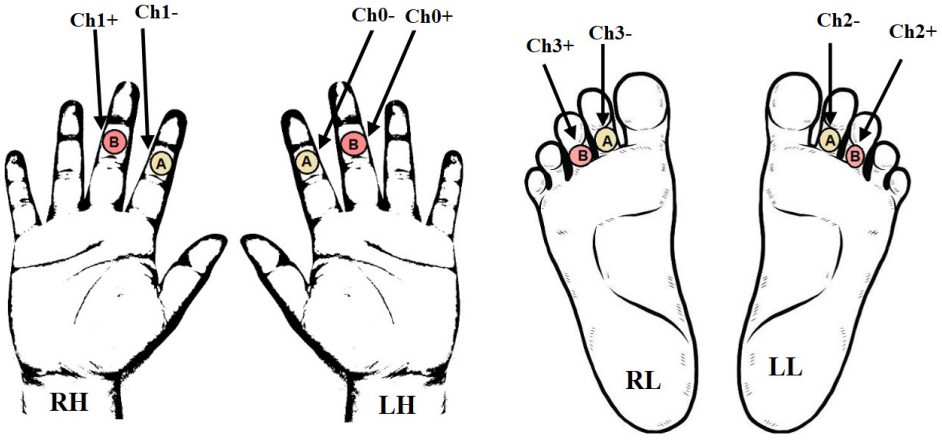

Figure 4.7: Electrode connections and placements in DS4

Data acquisition protocol

The data acquisition protocol for DS4 is essentially the same as that in DS2 (Section 4.2.2) except for the electrode connections, 4 in case of DS4 and 2 in case of DS2.

4.2.6 Measures for reliable signal acquisition

The human body is a complex system and the stochasticity in its biological communication processes plays a significant role in its overall development and evolution [121]. In order to record this essential stochasticity of the dermal potential reliably, all types of filters or filtering techniques have been avoided apart from the power line interference compensator.

Additionally, the following measures were taken to ensure that the recorded DDP signal is due to the physiological changes only.

1. It was ensured that the subject had not consumed any anticholinergic drug within 72 hours prior to the data acquisition.

2. The signal is acquired in DC mode only and so it responds mainly to the resistive components. Furthermore, the signal is acquired in differential mode with the electrodes being placed on similar surfaces of two adjacent fingers. So, it is relatively immune to sweat gland activity since the effects of similar resistances on the adjacent electrodes cancel out.

3. The input impedance of this acquisition system ($> 10G\Omega$) is much higher than the recommended input impedance of $10M\Omega$ for skin potential measurements [3].

4. Recommended bias voltage tests have been performed on the electrodes prior to every acquisition experiment.

5. Signal continuity is maintained by keeping the electrodes connected from start to end of the experiment as far as feasible.

6. The potentials are acquired in differential mode across two active, adjacent sites since this eliminates common mode noise (SNR $> 100dB$).

7. Systematic static and dynamic calibrations of the setup ensured the recordings to be noise free.

4.3 Experiment overview and related applications

This chapter contains details of all the 4 different experiments designed and conducted in this work. All 4 experiments follow a common preliminary protocol, followed by different data acquisition sequences.

The 4 different datasets are named here as DS1, DS2, DS3 and DS4. These are used for 6 applications in total.

An overview of the 4 experiments is given hereafter.:

DS1: DDP signals are acquired from only LH for 20 minutes which include 2 minutes in sitting posture, then 2 minutes during change in posture from sitting to supine and last 16 minutes in supine posture

DS2: DDP signals are acquired from LH and RH of supine subjects for 10 minutes

DS3: DDP signals are acquired from LH, RH of subjects for a specific set sequence: supine for 4 minutes, then sitting and then standing for 2 minutes each. This is followed by a no recording 1 minute activity session. Then subject sits again and DDP signals are acquired till a specified condition is met.

DS4: DDP signals acquired continuously from LH, RH, LL and RL of supine subjects for 10 minutes

All 4 datasets were used for 6 different applications. All these applications are enumerated hereafter with the associated datasets mentioned alongside.

Application1: Validation of the DDP signal by comparing it with standard recommended endosomatic EDA signals (golden reference) using DS1 dataset

Application2: Study unilateral characteristics of DDP signals using DS2, DS3 and DS4 datasets

Application3: Study bilateral characteristics of DDP signals using DS4 dataset

Application4: Classification of hypertensive and normotensive subjects using LH and RH of DS2

Application5: Classification of different postures using LH of DS1 and both LH and RH data of DS3

Application6: Determination of the effective duration of rest in supine posture from LH of DS1, both hands data (LH and RH) of DS2 and all 4 channel data (LH, RH, LL and RL) of DS4 datasets and in sitting posture from both hands data (LH and RH) of DS3 dataset

CHAPTER 5

Validation and characterization of DDP signals

The 4 experiments conducted for DDP data acquisition have been discussed in the previous Chapter. This chapter contains the first three (3) of the total 6 applications of the datasets listed there. These applications of the DDP signals include their

Application1: Validation by comparison with standard recommended endosomatic EDA signals using DS1 dataset

Application2: Unilateral characterization using DS2, DS3 and DS4 datasets

Application3: Bilateral characterization using DS4 dataset

At the outset, a physiological basis of the DDP signals is proposed based on their mode of measurement. This is followed by the validation of the signals in terms of their autocorrelation and by comparing them with their underlying standard endomatic EDA signals. Thereafter, their unilateral and bilateral characteristics have been studied. These include trends and polarities; various statistical, spectral and linear regression parameters; and lateralization coefficients. Some new bilateral characteristics have also been proposed in this Chapter.

5.1 Proposed physiological basis

As mentioned earlier, endosomatic EDA signals are acquired between an active and inactive site of two fingers of the left hand as per the standard recommendation [46]. However, the DDP signal is acquired between two active sites of the two fingers in differential mode. Hence, a physiological basis for the information content in these signals is proposed here.

A well accepted electrical equivalent circuit of the skin, as shown in Figure 5.1 (a), is given by Yamamoto et al. [6]. In this model, R_1 is the resistance of the epidermis that offers protection, while R_2 is the equivalent resistance of the dermis and hypodermis layer. R and C are the equivalent resistance and capacitance of the sweat glands, which primarily help in temperature regulation and water balance [3, 122]. The conventional scheme proposes that as the sweat glands get filled with sweat, the resistance of the glands decrease since sweat contains free ions. Along with that, the equivalent capacitances also change, causing the impedance (Z) of the sweat glands to change.

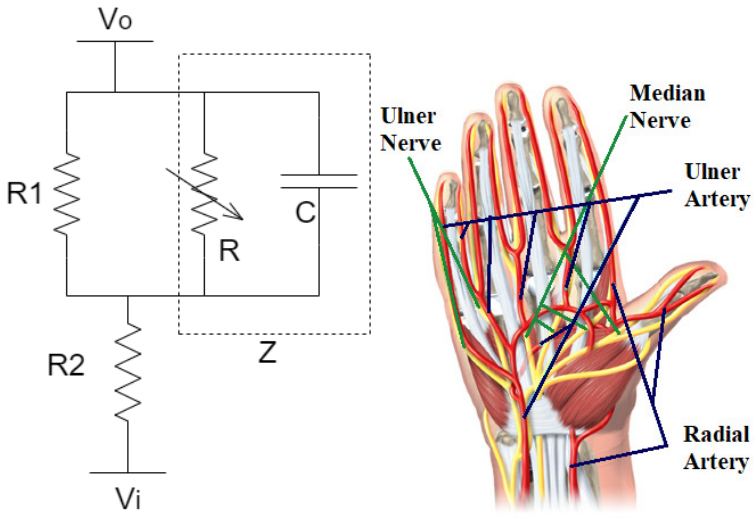

(a) (b)

Figure 5.1: (a) Electrical equivalent model of the skin proposed by Yamamoto et al. [6], (b) Anatomical view of palm with nerves and capillaries [7].

It is to be noted in this context that the DDP is always acquired in DC mode. Therefore, the capacitor acts as an open circuit and the equivalent circuit in Figure 5.1 (a) reduces to a resistive model. Furthermore, the differential potential is acquired across the intermediate phalanges of the index finger and the consecutive middle finger of the same hand (or feet). Hence R due to the sweat glands as well as R_1 due to the epidermis of both these *active, adjacent* sites may be considered almost identical as long as there is no scar or wound on the skin surface.

As mentioned, R_2 is the resistance of the dermis and hypodermis layers, which contain nerves as well as capillaries [3]. These contribute to the sensory function, immune function and communication of the skin surface and facilitate the heat and energy exchange at the epidermis as required by the autonomic nervous system (ANS) [123]. In fact, using optical techniques,

blood pressure and pulse rate can be measured directly at the wrist from the radial artery, which is also the largest artery in the hand [124].

As evident in Figure 5.1(b), the median nerve gives sensation to both the index and middle fingers along with the thumb and half of the ring finger on the palmar surface. As for the blood supply, a part of the index finger is supplied by the radial artery while the other part as well as the middle finger is supplied by the digital arteries of the ulnar artery [7]. It is thus hypothesized that the R_2 of these two fingers are not identical and differ primarily due to the difference in the flow in the capillaries and also due to differences in the information at the nerve endings at both fingers.

The differential potential acquired between these adjacent sites thus primarily responds to any change in the homeostasis of the subject or other physiological or psychophysiological process that affects the nervous system or blood flow in the capillaries. Small differences in sweat gland activity in both fingers may also affect the differential potential as non-identical R in both fingers. However, this effect is further reduced by the use of aqueous USG gel at the electrode-skin interface since this facilitates bio-potential acquisition while preventing additional conductivity due to ionic exchanges at the contact surfaces [46].

5.2 Validation of DDP signals

For the validation of the DDP signals, their auto-correlations were first studied and then they were compared with simultaneously acquired underlying endosomatic EDA signals.

5.2.1 Autocorrelation

3 sets of ACF have been studied: 1^{st} 2 minute window for sitting posture, 2^{nd} 2 minute window for change in posture and 3^{rd} to 10^{th} 2 minute windows for supine posture and the findings are stated below.

The ACF in all these cases are non-zero and broadly exhibit 2 distinct patterns, specifically

1. those with a single zero-crossing and a single minimum for the whole range

2. the others.

It is also found that the these ACF patterns cannot be ascribed in particular to any specific posture, age, gender or health conditions. Thus, it can

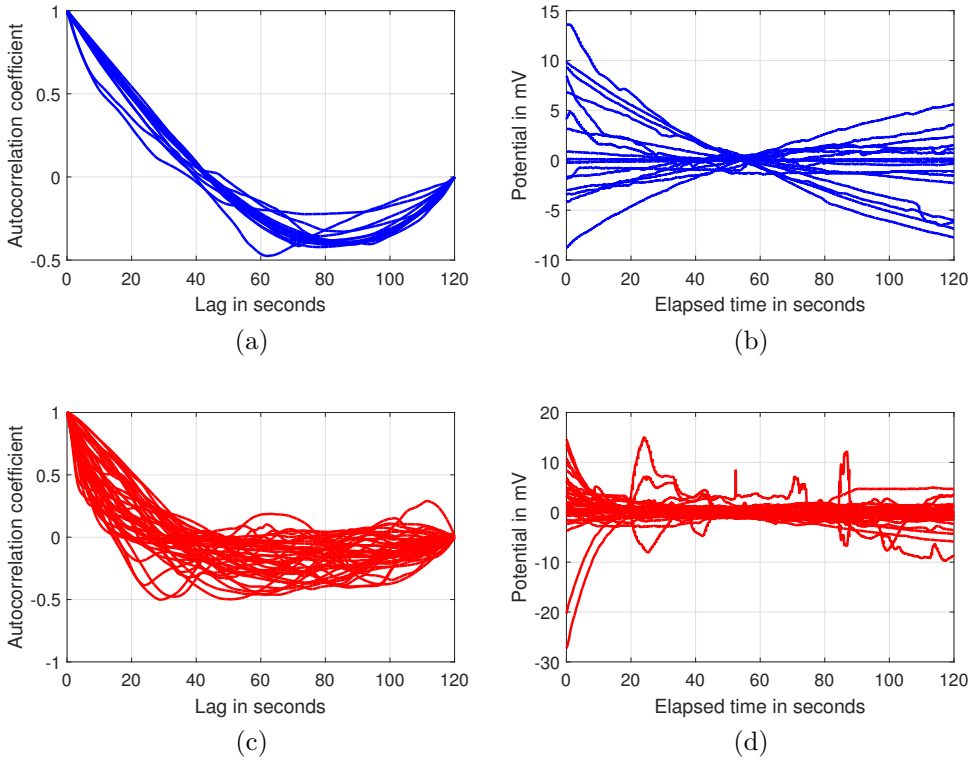

Figure 5.2: (a) Autocorrelation plot of all Type 1 signals and (b) Time-series plot of all Type 1 debiased signals. (c) Autocorrelation plot of all Type 2 signals and (d) Time-series plot of all Type 2 debiased signals.

be said that this non-random DDP owes its origin to systemic time-varying processes [125]. The underlying LH signals have accordingly been classified into 2 groups, named as Type 1 and Type 2 signals. The ACFs as well as the time-series plots of the mean subtracted signals, henceforth referred to as debiased signals, for both Type 1 and Type 2 signals in sitting posture are shown in Figure 5.2 and their characteristics are further described as follows.

The ACF of a Type 1 signal is smooth and similar to that for a linear signal, as shown in Figure 5.2(a). Specifically, the ACF starts from 1 and then decreases below 0 till a negative minima. Thereafter, it increases again and ends at 0. As expected, the underlying signals are quasi-linear in nature (Figure 5.2(b)).

The Type 2 signals show higher order dynamic characteristics from start till end (Figure 5.2(c)). In several cases, the ACF also crosses 0 correlation axis multiple times. As expected, the underlying debiased signals also display several higher order dynamics, as shown in Figure 5.2(d).

The proportion of signals showing these two types of ACF characteristics in all three postures are calculated. It is found that 33.76%, 33.33% and 33.99% signals showed Type 1 characteristics in sitting, change and supine postures respectively. Therefore, it can be said that irrespective of postures, Type 2 complex signals are almost 2 times more in count than the quasi-linear Type 1 signals.

5.2.2 Comparison with standard endosomatic EDA

As mentioned in the electrode placement details for experiment DS1 in Section 4.2.2, the DDP signal was acquired simultaneously with the two referenced signals, ML_{Ref} and IL_{Ref}. The DDP signals are validated against 3 types of standard signals, namely the respective ML_{Ref} and IL_{Ref} and their difference signal ($Diff_{MLIL}$). For this, the cross-correlations of the 3 types of standard signals with the DDP signals as well as the stability, settling times, statistical and spectral characteristics of all the 4 types of signals are studied and compared.

Cross-correlation

It is known that the referenced signals ML_{Ref} and IL_{Ref} are almost similar to each other, although a clear difference also exists between the two. A sample plot of 2 minutes data of all three simultaneously acquired signals in the sitting posture are shown in Figure 5.3. It is observed that in this case, both the referenced signals are positive and amplitudes are larger compared to that of the DDP signal.

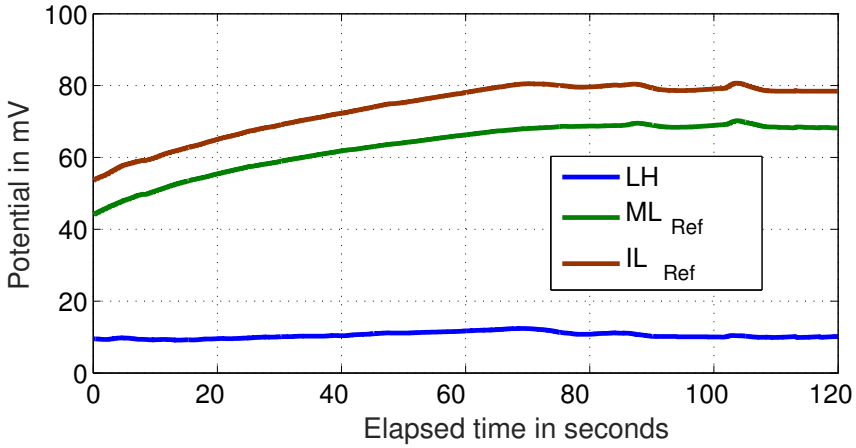

Figure 5.3: Sample 2 minute plot of LH, ML_{Ref} and IL_{Ref} signals during sitting posture

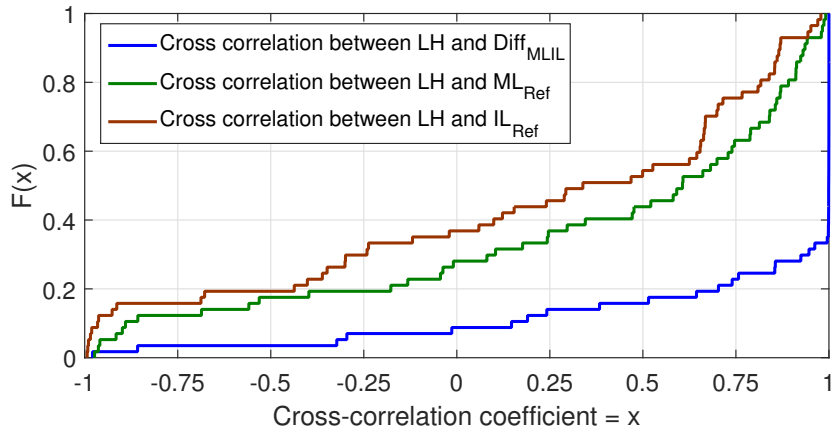

Figure 5.4: CDF plots of cross-correlation coefficients of (ML_{Ref} and LH), (IL_{Ref} and LH) and ($Diff_{MLIL}$ and LH) signals

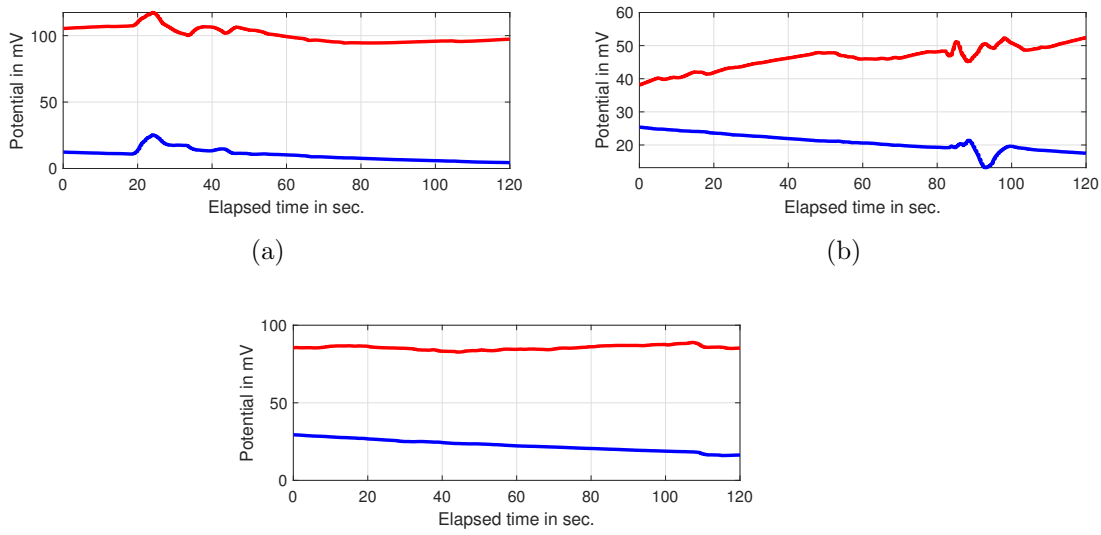

Figure 5.5: Sample plots of pairs of signals with cross-correlation coefficients within (a) +0.8 to +1.0, (b) -0.8 to -1.0 and (c) -0.8 to +0.8.

To examine whether there is any direct relation between any of these two referenced signals and the DDP signal in the short duration, the Pearson's correlation coefficient for 2 minutes data is calculated between the two pairs of signals, (ML_{Ref} and LH) and (IL_{Ref} and LH). Furthermore, since the differential signal is the potential difference between the middle and the index finger, it is expected that the DDP signal will be almost identical to the difference signal between ML_{Ref} and IL_{Ref}, denoted as $Diff_{MLIL}$. In order to verify this, Pearson's correlation coefficient is calculated between LH and $Diff_{MLIL}$ also. Cumulative distribution function (CDF) plots of all 3 correlation coefficients are plotted in Figure 5.4.

It can be seen that in case of (ML_{Ref} and LH) and (IL_{Ref} and LH), the correlation coefficients lie within -1 to -0.8 and 0.8 to 1 for more than 50% cases. For the remaining cases, the correlation coefficients are in the interim zone, within -0.8 to 0.8. These correlation characteristics are thus more weighted towards ± 1. It is also evident from the plot that ML_{Ref} is more likely to be negatively correlated with LH, while IL_{Ref} is more likely to be positively correlated.

Furthermore, on the basis of this cross-correlation coefficients, individual as well as pairwise characteristics are also studied. Sample plots of 3 types of pair of signals, having cross-correlation coefficients within +0.80 to +1.00,

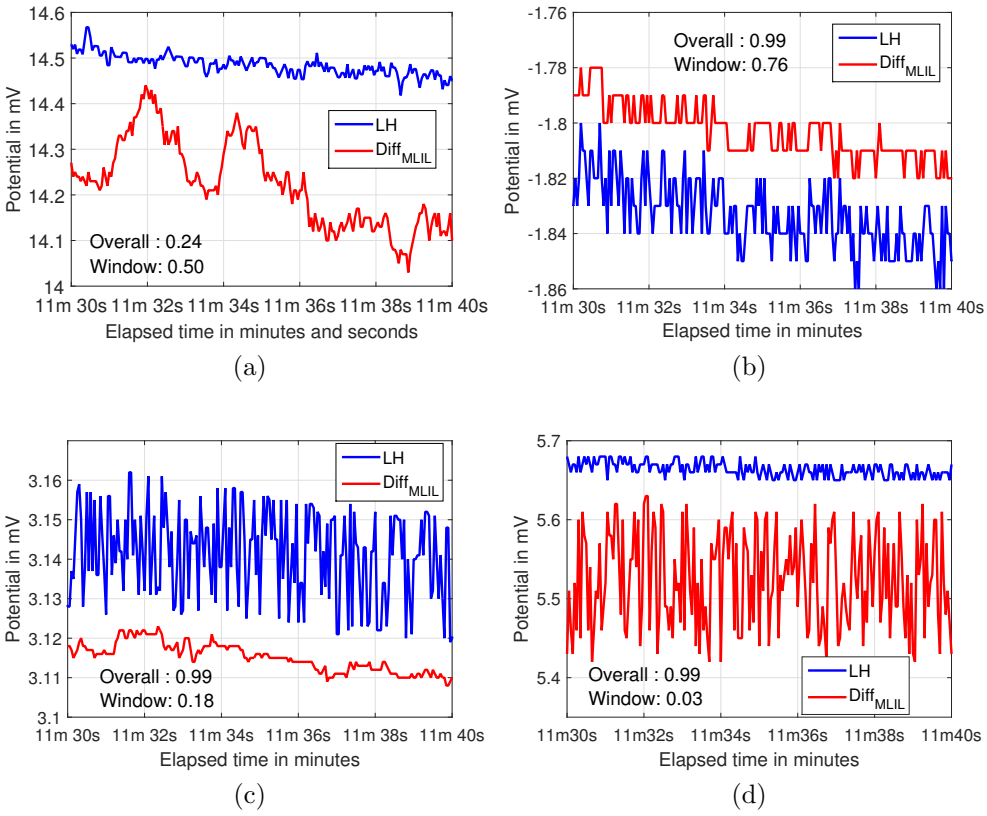

Figure 5.6: 4 sample time-series plots of $Diff_{MLIL}$ and LH signals zoomed in over a 10s window

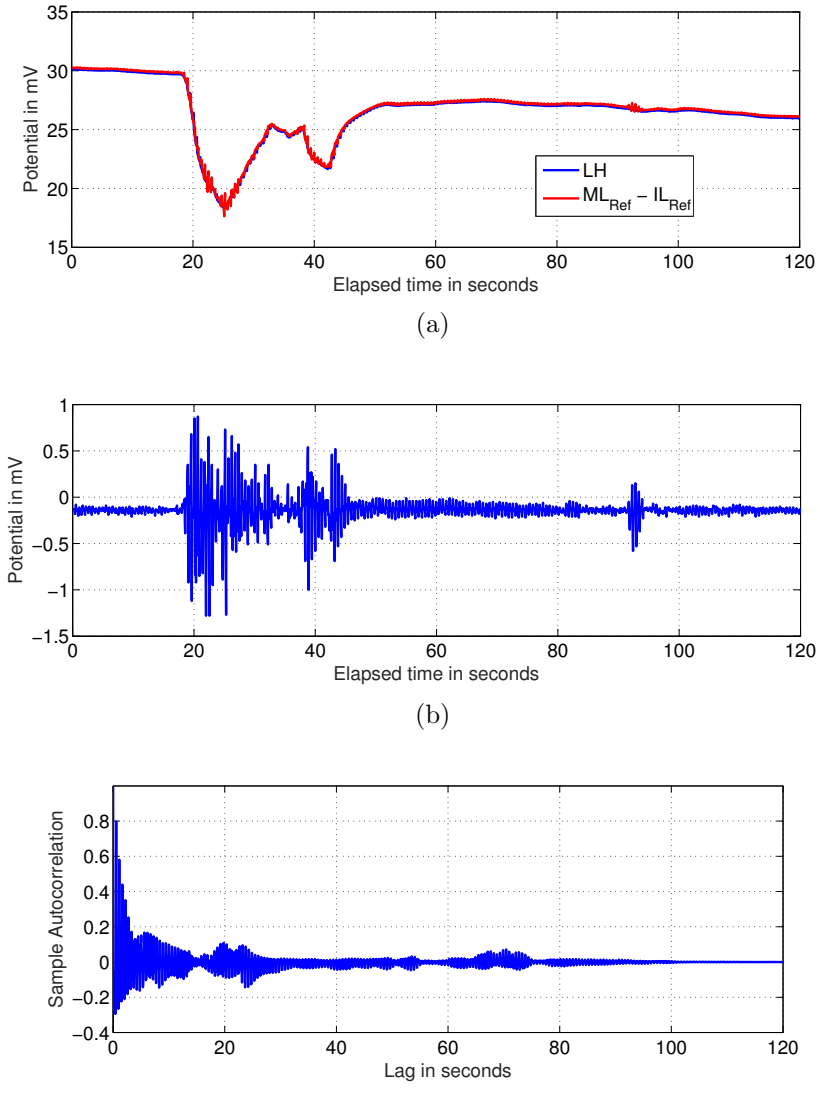

Figure 5.7: (a) Sample plot of $Diff_{MLIL}$ and LH, (b) Corresponding residual and (c) ACF of residual.

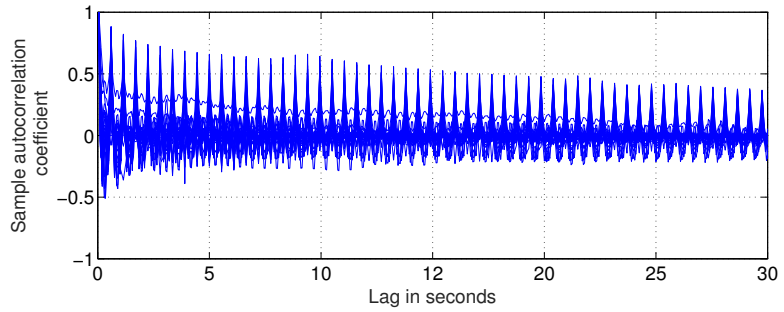

(a)

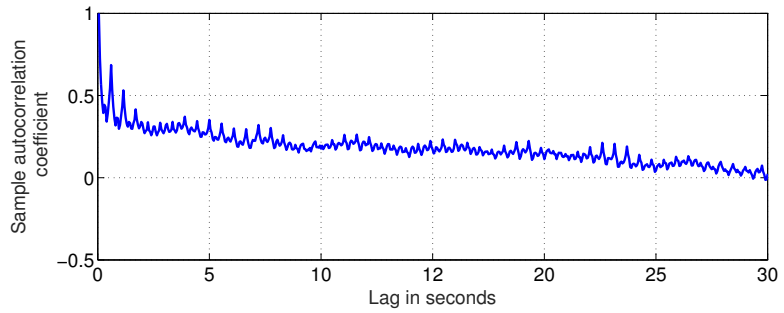

(b)

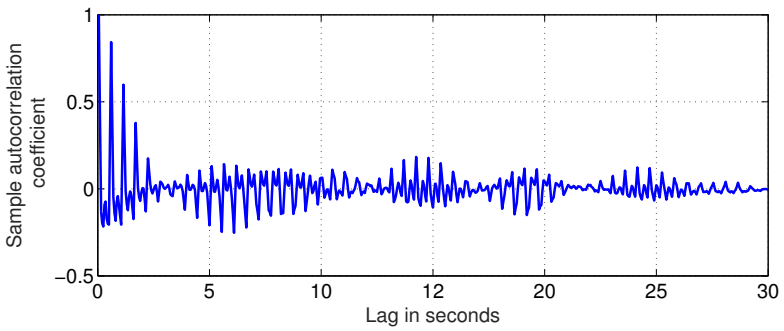

(c)

Figure 5.8: Sample autocorrelation plots of (a) all residuals, and 2 residuals zoomed within 400 samples lag (b) Example 1, (c) Example 2.

-0.80 to -1.00 and -0.80 to +0.80 respectively are shown in Figure 5.5. It can be said from the visual inspection that in case of strong positive correlation, the signal pairs are very similar to each other. In case of strongly negative correlated signals, as shown in Figure 5.5b, the signals are similar but with opposing trends, that is to say that while one of these two signals is increasing, the other one is decreasing in nature. Rest of the signals with cross-correlation coefficients within -0.80 to +0.80 are not similar in nature.

It is also observed that the cross-correlation coefficients of any LH and ML_{Ref} and its corresponding LH and simultaneously acquired IL_{Ref} may or may not be close to each other but the common factor is that the sign of these two coefficients are always same.

From Figure 5.4, it is further observed that the LH and corresponding $Diff_{MLIL}$ signals are strongly positively correlated. Their cross-correlation coefficient in more than 75% cases is more than 0.8, yet the signals are not identical. In order to verify this, 4 sample plots of these two signals have been shown in Figure 5.6 over a short duration of 10s window in the supine state. The elapsed time in all cases is chosen arbitrarily as 11 minutes 30 seconds, when the subject is expected to be in a deep restful condition. The cross-correlation coefficients of LH and $Diff_{MLIL}$ for the overall 20 minutes as well as for the 10 second window are stated in the figures.

It is observed that the overall cross-correlation value in Figure 5.6(a), is very low (0.24), while it is very high (> 0.99) in the other 3 cases. However, these values do not hold in the 10s windows. This finding establishes that although the overall LH signal is very similar to its corresponding $Diff_{MLIL}$ signal, yet it is not identical to it and this is evident from the signal characteristics in the sub-millivolt level.

This aspect is studied in more detail and accordingly, a sample plot of $Diff_{MLIL}$ and the corresponding LH is shown in Figure 5.7a. The residual of this set of signals (=LH- $Diff_{MLIL}$) is shown in Figure 5.7b, while the ACF plot of the residual is shown in Figure 5.7c. The significant dynamics in the ACF plot establish the non-trivial nature of the LH signal.

This observation holds for the ACF plots of all the residuals, as shown in Figure 5.8 (a) and is further evident from the zoomed ACF plots of 2 of the residuals shown in Figure 5.8 (b) and (c).

Thus, it is validated that the DDP signal carries unique information about the inherent system characteristics that is separate from the standard endosomatic signals or their difference signal.

Stability and settling times

In the next stage, the stability of all 4 types of signals and their settling times are compared. Figure 5.9 (a) and (b) show two sample time-series plots of the LH signal and the corresponding ML_{Ref} and IL_{Ref} signals acquired for 20 minutes. Figure 5.9 (c) and (d) show the respective $Diff_{MLIL}$ signal along with the LH signal. In the time-series plots, the red arrow indicates the data in sitting posture (0 to 2 minutes), green arrow indicates the data during transition from sitting to supine posture (2 to 4 minutes) and black arrow indicates the data in supine posture (4 to 20 minutes) for the complete daily set of data acquired in accordance with the DS1 experiment protocol.

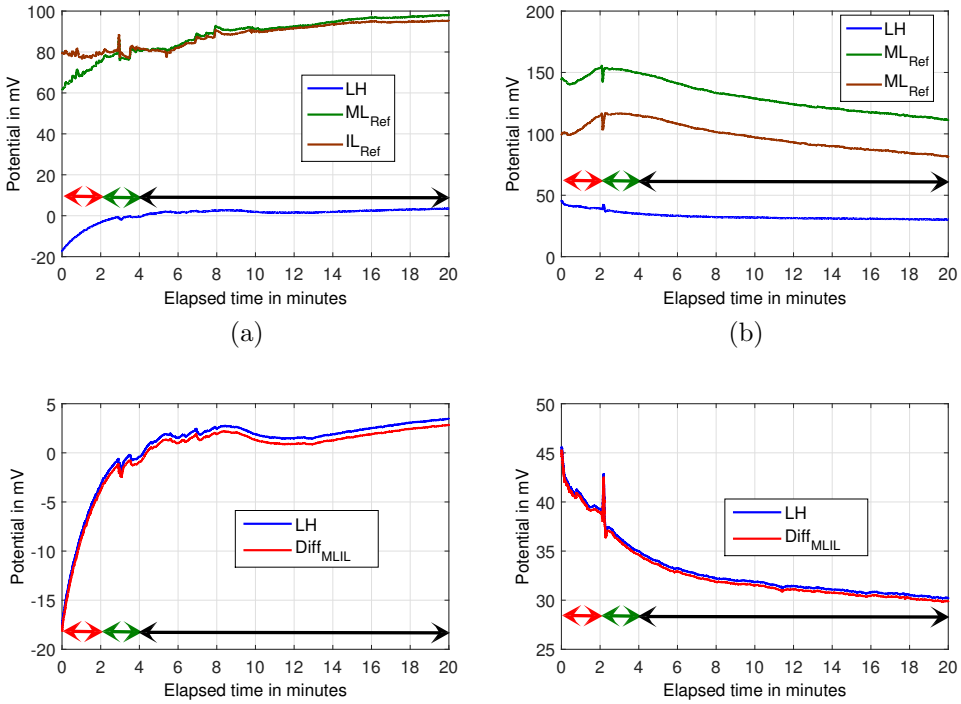

Figure 5.9: (a), (b) Two sample 20 minutes time-series plots of LH, ML_{Ref} and IL_{Ref} signals, (c), (d) Corresponding (Difference) $Diff_{MLIL}$ and (Differential) LH signals. Arrows in figures are indicative of following: red arrow - sitting posture, green arrow - transition from sitting to supine posture and black arrow - supine posture.

As expected, the signal amplitudes of the $Diff_{MLIL}$ and (Differential) LH signals are much smaller than those of the standard ML_{Ref} and IL_{Ref}

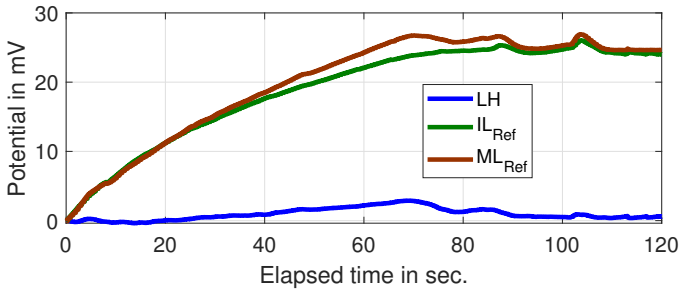

Figure 5.10: Plot of signals shown in Figure 5.3 with their first sample instant values subtracted.

signals. In order to observe the transient behaviours of these signals more clearly, the 2 minute signals shown in Figure 5.3 with their first sample instant values subtracted are plotted in Figure 5.10.

As reported [46], it is observed in these cases also that the transient effects are much more prominent and long lasting in both the referenced signals. This may be ascribed to the gel penetration in the sweat gland after the electrode connection to the skin.

In case of the differential LH signals, as also the difference ($Diff_{MLIL}$) signals, it is observed that this effect is not so prominent. This validates the expectations from the physiological basis (Section 5.1) that the transient effects due to the epidermis and sweat glands are minimized when the signal is acquired in the differential, or even the difference, mode.

Considering RS_i to be the running slope of i^{th} instant, x_i as the data point at i^{th} instant and hence x_1 as the data point at the 1^{st} instant, the running slopes of all the signals are calculated over the 20 minutes duration using the formula 5.1

$$RS_i = \frac{x_i - x_1}{i} \tag{5.1}$$

A sample plot of the running slopes (in mV/instant) of all three simultaneously acquired signals are plotted in Figure 5.11. It is seen from this plot that the running slope of the LH is very low compared to that of the ML_{Ref} and IL_{Ref} signals. The histogram of the running slopes of these signals for all the acquired datasets is shown in Figure 5.12. From this figure, it can be seen that the peakedness (or kurtosis) of the DDP signal is much higher and typically centred at 0mV/instant. Quantitatively it can be said that more than 90% of running slopes of LH signals lie within ±0.05 mV/instant, whereas less than 60% of running slopes of ML_{Ref} and IL_{Ref} signals lie within ±0.05 mV/instant.

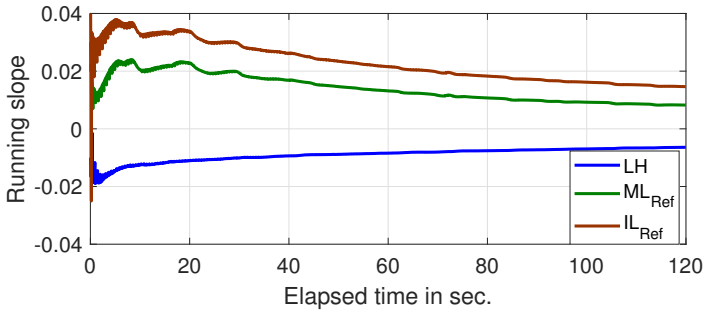

Figure 5.11: Sample plot of the running slopes (in mV/instant) of (a) LH and corresponding (b) ML_{Ref} and (c) IL_{Ref} signals

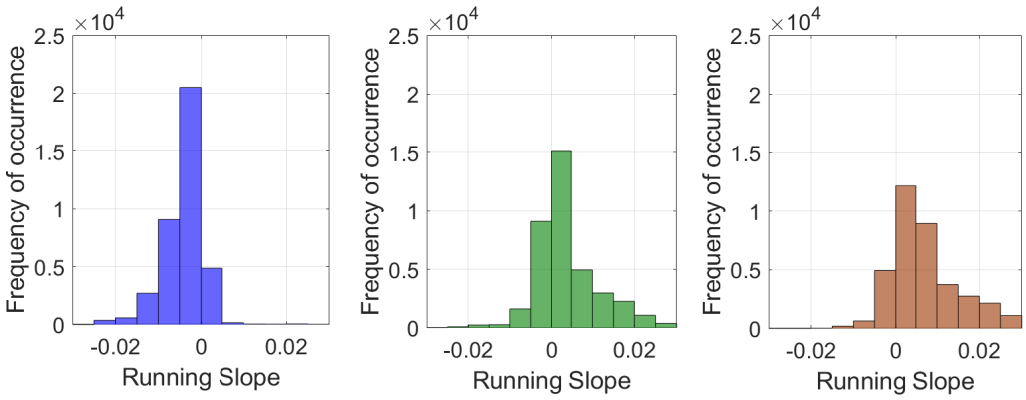

Figure 5.12: Histograms of the running slopes of (a) LH , (b) ML_{Ref} and (c) IL_{Ref} signals

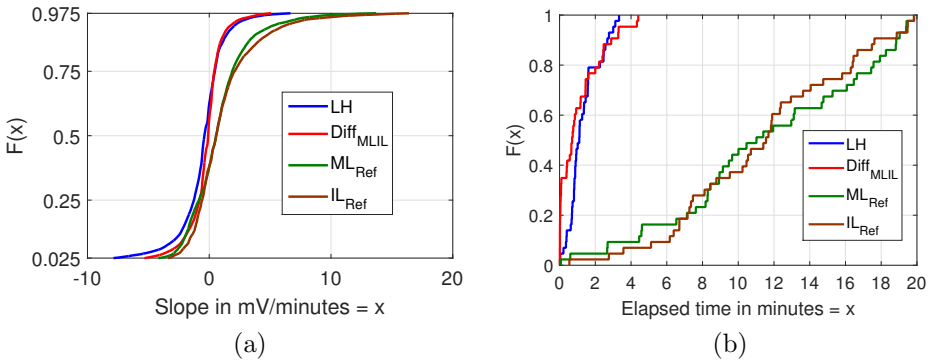

Figure 5.13: CDF plots of (a) running slopes for the overall span of 20 minutes, (b) settling time of all 4 signals.

Further to this, the CDF plots as well as the signal settling times for all the 4 types of signals are shown in Figure 5.13 (a) and (b) respectively for 2.5% to 97.5% of data. It can be seen from Figure 5.13(a) that 95% of the running slope of ML_{Ref}, IL_{Ref}, $Diff_{MLIL}$ and LH signals lie within -4.12 mV/minute to 13.54 mV/minute, -3.27 mV/minute to 16.26 mV/minute, -5.27 mV/minute to 5.01 mV/minute and -7.82 mV/minute to 6.63 mV/minute respectively. Thus, the ML_{Ref} and IL_{Ref} both exhibit more dynamic characteristics while the LH and $Diff_{MLIL}$ signals are relatively steady with inherent low amplitude stochastic characteristics as seen earlier.

The reason is that the LH signal settles down in a much shorter time as compared to the reference signals. This is evident from the mean and SD, represented as a set as mean(SD), of the settling time for all the acquired ML_{Ref}, IL_{Ref} and LH signals, which are 690.39(335.34)s, 680.95(288.85)s and 81.17(59.63)s respectively. These have been calculated after the transition to the supine posture. The settling times of the $Diff_{MLIL}$ signals with mean(SD) of 83.03(163.34)s are comparable in the mean to those of the LH signals but have a much larger SD indicating larger variability.

5.2.3 Signal characteristics

Prior to the unilateral and bilateral characterization of the DDP signals, a comparison of the statistical and spectral characteristics of the LH signal and its associated ML_{Ref}, IL_{Ref} and $Diff_{MLIL}$ signals as recorded in the DS1 experiment are stated hereafter.

Statistical characteristics

As mentioned, the statistical parameters of all 4 types of signals, namely LH, ML_{Ref}, IL_{Ref} and $Diff_{MLIL}$ are determined, as shown in Table 5.1, for all the 60 data sets in 3 segments: the 2 minutes of the sitting posture, the 2 minutes during change of posture and the 16 minutes of the supine posture. For this, the minimum, maximum, mean, SD, skewness and kurtosis for subsequent 2 minute windows have been calculated.

Of these parameters, the averages are calculated for the z-normalized data of the mean, SD and kurtosis for subsequent 2 minute windows. Z-normalized data is obtained by dividing the respective debiased, or mean subtracted, signal with its SD. The plots are shown in Figure 5.14 (a), (b) and (c) respectively for all 4 types of signals.

Let us first compare the recorded values as stated in Table 5.1 and Figure 5.14 with the DAS calibration characteristics in Table 3.7 to Table 3.9

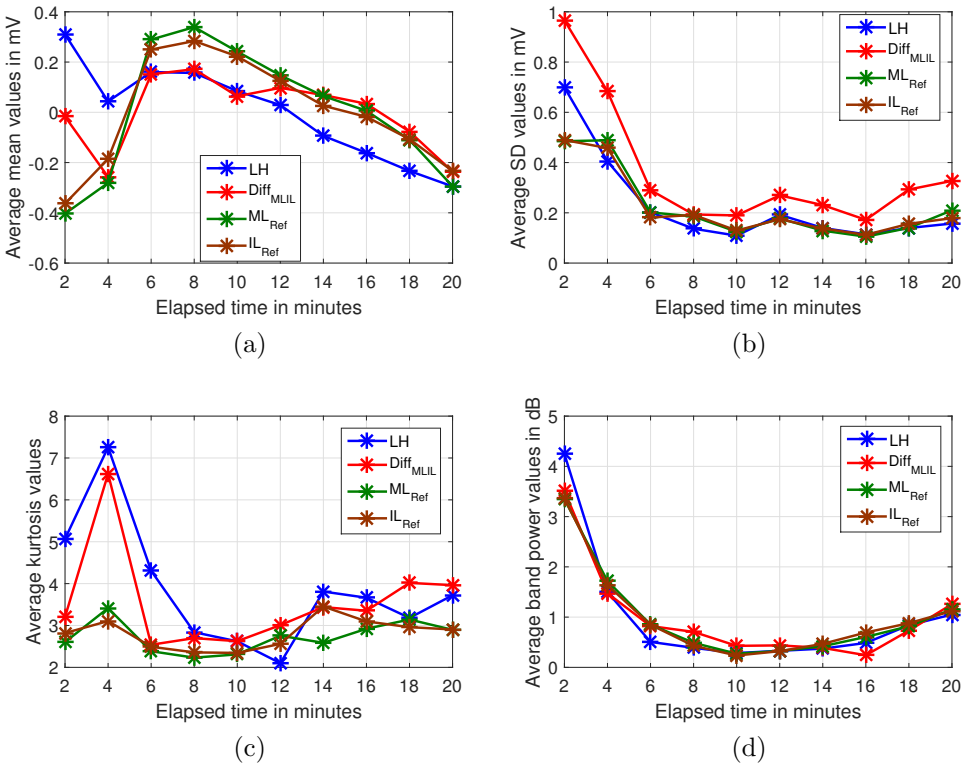

Figure 5.14: Plots of averages of (a) mean, (b) standard deviation (SD), (c) kurtosis and (d) average band power for subsequent 2 minutes windows over the 20 minutes duration

Table 5.1: Standard statistical parameters of signals collected in all three postures

Posture	Signals	Min in mV	Max in mV	Mean in mV	SD in mV	Skewness	Kurtosis
Sitting	LH	-44.18	45.62	3.09	19.21	-0.44	2.72
	$Diff_{MLIL}$	-41.32	45.28	7.82	16.38	-0.44	3.19
	ML_{Ref}	10.09	186.82	82.62	43.27	0.40	2.61
	IL_{Ref}	10.15	183.02	73.23	40.83	0.57	3.07
Change	LH	-44.42	48.90	2.25	17.85	-0.56	3.03
	$Diff_{MLIL}$	-39.43	42.57	6.65	15.24	-0.40	3.44
	ML_{Ref}	9.95	182.79	84.07	43.77	0.34	2.64
	IL_{Ref}	9.23	185.90	76.13	40.55	0.45	3.09
Supine	LH	-43.83	39.69	2.41	18.12	-0.56	3.09
	$Diff_{MLIL}$	-38.80	39.61	7.06	15.71	-0.36	3.66
	ML_{Ref}	9.24	175.56	86.51	44.49	0.20	2.54
	IL_{Ref}	9.13	183.50	78.33	41.16	0.25	2.95

. It is observed that the LH signals lie within $\pm$50mV in all 3 postures. The maximum static error in that range is 0.38mV which is 0.76% of the maximum static error stated in Table 3.8. The time varying characteristics of the signal is recorded in terms of its SD. This lies in the range of 0.1mV to 0.7mV (Figure 5.14), which is an order higher than the SD of 0.01mV obtained from the DAS (Table 3.9), thus validating the measured signal.

A comparison of the parameters of the LH signal with those of the $Diff_{MLIL}$ signals as well as the two referenced signals themselves from Table 5.1 and Figure 5.14 yield the following.

1. As is to be expected, the parameters for the LH and $Diff_{MLIL}$ signals are similar in magnitude and sign, while those of the two referenced signals are similar in all cases.

2. The trends for the mean values of the referenced signals are quite different from those of the difference and DDP signals. For the reference signals, these increase when the subject changes to the supine posture and then decreases slightly with longer rest. However, for the LH and the $Diff_{MLIL}$ signals, the mean decreases sharply due to change in posture and then decreases steadily as the subject enters a more restful condition.

3. The SD ranges for the referenced signals, typically in $40-45$mV range, are > 2 times than those of the LH and $Diff_{MLIL}$ signals. The SD

of the LH and $Diff_{MLIL}$ signals are within 15−20mV. This corroborates with the findings of the earlier studies for the differential signals [92, 113]. However, it is observed from the average SD plots in Figure 5.14(b) that the signal dynamics like posture change or long duration of rest are captured equally well in all 4 cases.

4. Skewness values are overall low, and hence negligible, for all cases. However, the trends are opposing for the referenced signals (right skewed) as compared to the LH and $Diff_{MLIL}$ signals (left-skewed).

5. The kurtosis values are close to 3 in all cases and are almost comparable all through the experiment for the reference signals. In case of the z-normalized data of the LH (and to a lesser extent, the $Diff_{MLIL}$) signals, it is observed that the kurtosis increases significantly and then drops again as the posture changes from sitting to supine, indicating the effect of orthostatic hypotension [126].

Spectral characteristics

Two spectral characteristics of these signals, namely the Welch Power Spectral Density (PSD) and the average band power, are also determined using the respective z-normalized data. The effect of the posture change on the PSD characteristics of all 4 signals are shown in Figure 5.15 (a)-(d). Each plot contains the average PSDs of all 60 sets of data in the range of 0 to 1Hz for 5 conditions: during the sitting posture, change of posture, the first 2 minutes of supine state (termed Sup 1), during 5 to 6 minutes of the supine state (9 to 10 minutes of elapsed time) (termed Sup 3) and last 2 minutes of supine state (termed Sup 8). As expected, the maximum power in all these signals is concentrated in the DC bias level and reduces drastically beyond this frequency. The PSD of the LH and $Diff_{MLIL}$ signals are almost identical in all cases and are significantly larger and exhibit slightly different characteristics than those of the reference signals.

The average band power of the signals, as plotted in Figure 5.14(d) for all 10 windows, is observed to be almost similar but not identical for all 4 types of signals. A common feature in all 3 plots is that the band power starts from a high value and continuously decreases till a certain value and then increases again. It can be interpreted that when the acquisition started, the (human) system was in a higher energy state. As the subjects get into (physical and mental) restful states, the energy level drops till the minima. When the maximum restfulness is achieved, the energy level starts increasing again. This may be in part due to the eagerness of the subjects to resume their routine work.

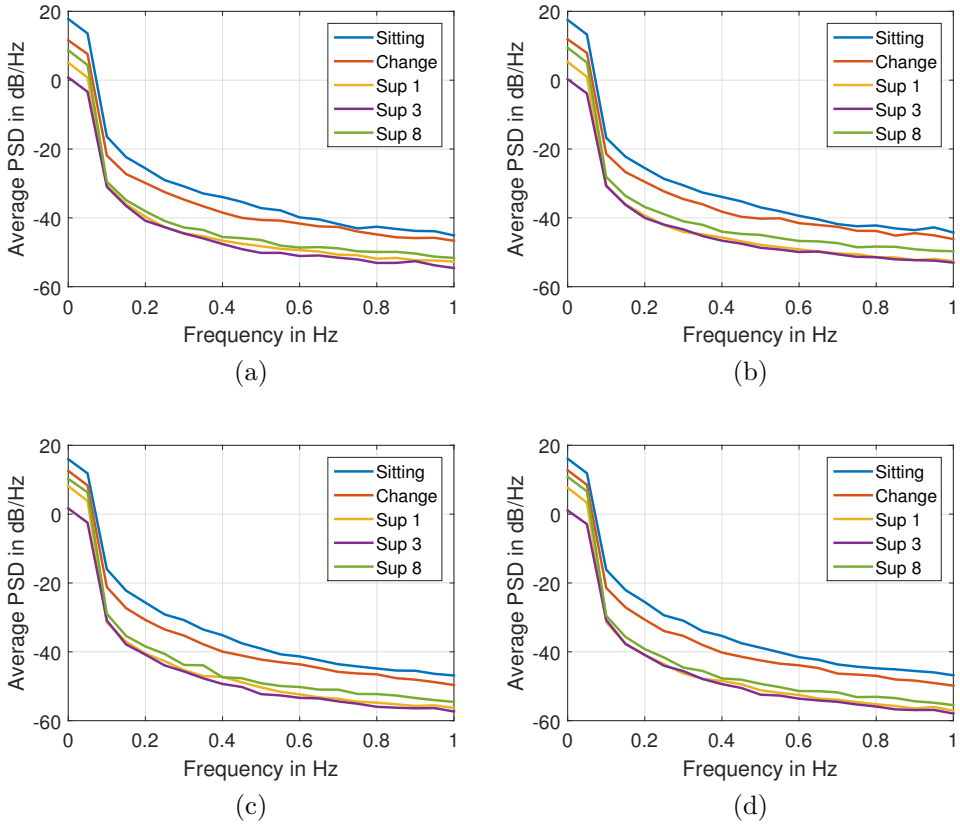

Figure 5.15: Average PSD within 0 to 1Hz at 5 different elapsed times of (a) LH signal, (b) $Diff_{MLIL}$ signal, (c) ML_{Ref} signal and (d) IL_{Ref} signal.

These characteristics and their changes with the different conditions of the experiment DS1 indicate the utility of the DDP signal in similar and other physiological applications.

5.3 Unilateral characteristics

In order to use the acquired DDP signal in any application, it is needed to establish key features and characteristics of these signals which might be useful in subsequent classification or analysis studies. As a first step for that, all DDP signals acquired during DS2, DS3 and DS4 have been collected together and segregated in to the 4 classes of LH, RH, LL amd RL signals. Since the acquired datasets are typically long term and varying in length, so all the datasets have been quantized into suitable number of 2 minutes data subsets. Then the unilateral characteristics of these 4 classes of 2 minutes signals have been studied in detail in this Section.

5.3.1 Characterization of acquired signals

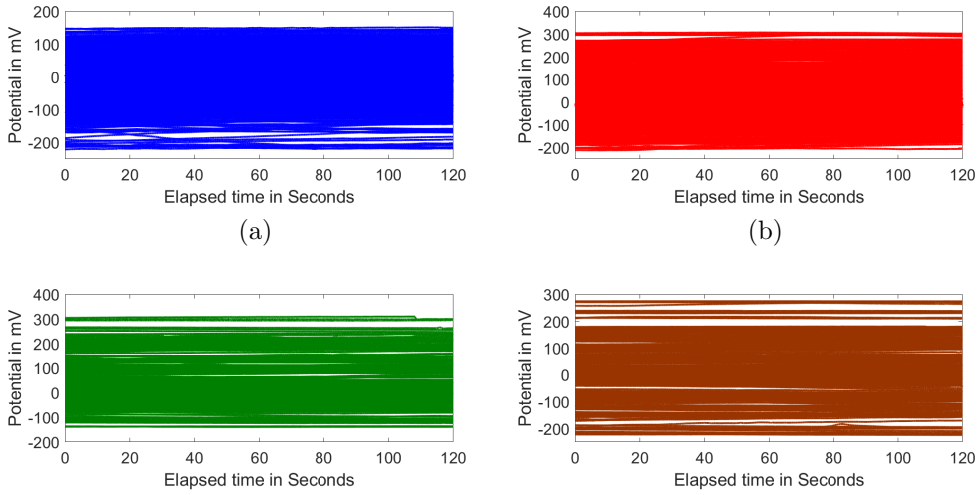

Figure 5.16: Time series plots of all (a) LH, (b) RH, (c) LL and (d) RL signals

The time series plots of all 2 minute signals for all 4 classes of acquired signals, namely LH, RH, LL and RL signals, are plotted in Figure 5.16a, Figure 5.16b, Figure 5.16c and Figure 5.16d respectively while their ranges

are stated in Table 5.2. It is observed that all the acquired signals lie approximately in the range of $\pm 300mV$.

From the study of Bhattacharya in [5], it is known that the set of simultaneously acquired DDP signals differ from each other. So, two signals collected simultaneously from both hands are different. Furthermore, though these signals look almost constant, but they vary continuously with time. Hence, a particular signal differs for different subjects and on different days for the same subject.

As stated earlier, DDP signals from both hands and both feet have been acquired in this study. It is observed that as in the case of the hand signals, the feet signals are also almost constant. Also, no two signals out of the LH, RH, LL and RL signals acquired simultaneously are identical to each other or to the same signal acquired subsequently from the same subject or from a different subject.

To understand the statistical distribution of the signals, standard statistical quantities of these acquired signals, namely the range, mean (μ), median, SD (σ), skewness and kurtosis, are tabulated in Table. 5.2. It can be seen that more than 95% of acquired signals lie within $\pm$250mV, whereas 90% of feet signals lie within $\pm$200mV. Among all, the span of the LH signals is minimum with 95% of the signals lying within (-110.06) mV to 107.93 mV, which is less than half of the typical DDP signal range of $\pm$250mV. Overall mean of the LH signals is also very close to 0, but for the others, the mean values are higher. Overall SD value of LH is also lower compared to that of the other acquired signals. Skewness values are close to normal for all 4 classes but kurtosis of the LH and RH are higher compared to LL and RL signals.

Table 5.2: Statistical characteristics of 4 types of acquired signals

Parameters	Range in mV		μ in	Median	σ in	Skewness	Kurtosis
	Min	Max	mV	in mV	mV		
LH	-294.03	151.37	-1.52	-1.36	48.10	-0.33	5.34
RH	-211.91	307.96	14.36	7.58	79.21	0.57	4.52
LL	-139.41	309.99	36.79	18.96	86.98	0.68	3.33
RL	-224.10	274.28	13.59	6.88	96.30	0.12	3.33

5.3.2 Polarity and trend of individual signals

In the previous study by Bhattacharya [5], it has been reported that the acquired signals are almost equally likely to be of either positive or nega-

tive polarity and in some cases, there are even transitions from negative to positive or vice versa.

Furthermore, the signals are likely to have either increasing or decreasing trends or are almost constant all through the 2 minute duration. These characteristics also differ for the signals acquired simultaneously.

These earlier reported findings have been reviewed for the signals acquired in the present study.

Polarity

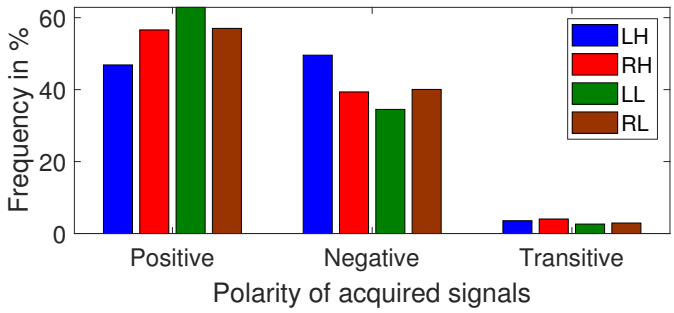

Figure 5.17: Bar plot of different polarities in LH, RH, LL and RL signals.

It is evident from Figure 5.16 that all the acquired DDP signals are distributed over all 3 classes, namely Positive, Negative and Transitive, as already defined by Bhattacharya [5]. The conditions for these 3 classes are as follows.

Let x_i denote the DDP at the i-th instant. Then, for any particular dataset x_i, $\forall \ \ i \in [1, 2400]$,

$$Signal\ is \begin{cases} Positive & if,\ x_i \geq 0.01mV \\ Negative & if,\ x_i \leq -0.01mV \\ Transitive & Otherwise \end{cases}$$

Polarities of all 4 classes of acquired signals are calculated and tabulated in Table 5.3 and represented as bar plots in Figure 5.17. It can be seen from the results that signals are more likely to have positive polarity, followed by negative polarity. In any particular class of signals, less than 4% of the signals are transitive in nature.

Table 5.3: Occurrence (in %) of different polarities in LH, RH, LL and RL signals.

Parameters	Positive in %	Negative in %	Transitive in %
LH	46.76	49.57	3.56
RH	56.60	39.36	4.04
LL	62.87	34.52	2.63
RL	57.12	40.06	2.92

Trends of individual signals

Three signal trends, namely increasing, decreasing and constant, are defined by Bhattacharya [5]. Considering a nominal tolerance of 2 mV, these 3 trends are defined in terms of the DDP values at the initial and final instants as follows.

For a particular data set $x_i, i \in [1, 2400]$, let $diff = x_1 - x_{2400}$.

$$Signal\ is \begin{cases} Decreasing & if,\ diff > +2mV \\ Increasing & if,\ diff < -2mV \\ Constant & ,Otherwise \end{cases}$$

The occurrence of these three trends in all 4 classes of signals are calculated in % and are tabulated in Table 5.4 while their bar plots are shown in Figure 5.18. The results show that in these cases also, all trends are almost equally likely but among them, the constant trend is most prevalent followed by the increasing and then the decreasing trends.

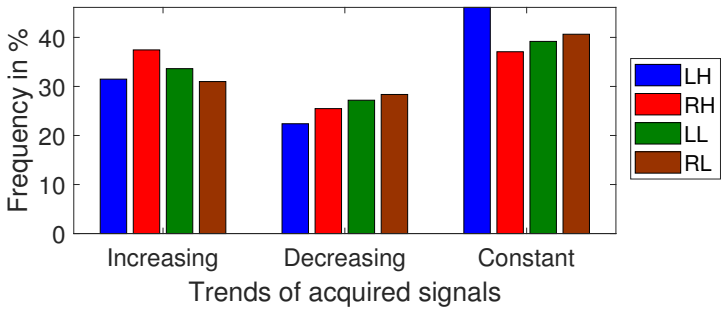

Figure 5.18: Bar plot of different trends in LH, RH, LL and RL signals.

Table 5.4: Occurrence (in %) of different trends in LH, RH, LL and RL signals.

Parameters	Increasing in %	Decreasing in %	Constant in %
LH	31.49	22.39	46.11
RH	37.45	25.48	37.07
LL	33.63	27.19	39.18
RL	30.99	28.36	40.64

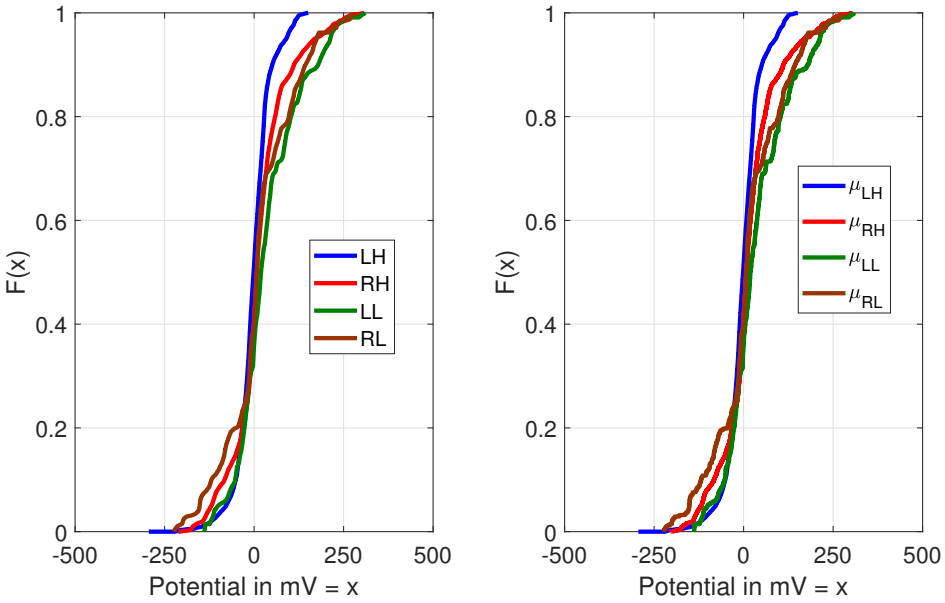

(a) (b)

Figure 5.19: Cdf plots of (a) 4 acquired signals, (b) their mean values (μ).

5.3.3 Bias of the signals

The bias of a particular DDP signal is considered to be its mean value for the whole duration of the dataset or in other words, its setwise mean value. Plots of the CDF of the 4 acquired DDP signals and their mean values are shown in Figure 5.19a and Figure 5.19b respectively.

Standard statistical quantities of the mean values of all 2 minute signals for the 4 classes of acquired signals are tabulated in Table 5.5. It is found

that the overall average of the LL signals are higher than that of the LH and also the RH signals, but the RH and RL signals have similar statistical characteristics.

From a comparison of the cdf plots in Figure 5.19a and Figure 5.19b as well as the statistical parameters in Table 5.5 and Table 5.2, it is observed that they are almost identical. Hence, it can be said that the DDP signal mean can be considered as one of its representative features.

Table 5.5: Standard statistical parameters of subsetwise mean values of LH, RH, LL and RL signals

Parameters	Range in mV		μ in mV	Median in mV	σ in mV	Skewness	Kurtosis
	Min	Max					
μ_{LH}	-216.11	149.30	-1.52	-1.47	48.04	-0.32	5.32
μ_{RH}	-205.13	305.59	14.36	7.77	79.14	0.57	4.51
μ_{LL}	-138.54	307.22	36.79	18.76	87.08	0.68	3.33
μ_{RL}	-222.72	274.06	13.59	6.55	96.40	0.12	3.33

Chi-square goodness of fit tests were performed with 5% and 10% significance levels to check the normality of the signal mean, or bias, values. The test results for acquired signals from hand are tabulated in Table 5.6, whereas, feet signals are tabulated in Table 5.7. Results show that none of these DDP signals follow normal distribution.

Table 5.6: Chi-square goodness of fit tests for μ_{LH} and μ_{RH}

Hypothesis	H_0: μ_{LH} is normally distributed H_A: μ_{LH} is not normally distributed		H_0: μ_{RH} is normally distributed H_A: μ_{RH} is not normally distributed	
df=15	$\chi^2_{0.10}$	$\chi^2_{0.05}$	$\chi^2_{0.10}$	$\chi^2_{0.05}$
Theoretical	22.307	24.996	22.307	24.996
Experimental	39.704	39.704	85.465	85.465
Conclusion	H_0 rejected	H_0 rejected	H_0 rejected	H_0 rejected

5.3.4 Debiased signals

In order to study the dynamic nature of these signals in more detail, the mean value of the individual signal is subtracted from the corresponding signal for all 4 acquired signals. Name of all these 4 signals are given hereafter. The characteristics of these signals are studied in this section.

Table 5.7: Chi-square goodness of fit tests for μ_{LL} and μ_{RL}

Hypothesis	H_0: μ_{LL} is normally distributed H_A: μ_{LL} is not normally distributed		H_0: μ_{RL} is normally distributed H_A: μ_{RL} is not normally distributed	
df=15	$\chi^2_{0.10}$	$\chi^2_{0.05}$	$\chi^2_{0.10}$	$\chi^2_{0.05}$
Theoretical	22.307	24.996	22.307	24.996
Experimental	39.704	39.704	85.465	85.465
Conclusion	H_0 rejected	H_0 rejected	H_0 rejected	H_0 rejected

1. debiased LH : Corresponding mean subtracted left hand signal = LH_k - mean(LH_k)

2. debiased RH : Corresponding mean subtracted right hand signal = RH_k - mean(RH_k)

3. debiased LL : Corresponding mean subtracted left feet signal = LL_k - mean(LL_k)

4. debiased RL : Corresponding mean subtracted right feet signal = RL_k - mean(RL_k)

where, k represents the individual 2 minute subset.

The superimposed line plots of the debiased LH, debiased RH, debiased LL and debiased RL signals corresponding to Figure 5.16 for the all subjects are shown in Figure 5.20. Most of the signals show a quasilinear nature and the majority of the signals, and/or their major portions, lie within $\pm 6mV$, as can be expected from the CDF plot of their SD in Figure 5.21a.

A typical characteristic of these signals, as evident in Figure 5.16, is that the cluster of all the 4 types of debiased acquired signals exhibit similar butterfly like patterns, mostly within $\pm 10mV$. This pattern appears since the majority of these quasilinear signals cross zero in the middle epoch, within 800 to 1600 instant (out of 2400 instants).

Standard statistical quantities of the debiased LH, debiased RH, debiased LL and debiased RL signals are tabulated in Table 5.8, while their CDF plots as well as the corresponding zoomed CDFs in the range $\pm 10mV$ are shown in Figure 5.21.

It is observed that the range of hand signals is higher than that of the feet signals. It can also be seen that the overall characteristics of the instantaneous debiased LH and RH signals are almost identical. Furthermore, in all 4 cases, the data are almost equitably distributed about the median value, which is close to 0 mV. Additionally, the kurtosis of the signals is very

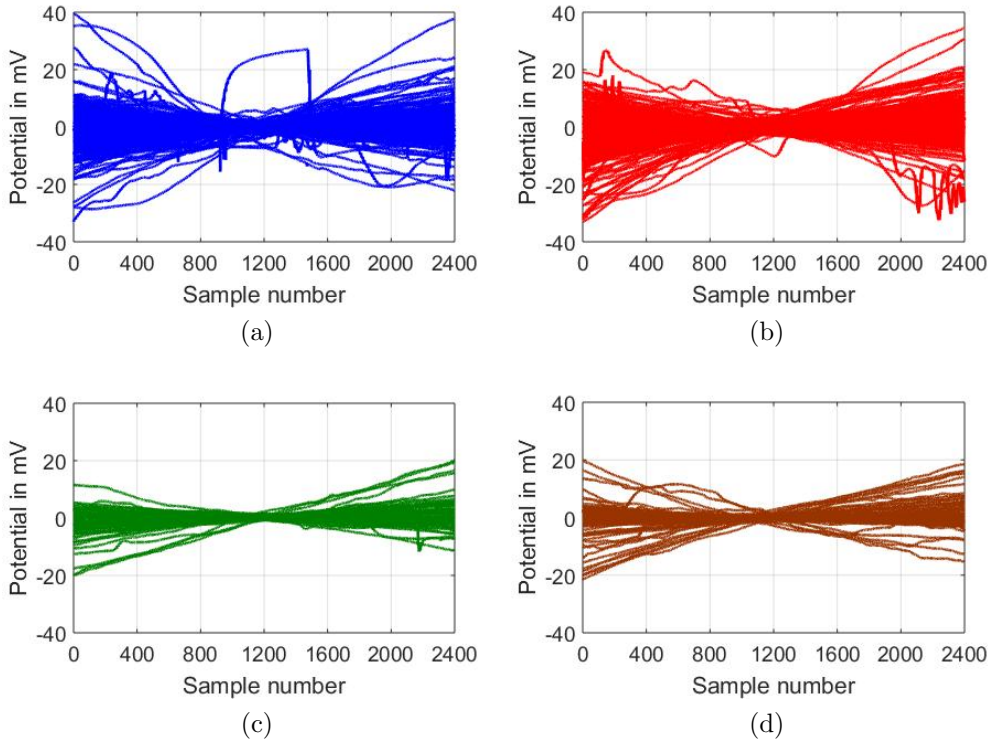

Figure 5.20: Time series plots of all debiased signals of (a) LH, (b) RH, (c) LL and (d) RL signals

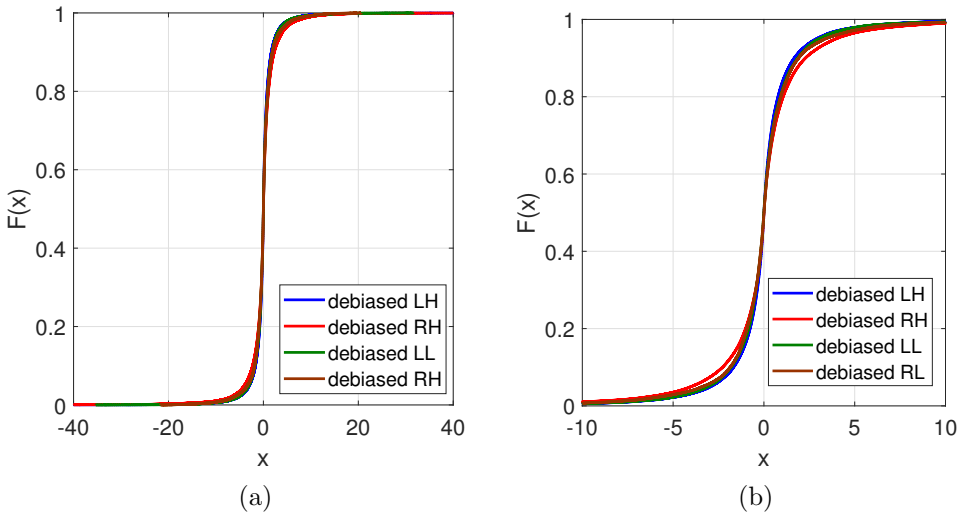

Figure 5.21: CDF plots of (a) all debiased acquired signals, (b) their zoomed plots within $\pm 10mV$

Table 5.8: Standard statistical parameters of debiased LH, RH, LL and RL signals

Parameter	Range in mV		σ in	Skewness	Kurtosis
	Min	Max	mV		
debiased LH	-33.00	39.50	3.09	0.66	27.14
debiased RH	-33.04	34.58	3.41	-0.59	17.69
debiased LL	-20.02	20.04	3.36	-0.07	11.61
debiased RL	-21.58	19.69	4.09	-0.22	8.15

high with typically more than 95% (2.5% to 97.5%) of the data lying within $\pm 6mV$. Characteristics of debiased LL is quite similar to that of debiased LH and debiased RH but the characteristics of debiased RL signls are slightly different, particularly in the mean and the kurtosis.

5.3.5 Linear regression parameters

In view of the mean as a characteristic feature of the DDP signal and the similar quasistatic natures of the debiased signals, the linear regression equation (5.2) that was proposed in [5] is considered in this study also. Here, ZCI is the Zero Crossing Instant, defined as the time instant when the debiased signal crosses the 0mV axis closest to its mid point, y_k is the acquired signal, μ is the mean and e_k is the residual of the acquired signal from the linear fit at the k_{th} instant. The slope m is defined in 5.3.

$$y_k = \mu + m \times (k - ZCI) + e_k; \tag{5.2}$$

$$m = [\frac{\sum_{k=1}^{N}(k - ZCI)y_k}{\sum_{k=1}^{N}(k - ZCI)^2}] \tag{5.3}$$

Zero Crossing Instant

From Figure 5.20, it is observed that most of the debiased signals cross 0mV axis in the middle epoch (within 800 to 1600 instant). These instants are termed as the Zero Crossing Instants (ZCI). The CDF plots of the zero crossing instants (ZCI) of the debiased LH and RH signals of all subjects, denoted as ZCI_{LH} and ZCI_{RH} respectively, are shown in Figure 5.22a. The likelihood of occurrences of the ZCI_{LH} and ZCI_{RH} in 50% of the cases

(F(x)=0.5 to 1) are almost identical. Statistical characterization of ZCI_{LH} and ZCI_{RH} are done in Table 5.9. From this table it can be said that ZCI_{LH} and ZCI_{RH} lies within 400 to 2000 instants and mean values lie very close to 1200. No strong skewness can be seen in either of two sides.

Table 5.9: Statistical characterization of ZCI_{LH}, ZCI_{RH}, ZCI_{LL} and ZCI_{RH}

Parameters	Range in mV		μ in mV	σ in mV	Skewness	Kurtosis
	Min	Max				
ZCI_{LH}	485	1928	1150.73	197.20	0.43	5.39
ZCI_{RH}	454	1924	1130.24	218.75	0.21	4.34
ZCI_{LL}	583	1848	1161.53	190.40	0.33	6.06
ZCI_{RL}	662	1881	1174.32	199.68	0.67	5.20

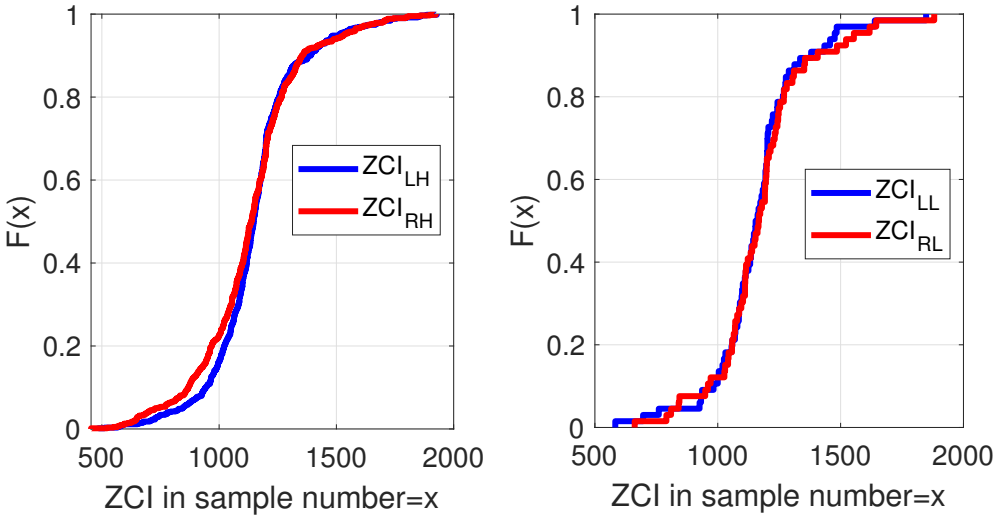

(a) (b)

Figure 5.22: CDF plot of (a) ZCI_{LH} and ZCI_{RH} and (b) ZCI_{LL} and ZCI_{RL}

ZCI of feet signals are also studied. Here almost 90% of ZCI_{LL} and ZCI_{RL} lie within their middle epoch. This can be seen in the CDF plot of ZCI_{LL} and ZCI_{RL} in Figure 5.22b also. The standard statistical parameters for the ZCI of all 2 minute LL and RL signals are also tabulated in Table 5.9. It is observed that the span of ZCI_{LL} and ZCI_{RL} are close to the span of

ZCI_{LH} and ZCI_{RH}. Figure 5.22b and Table 5.9 both have confirmed that the kurtosis of the ZCI distributions are on the higher side.

Slope (m) of signals

The findings about the locations of the pairwise ZCI lead to an investigation of the overall deviation occurring in these quasilinear signals. For this reason, straight lines passing through the respective ZCI are fitted to the debiased LH and RH signals. Slopes of these straight lines are denoted as m_{LH} and m_{RH} respectively. The CDF plots of m_{LH} and m_{RH} are shown in Figure 5.23a. It is observed that in both cases, the slopes vary between $\pm 0.04 mV/instant$ and almost 99% of the data lie within $\pm 0.01 mV/instant$. However, in more than 80% cases(F(x)=0.1 to 0.9), m_{LH} values are likely to be slightly more negative than m_{RH}.

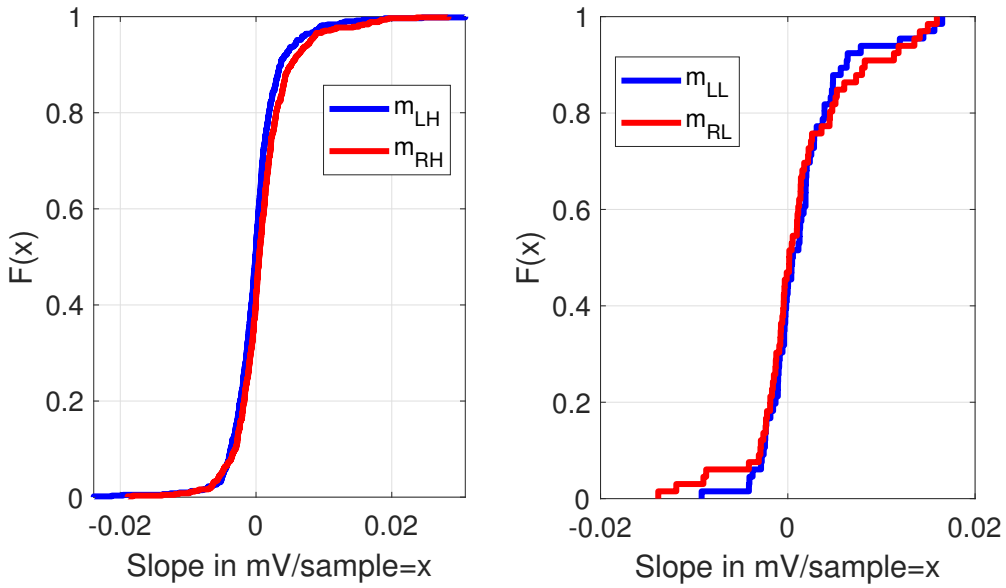

(a) (b)

Figure 5.23: CDF plot of (a) m_{LH} and m_{RH} and (b) m_{LL} and m_{RL}

Statistical properties of m_{LH} and m_{RH} are stated in Table 5.10. It can be seen from the table that range of m_{LH} and m_{RH} lie within -0.024mV/instant to 0.03mV/instant, though their mean are 0. It is found that m_{LH} and m_{RH} both have same SD values. Both m_{LH} and m_{RH} have positive skewness and very high kurtosis.

Table 5.10: Statistical characterization of m_{LH}, m_{RH}, m_{LL} and m_{RL}

Parameters	Range in mV		μ in mV	σ in mV	Skewness	Kurtosis
	Min	Max				
m_{LH}	-0.024	0.03	0	0.004	0.95	15.35
m_{RH}	-0.018	0.028	0	0.004	1.18	9.98
m_{LL}	-0.0092	0.0165	0.0015	0.0045	1.3747	6.0347
m_{RL}	-0.0138	0.0159	0.0012	0.0056	0.4464	4.4140

Slope of the debiased feet signals are calculated and their CDF plots are shown in Figure 5.23b while their statistical parameters are tabulated in Table 5.10. Slope of LL and RL signals are denoted as m_{LL} and m_{RL} respectively. It is observed that m_{LL} varies within -0.0092mV/instant to 0.0165mV/instant while m_{RL} varies within -0.0138mV/instant to 0.0159mV /instant. These are very low compared to $\pm 4mV$, which is the typical range of m_{LH} and m_{RH} signals. In these cases also, more than 90% of data lies within $\pm 1mV$ range. Mean value of m_{LL} and m_{RL} lies very close to 0mV/instant.

5.3.6 Spectral features

Certain spectral features of the LH, RH, LL and RL signals have also been studied in order to observe their overall characteristics across the various experiments.

Power spectral density

The power spectral density (PSD) analysis is a major analysis technique in the frequency domain. It is known that any time varying signal can be decomposed into its composite frequency components. Power spectral density describes the distribution of power in these different frequency components. It can be calculated by taking the Fourier transform of the signal ACF [127].

PSD of all 4 classes of signals are studied and plots of PSD of the LH, RH, LL and RL signals of 2 arbitrarily chosen sets are shown in Figure 5.24.

It can be seen in these plots that the spectral energy is mostly concentrated very close to the origin, though these signals are dynamic. Therefore, it can be inferred that these signals contain very low frequency components which are not directly observed from the PSD plots.

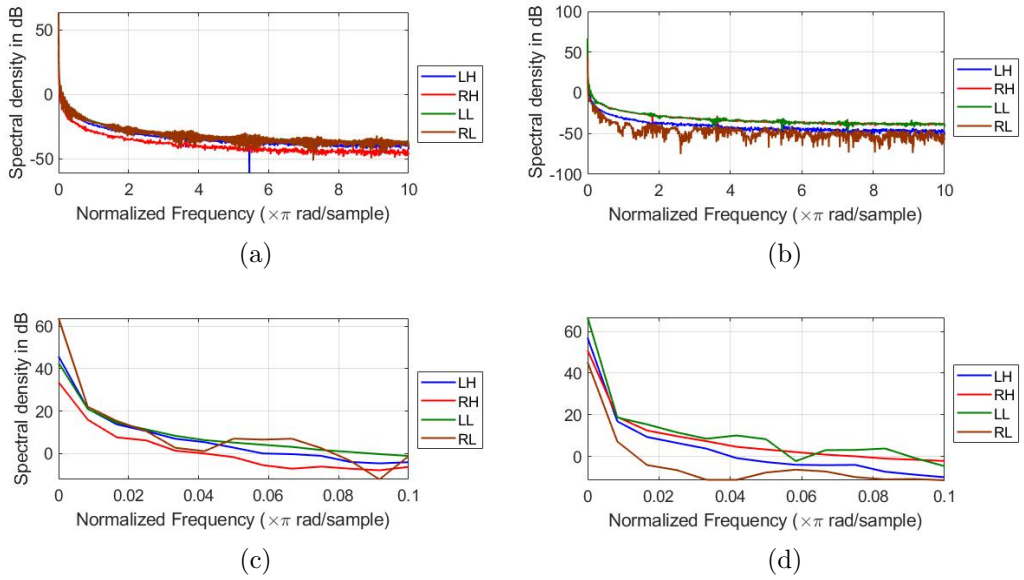

Figure 5.24: Sample PSD plots of arbitrarily chosen (a) Example 1 and (b) Example 2 and zoomed plots of (c) Figure 5.24a and (d) Figure 5.24b within 0.1 Hz normalised frequency.

Mean frequency and Power at mean frequency

The mean frequency (MNF) is defined as the ratio between the sum of products of the instantaneous frequencies and the power at those frequencies and the total power (Equation 5.4) [128, 129]. Here, k is the instant and N is the highest instant while the power at that mean frequency instant MNF is denoted as P_{MNF}.

$$MNF = \frac{\sum_{k=1}^{N} f_k P_k}{\sum_{k=1}^{N} P_k} \tag{5.4}$$

Table 5.11 represents the statistical characteristics of the MNF and the P_{MNF} whereas Figure 5.25 represents the box plots of the MNF and the P_{MNF}. It has been found from both table and figure that range of MNF for LH is maximum, followed by RH, LL and RL. Along with that, the mean values are also maximum for LH, followed by RH, LL and RL. The median values of MNF for all 4 classes of signals are exactly identical to 0.0022. The SD, skewness and kurtosis of MNF are all are higher for LH, followed by RH, LL and RL.

In case of the P_{MNF}, mean value is little low in LH, followed by RH, LL and RL in the ascending order along with the median and standard deviation

Table 5.11: Standard statistical quantities of MNF and P_{MNF} of 4 acquired signals

Parameters	Signal	Range in Hz		μ in Hz	Median in Hz	σ in Hz	Skewness	Kurtosis
		Min	Max					
MNF	LH	0.0019	4.9989	0.0087	0.0022	0.1424	28.7535	909.55
	RH	0.0018	0.3810	0.0036	0.0022	0.0132	18.5370	440.52
	LL	0.0021	0.0494	0.0025	0.0022	0.0027	15.1995	255.91
	RL	0.0020	0.0196	0.0024	0.0022	0.0012	10.9192	142.07
Parameters	Signal	Range in dB		μ in dB	Median in dB	σ in dB	Skewness	Kurtosis
		Min	Max					
P_{MNF}	LH	-24.1213	65.0966	26.4637	27.7776	9.7937	-0.7550	4.0772
	RH	-24.9699	49.7277	28.8756	30.6082	11.9576	-0.7715	3.6341
	LL	-7.1924	49.7821	31.4503	32.5355	11.3410	-0.9468	3.8401
	RL	-4.2798	48.7599	30.9012	33.1523	12.0013	-0.5648	2.5099

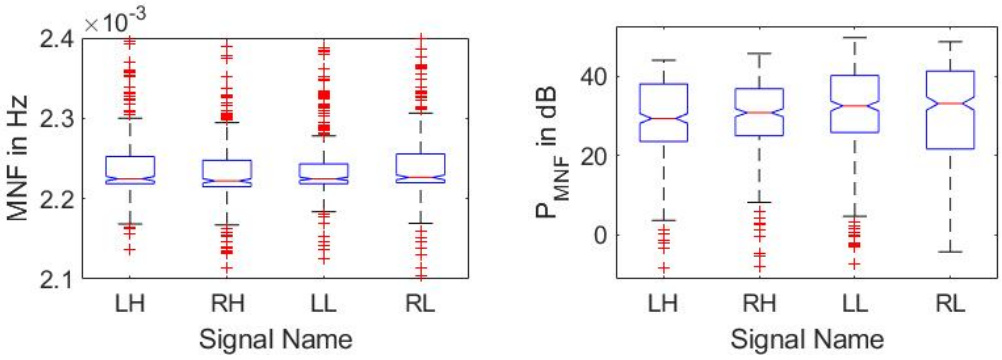

(a) (b)

Figure 5.25: Box plots of (a) Mean frequency and (b) Power at mean frequency of all 4 classes of signals

also. It can also be observed that the span of RL (difference between upper adjacent and lower adjacent) is maximum for the range of -4.28 to 48.75, followed by LL, LH, and RH with the range of 4.67 to 49.78, 3.65 to 44.08 and 8.21 to 45.78 respectively in descending order.

Median frequency and Power at median frequency

Median frequency (MDF) is defined as the frequency which actually divides the total spectrum into two parts of equal power, so that each half has similar total power [129]. It is presented in Equation 5.5. Power at MDF is defined as P_{MDF}.

$$\sum_{k=1}^{MDF} P_k = \sum_{k=MDF}^{N} P_k = \frac{1}{2}\sum_{k=1}^{N} P_k \tag{5.5}$$

Statistical parameters of MDF and P_{MDF} are given in Table 5.12 and box plots of MDF and P_{MDF} are plotted in Figure 5.26 for all 4 signals. Comparing Table 5.11 and Table 5.12, it can be seen that all the parameters are very close to each other. Median of the MDF for all 4 signals lie at 0.0028. This is the case for P_{MDF} also. Both the P_{MNF} in Table 5.11 and P_{MDF} in Table 5.12 are almost identical.

Comparing Figure 5.25 and Figure 5.26, it can be said that the MNF and MDF characteristics are almost identical. The upper adjacent and the lower adjacent of MDF of LH signal are 2.87 $\times$ $10^{-}3$ and 2.82 $\times$ $10^{-}3$. The values are similar in case of the other 3 signals also. Compared to the range of MNF of nearly 1.5 $\times$ $10^{-}4$ Hz, the range of MDF at nearly 5 $\times$ $10^{-}5$ Hz is low. On the other hand, median of all 4 signals in MDF lies at 2.84 $\times$ $10^{-}3$.

Overall span of the P_{MDF} lies within -4.27 dB to 49.78 dB, which is almost identical to that of P_{MNF}. Similarly, range of other 3 signals are almost identical to the case of P_{MNF}.

Peak frequency and Power at peak frequency

The peak frequency (PKF) is the frequency at which the maximum power occurs and its power is called P_{PKF} [130]. Box plots of PKF and P_{PKF} are plotted in Figure 5.27. It has already been seen in PSD plots in Figure 5.24 that maximum power lies very close to 0. From Figure 5.27a, it is evident that the maximum power occurs at 0Hz for all signals, which is actually the DC component. For this reason, this parameter has not been studied further and is not used as a feature in any of the applications.

$$PKF = max(P_k),\ k = 1, 2, 3, ..., N \tag{5.6}$$

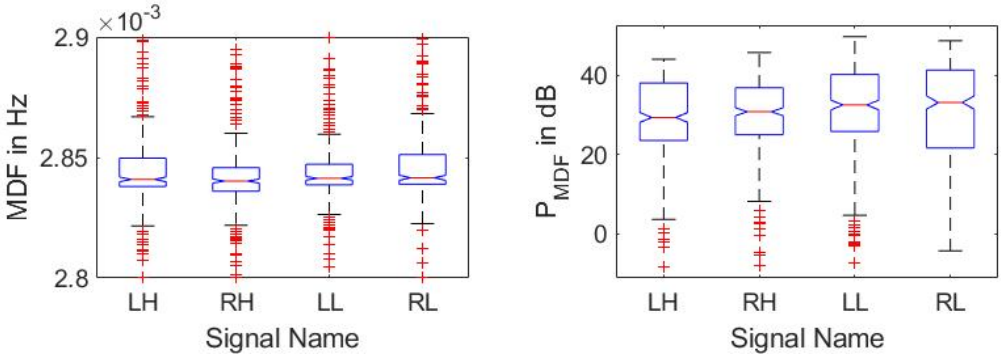

(a) (b)

Figure 5.26: Box plots of (a) Median frequency and (b) Power at median frequency of all 4 signals

Table 5.12: Standard statistical quantities of MDF and P_{MDF} of 4 acquired signals

Parameters	Signal	Range in Hz		μ in Hz	Median in Hz	σ in Hz	Skewness	Kurtosis
		Min	Max					
MDF	LH	0.0026	4.9989	0.0087	0.0028	0.1293	39.749	1.64×10^3
	RH	0.0025	0.0520	0.0030	0.0028	0.0020	18.2363	391.04
	LL	0.0028	0.0079	0.0029	0.0028	3.28×10^{-4}	12.3676	174.99
	RL	0.0027	0.0098	0.0029	0.0028	5.55×10^{-4}	10.0699	110.1617
Parameters	Signal	Range in dB		μ in dB	Median in dB	σ in dB	Skewness	Kurtosis
		Min	Max					
P_{MDF}	LH	-24.1213	65.0966	26.4637	27.7776	9.7937	-0.7550	4.0772
	RH	-24.9699	49.7277	28.8756	30.6082	11.9576	-0.7715	3.6341
	LL	-7.1924	49.7821	31.4503	32.5355	11.3410	-0.9468	3.8401
	RL	-4.2798	48.7599	30.9012	33.1523	12.0013	-0.5648	2.5099

Table 5.13: Standard statistical quantities of P_{PKF} of 4 acquired signals

Parameters	Signal	Range in dB		μ in dB	Median in dB	σ in dB	Skewness	Kurtosis
		Min	Max					
P_{PKF}	LH	-5.3809	66.1589	45.8509	47.2214	9.8267	-0.8177	4.0791
	RH	-9.5719	69.1666	48.2498	50.0512	12.0757	-0.8069	3.7766
	LL	11.3873	69.2218	50.8642	51.9804	11.4144	-0.9720	3.9232
	RL	14.4181	68.2051	50.3183	52.5857	12.0441	-0.5745	2.5393

The mean value of P_{PKF} is higher compared to the P_{MNF} and P_{MDF}, which is evident as it is the highest power component. The SD, skewness and kurtosis values of P_{PKF} are very close to those of P_{MNF} and P_{MDF}.

The overall pattern of P_{PKF} is very much similar to that of P_{MNF} and P_{MDF} but the range of the P_{PKF} is higher compared to the other two as in Figure 5.27b. Arranging all 4 signals in terms of their range of P_{PKF} in descending order, it can be found that RL is most spread out with the range of 14.42 dB to 68.20 dB, followed by LL (23.81dB to 69.22 dB), LH (22.80 dB to 63.52 dB) and RH (27.50 dB to 65.21 dB) respectively.

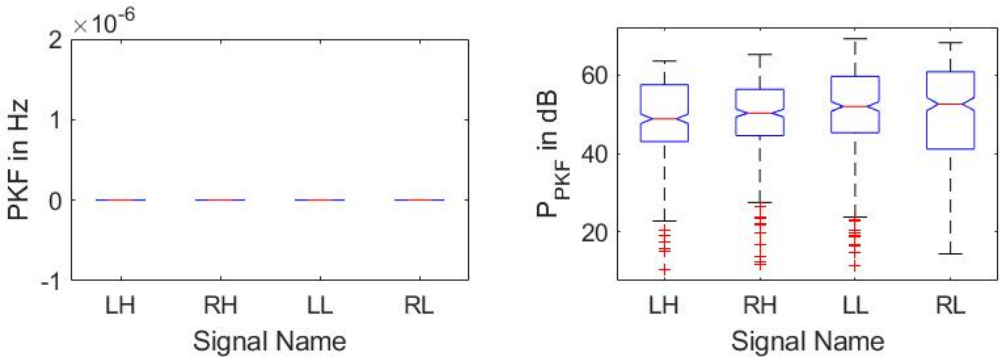

(a) (b)

Figure 5.27: Box plots of (a) Peak frequency and (b) Power at peak frequency of all 4 signals

Band power

Band power is defined as the average power of a signal in the spectral domain. Box plots for the band power for all 4 signals are shown in Figure 5.28. Comparing with the P_{MNF} and P_{MDF} in Figure 5.25b and Figure 5.26b, it is found that all these 3 are exactly similar to each other. Comparing the values in Table 5.11, Table 5.12 and Table 5.14, it is found that all three

tables are exactly identical to each other. Therefore, it can be said that all three parameters are identical.

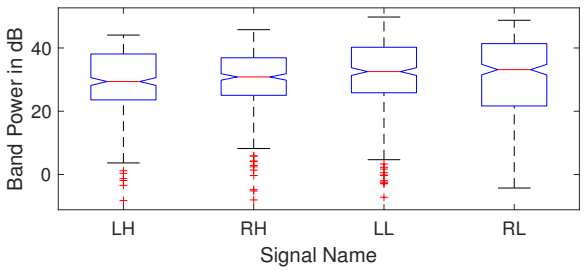

Figure 5.28: Box plots of band power of all 4 signals

Table 5.14: Standard statistical quantities of band power of 4 acquired signals

Parameters	Signal	Range in dB		μ in dB	Median in dB	σ in dB	Skewness	Kurtosis
		Min	Max					
$BandPower$	LH	-24.1213	65.0966	26.4637	27.7776	9.7937	-0.7550	4.0772
	RH	-24.9699	49.7277	28.8756	30.6082	11.9576	-0.7715	3.6341
	LL	-7.1924	49.7821	31.4503	32.5355	11.3410	-0.9468	3.8401
	RL	-4.2798	48.7599	30.9012	33.1523	12.0013	-0.5648	2.5099

SM1, SM2 and SM3

SM1, SM2 and SM3 are the three spectral moments. SM1 is defined as the sum of product of the instantaneous frequency and power. Therefore, SM1 can be considered as the gain-bandwidth product of the frequency spectrum. Similarly, SM2 and SM3 are the sum of the product of the square of instantaneous frequency and power and the sum of the product of the cube of instantaneous frequency and power respectively. SM1, SM2 and SM3 are shown in Equation 5.7.

$$\begin{aligned} SM1 &= \sum_{k=1}^{N} f_k P_k \\ SM2 &= \sum_{k=1}^{N} f_k^2 P_k \\ SM3 &= \sum_{k=1}^{N} f_k^3 P_k \end{aligned} \tag{5.7}$$

All their statistical parameters are calculated and tabulated in Table 5.15. It can be seen that the overall ranges of LH and RH for SM1, SM2 as well as SM3 are high compared to that of the LL and RL signals though the mean, median and SD of all 4 signals and all 3 SM are comparable to each other. But, skewness and kurtosis are both high for LH signals in all three cases.

Box plots of SM1, SM2 and SM3 of all 4 signals are plotted in Figure 5.29. It can be seen from all these three plots that there is not much difference between all 4 signals in terms of SM1, SM2 and SM3 respectively.

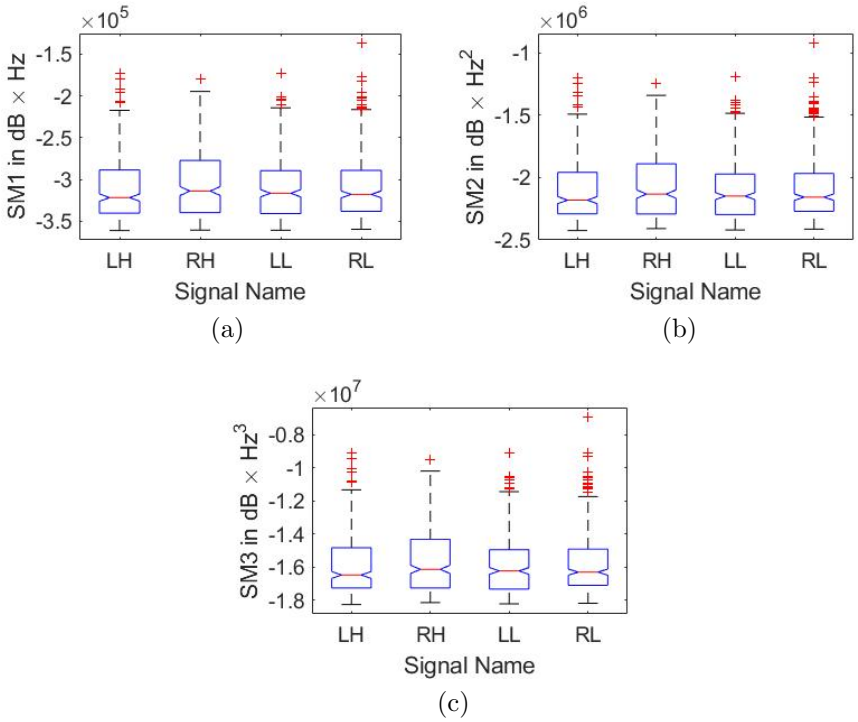

Figure 5.29: Box plots of (a) SM1, (b) SM2 and (c) SM3 of all 4 signals

Spectral entropy

The Shannon entropy of the signal is calculated for the power spectral distribution of this signal since this is widely used in biomedical signal processing [131]. The spectral entropy of a signal is defined as Equation 5.8 in terms of the probability distribution $P(k)$ (defined as in 5.9) as follows.

$$E = -\sum_{k=1}^{N} P(k) log_2 P(k), \tag{5.8}$$

Table 5.15: Standard statistical quantities of SM1, SM2 and SM3 of 4 acquired signals

Parameters	Signal	Range in $dBHz$		μ in $dBHz$	Median in $dBHz$	σ in $dBHz$	Skewness	Kurtosis
		Min	Max					
SM1	LH	-3.76 $\times 10^5$	3.31 $\times 10^5$	-3.06 $\times 10^5$	-3.16 $\times 10^5$	4.68 $\times 10^4$	2.9707	25.9786
	RH	-3.60 $\times 10^5$	3.95 $\times 10^4$	-2.97 $\times 10^4$	-3.05 $\times 10^5$	4.42 $\times 10^4$	1.2881	6.6009
	LL	-3.61 $\times 10^5$	-1.73 $\times 10^5$	-3.11 $\times 10^5$	-3.16 $\times 10^5$	3.61 $\times 10^4$	0.8879	3.4361
	RL	-3.59 $\times 10^5$	-1.37 $\times 10^5$	-3.09 $\times 10^5$	-3.18 $\times 10^5$	3.87 $\times 10^4$	1.2037	4.3810
Parameters	Signal	Range in $dBHz^2$		μ in $dBHz^2$	Median in $dBHz^2$	σ in $dBHz^2$	Skewness	Kurtosis
		Min	Max					
SM2	LH	-2.56 $\times 10^6$	2.21 $\times 10^6$	-2.07 $\times 10^6$	-2.15 $\times 10^6$	3.08 $\times 10^5$	3.1852	28.3957
	RH	-2.45 $\times 10^6$	2.22 $\times 10^5$	-2.02 $\times 10^6$	-2.07 $\times 10^6$	2.89 $\times 10^6$	1.3752	6.9766
	LL	-2.42 $\times 10^6$	-1.19 $\times 10^6$	-2.11 $\times 10^6$	-2.15 $\times 10^6$	2.34 $\times 10^5$	0.9637	3.5990
	RL	-2.41 $\times 10^6$	-9.21 $\times 10^5$	-2.09 $\times 10^6$	-2.16 $\times 10^6$	2.52 $\times 10^5$	1.3118	4.7953
Parameters	Signal	Range in $dBHz^3$		μ in $dBHz^3$	Median in $dBHz^3$	σ in $dBHz^3$	Skewness	Kurtosis
		Min	Max					
SM3	LH	-1.94 $\times 10^7$	1.65 $\times 10^7$	-1.56 $\times 10^7$	-1.62 $\times 10^7$	2.29 $\times 10^6$	3.2986	29.7448
	RH	-1.86 $\times 10^7$	1.53 $\times 10^6$	-1.52 $\times 10^7$	-1.56 $\times 10^6$	2.15 $\times 10^6$	1.4210	7.1704
	LL	-1.82 $\times 10^7$	-9.11 $\times 10^6$	-1.59 $\times 10^7$	-1.62 $\times 10^7$	1.73 $\times 10^6$	1.0062	3.7004
	RL	-1.82 $\times 10^7$	-6.93 $\times 10^6$	-1.58 $\times 10^7$	-1.63 $\times 10^7$	1.86 $\times 10^6$	1.3697	5.0306

For a signal $x(n)$, the power spectrum is $S(k) = |X(k)|^2$. Here $X(k)$ is the discrete Fourier transform of $x(n)$. Then,

$$P(k) = \frac{S(k)}{\sum_i S(i)} \tag{5.9}$$

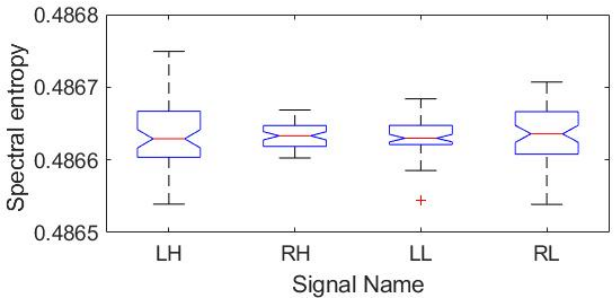

Figure 5.30: Spectral entropy of all 4 signals

All the statistical parameters measured are given in Table 5.16 while the box plots of the spectral entropy of all 4 signals are plotted in Figure 5.30. It can be seen from the table as well as plots that the overall range lies within 0.4868 and 0.5674, while the median values are exactly at 0.4868. The interquartile range in Figure 5.30 of LH and RH are comparably higher

Table 5.16: Standard statistical quantities of spectral entropy of 4 acquired signals

Parameters	Signal	Range		μ	Median	σ	Skewness	Kurtosis
		Min	Max					
Entropy	*LH*	0.4868	0.5477	0.4872	0.4868	0.0030	12.0192	184.1697
	RH	0.4868	0.5674	0.4875	0.4868	0.0047	10.9010	143.9715
	LL	0.4868	0.5315	0.4871	0.4868	0.0027	14.2498	228.7668
	RL	0.4868	0.5020	0.4870	0.4868	0.0013	8.4672	80.1640

than LL and RL although value-wise these are very close since the difference is in the range of 10^{-5}. All the 4 signals are right skewed with very high kurtosis.

5.4 Bilateral characteristics

Hereafter, the bilateral characteristics of the DDP signals have been studied using the DS4 dataset comprising of simultaneously acquired LH, RH, LL and RL signals.

5.4.1 Signal interactions

It is obvious that the 4 DDP signals may exhibit 3 types of 2 channel interactions. These are
Bilateral: Interrelation between two bilateral location signals like LH and RH or LL and RL.
Sidewise: Interrelation between two locations of same side (right or left) like LH and LL or RH and RL
Cross: Interaction between signals of cross-limbs like LH and RL or RH and LL.

Signal cross-correlations

Cross-correlations of these sets of signals have been studied and the histograms of all 6 cross-correlation coefficients are shown in Figure 5.31. Here Figure 5.31a and Figure 5.31b are the bilateral cross-correlation coefficients of LH-RH and LL-RL respectively. Similarly Figure 5.31c (LH-LL cross-correlation) and Figure 5.31d (RH-RL cross-correlation) represent the sidewise and Figure 5.31e (LH-RL cross-correlation) and Figure 5.31f (RH-LL cross-correlation) represent the crosswise relationships of DDP signals.

It can be seen from the figures that the cross-correlation coefficients mostly lie within ±0.8 to ±1 in all 6 cases. In case of bilateral interactions, more than 66% of data lies within these limits as evident in Figure 5.31a and Figure 5.31b. In the other 4 cases (Figure 5.31e - Figure 5.31f), less than 50% of cases are highly correlated. Therefore, it can be said that bilateral relationship is the most significant among all 3 types of interactions and need to be studied in details.

Lateralization coefficients

Lateralization coefficient for electrodermal signals, denoted henceforth as LC1, was proposed by Myslobodsky and Rattok [132] and is defined as stated in Equation 5.10. Here, EDR$_{right}$ and EDR_{left} denote the electrodermal response of right and left hand, whereas EDR_{max} is the maximum of EDR_{right} and EDR_{left}. Another lateralization coefficient, denoted henceforth as LC2 was proposed by Schulter and Papousek [133], also in terms of EDR_{right} and EDR_{left} as stated in Equation 5.11. The difference in the two are the normalization factors, which is EDR_{max} in case of LC1 and $EDR_{right}+EDR_{left}$ in case of LC2.

$$LC1 = \frac{EDR_{right} - EDR_{left}}{EDR_{max}} \tag{5.10}$$

$$LC2 = \frac{EDR_{right} - EDR_{left}}{EDR_{right} + EDR_{left}} \tag{5.11}$$

Table 5.17: Statistical parameters of LC1H, LC1L, LC2H and LC2L for the mean of the DDP signals

Parameters	Range		μ	Median	σ	Skewness	Kurtosis
	Min	Max					
LC1H	2.54 $\times 10^3$	1.42 $\times 10^3$	-1.77	-0.53	96.77	-16.95	529.68
LC1L	-397.04	805.34	0.94	-0.21	30.40	16.87	430.52
LC2H	-117.33	56.96	-0.32	0.72	9.88	-6.33	76.74
LC2L	-9.66 $\times 10^3$	165.13	-27.69	0.28	522.74	-18.37	339.02

In this work, LC1 and LC2 have been calculated for both the hand and the leg signals, considering the EDR to be the mean of the respective signal. Hence, LC1H and LC1L (alternatively, LC2H and LC2L) denote the LC1 (alternatively, LC2) parameters for the mean of the (LH, RH) and (LL, RL) signals respectively. The statistical characteristics of these parameters are listed in Table 5.17. It can be seen that the overall ranges are high, though

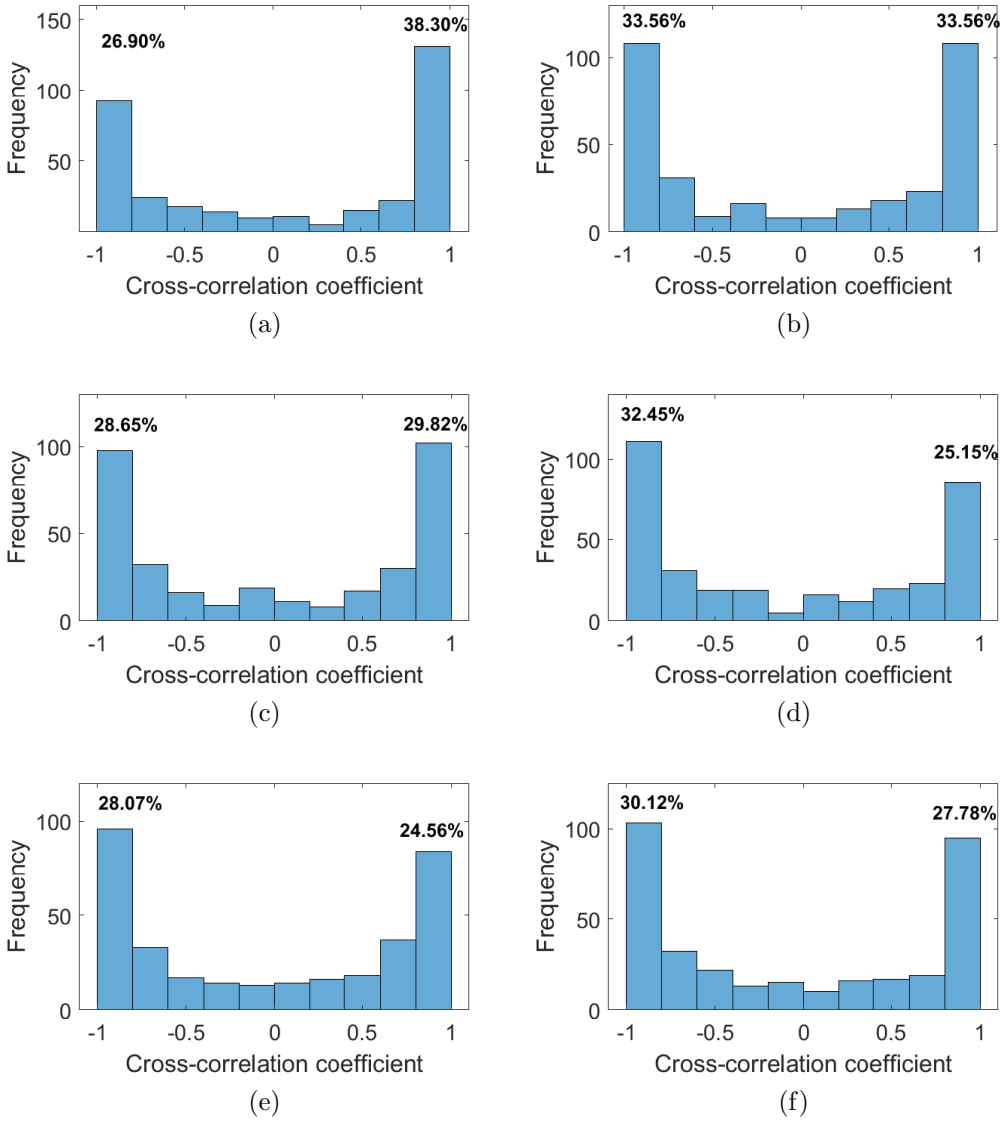

Figure 5.31: Histograms of the cross-correlation coefficients of (a) LH and RH, (b) LL and RL, (c) LH and LL, (d) RH and RL, (e) LH and RL and (f) RH and LL respectively.

the mean values are very low except for LC2L. The median values lie within ± 1 in all 4 cases. The SD value is minimum for LC2H, but is a very high maximum for LC2L. Among the other 2 cases, the SD for LC1H is higher than that for LC1L. These parameters are all highly left skewed except LC1L which is highly right skewed. Kurtosis is also very high compared to the normal distribution in all cases with that for LC2H being reasonably less.

Hence, it is evident from the characteristics of these coefficients also that the bilaterality of the DDP signals carry significant information and further, that this information varies for the hand and the leg signals. More specifically, while the LC1 parameters for the hand and leg signals are similar in magnitude and indicative of their similarity, the respective LC2 parameters being distinctly different are useful in differentiating the two sets of signals.

5.4.2 Bilaterality of DDP signals

Hence, the bilaterality of the DDP signals have been explored in more detail in terms of their trends, bias, debiased signals as well as similar features for a set of derived signals.

Trends of pairs of bilateral signals

To understand the bilateral relationship between left and right, signals are considered as pair, namely the LH signal with the corresponding RH signal and the LL signal with its corresponding RL signal. As these individual signals are either increasing, decreasing or constant, therefore possible 4 types of pairs can be observed. These are converging, diverging, cross-over and parallel [5]. For the study of individual signal trends, the limit of classification is considered as $\pm 2mV$. Hence the limit for classifying pair of signals is taken to be $\pm 4mV$. The conditions for these 4 classes have been given as follows.

Let the first difference be denoted as $d_1 = x_{left1} - x_{right1}$ and the last difference be denoted as $d_{2400} = x_{left2400} - x_{right2400}$.

$$Pair\ \ of\ \ signal \begin{cases} Crossing: & if\ d_1 > 0mV\ and\ d_{2400} < 0mV\ or\ vice\ versa \\ Converging: & if\ (d_1 - d_{2400}) > +4mV\ with\ same\ sign \\ Diverging: & if\ (d_1 - d_{2400}) < -4mV\ with\ same\ sign \\ Parallel: & if\ -4mV \leq (d_1 - d_{2400}) \leq +4mV,\ same\ sign \end{cases}$$

Examples of all 4 trends of pair of signals are shown in Figure 5.36. These different patterns have been recorded at different times from 4 randomly selected subjects. The % occurrence of these trends for the (LH, RH) and

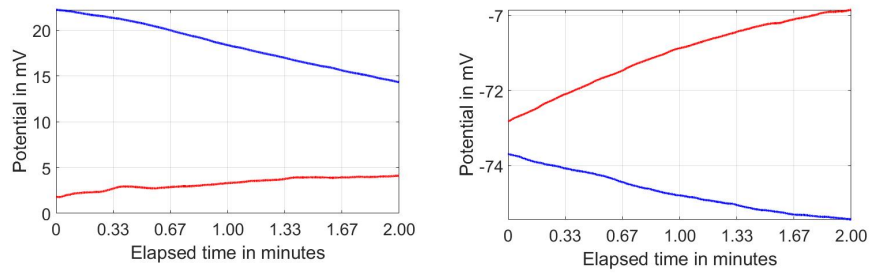

(a)

(b)

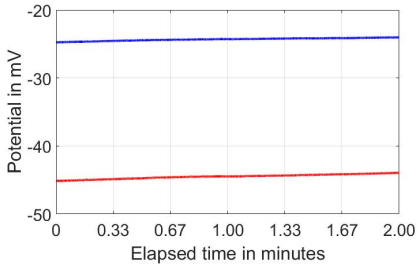

(c)

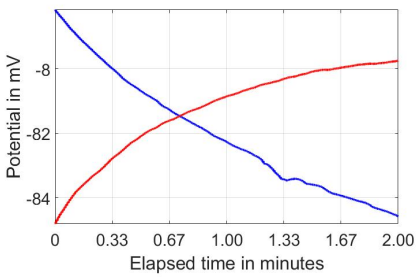

(d)

Figure 5.32: Representative time series plots of (a) Converging pair, (b) Diverging pair, (c) Parallel pair and (d) Cross-over pair of signals

(LL, RL) pairs of signals have been calculated and tabulated in Table 5.18 while their bar plots are shown in Figure 5.33.

From the analysis, it is found that the % occurrence of converging, diverging and parallel pairs are very close to each other for both the hand and leg pairs of signals. Among these three, parallel type dominates with 36.59% and 40.35% for the LH-RH pair and LL-RL pair respectively. This is followed by diverging type with 35.64% and 28.95% and converging type with 24.95% and 28.36% occurrences respectively. Cross-over patterns appear in only 2.82% and 2.34% for the LH-RH pairs and LL-RL pairs.

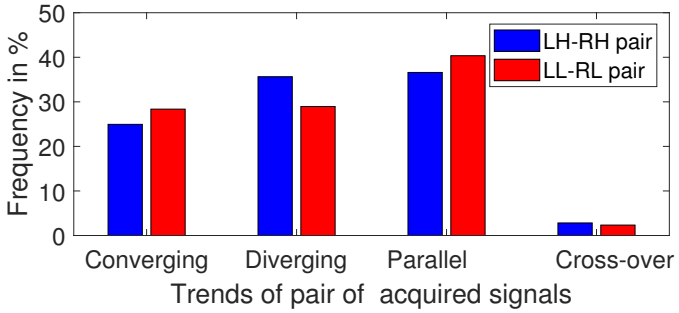

Figure 5.33: Bar plot of different trends of pairs of acquired hand and feet signals

Table 5.18: Occurrence in % of different trends of 2 pairs of acquired signals

Parameters	Converging in %	Diverging in %	Parallel in %	Cross-over in %
LH-RH pair	24.94	35.64	36.60	2.82
LL-RL pair	28.36	28.95	40.35	2.34

Derived signals

As suggested in Bhattacharya [5], 4 bilateral interaction signals, henceforth also referred to as the derived signals, have been considered in this case also. These 4 signals are defined as:

GapH : Gap signal of hand = LH_k - RH_k

PSH : Pair sum signal of hand = LH_k + RH_k

GapL : Gap signal of leg = LL_k - RL_k

PSL : Pair sum signal of leg = LL_k + RL_k

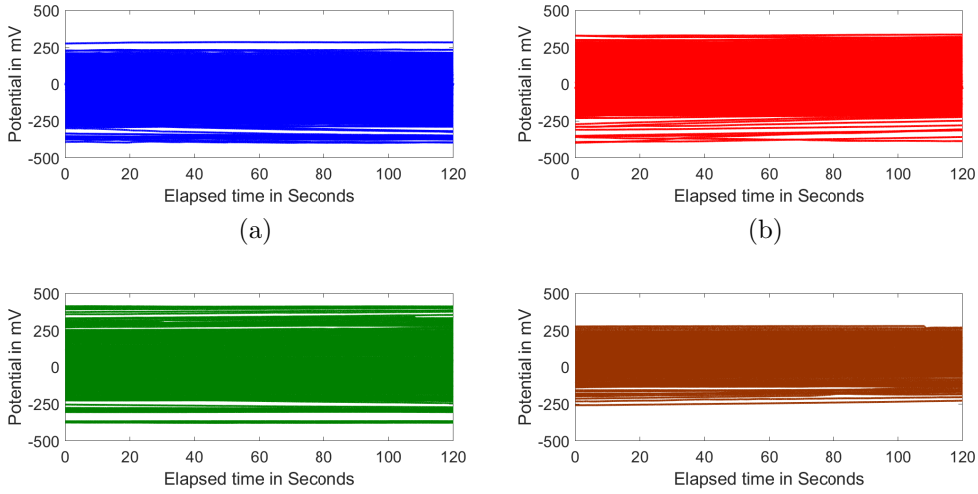

Figure 5.34: Time series plots of all (a) GapH, (b) PSH, (c) GapL and (d) PSL signals

The time series plots of all the 4 types of derived signals are shown in Figure 5.34 while their ranges have been tabulated in Table 5.19. It can be seen that as in the case of the acquired DDP signals, the derived signals also seem constant in these plots. However, the span of these derived signals are higher compared to the acquired signals and lie within $\pm 400mV$.

The CDF plots of the 4 acquired DDP signals as well the 4 derived signals are shown in Figure 5.35a and Figure 5.35b respectively for comparison. The standard statistical parameters of the derived signals are tabulated in Table. 5.19. These can be compared to those of the acquired signals as tabulated in Table. 5.2.

It can be seen that more than 95% of acquired hand signals lie within ±200mV, whereas 90% of feet signals lie within ±200mV. In case of derived hand signals, 90% of signals lie within ±200mV, whereas more than 80% of derived feet signals lie within ±200mV. SD (σ) values of acquired hand signals are higher than that of acquired feet signals. In case of derived signals also, σ values are higher for hand signals than that of feet signals. Skewness and kurtosis values are close to normal but none of these 8 acquired and derived signals are normally distributed.

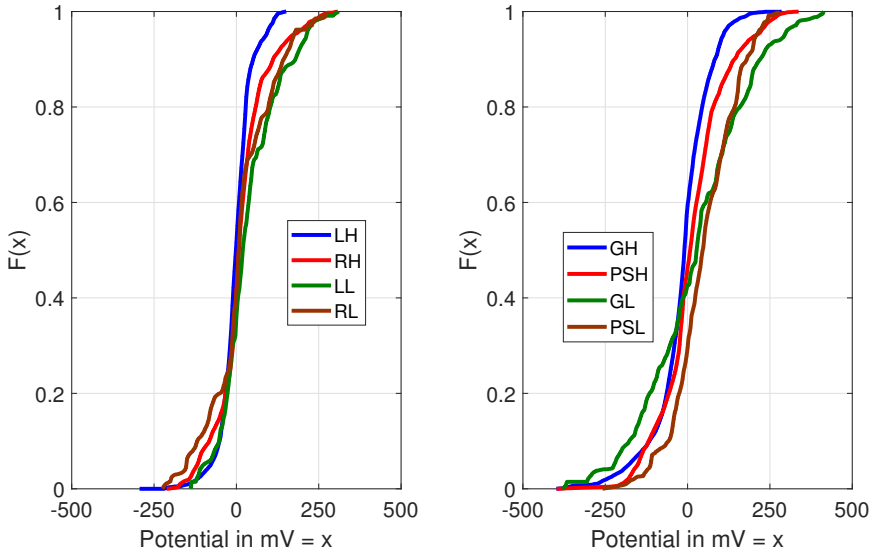

(a) (b)

Figure 5.35: CDF plots of (a) 4 acquired signals (b) 4 derived signals

Table 5.19: Statistical characteristics of 4 types of derived signals

Parameters	Range in mV		μ in mV	Median in mV	σ in mV	Skewness	Kurtosis
	Min	Max					
GH	-398.37	286.47	-15.88	-9.76	84.92	-0.86	5.40
PSH	-397.80	337.12	12.83	7.76	99.82	0.19	3.72
GL	-378.16	413.38	23.20	27.47	156.33	-0.03	2.84
PSL	-258.90	280.10	50.38	46.13	96.13	-0.13	2.90

Bias of the derived signals

As stated earlier, the setwise mean value is considered as the bias of the corresponding signal in this work.

Plots of the CDF of the mean values of the 4 acquired and 4 derived DDP signals are shown in Figure 5.36. It is observed that these plots are almost identical to the CDF plots of the acquired and derived DDP signals in Figure 5.35. So, the bias of the signals can be considered to be representative of the actual signals for both the acquired and the derived set of signals.

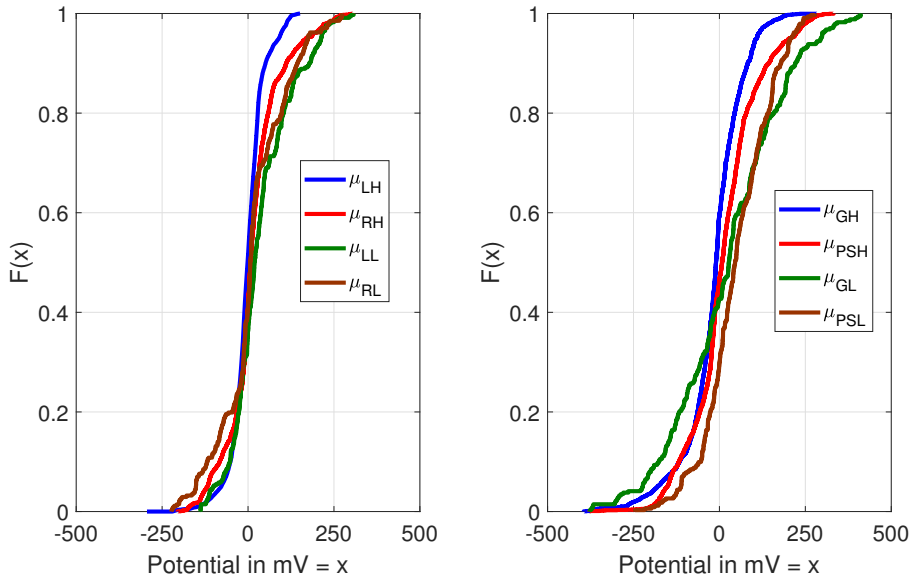

(a) (b)

Figure 5.36: CDF plots of mean values (μ) of (a) 4 acquired signals (b) 4 derived signals

Standard statistical quantities of 4 acquired signals are tabulated in Table 5.5, whereas, standard statistical quantities for 4 derived signals are tabulated in Table 5.20. Comparing these two tables with Table 5.2 and Table 5.19, it can be said that the mean can be treated as the representative of the actual signals. It can further be seen from these two tables that the span of the derived signals are significantly higher than that of the acquired signals. Additionally, the SD of both acquired and derived feet signals are higher than that of hand signals. The other parameters are close to each other.

Table 5.20: Standard statistical parameters of subsetwise mean values of GapH,PSH, GapL and PSL signals

Parameters	Range in mV		μ in mV	Median in mV	σ in mV	Skewness	Kurtosis
	Min	Max					
μ_{GapH}	-394.80	284.37	-15.88	-9.95	84.82	-0.86	5.40
μ_{PSH}	-378.38	332.48	12.83	7.87	99.73	0.19	3.71
μ_{GapL}	-377.22	411.31	23.20	27.24	156.51	-0.04	2.84
μ_{PSL}	-245.53	278.28	50.38	45.51	96.21	-0.13	2.89

Debiased derived signals

In a further study, the debiased derived signals are obtained by subtracting the setwise mean from the derived signal dataset, as has been done to obtain the debiased signals for the acquired DDP signals. These have been studied in order to compare their characteristics with those of the debiased acquired signals.

In order to study the deviation characteristics of derived signals, debiased GapH, debiased PSH, debiased GapL and debiased PSL signals are plotted in Figure 5.37 while their standard statistical parameters are tabulated in Table 5.21. As expected, these derived signals have natures that are quite similar to those of the acquired signals. In this case also, the debiased signals are butterfly like in nature and the ranges of the derived hand signals are higher than that of the derived feet signals.

Since neither of these debiased derived signals are totally 0, nor totally positive or negative, hence it may be interpreted that they are instrumental in ensuring the interdependence between the pair of bilateral signals.

Table 5.21: Standard statistical parameters of debiased GapH, PSH, GapL and PSL signals

Parameter	Range in mV		σ in mV	Skewness	Kurtosis
	Min	Max			
debiased GapH	-35.87	68.32	4.44	1.13	25.12
debiased PSH	-60.32	27.58	4.75	-0.23	25.68
debiased GapL	-33.05	34.60	5.50	0.06	9.49
debiased PSL	-28.59	22.03	5.08	-0.30	6.57

The CDF plots of the debiased derived signals as well as the corresponding

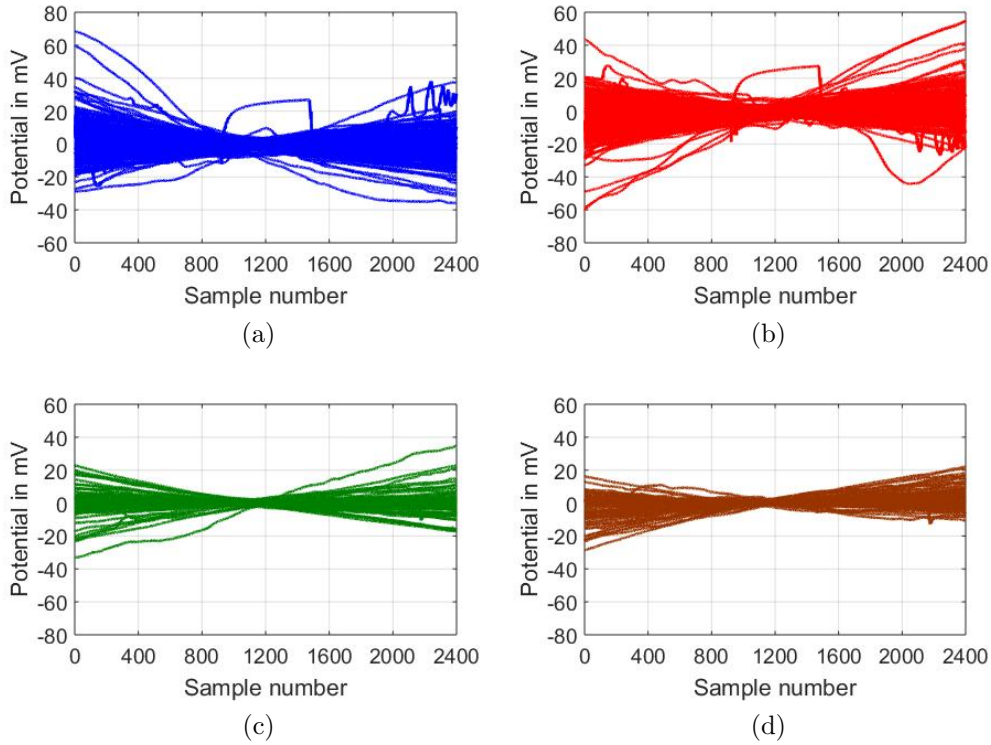

Figure 5.37: Time series plots of all (a) debiased GapH, (b) debiased PSH, (c) debiased GapL and (d) debiased PSL signals

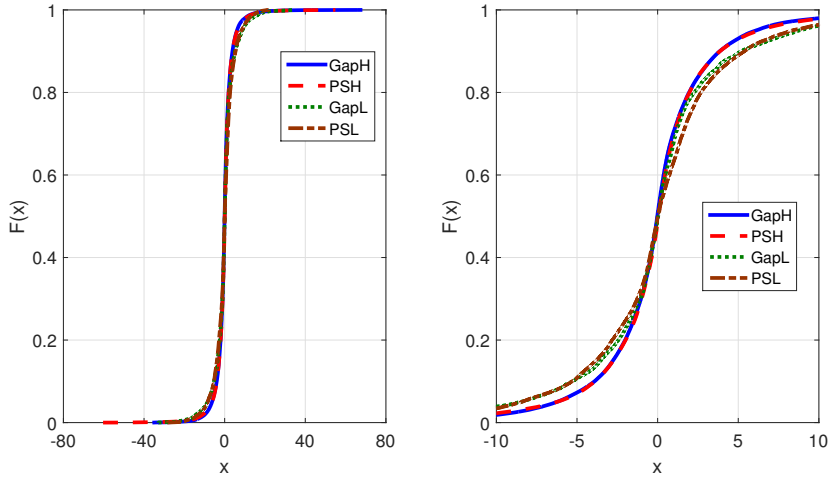

Figure 5.38: CDF plots of (a) all debiased derived signals (b) their zoomed plots within ±10 mV

zoomed CDFs in the range ±10mV are shown in Figure 5.38. From the plot, it can be said that the debiased GapH and PSH signals are very much similar to each other, while the debiased GapL and PSL signals are similar to each other. More than 80% of these 4 debiased derived signals lie within ±10 mV.

5.4.3 Interdependencies of means, ZCIs and slopes

Interdependence of signal mean values: In view of the observed interdependence of the LH and RH signals, the pairwise characteristics of their respective mean values, μ_{LH} vs. μ_{RH}, are observed using a scatter plot in Figure 5.39. Considering (0,0) mV as reference point, it is observed that the pairwise mean values mostly lie in a region very close to the reference point, but spread in all four quadrants. The first quadrant contains those pairs for which both μ_{LH} and μ_{RH} are positive. Similarly, those pairs with μ_{LH} negative and μ_{RH} positive lie in the second quadrant. The third quadrant contains pairs in which both μ_{LH} and μ_{RH} are negative, while those pairs with μ_{LH} positive and μ_{RH} negative lie in the fourth quadrant.

Furthermore, for an in-depth study, each quadrant is bisected into two segments using the lines $\mu_{LH} = \mu_{RH}$ for quadrants I and III and $\mu_{LH} = -\mu_{RH}$ for quadrants II and IV. All 8 sub-regions and their corresponding names are shown in Figure 5.39. Characteristics of data points belonging to these 8 sub-regions are stated in Table 3 along with the % data points present in

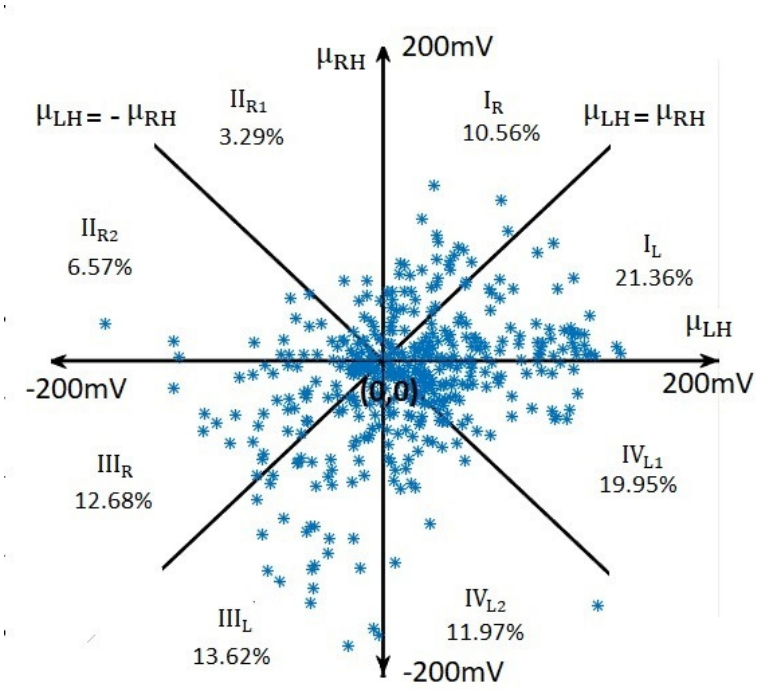

Figure 5.39: Scatter plot of μ_{LH} vs.μ_{RH} with marked 8 sub-regions

Table 5.22: Different conditions and data present in % in 8 sub-regions of (μ_{LH}, μ_{RH})

Sub-regions	Properties of (μ_{LH}, μ_{RH})	Count in % of (μ_{LH}, μ_{RH})
I_L	$\mu_{LH} \geq \mu_{RH} \geq 0$	21.35
I_R	$\mu_{RH} \geq \mu_{LH} \geq 0$	10.56
II_{R1}	$\mu_{RH} \geq 0 \geq \mu_{LH}$, $\lvert\mu_{RH}\rvert \geq \lvert\mu_{LH}\rvert$	3.29
II_{R2}	$\mu_{RH} \geq 0 \geq \mu_{LH}$, $\lvert\mu_{RH}\rvert \leq \lvert\mu_{LH}\rvert$	6.57
III_R	$\mu_{LH} \leq \mu_{RH} \leq 0$	12.68
III_L	$\mu_{RH} \leq \mu_{LH} \leq 0$	13.62
IV_{L2}	$\mu_{RH} \leq 0 \leq \mu_{LH}$, $\lvert\mu_{LH}\rvert \leq \lvert\mu_{RH}\rvert$	11.97
IV_{L1}	$\mu_{RH} \leq 0 \leq \mu_{LH}$, $\lvert\mu_{RH}\rvert \leq \lvert\mu_{LH}\rvert$	19.95

each region. It can be seen from Figure 8 and Table 3 that more than 66% signals lie below the $\mu_{LH} = \mu_{RH}$ line. Hence, $\mu_{LH} \geq \mu_{RH}$ is more likely than the other alternative by more than 2 times.

In order to understand the interdependence between the bias values of feet signals and hand signals μ_{LL} vs. μ_{RL} is plotted in Figure 5.40. Here also the whole region is divided into 8 sub regions. Conditions of these sub regions are tabulated in Table 5.23. Amount of data present in % in these regions have also been tabulated in this table. It is found from the study that 66.66% of data lie at the positive side of μ_{LL}. Therefore only 33.37% data lies at the negative side of μ_{LL}. This finding little differs from the analysis of Figure 5.39 that for most of the cases $\mu_{LH} > \mu_{RH}$.

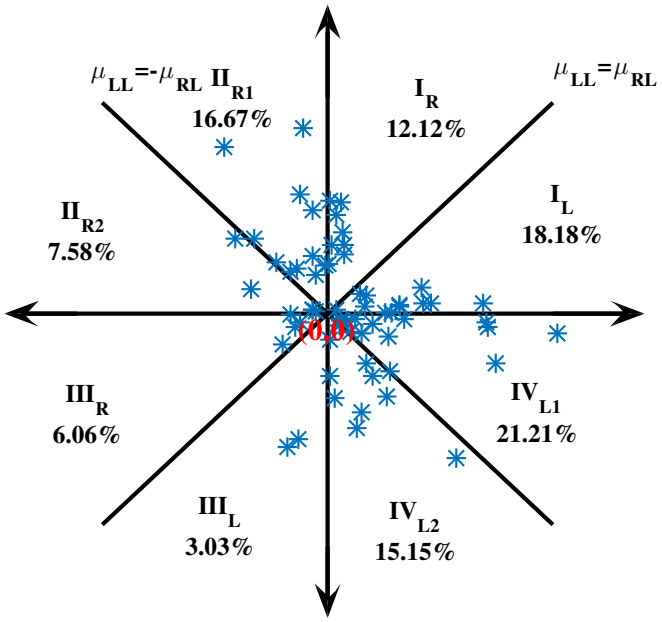

Figure 5.40: Scatter plot of μ_{LL} vs.μ_{RL} with marked 8 sub-regions

Interdependence of ZCIs: Pairwise nature of the ZCI of the debiased LH and RH signals is studied. For this, the scatter plot of ZCI_{LH} and ZCI_{RH} is plotted in Figure 5.41 containing 8 sub-regions similar to that used to study the μ_{LH} vs. μ_{RH} characteristics. The characteristics of the data points in these 8 sub-regions and their counts in % are tabulated in in Table 5.24. Here the (1200, 1200) instants is considered as the reference point. The sub-regions in this case are similarly denoted as in case of Figure 5.39 and may be similarly interpreted.

Table 5.23: Different conditions and data present in % in 8 sub-regions of (μ_{LL}, μ_{RL})

Sub-regions	Properties of (μ_{LL}, μ_{RL})	Count in % of (μ_{LL}, μ_{RL})
I_L	$\mu_{LL} \geq \mu_{RL} \geq 0$	18.18
I_R	$\mu_{RL} \geq \mu_{LL} \geq 0$	12.12
II_{R1}	$\mu_{RL} \geq 0 \geq \mu_{LL}$, $\lvert\mu_{RL}\rvert \geq \lvert\mu_{LL}\rvert$	16.67
II_{R2}	$\mu_{RL} \geq 0 \geq \mu_{LL}$, $\lvert\mu_{RL}\rvert \leq \lvert\mu_{LL}\rvert$	7.58
III_R	$\mu_{LL} \leq \mu_{RL} \leq 0$	6.06
III_L	$\mu_{RL} \leq \mu_{LL} \leq 0$	3.03
IV_{L2}	$\mu_{RL} \leq 0 \leq \mu_{LL}$, $\lvert\mu_{LL}\rvert \leq \lvert\mu_{RL}\rvert$	15.15
IV_{L1}	$\mu_{RL} \leq 0 \leq \mu_{LL}$, $\lvert\mu_{RL}\rvert \leq \lvert\mu_{LL}\rvert$	21.21

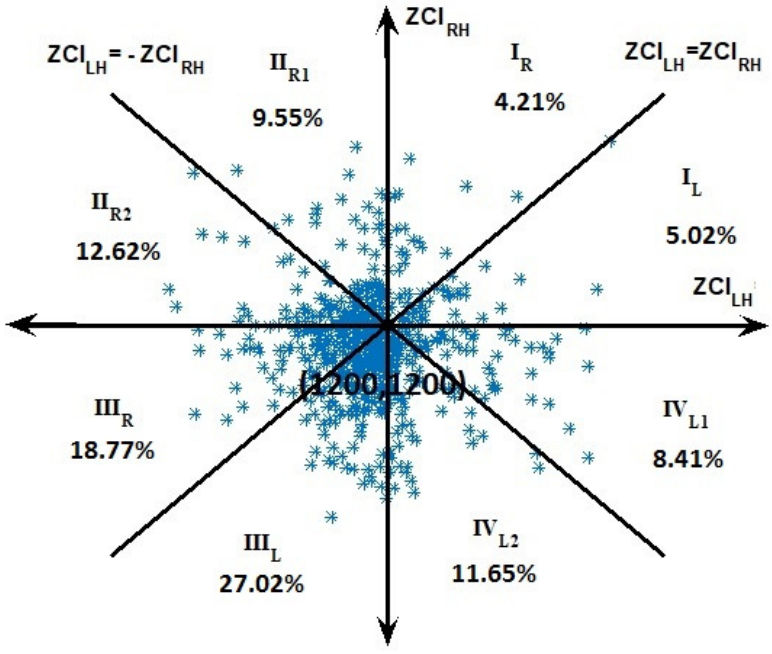

Figure 5.41: Scatter plot of ZCI_{LH} vs.ZCI_{RH} with marked 8 sub-regions

Table 5.24: Different conditions and data present in % in 8 sub-regions of (ZCI_{LH}, ZCI_{RH})

Sub-regions	Properties of (ZCI_{LH}, ZCI_{RH})	Count in % of (ZCI_{LH}, ZCI_{RH})
I_L	$ZCI_{LH} \geq ZCI_{RH} \geq 0$	5.02
I_R	$ZCI_{RH} \geq ZCI_{LH} \geq 0$	4.21
II_{R1}	$ZCI_{RH} \geq 0 \geq ZCI_{LH}$, $\lvert ZCI_{RH}\rvert \geq \lvert ZCI_{LH}\rvert$	9.55
II_{R2}	$ZCI_{RH} \geq 0 \geq ZCI_{LH}$, $\lvert ZCI_{RH}\rvert \leq \lvert ZCI_{LH}\rvert$	12.62
III_R	$ZCI_{LH} \leq ZCI_{RH} \leq 0$	18.77
III_L	$ZCI_{RH} \leq ZCI_{LH} \leq 0$	27.02
IV_{L2}	$ZCI_{RH} \leq 0 \leq ZCI_{LH}$, $\lvert ZCI_{LH}\rvert \leq \lvert ZCI_{RH}\rvert$	11.65
IV_{L1}	$ZCI_{RH} \leq 0 \leq ZCI_{LH}$, $\lvert ZCI_{RH}\rvert \leq \lvert ZCI_{LH}\rvert$	8.41

In this case also, the pairwise points (ZCI_{LH}, ZCI_{RH}) are spread in all four quadrants in a region very close to the reference point. It is further noted that both the signals do not necessarily cross the zero value simultaneously. However, the 3^{rd} quadrant contains 45.79% of the data and the 1_{st} quadrant contains only 9.23% of the total data. Following this analysis further, it is observed that only 28% of ZCI pairs lie above the $ZCI_{LH} = -ZCI_{RH}$ line. Analytically, this region satisfies the condition $(ZCI_{LH} - 1200) > -(ZCI_{RH} - 1200)$ and so, $(ZCI_{LH} + ZCI_{RH}) > 2400$. This indicates that in majority cases, ZCI_{LH} and ZCI_{RH} are significantly likely to be less than 1200 individually and less than 2400 as a pair.

Interdependence between ZCI_{LL} and ZCI_{RL} has also been studied by plotting scatter plot in Figure 5.42. The same study was performed in sec. 5.3.5 also. Comparing Figure 5.42 with Figure 5.41 it can be said that in hand and feet signals more than 45% data lies at the third quadrant. Whereas data at rest of three quadrants are almost equally likely. Different conditions at all of 8 subregions of the Figure 5.42 along with data present in % are tabulated in Table 5.25.

Interdependence of signal slopes Furthermore m_{LH} vs. m_{RH} plot is done in order to study the hemispheric dominance in terms of signal slope. Figure 5.43 represents the scatter plot.Reference is considered at (0,0)mV/instant. The characteristics of the data in 8 sub-regions marked on the scatter plot along with the % data count in each sub-region are stated

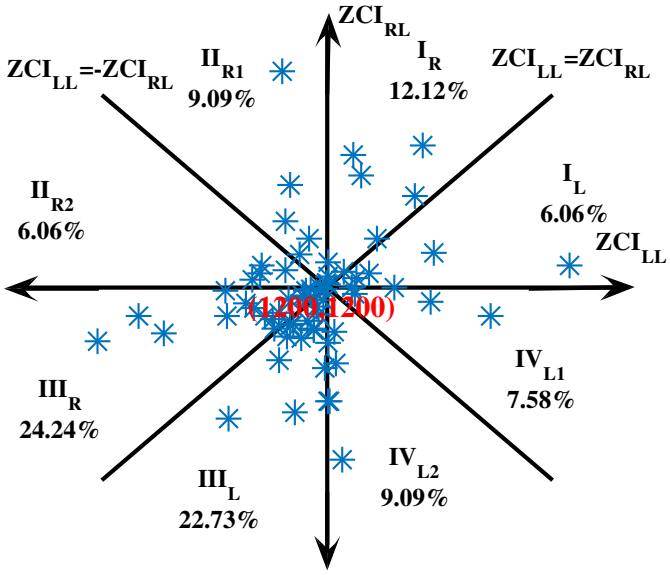

Figure 5.42: Scatter plot of ZCI_{LL} vs.ZCI_{RL} with marked 8 sub-regions

Table 5.25: Different conditions and data present in % in 8 sub-regions of (ZCI_{LL}, ZCI_{RL})

Sub-regions	Properties of (ZCI_{LL}, ZCI_{RL})	Count in % of (ZCI_{LL}, ZCI_{RL})
I_L	$ZCI_{LL} \geq ZCI_{RL} \geq 0$	6.06
I_R	$ZCI_{RL} \geq ZCI_{LL} \geq 0$	12.12
II_{R1}	$ZCI_{RL} \geq 0 \geq ZCI_{LL}$, $\lvert ZCI_{RL}\rvert \geq \lvert ZCI_{LL}\rvert$	9.09
II_{R2}	$ZCI_{RL} \geq 0 \geq ZCI_{LL}$, $\lvert ZCI_{RL}\rvert \leq \lvert ZCI_{LL}\rvert$	6.06
III_R	$ZCI_{LL} \leq ZCI_{RL} \leq 0$	24.24
III_L	$ZCI_{RL} \leq ZCI_{LL} \leq 0$	22.73
IV_{L2}	$ZCI_{RL} \leq 0 \leq ZCI_{LL}$, $\lvert ZCI_{LL}\rvert \leq \lvert ZCI_{RL}\rvert$	9.09
IV_{L1}	$ZCI_{RL} \leq 0 \leq ZCI_{LL}$, $\lvert ZCI_{RL}\rvert \leq \lvert ZCI_{LL}\rvert$	7.58

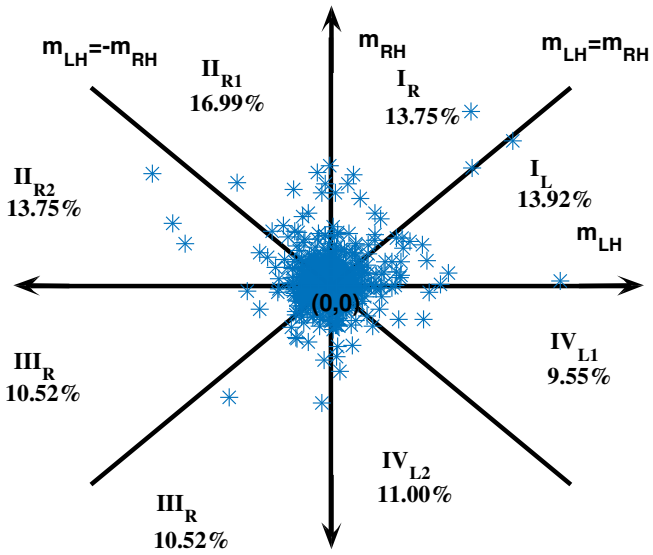

Figure 5.43: Scatter plot of m_{LH} vs.m_{RH} with marked 8 sub-regions

in Table 5.26. It is observed that both debiased LH as well as the debiased RH signals have larger or smaller slopes as well as negative and positive slopes. In several cases, the slopes are likely to be opposite in signs also. Hence, almost all debiased signal pairs are crossing in nature. From the % count of the data in the various sub-regions, it is observed that more than 55% data belong to the region above $m_{LH} = m_{RH}$. This can be interpreted as a significant probability of m_{RH} being larger than m_{LH}.

In order to understand the hemispheric dominance in feet signals scatter plot of m_{LL} vs. m_{RL} is plotted in Figure 5.44 as like as Figure 5.43. In same way the whole region is divided into 8 sub regions. Conditions of all 8 subregions with number of data present in % are tabulated in Table 5.27. From this analysis it can be seen that more than 55% data lies below $m_{LL} = m_{RL}$ line. This completely opposite finding from the finding of the study of slope of hand signals.

5.4.4 Proposed bias parameters

Differential bias (μ_{diff}) A new parameter differential bias (μ_{diff}) is proposed which is the difference between setwise mean values of LH and corresponding RH signals. This can also be considered as the mean of

Table 5.26: Different conditions and data present in % in 8 sub-regions of (m_{LH}, m_{RH})

Sub-regions	Properties of (m_{LH}, m_{RH})	Count in % of (m_{LH}, m_{RH})
I_L	$m_{LH} \geq m_{RH} \geq 0$	13.92
I_R	$m_{RH} \geq m_{LH} \geq 0$	13.75
II_{R1}	$m_{RH} \geq 0 \geq m_{LH}$, $\lvert m_{RH}\rvert \geq \lvert m_{LH}\rvert$	16.99
II_{R2}	$m_{RH} \geq 0 \geq m_{LH}$, $\lvert m_{RH}\rvert \leq \lvert m_{LH}\rvert$	13.75
III_R	$m_{LH} \leq m_{RH} \leq 0$	10.52
III_L	$m_{RH} \leq m_{LH} \leq 0$	10.52
IV_{L2}	$m_{RH} \leq 0 \leq m_{LH}$, $\lvert m_{LH}\rvert \leq \lvert m_{RH}\rvert$	11.00
IV_{L1}	$m_{RH} \leq 0 \leq m_{LH}$, $\lvert m_{RH}\rvert \leq \lvert m_{LH}\rvert$	9.55

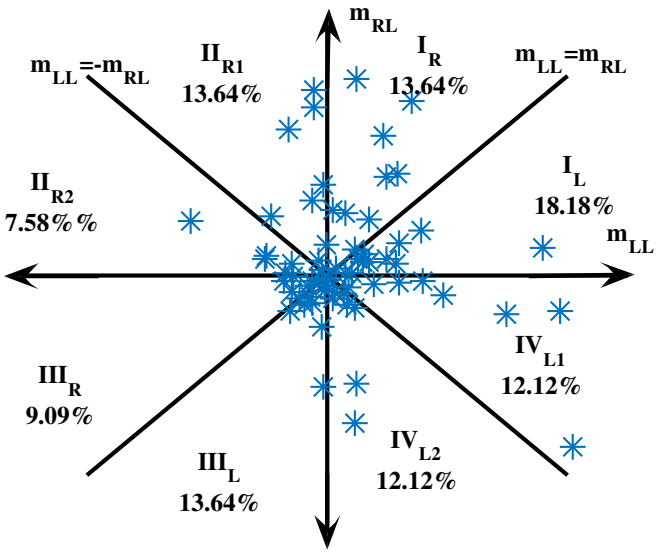

Figure 5.44: Scatter plot of m_{LL} vs.m_{RL} with marked 8 sub-regions

Table 5.27: Different conditions and data present in % in 8 sub-regions of (m_{LL}, m_{RL})

Sub-regions	Properties of (m_{LL}, m_{RL})	Count in % of (m_{LL}, m_{RL})
I_L	$m_{LL} \geq m_{RL} \geq 0$	18.18
I_R	$m_{RL} \geq m_{LL} \geq 0$	13.64
II_{R1}	$m_{RL} \geq 0 \geq m_{LL}$, $\lvert m_{RL}\rvert \geq \lvert m_{LL}\rvert$	13.64
II_{R2}	$m_{RL} \geq 0 \geq m_{LL}$, $\lvert m_{RL}\rvert \leq \lvert m_{LL}\rvert$	7.58
III_R	$m_{LL} \leq m_{RL} \leq 0$	9.09
III_L	$m_{RL} \leq m_{LL} \leq 0$	13.64
IV_{L2}	$m_{RL} \leq 0 \leq m_{LL}$, $\lvert m_{LL}\rvert \leq \lvert m_{RL}\rvert$	12.12
IV_{L1}	$m_{RL} \leq 0 \leq m_{LL}$, $\lvert m_{RL}\rvert \leq \lvert m_{LL}\rvert$	12.12

Gap signals. Thus,

$$\begin{aligned} \mu_{diffH} &= \mu_{LH} - \mu_{RH} \\ \mu_{diffL} &= \mu_{LL} - \mu_{RL} \end{aligned} \tag{5.12}$$

In order to characterize the differential bias, its statistical parameters are tabulated in Table 5.28. The corresponding CDF plot and quantile-quantile plot (QQ plot) are shown in Figure 5.45, while the chi-square test results for normality are tabulated in Table 5.29.

Table 5.28: Standard statistical parameters of μ_{diffH} and μ_{diffL}

Para-meters	Range in mV		μ in mV	median in mV	σ in mV	Skewness	Kurtosis
	Min	Max					
μ_{diffH}	-301.55	284.37	6.13	12.92	68.15	-0.42	4.06
μ_{diffL}	-377.22	380.02	20.26	30.28	146.82	-0.10	3.12

As shown in Figure 5.45a, the nature of CDF of μ_{diffH} shows a normal like distribution. From this figure and the chi-square test results, it can be seen that the data lies within the 97.5% confidence limit for the total range. It is to be noted that in comparison to the mean and median of the parameters μ_{LH} ($8.59mV$ and 10.35 respectively) and μ_{RH} ($2.46mV$ and $1.55mV$ respectively), the mean ($6.13mV$) and the median ($12.92mV$) for μ_{diffH} are very close to each other. The QQ

Table 5.29: Chi square test for μ_{diffH} and μ_{diffL}

Hypothesis	H_0: μ_{diffH} is normally distributed H_A: μ_{diffH} is not normally distributed			
df=11	$\chi^2_{0.975}$	$\chi^2_{0.95}$	$\chi^2_{0.05}$	$\chi^2_{0.025}$
Theoretical	3.816	4.575	19.675	21.920
Experimental	3.639	3.639	3.639	3.639
Conclusion	H_A rejected	H_A rejected	H_A rejected	H_A rejected
Hypothesis	H_0: μ_{diffL} is normally distributed H_A: μ_{diffL} is not normally distributed			
df=4	$\chi^2_{0.975}$	$\chi^2_{0.9}$	$\chi^2_{0.1}$	$\chi^2_{0.025}$
Theoretical	0.48	1.06	7.78	11.143
Experimental	1.7018	1.7018	1.7018	1.7018
Conclusion	H_0 rejected	H_0 rejected	H_A rejected	H_A rejected

plot also shows that till the 2nd quantile, the data almost follows the normal probability fit line. Therefore, it can be said that the parameter μ_{diffH} varies within $6.13 \pm 136.30mV$ for 95% of the generally healthy population considered in this study. Hence, it can be said that in a healthy person, the dynamically changing LH and RH biopotentials will not be identical. This is typically characterized by a non-zero differential bias.

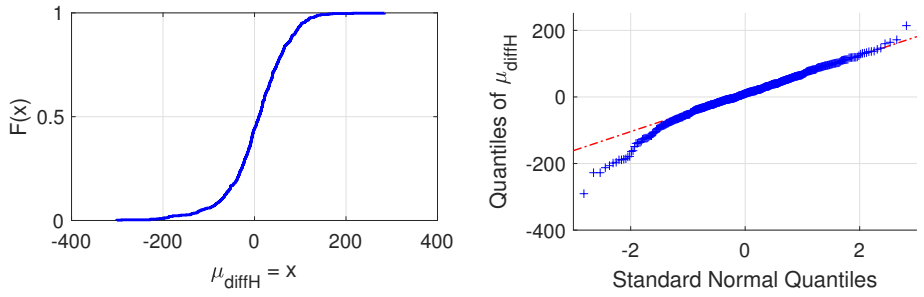

(a) (b)

Figure 5.45: (a) Cumulative distribution function (CDF) and (b) quantile-quantile (QQ) plots of differential bias

Differential bias (μ_{diffL})is studied and standard statistical quantities are calculated for feet signals also. Results are tabulated in Table 5.28. Comparing with μ_{diffH}, it can be said that span of (μ_{diffL}) of feet signals is much higher than that of hand signals. Mean and median values are also much more positive. Standard deviation is also more than 2 times of hand signals. Skewness and kurtosis values are close to a normal distribution.

CDF plot is done to study the distribution of this parameter in Figure 5.46a, which shows a normal like 'S' shape distribution. Chi-square goodness of fit test is performed to test for normality in Table 5.29. The result confirms the normality of μ_{diffL} with 90% confidence limit. Furthermore, q-q plot have also been done in Figure 5.46b. From this figure it can be seen that this plot is linear roughly from -1 to +2 quantile.

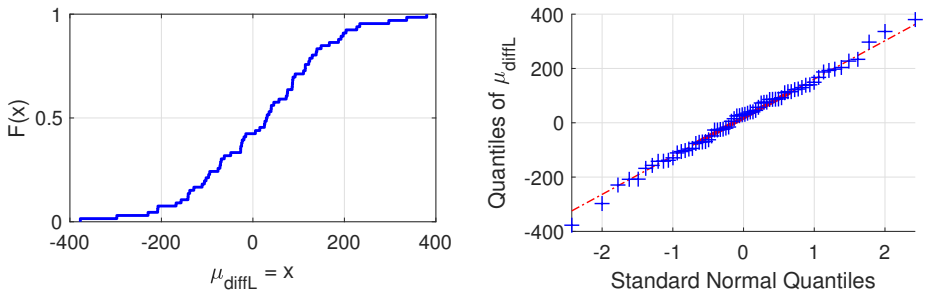

(a) (b)

Figure 5.46: (a) Cumulative distribution function (CDF) and (b) quantile-quantile (QQ) plots of differential bias of the feet signals

Common mode bias (μ_{cb}) A new parameter, common mode bias (μ_{cbH} and μ_{cbL}), is proposed which is the sum between setwise mean values of LH and corresponding RH signals or LL and corresponding RL signals. This can also be considered as the mean of PS signals. Thus,

$$\begin{aligned} \mu_{cbH} &= \mu_{LH} + \mu_{RH} \\ \mu_{cbL} &= \mu_{LL} + \mu_{RL} \end{aligned} \tag{5.13}$$

To characterize the common mode bias, its statistical parameters are tabulated in Table 5.30. Along with corresponding CDF plot and quantile-quantile plot (QQ plot) have also been plotted in Figure 5.47. The chi-square test results for normality are tabulated in Table 5.31.

Table 5.30: Standard statistical parameters of μ_{cbH} and μ_{cbL}

Parameters	Range in mV		μ in mV	Median in mV	σ in mV	Skewness	Kurtosis
	Min	Max					
μ_{cbH}	-348.71	271.82	11.05	34.38	88.18	-0.25	3.98
μ_{cbL}	-245.53	278.28	42.78	35.21	102.51	-0.23	3.24

Table 5.31: Chi square test for μ_{cbH} and μ_{cbL}

Hypothesis	H_0: μ_{cbH} is normally distributed H_A: μ_{cbH} is not normally distributed			
df=7	$\chi^2_{0.975}$	$\chi^2_{0.95}$	$\chi^2_{0.05}$	$\chi^2_{0.025}$
Theoretical	1.690	2.167	14.067	16.013
Experimental	35.99	35.99	35.99	35.99
Conclusion	H_0 rejected	H_0 rejected	H_0 rejected	H_0 rejected
Hypothesis	H_0: μ_{cbL} is normally distributed H_A: μ_{cbL} is not normally distributed			
df=4	$\chi^2_{0.975}$	$\chi^2_{0.90}$	$\chi^2_{0.10}$	$\chi^2_{0.025}$
Theoretical	0.207	1.064	7.779	11.143
Experimental	3.9658	3.9658	3.9658	3.9658
Conclusion	H_0 rejected	H_0 rejected	H_A rejected	H_A rejected

It can be seen from Table 5.30 that range of this parameter is 620.53mV, quite high than differential bias parameter. Standard deviation (σ) is also very high, although skewness and kurtosis values are close to a normal distribution. Figure 5.47a represents CDF of μ_{cbH}, shows a normal like distribution pattern, though Q-Q plot in Figure 5.47b and Table 5.31 have confirmed that the data is not distributed normally. Hence, it can be said that in a healthy person, the common mode bias of hand signals is not normally distributed.

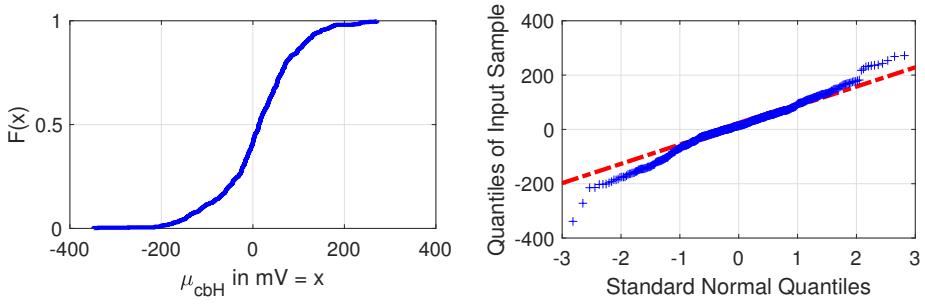

(a) (b)

Figure 5.47: (a) Cumulative distribution function (CDF) and (b) quantile-quantile (QQ) plots of common mode bias

Furthermore, common mode bias is studied for feet signals also and named as μ_{cbL}. Standard statistical parameters are also calculated for μ_{cbL} of feet signals in Table 5.30. Unlike the hand signals, range of μ_{cbL} of feet signals is very low, though overall σ is higher. Chi-square goodness of fit test shows normality of the parameter for feet signal. Result of this test is also tabulated in Table 5.31.

5.4.5 Proposed debiased signal parameters

In order to quantify the interdependent dynamic character of the acquired biopotentials, three new parameters are proposed. These parameters are related to the debiased signals. These proposed parameters are

Slope ratio : A new parameter termed as slope ratio (m_{ratioH} and m_{ratioL}) is proposed to compare the overall deviations in a pair of LH and RH signals and LL and RL signals. This parameter is described in 5.14. Here m_{ratioH} is the ratio of m_{LH} and m_{RH}, whereas, m_{ratioL} is the ratio of m_{LL} and m_{RL}. Statistical characteristics of these parameters are

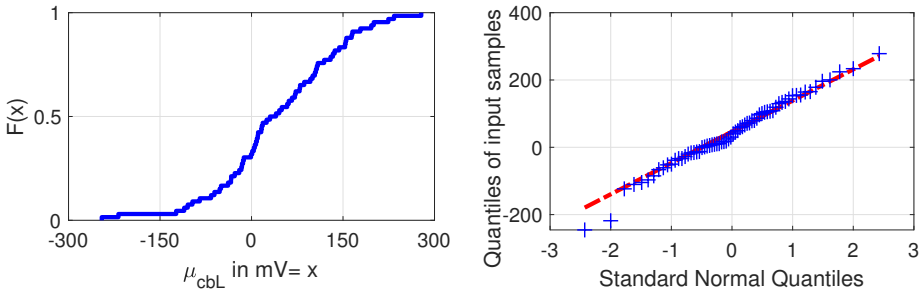

(a) (b)

Figure 5.48: (a) Cumulative distribution function (CDF) and (b) quantile-quantile (QQ) plots of μ_{cbL}

tabulated in Table 5.32 and the zoomed CDF plot from 5% to 95% data of m_{ratioH} and m_{ratioL} are shown in Figure 5.49.

$$\begin{aligned} m_{ratioH} &= \frac{m_{LH}}{m_{RH}} \\ m_{ratioL} &= \frac{m_{LL}}{m_{RL}} \end{aligned} \tag{5.14}$$

Table 5.32: Statistical characterization of m_{ratioH} and m_{ratioL}

Parameters	Range in mV		μ in	σ in	Skewness	Kurtosis
	Min	Max	mV	mV		
m_{ratioH}	-230.51	457.13	1.09	25.99	10.55	199.29
m_{ratioL}	-20.73	19.29	0.12	4.82	-0.34	11.15

It is observed that the overall range of $_{mratioH}$ is [-230.51, 457.13]. But from Figure 5.49 it can be observed that 90% of the data lies within [-6.29, 6.69]. Mean of the ratio is slightly higher than 1, which signifies that m_{LH} is little higher than m_{RH}. Distribution of m_{ratioH} is very much right skewed. From the CDF plot it can be seen that F(0)=0.51. Therefore it can be said that probability of sign of slope of LH and RH signals to be same or not, is almost equal.

Standard statistical quantities of m_{ratioL} are also tabulated in Table 5.32. Along with CDF is plotted for 0.05% to 0.95% data in Figure 5.49b. It can be seen that the range of m_{ratioL} lie almost $\pm 20mV$, but more than 90% data lie within $\pm 7mV$ which is similar to that of the m_{ratioL}.

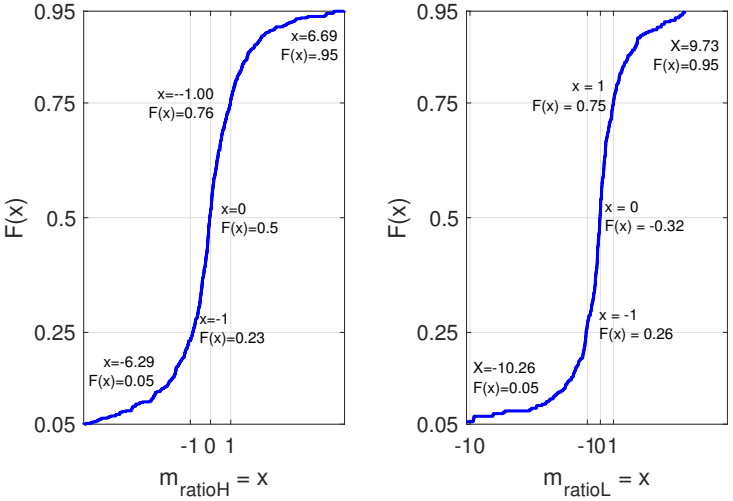

Figure 5.49: CDF plot of (a) m_{ratioH} and (b) m_{ratioL}

Among these 43% data lies within $\pm 1mV$ only. Comparing m_{ratioH} and m_{ratioL} in Table 5.32 it can be seen that the overall range of m_{ratioL} is much lower than that of m_{ratioH}. Mean value of m_{ratioL} is close to 0, but it was close to 1 for hand signals. Along with that, standard deviation value also is very low for m_{ratioL}. Skewness for m_{ratioL} is slightly negative and kurtosis is much lower than that of m_{ratioH}. Though it is quite higher than a normal distribution.

ZCI ratio : To characterize the interrelationship a new ratio parameter is proposed, namely ZCI_{ratio}. This parameter was calculated for both hand and leg signals and these are named after ZCI_{ratioH} and ZCI_{ratioL} respectively. This parameter is explained in 5.15. The statistical characteristics of these are stated in Table 5.33. The CDF plot of ZCI_{ratioH} is shown in Figure 5.50a, whereas ZCI_{ratioL} is shown in Figure 5.50b. The whole span is divided into 4 sub-regions. These sub-regions have also been marked in Figure 5.50. It is to be noted that in 9 cases, $ZCI_{RH} = 1200$ and hence the ZCI_{ratioH} in these cases is undetermined and are omitted from the plots. Considering all other signals, the range of ZCI_{ratioH} is [-134,358]. Though for 0.05 to 0.95, i.e. for 90% cases this ratio lies within -10.98 to 4.79. From Figure 5.50 it can be seen that likelihood of samples to occur within 0 to 1 is slightly higher than other 3 regions.

Inspite of the higher range of ZCI_{ratioL} of all feet signals, 90% of these lie within -6 to 7. Furthermore, 55% of these lie within ±1. This is similar to that of hand signals. It is noticeable that 66% of these are positive in nature. It is little higher than that of hand signals. For hand signals 53% of these were positive.

$$ZCI_{ratioH} = \frac{ZCI_{LH} - 1200}{ZCI_{RH} - 1200}$$
$$ZCI_{ratioL} = \frac{ZCI_{LL} - 1200}{ZCI_{RL} - 1200} \tag{5.15}$$

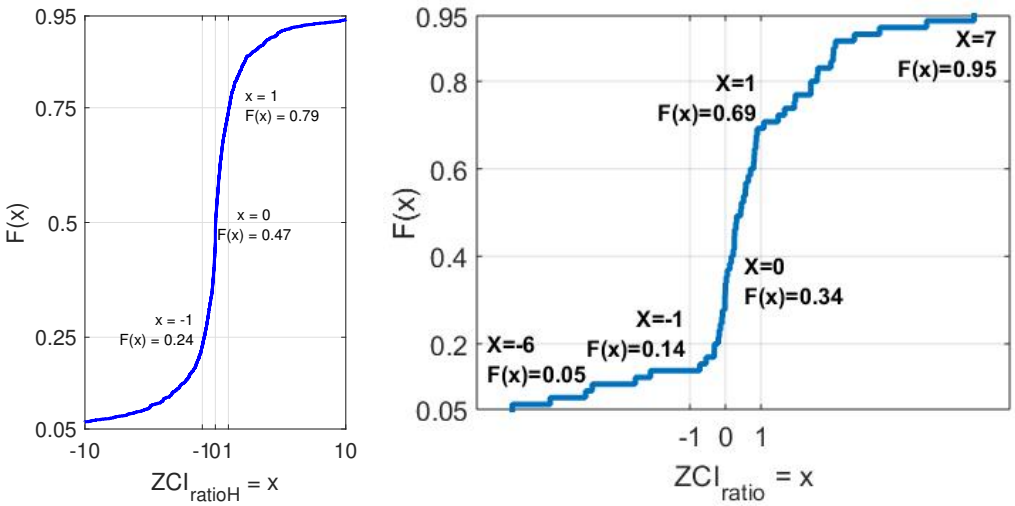

(a) (b)

Figure 5.50: CDF plot of (a) ZCI_{ratioH} and (b) ZCI_{ratioL}

Table 5.33: Statistical characterization of ZCI_{ratioH} and ZCI_{ratioL}

Parameters	Range in mV		μ in	σ in	Skewness	Kurtosis
	Min	Max	mV	mV		
ZCI_{ratioH}	-229.18	471.28	0.53	27.34	10.67	219.86
ZCI_{ratioL}	-180.00	34.25	-1.99	23.36	-6.93	53.58

Debias ratio : To obtain an insight into the instantaneous behaviour of the debiased pair of hand as well as feet signals, a new instantaneous

parameter is proposed as Debias ratio or DR_k, This parameter is defined underneath in 5.16, while the statistical quantities are tabulated in Table 5.32.

$$\begin{aligned} DR_{kH} &= \frac{debiasedLH_k}{debiasedRH_k} \\ DR_{kL} &= \frac{debiasedLL_k}{debiasedRL_k} \end{aligned} \tag{5.16}$$

for all $k \in [1, 2400]$.

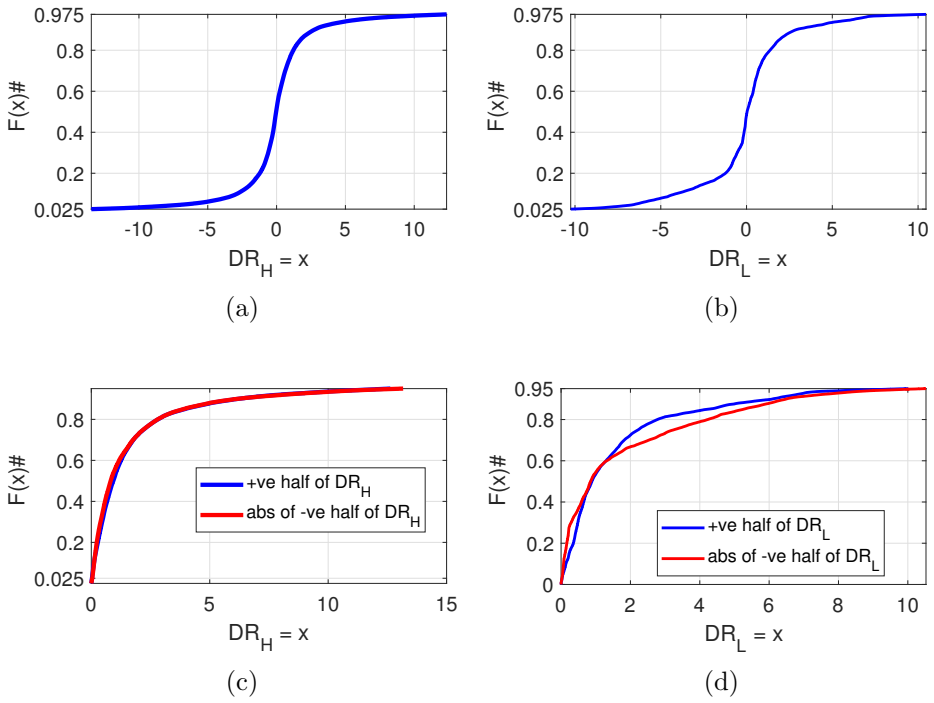

Figure 5.51: CDF plot of (a) DR_H, (b) DR_L, (c) positive half of DR and absolute of negative half of (c) DR_H, (d) DR_L

The CDF plots of overall DR for the range 2.5% till 97.5% is shown in Figure 5.51a and Figure 5.51b. It is observed that this 95% of the DR_H values, lie within a small range of [-13.56, 12.69]. Beyond this, the values are very high or infinity and they occur when the debiased RH signal values are zero or negligibly small as compared to the respective debiased LH signal. Inspite of a larger range of debias ratio DR_L of feet signals, 2.5% to 97.5%, i.e. 95% of data lies within a smaller range

Table 5.34: Statistical characterization of DR_H and DR_L

Parameters	Range in mV		μ in	σ in	Skewness	Kurtosis
	Min	Max	mV	mV		
DR_H	-13.42	12.31	0.30	3.00	-0.18	7.76
DR_L	-10.22	10.38	0.10	2.68	-0.35	6.88

of almost ± 10 in the CDF plot Figure 5.51b. This is close to the range of DR_H.

Table 5.34 contains the statistical quantities of DR_L. Comparing Table 5.34 it can be said that μ is smaller compared to the DR_H. Both are positively skewed but the value is larger in case of hand signals. But kurtosis value of DR_L is very much larger than that of hand signals.

Furthermore, it is observed that within the range observed in Figure 5.51, the DR values are equally likely to be positive or negative. In order to study this similarity further, the positive segment of the CDF plot in Figure 5.51a is overlapped with absolute of its negative segment in Figure 5.51c. It can be seen that the nature of distribution of these two halves are almost identical and hence the characteristics of the absolute values of DR are representative of the debiased signal pair in Figure 5.51c and Figure 5.51d respectively. Furthermore two halves of this CDF is compared by plotted CDF of the positive half and absolute of the negative half together in Figure 5.51d. Unlike the DR_k of hand signals, these two halves are not overlapping in case of DR_k of feet signals.

Log SD ratio : In view of the findings from the DR, another new parameter is proposed which is representative of a particular signal pair. This is termed as log SD ratio. Definition of Log SD ratio is given in 5.17. The CDF and Q-Q plots of ξ_{SD} are shown in Figure 5.52 and its statistical characteristics are stated in Table 5.35.

$$\begin{aligned} \xi_{SDH} &= log_{10}\frac{SD_{LH}}{SD_{RH}} \\ \xi_{SDL} &= log_{10}\frac{SD_{LL}}{SD_{RL}} \end{aligned} \tag{5.17}$$

The range of ξ_{SDH} is [-1.45, 1.77] and its median is very close to 0, as evident from Figure 5.52a. Furthermore, the skewness and kurtosis

values are indicative of a normal distribution for this parameter. This is supported by the observations from the Q-Q plot in Figure 5.52b, which shows good linearity almost up to ±2 quantile. This has also been validated using the chi-square goodness of fit test. In 95% cases, ξ_{SDH} lies within [-1,1]. It is to be noted that negative values of ξ_{SDH} indicate that SD_{LH} is smaller than SD_{RH}, while the reverse is true for positive values. Thus, in these cases, the ratio of the SD of LH and RH signal pairs lie approximately within 0.10 to 10 times following a log-normal distribution and there is no significant hemispheric dominance in this parameter for the overall data collected for this population.

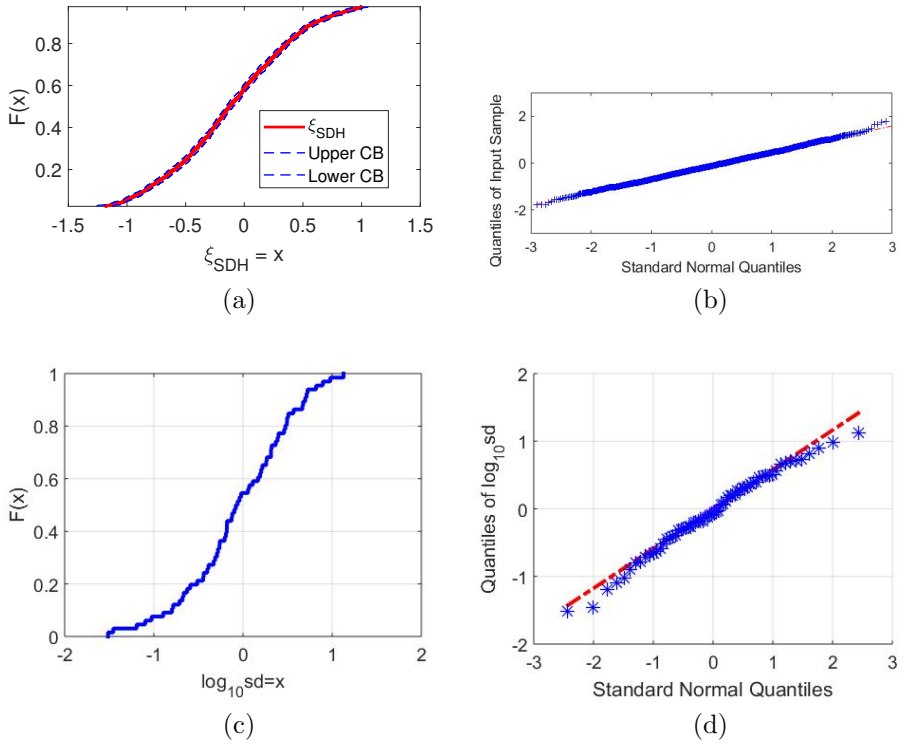

Figure 5.52: (a) CDF plot of ξ_{SDH} of hand signals with 95% confidence bound (CB) and (b) Quantile-Quantile plot of ξ_{SDH} of hand signals, (c) CDF plot of ξ_{SDL} of feet signals with 95% confidence bound (CB) and (b) Quantile-Quantile plot of ξ_{SDL} of feet signals

Whereas, ξ_{SDL} lie within (-1.51, 1.13) in Table 5.35. This can also be seen in Figure 5.52c. This range is very close to that of ξ_{SDH}. All the statistical quantities are very close for ξ_{SDH} and ξ_{SDL} in Table 5.35. To test the normality in distribution of ξ_{SDL}, Q-Q plot is done in Figure 5.52d. Figure shows linearity upto almost ±2 quantiles. This can

Table 5.35: Statistical characterization of ξ_{SDH} and ξ_{SDL}

Parameters	Range in mV		μ in	σ in	Skewness	Kurtosis
	Min	Max	mV	mV		
ξ_{SDH}	-1.45	1.77	-0.07	0.53	0.16	3.15
ξ_{SDL}	-1.51	1.13	-0.05	0.59	-0.33	2.73

also be found in the study of ξ_{SDH}. To validate the result chi-square test is performed on ξ_{SDL} and the result shows the normality with 95% confidence limit.

5.5 Discussions

In this Chapter, the physiological basis for the information content in the DDP signals has been analyzed at the outset. It is established that as the recording is done in DC mode, so the information recorded in differential mode from the dermal surface is due to differences in electrical activities at the nerve endings and/or the capillaries of the dermis and hypodermis layers. It is also established that the effect of sweat gland activity in the DDP signals is minimal.

Thereafter, the DDP signals acquired in the DS1 experiment (Section 4.2.2) have been validated in Section 5.2 in terms of its autocorrelation and by comparing with the underlying standard referenced endosomatic EDA signals as stated in [46] and their difference signal. As part of this validation, the statistical and spectral characteristics of these DDP signals have also been compared with those of the underlying endosomatic EDA signals and their difference signal.

This validation is followed by a detailed study of the unilateral characteristics of the DDP signals acquired in the DS2, DS3 and DS4 experiments. For this, the individual LH, RH, LL and RL signals in these datasets have been subdivided into 2 minute subsets and these have then been clubbed together. In the statistical characterization, it is observed that the LH and RH signals lie within $\pm 300mV$, whereas LL and RL signals lie within $\pm 400mV$. Of all signals, the LH signal has the lowest standard deviation. It is observed that 90% data of all the LH, RH, LL and RL signals lie within ±200mV. These individual signals typically exhibit mostly positive or negative polarities, show mostly converging and diverging trends with only 4% signals being constant.

From this study, it is observed that the signal mean is a representative of the individual signals with statistical characteristics similar to that of the

acquired signals.

Thereafter, the (mean subtracted) debiased signals, alternatively termed as deviation signals, have also been studied. More than 95% of these debiased signals lie within ±6mV. Along with that, ZCI lie within the middle of the 2 minute segment, *i.e.* between 40s to 80s. The slope m of all these 4 signals are of the order of 10^{-2} mV/instant.

The spectral characteristics of all 4 classes of signals are similar with overall range of mean frequency (MNF) and median frequency (MDF) within 2.16×10^{-3} to 2.3×10^{-3} and 2.87×10^{-3} and 2.82×10^{-3} respectively. From a study of the spectral entropy, it is observed that it is of the order of 10^{-4} and is maximum for LH, followed by RL, LL and RH.

Subsequently, the bilateral characteristics of these 4 signals have been studied based on the simultaneously acquired signals in the DS4 experiment. In this study, 4 derived signals named as GapH, PSH, GapL and PSL have also been generated from the 4 classes of acquired signals. These derived signals are little higher in magnitude, though the debiased derived signals also range within ±6mV for 95% cases. The band-limited characteristics of these derived signals indicate the bilateral interdependence of the acquired signals. The interdependencies of the various pairs of signals have been studied and this establishes that the bilateral interdependence is the most dominant. Thereafter, a study of the bilateral interdependencies in terms of mean, ZCI and slope have been studied.

Based on the aforementioned studies, total 6 number of bilateral parameters have been proposed in this study. The two bias parameters are differential bias μ_{diff} and common mode bias μ_{cb}, while the four debiased signal parameters are the slope and ZCI ratios m_{ratio}, ZCI_{ratio}, debias ratio DR and log SD ratio ξ_{SD} for hands as well as feet signals. The statistical, time domain and spectral characteristics of all these parameters have also been studied.

CHAPTER 6

Applications in human condition monitoring

All the unilateral and bilateral characteristics of the DDP signals, which include their statistical, time domain, spectral and proposed interaction parameters (or, features), that have been studied in Chapter 5 have been used in this Chapter to perform human condition monitoring studies.

Three specific applications of the DDP signals have been studied using the datasets recorded in all four experiments, namely DS1, DS2, DS3 and DS4 as replicated from Section 4.3.

Application4: Classification of hypertensive and normotensive subjects using LH and RH of DS2

Application5: Classification of different postures using LH of DS1 and both LH and RH data of DS3

Application6: Determination of the effective duration of rest in supine posture from LH of DS1, both hands data (LH and RH) of DS2 and all 4 channel data (LH, RH, LL and RL) of DS4 datasets and in sitting posture from both hands data (LH and RH) of DS3 dataset

At the outset of this Chapter, the materials and methods used for all 3 applications have been stated. This includes the details of the data preprocessing, followed by the details of the classification method and procedure used in the first two applications. Thereafter, the three different applications have been detailed.

6.1 Preprocessing

In order to make the acquired DDP datasets in the 4 experiments ready for the classification and inference applications, it was necessary to perform data cleaning, z-normalization, data quantization and feature extraction.

6.1.1 Data cleaning

This is an essential step to have valid data for the applications. Hence, all the acquired signals were manually examined as soon as they were recorded. In case abnormal local spikes, random missing bits or NaN (not a number) appeared in the acquired data, these were replaced by the mean value of the previous and the next data. For any other larger abnormality, the particular dataset was discarded and a fresh dataset was acquired in the experiment.

6.1.2 Z-normalization

As stated earlier, the span of the majority of acquired DDP signals is $\approx \pm 300$mV, whereas the variation of an individual signal is very less at only $\approx$20mV. As is usual in trend analysis of signals, in this case also all the individual long datasets with mean μ_t and standard deviation σ_t were Z-normalized as follows.

$$\hat{X} = \frac{X - \mu_t}{\sigma_t} \tag{6.1}$$

This is done to remove the overall bias in the acquired long datasets and normalize all of these datasets to zero mean and furthermore, to standardize their variance to unity.

6.1.3 Data quantization

The z-normalized signals are thus SD normalized versions of the debiased signals studied in Chapter 5. This enables a comparison of the 2 minute long subsets of a longer dataset on an uniform basis.

DS1

As stated at the outset, the DS1 dataset is used for the posture change classification and rest duration determination studies.

For this, the long 20 minute dataset has been quantized into 10 subsets of 2 minutes each. Specifically, the first 2 minute subset pertains to the sitting posture and is denoted as Sitting. Since the next 2 minute subset is acquired during change of posture from sitting to supine so it is not considered for the study. The subsequent 8 subsets acquired in supine posture are denoted as Sup 1 to Sup 8. Description of the 9 subsets pertaining to sitting and supine postures are tabulated in Table 6.1.

Table 6.1: List and description of different classes in DS1

Posture	Subset	Duration in minutes	Description
Sitting	Sitting	0 to 2	Acquisition started with subject in sitting posture.
Supine	Sup 1	4 to 6	16 minutes in restful nap supine posture, divided into 8 subsets. Each subset represents a state of restfulness. Effective duration of rest has been identified from the analysis of these states
	Sup 2	6 to 8	
	Sup 3	8 to 10	
	Sup 4	10 to 12	
	Sup 5	12 to 14	
	Sup 6	14 to 16	
	Sup 7	16 to 18	
	Sup 8	18 to 20	

Of these, the Sitting and the Sup 1 subsets were compared for posture classification, while the Sup 1 to Sup 8 subsets were considered for the estimation of the duration of effective rest. Since the data for change in posture has not been used for this study, it is neglected henceforth.

However, for classification type applications, as undertaken in this study, a higher level of quantization is needed. So, a data matrix $A1$ has been generated as follows in order to increase the resolution.

$$A1 = \begin{bmatrix} Sitting_1 & Sup\ 1_1 & \dots & Sup\ 8_1 \\ Sitting_2 & Sup\ 1_2 & \dots & Sup\ 8_2 \\ \vdots & \vdots & \vdots & \vdots \\ Sitting_{684} & Sup\ 1_{684} & \dots & Sup\ 8_{684} \end{bmatrix}$$

Thus, 57 numbers of 20 minute long datasets were considered after data cleaning. Each dataset is then primarily quantized into 9 numbers of 2 minute subsets, ignoring the change in posture subset as mentioned.

Thereafter, each 2 minute subset is further divided into 12 small subsets of 10s data. Therefore, the overall dataset of 57 sets contains 12 *small sets* $\times$ 57 *sets* $=$ 684 *small sets* in each of the 9 subsets. Thus, $Sitting_1$ to $Sitting_{12}$ are 12 small subsets of 10s duration of the original 2 minutes long *Sitting* subset of the first dataset. The other entries can be interpreted accordingly.

DS2 and DS4

The DS2 and DS4 datasets both contain 10 minutes long continuous signals. This 10 minute long data is quantized into 5 subsets of 2 minutes each, termed as Sup 1 to Sup 5. Each of the 5 subsets are described in Table 6.2.

As described for the DS1 dataset, the 2 minute subsets of the DS2 dataset are further quantized into 12 small sets of 10s length and arranged into a matrix form.

Table 6.2: List and description of different states in DS2 an DS4

State	Duration in minutes	Description
Sup 1	0 to 2	Acquisition started for supine subject.
Sup 2	2 to 4	2 minutes of acquisition completed; duration of rest more than in Sup 1.
Sup 3	4 to 6	4 minutes of acquisition completed; duration of rest more than in Sup 2.
Sup 4	6 to 8	6 minutes of acquisition completed; duration of rest more than in Sup 3.
Sup 5	8 to 10	8 minutes of acquisition completed; maximum duration of rest.

DS2 contains total 98 datasets of 10 minutes each. Therefore, there are 98 datasets in each of the 5 numbers of 2 minutes long states. As in case of DS1, here too the number of data subsets increase to 1176 small sets (=12 *small sets* $\times$ 98 *sets*) after quantization. This data matrix is represented as A2. Similarly, since DS4 contains 66 datasets of 10 minutes each, so the number of subsets increase to 792 small sets (=12 *small sets* $\times$ 66 *sets*), represented as the A4 matrix. The forms of A2 and A4 matrices are given hereafter.

$$A2 = \begin{bmatrix} Sup\ 1_1 & Sup\ 2_1 & Sup\ 3_1 & Sup\ 4_1 & Sup\ 5_1 \\ Sup\ 1_2 & Sup\ 2_2 & Sup\ 3_2 & Sup\ 4_2 & Sup\ 5_2 \\ \vdots & \vdots & \vdots & \vdots & \vdots \\ Sup\ 1_{1176} & Sup\ 2_{1176} & Sup\ 3_{1176} & Sup\ 4_{1176} & Sup\ 5_{1176} \end{bmatrix}$$

$$A4 = \begin{bmatrix} Sup\ 1_1 & Sup\ 2_1 & Sup\ 3_1 & Sup\ 4_1 & Sup\ 5_1 \\ Sup\ 1_2 & Sup\ 2_2 & Sup\ 3_2 & Sup\ 4_2 & Sup\ 5_2 \\ \vdots & \vdots & \vdots & \vdots & \vdots \\ Sup\ 1_{792} & Sup\ 2_{792} & Sup\ 3_{792} & Sup\ 4_{792} & Sup\ 5_{792} \end{bmatrix}$$

DS3

In case of DS3 experiment, the acquired data vary in length as different subjects settled down to satisfy the stated condition at different times. This

settling time also varied for the same subject in different acquisition trials and so was not subject specific at all.

In this case also, the overall length of a dataset was quantized into a number of multiple subsets, named as states, of 2 minutes length. The names and descriptions of these states or subsets are tabulated in Table 4.1 and repeated here for ready reference as Table 6.3.

Table 6.3: Different states of the DS3 data with their details

State no.	Posture	Name	Condition
1	Supine	Sup 1	Left and Right BP, then DDP+PR+SpO2.
2		Sup 2	DDP+PR+SpO2, then Left and Right BP.
3	Sitting	Sit 1	Left BP and PR, then DDP+PR+SpO2.
4	Standing	Stand 1	Left BP and PR, then DDP+PR+SpO2.
5	Climb down and up a flight of stairs in 1 min		
6	Sitting	Sit i, i∈(2,3,...,n)	DDP+PR+SpO2, then Left BP and PR. Repeat for every 2 minutes until BP matches that in state 3 (Sit 1).

In this case, total 65 datasets were acquired. After the final quantization of each of these datasets, the data matrix A3 has 780 small sets (=12 *small sets* × 65 *sets*) for each state as shown hereafter.

It is to be noted that since all datasets contain at least upto Sit 5, *i,e,* 4 subsets after 1 minute of exercise, the datasets have been considered till that state. All further states have been truncated in order to maintain the same number of columns for each dataset and its subsets.

$$A3 = \begin{bmatrix} Sup\ 1_1 & Sup\ 2_1 & Sit\ 1_1 & Stand\ 1_1 & Sit\ 2_1 & \dots & Sit\ 5_1 \\ Sup\ 1_2 & Sup\ 2_2 & Sit\ 1_2 & Stand\ 1_2 & Sit\ 2_2 & \dots & Sit\ 5_2 \\ \vdots & \vdots & \vdots & \vdots & \vdots & \vdots & \vdots \\ Sup\ 1_{780} & Sup\ 2_{780} & Sit\ 1_{780} & Stand_{780} & Sit\ 2_{780} & \dots & Sit\ 5_{780} \end{bmatrix}$$

6.1.4 Feature extraction and attribute selection

As stated earlier, all the features described in Chapter 5 have been used as the features for these applications.

Two additional statistical parameters, namely normalized variance and normalized kurtosis, have also been considered as features. Normalized vari-

ance is the variance of each subset of a long dataset normalized in terms of (i.e. divided by) the variance of the last subset. Similarly, the normalized kurtosis of a subset is obtained by normalizing it in terms of the kurtosis of the last subset.

The list of all these features are given hereafter.

- Unilateral features of all 4 individual signals

  Basic characteristics: Polarity, Trend

  Statistical features: Mean, SD, variance, normalized variance, skewness, kurtosis and normalized kurtosis.

  Linear model: ZCI, m

  Spectral features: MNF, P_{MNF}, MDF, P_{MDF}, SM1, SM2, SM3, E

- Bilateral features of LH-RH and LL-RL pairs

  Pair of signals: Trend

  Derived signals: Mean, SD, skewness, kurtosis of GapH, GapL, PSH and PSL

  Lateralisation coefficients: LC1 and LC2

  Proposed features: μ_{diff}, μ_{cb}, ZCI_{ratio}, m_{ratio}, DR_k, ξ_{sd}

Among all these, the attributes that are most suitable for the particular application are selected. Attribute selection has been done in the open source data mining software WEKA, version 3.9.4 [134, 135]. Attribute selection is helpful in reducing dimensionality, training time as well as over-fitting of the data. Out of the various attribute evaluators available in the WEKA software, the *AttributeSelection* filter was used in this experiment. It is a very flexible supervised attribute filter and allows the use of various combinations of search and evaluation methods.

6.2 Classification

Both the classification studies were done in WEKA using the random forest (RF) classifier [136]. RF is actually an ensemble of different classification trees. Each tree predicts a result and all results are ensembled to produce the actual prediction of the classification. For this reason, RF minimizes error. It also works well for imbalanced dataset and is capable of handling missing data. But its main drawback is its complexity due to the large number of

decision trees created. For this reason, the training time for RF classifier increases exponentially as the number of features increase. However, in the present study, the total number of features is reasonable with the minimum of 19 features for DS1 and the maximum of 245 features for DS2 datasets.

The end result of the classification is the 2 × 2 confusion matrix which is used for its performance assessment. This matrix, as shown in Table 6.4 actually represents the true positive (TP), false positive (FP), true negative (TN) and false negative (FN) predictions among all the actual cases.

Table 6.4: Structure of a confusion matrix.

		Predicted output		
		Positive	Negative	Total
Actual incident	Positive	TP	FN	$TP + FN$
	Negative	FP	TN	$FP + TN$
	Total	$TP + FP$	$FN + TN$	N

TP (TN) or true positive (negative) is defined as the number of incidents predicted positive (negative) among all the actual positive (negative) incidents. On the other hand, the total number of false predictions among all the positive (negative) counts are defined as the false positive (negative) or FP (FN). These 4 quantities are used to calculate performance of the classification in terms of accuracy, True Positive Rate (TPR), True Negative Rate (TNR), F1 score, precision, Receiver Operating Characteristic (ROC) and Precision-Recall area under the curve (PRC AUC).

Accuracy is defined as the true predictions among all predictions and is calculated as in (6.2). Two other terms TPR (alternatively Recall or Sensitivity) and TNR (alternatively Specificity) are calculated as in (6.3). Of these, TPR is the ratio of the true positive outcomes to the actual positive counts, while TNR is the ratio of the true negative outcomes to the actual negative counts. Accuracy is alternatively determined using the weighted accuracy (WA) formula, which is the average of TPR and TNR.

$$accuracy = \frac{TP + TN}{TP + TN + FP + FN}; \tag{6.2}$$

$$TPR = \frac{TP}{TP + FN}; \;\; TNR = \frac{TN}{TN + FP} \tag{6.3}$$

$$Precision(PPV) = \frac{TP}{TP + FP} \tag{6.4}$$

$$NPV = \frac{TN}{TN + FN} \tag{6.5}$$

$$F1 - score = \frac{2 \times Recall \times Precision}{Recall + Precision} \tag{6.6}$$

In case of a heterogeneous dataset, *i.e.* where all the classes are not equally numbered, the accuracy is predicted in terms of the F1 score 6.6, which is calculated in terms of precision and recall. Precision (6.4), also known as positive prediction value (PPV), has also been calculated along with negative prediction value (NPV) 6.5. NPV is defined as the actual negative incidents among all the negative outcomes. The trade-off between the TPR and the FPR is studied from the ROC-AUC along with the PRC-AUC.

Three cross validation techniques are used in this experiment, namely 10 fold cross validation (10FCV), leave one out cross validation (LOOCV) and leave one subject out cross validation (LOSOCV).

In 10FCV, the total dataset is grouped into 10 number of subsets with equal populations. Among these, 9 subsets are used to train the model and the remaining 1 subset is kept for testing purpose. In the next cycle, a different subset is used for testing while the remaining 9 are used for training purpose. This process is repeated for 10 iterations. Performance is calculated by averaging all 10 predictions.

LOOCV is similar to 10FCV but with all subsets being considered at a time in place of 10 groups. So, the number of iterations in this case is the same as the number of subsets.

In LOSOCV, which is used to eliminate the subject bias, all the datasets of one subject are kept for testing purpose in a particular iteration, while the rest are considered as training sets. Thus, in this case, the number of iterations is the number of subjects.

6.3 Hypertensive and normotensive classification

In this study, a method is proposed to classify hypertensive and normotensive subjects using the changes in DDP signal characteristics during extended periods of rest. This assumes that the progression of rest is dependent upon blood pressure. The hypertensive and normotensive subject classification has been done using DS2 dataset where the subjects are supine for 10 minutes.

6.3.1 Selected attributes

Total 5 attributes were selected out of a total set of 245 features. The selected attributes are tabulated in Table 6.5.

Table 6.5: List of selected attributes for hypertensive and normotensive subject classification

Attributes	Parameter	Signal	State No.
SDLH3	SD	LH	State 3
mGapH3	Slope (m)	Gap	State 3
mGapH4	Slope (m)	Gap	State 4
mPSH3	Slope (m)	PS	State 3
LC1μ2	LC1 of mean	LH and RH	State 2

It is observed that the SD of the left hand, which is physically located closer to the heart, is the most preferred attribute for differentiating hypertension. It is also important to note the contributions of the derived signals GapH and the common mode signal PSH. The variations in their signal slopes with increased duration of rest are different for normal and hypertensive subjects. In addition, the lateralization coefficient of the mean also performs effectively in differentiating the two classes.

6.3.2 Result and findings

The results of the RF classification for 10FCV, LOOCV and LOSOCV are given in Table 6.6. It can be seen from the analysis of the 10FCV results that out of 98 instants, the classifier model successfully classified 75 instants, which yields an overall accuracy of 0.765 with precision and F1 score of 0.752. The weighted average (WA) of precision and recall are 0.774 and 0.776 respectively. Furthermore, the weighted averages of F1-score and PRC area under the curve (AUC) are 0.749 and 0.776 respectively. The consistency of all these measures are indicative of the efficacy of the classification.

The LOOCV and LOSOCV results are similar to that of the 10FCV results. The weighted average (WA) of the TPR in both LOOCV and LOSOCV are 0.769 and 0.739 respectively. The F1 score in these two cases are 0.756 and 0.738 respectively. The ROC-AUC is marginally low in LOOCV and LOSOCV, but PRC-AUC is relatively high in all 3 cross-validation tests.

Box plot representations of the 5 selected attributes for both classes, hypertensive and normotensive, are shown in Figure 6.1. As expected, the

Table 6.6: Results of RF classification of hypertensive and normotensive subjects

Application		TPR	TNR	Precision	F-1 score	PRC-AUC	ROC-AUC
10FCV	Hypertensive	0.700	0.793	0.767	0.732	0.749	0.747
	Normotensive	0.793	0.700	0.742	0.767	0.749	0.797
	WA	0.765	0.739	0.752	0.752	0.749	0.776
LOOCV	Hypertensive	0.810	0.742	0.739	0.772	0.688	0.758
	Normotensive	0.742	0.810	0.748	0.745	0.688	0.755
	WA	0.769	0.782	0.744	0.756	0.688	0.756
LOSOCV	Hypertensive	0.753	0.729	0.739	0.746	0.666	0.748
	Normotensive	0.729	0.753	0.740	0.734	0.666	0.769
	WA	0.739	0.743	0.739	0.738	0.666	0.760

Table 6.7: Comparison of different classification techniques in 10FCV

Technique	PPV	NPV	Sensitivity	Specificity	F1-score
RF	0.75	0.82	0.76	0.73	0.75
SVM	0.54	0.67	0.58	0.64	0.61
k-NN	0.58	0.72	0.65	0.65	0.65

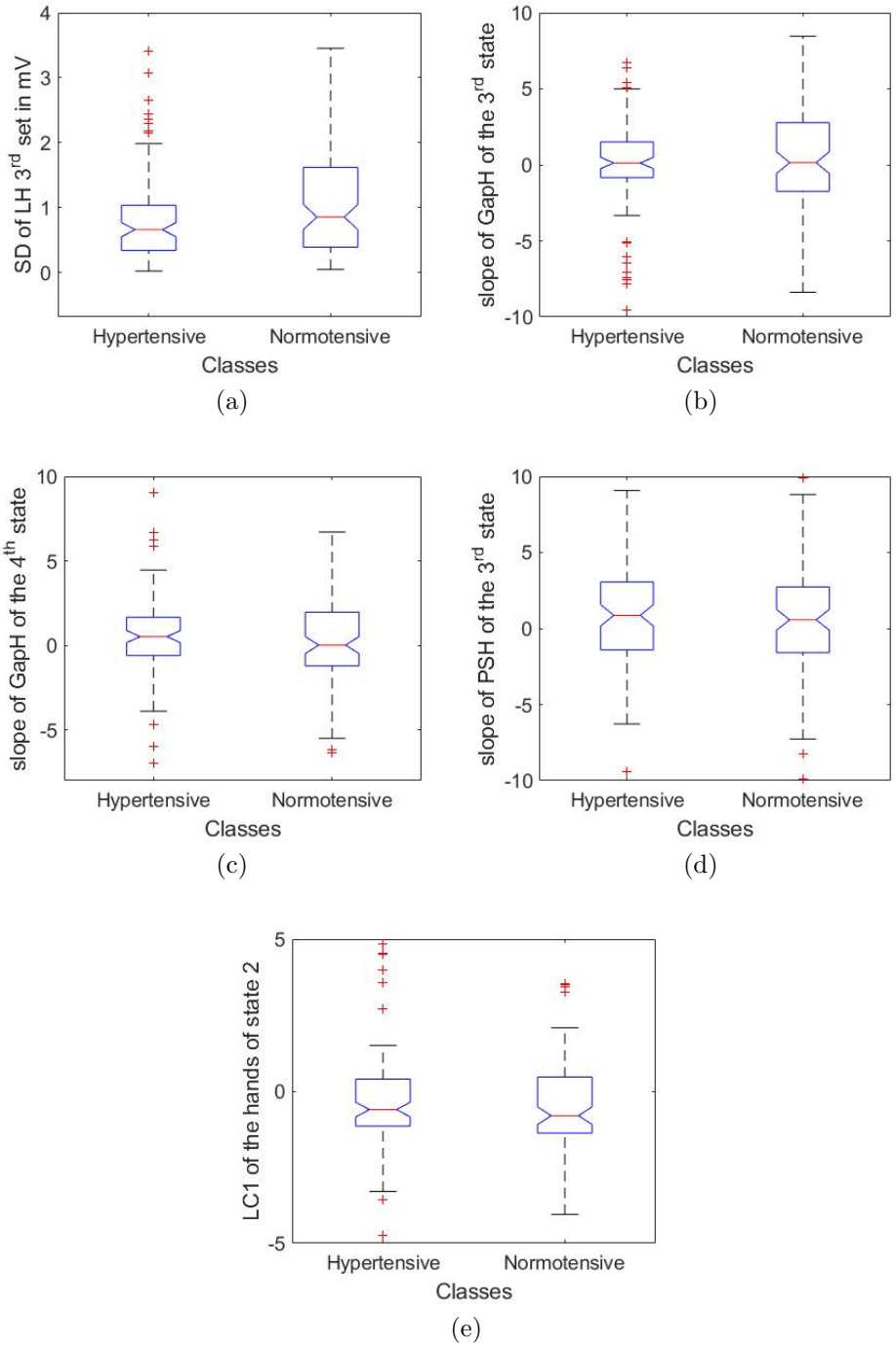

Figure 6.1: Box plots of (a) SD of LH of the Sup 3, (b)slope (m) of the GapH of the sup 3, (c) slope (m) of the GapH of the sup 4, (d) slope (m) of the PSH of the sup 3, (e) LC1 of hands of sup 2.

box plots of the SD of LH 3^{rd} state as well as the GapH of the 3^{rd} and 4^{th} states are easily distinguishable for the normotensive and hypertensive classes. The contribution of the remaining 2 parameters are significantly less as also apparent from their box plots.

Comparison of the results of RF classifier with those of SVM and k-NN classifiers for 10FCV is presented in Table 6.7. The 5 measures compared are PPV, also called precision; NPV; sensitivity, also called TPR; specificity, also called TNR; and the F1-score. From the results, it is seen that among all three techniques tested, RF performed best in terms of all 5 measures presented in Table 6.7.

All these results are satisfactory to say that hypertensive and normotensive subjects can be classified using this technique.

6.3.3 Comparison with existing methods

Hypertension causes many severe health complications like heart problem, stroke or even death. According to the WHO report [137], 17.9 million people have died in 2019 due to cardiovascular diseases. Among these, 85% were due to heart attack and stroke [138]. 63% of the total deaths in India are due to noncommunicable diseases, of which 27% are due to cardiovascular diseases [139]. The different stages of hypertension are detailed in [140]. Since this fatality occurs due to lack of awareness, lack of primary care and follow up, so it is essential to have a simple, reliable automated screening system along with the usual BP monitoring system.

Table 6.8: Comparison of the existing methods for classifying hypertension

Serial	Authors & year	Experiment	Classification technique	Accuracy
1	Yongbo Liang *et al.* (2018) [37]	Hypertension assessment using ECG and PPG	Logistic Regression, AdaBoost Tree, Bagged Tree, and k-NN	F1 score of 94.84%
2	Gabor Kovacs *et al.* (2016) [141]	Pulmonary hypertension assessment using ECG and other non-invasive tools	multivariate logistic regression	PPV:92%, NPV:97%
3	J. S. Rajput *et al.* (2019) [38]	Discrimination of high-risk hypertension ECG signals	optimal orthogonal wavelet filter bank	$p<0.01$
4	P. Y. Courand *et al.* (2014) [39]	R wave of ECG in aVL lead as hypertension index	ECG recordings were analyzed in a prospective cohort	$p<0.05$
5	J. S. Rajput *et al.* (2020) [40]	Automatic detection of severity of hypertension ECG signals	Optimal bi-orthogonal wavelet filter bank	Average accuracy 99.95%
6	Hongbo Ni *et al.* (2015) [140]	Severity of hypertension	Multiscale fine-grained hart rate variability (HRV) analysis	Precision 95.1%
7	M. Simjanoska *et al.* (2018) [41]	Blood pressure classification from ECG signals	Complexity analysis-based machine learning	Precision 96.68%

Table 6.8 – continued from previous page

Serial	Authors & year	Experiment	Classification technique	Accuracy
8	Tim Seidler *et al.* (2019) [42]	Pulmonary hypertension detection from electrocardiographic signals	random forest of classification trees and regression trees, lasso penalized logistic regression, boosted classification trees, support vector machines	Accuracy of 95% with area under curve 0.87
9	M.G.Poddar *et al.* (2019) [43]	automated hypertension classification technique from the HRV analysis	PNN, k-NN, and SVM classifiers	96.67% in SVM
9	Present method	Features of DDP signals	RF	Accuracy of 80.60%

A comparison of the existing methods for classifying hypertensive subjects is presented in Table 6.8. It is observed that there exists methods based on ECG with accuracies well above 90%. In comparison, the classification accuracy of the DDP signals based method is at most 80.60%. Yet, the simplicity of its acquisition even by nominally skilled health workers and the minimal subject discomfort during its acquisition using the simple 10 minutes rest protocol can be useful for primary monitoring and screening purposes.

6.4 Posture classification

In this study, changes in the features of the DDP signals have been used to classify the sitting and supine and/or standing postures. Accordingly, only the sitting and supine posture components of the DS1 datasets, specifically the Sitting and Sup 1 states listed in Table 6.1, have been considered for a binary classification. In case of the DS3 datasets, the three states Sup 2, Sit 1 and Stand 1 listed in Table 6.3 have been considered for classification into one of 3 classes. As already known, the DS1 datasets contain LH data only, whereas the DS3 datasets contains LH and RH data.

6.4.1 Selected attributes

List of the selected attributes for the DS1 and DS3 feature sets are tabulated in Table 6.9. It is observed that in case of DS1, only 3 variables were selected out of 19 features of LH signals provided to perform the binary classification of sitting and supine posture. These are the mean (μ_{LH}), SD (σ_{LH}) and normalized variance ($Nvar_{LH}$).

For the supine, sitting and standing posture classifications in DS3, 4 more features have been selected along with the 3 selected features as in DS1 out of a total of 49 features. Thus the selected features are the mean, SD and normalized variance of both LH and RH and the lateralization coefficient of the mean ($LC1_H$) of the signals.

6.4.2 Result and findings

The confusion matrices of the RF classification for 10FCV, LOOCV and LOSOCV are shown in Table 6.10, while the results of these classifications are stated in Table 6.11. It is to be noted that since this study deals with balanced data, *i.e.* the total number of sets available for each of the two (or three) classes are the same, so the overall accuracy, TPR, F1 score and TNR are equivalent to each other [142, 143].

Table 6.9: List of selected attributes for posture classification in application 4 using DS3

Sl. No	Attributes		Description
	DS1	DS3	
1	μ_{LH}	μ_{LH}	Mean value of the LH signal
2	σ_{LH}	σ_{LH}	Standard deviation of LH
3	$Nvar_{LH}$	$Nvar_{LH}$	Normalized variance of the LH signal
4	×	μ_{RH}	Mean value of the RH signal
5	×	σ_{RH}	Standard deviation of RH
6	×	$Nvar_{RH}$	Normalized variance of the RH signal
7	×	$LC1_{\mu}$	Lateralization coefficient 1 of the mean values

Table 6.10: Confusion matrices of RF classifier for posture classification of DS1 and DS3 datasets

			Prediction					
			DS1, N=684			DS3, N=792		
			Supine	Sitting	Standing	Supine	Sitting	Standing
Actual	10FCV	Supine	682	2	×	722	39	31
		Sitting	0	684	×	34	682	76
		Standing	×	×	×	36	103	653
	LOOCV	Supine	678	6	×	713	37	42
		Sitting	9	675	×	40	673	79
		Standing	×	×	×	48	106	638
	LOSOCV	Supine	652	32	×	717	40	35
		Sitting	51	633	×	43	645	104
		Standing	×	×	×	38	126	628

Table 6.11: Results for posture classification of DS1 and DS3 datasets using RF classifier

Application			TPR	Precision	PRC-AUC	ROC-AUC
10FCV	DS1	Supine	0.997	1.000	1.000	1.000
		Sitting	1.000	0.997	1.000	1.000
		WA	0.999	0.999	1.000	1.000
	DS3	Supine	0.912	0.912	0.969	0.982
		Sitting	0.861	0.828	0.907	0.953
		Standing	0.824	0.859	0.913	0.951
		WA	0.866	0.866	0.930	0.962
LOOCV	DS1	Supine	0.991	0.987	0.989	0.983
		Sitting	0.987	0.991	0.989	0.985
		WA	0.989	0.989	0.989	0.984
	DS3	Supine	0.900	0.886	0.958	0.976
		Sitting	0.854	0.825	0.900	0.948
		Standing	0.808	0.848	0.907	0.947
		WA	0.853	0.853	0.922	0.957
LOSOCV	DS1	Supine	0.953	0.904	0.939	0.919
		Sitting	0.926	0.926	0.940	0.966
		WA	0.939	0.915	0.939	0.942
	DS1	Supine	0.905	0.898	0.960	0.976
		Sitting	0.814	0.795	0.873	0.935
		Standing	0.793	0.819	0.887	0.934
		WA	0.838	0.838	0.907	0.948

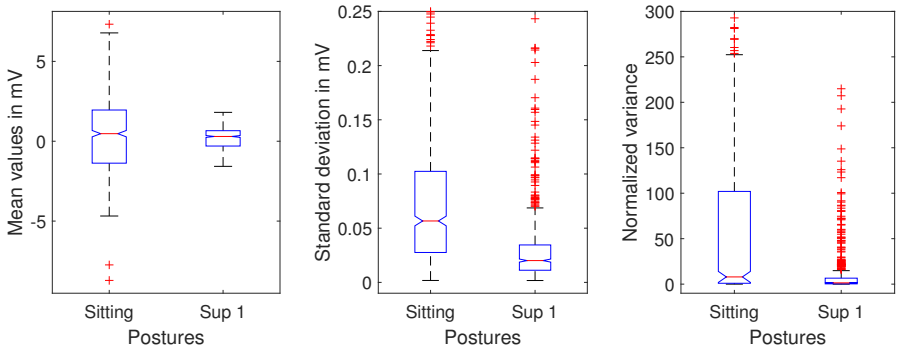

(a) (b) (c)

Figure 6.2: Box plots of (a) mean values, (b) standard deviation (SD) values and (c) normalized variance of the z-normalized preprocessed signals of sitting and supine postures in application 4 using DS1

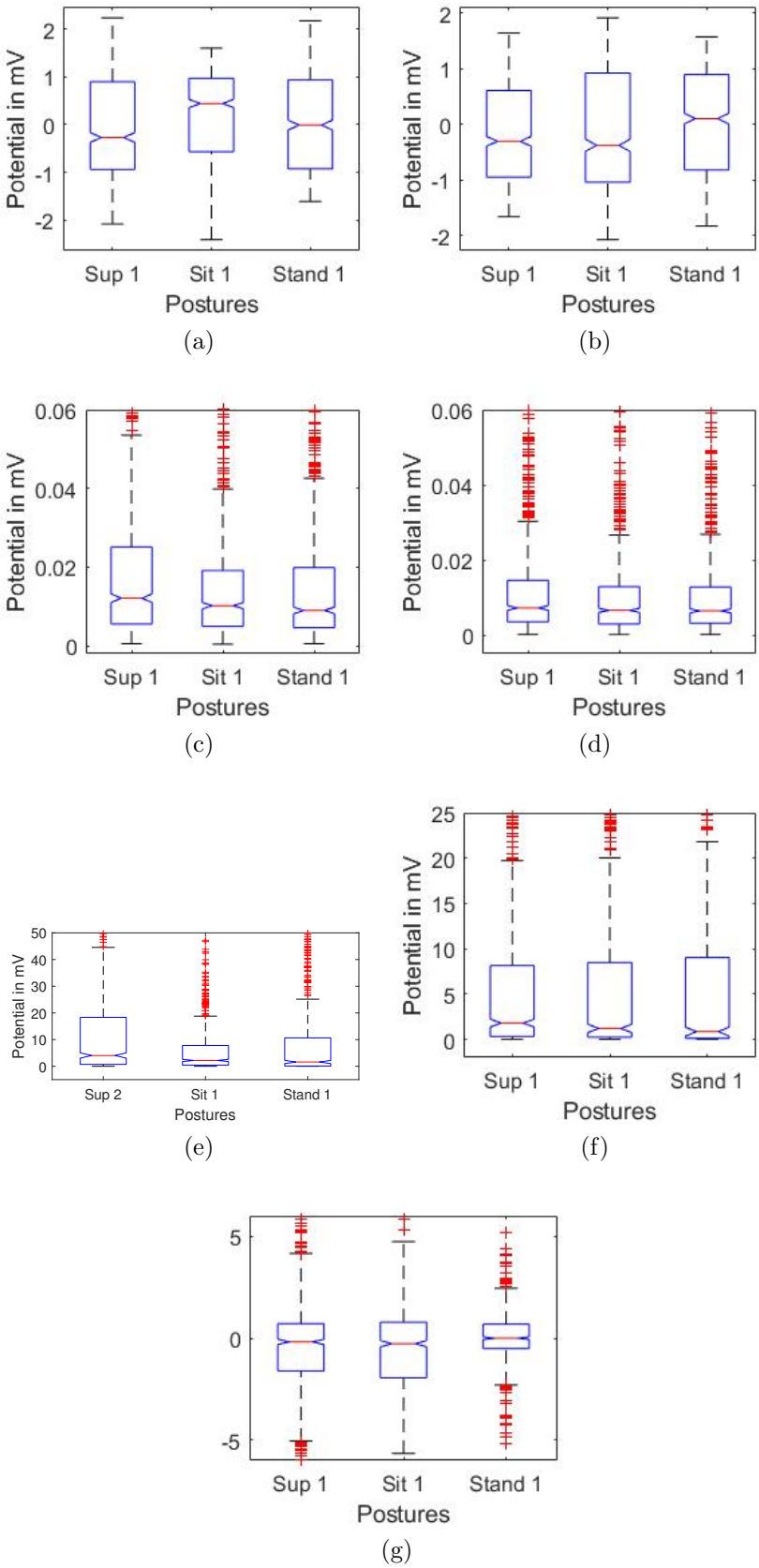

Figure 6.3: Box plots of (a) Mean of LH, (b)Mean of RH, (c) SD of LH, (d) SD of RH, (e)Normalized variance of LH, (f) Normalized variance of RH and (g) LC1 of the mean values of all three classes.

It is seen from Table 6.10 that out of the 684 instances for DS1, the RF model can predict 684 and 675 sitting postures as well as 682 and 678 supine postures correctly in 10FCV and LOOCV experiments respectively. Therefore, the overall accuracy (or TPR) in 10FCV and LOOCV are 0.999 and 0.989 respectively (Table 6.11). Furthermore, precision, (PRC-AUC) and (ROC-AUC) for 10FCV experiments are 0.999, 1.000 and 1.000 respectively and for LOOCV experiments are 0.989, 0.989 and 0.984 respectively. Both these results are thus consistent and significantly high.

In case of subject wise analysis using the LOSOCV experiment, 633 sitting instants and 652 supine instants out of 684 instances have been detected correctly. Thus, the results of LOSOCV experiments yield overall accuracy and PRC-AUC of 0.939, ROC-AUC of 0.942 and a precision of 0.915. Since these are also consistently above 0.9, thus it can be said that subject biases are not very relevant in this experiment.

In the 3 level classification in DS3, it is observed that 10FCV can predict 722, 682 and 653 instants correctly, whereas LOOCV can predict 713, 673 and 638 instants correctly for supine, sitting and standing classes respectively among 792 instants. The results of LOSOCV are also similar to that of other two cross validations and the numbers in this case are 717, 645 and 628 respectively. Therefore, the accuracy of all 3 cross validation tests - 10FCV, LOOCV and LOSOCV - are 0.866, 0.853 and 0.838 respectively. Along with that, the PRC area under the curve is found to be 0.930, 0.922 and 0.907 for the 3 cross-validations respectively, which is significantly high. Furthermore, ROC-AUC values are 0.962, 0.957 and 0.948 respectively, which are also very high.

Box plots of the underlying 3 selected attributes in DS1, namely μ_{LH}, σ_{LH} and $Nvar_{LH}$, are shown in Figure 6.2 and their statistical parameters are stated in Table 6.12. It is observed that the range and inter quartile range (IQR) of these parameters, as well as their median values are comparatively higher in sitting posture than in the supine posture.

It is to be noted that while the mean represents the slow changing tonic component, the SD and normalized variance represent the quick changing phasic component of the normalized signal. This analysis thus establishes that the acquired biopotentials differ in both these aspects for these two postures.

Box plots of the 7 selected attributes in DS3 are shown in Figure 6.3 and their statistical parameters are stated in Table 6.12. The differences among the three postures for the 7 select4d attributes of DS3 are clearly visible from the box plots, as also validated from Table 6.12. These differences are most prominent in the signal mean for both hands, μ_{LH} and μ_{RH}, and the normalized variance for the left hand $Nvar_{LH}$.

Table 6.12: Box plot parameters for posture classification using DS1 and DS3 datasets

DS	Signals	Posture	Lower Adjacent	Lower Quantile	Median	Upper Quantile	Upper Adjacent
DS1	μ_{LH}	Sitting	-4.68	-1.37	0.47	1.95	6.78
		Supine	-1.57	-0.30	0.29	0.66	1.81
	σ_{LH}	Sitting	0	0.03	0.06	0.10	0.21
		Supine	0.00	0.01	0.02	0.03	0.68
	$Nvar_{LH}$	Sitting	0.00	0.95	7.93	101.98	252.36
		Supine	0.00	0.3	1.39	6.57	14.83
DS3	μ_{LH}	Supine	-2.08	-0.94	-0.27	0.90	2.24
		Sitting	-2.41	-0.56	0.44	0.97	1.60
		Standing	-1.61	-0.92	-0.01	0.93	2.18
	σ_{LH}	Supine	0.00	0.00	0.01	0.02	0.05
		Sitting	0.00	0.00	0.01	0.02	0.04
		Standing	0.00	0.00	0.01	0.02	0.04
	$Nvar_{LH}$	Supine	0.00	0.71	4.04	18.33	44.54
		Sitting	0.00	0.44	2.59	7.78	18.79
		Standing	0.00	0.09	1.61	10.64	25.14
	μ_{RH}	Supine	-1.66	-0.95	-0.31	0.61	1.64
		Sitting	-2.07	-1.04	-0.38	0.92	1.92
		Standing	-1.83	-0.82	0.10	0.89	1.57
	σ_{RH}	Supine	0.00	0.00	0.00	0.01	0.03
		Sitting	0.00	0.00	0.00	0.01	0.02
		Standing	0.00	0.00	0.00	0.01	0.02
	$Nvar_{RH}$	Supine	0.00	0.32	1.79	8.13	19.71
		Sitting	0.00	0.25	1.20	8.47	20.03
		Standing	0.00	0.00	0.85	9.02	21.81
	$LC1_H$	Supine	-5.04	-1.60	-0.18	0.70	4.74
		Sitting	-5.65	-1.94	-0.27	0.78	4.74
		Standing	-2.30	-0.51	-0.07	0.69	2.45

6.4.3 Comparison with existing methods

A comparison of recent methods for posture classification is presented in Table 6.13. In a study, Foubert *et al.* proposed a sitting and supine classification technique using bed-based pressure sensor array and videography [144]. Results show very low miss rate with significantly high accuracy. In another study, a smart chair system has been developed combining six infra-red reflective distance with pressure sensor array for posture classification [145]. Use of IMU (inertial measurement unit) sensor in posture classification shows mixed performances in terms of accuracy [146, 147]. Overall accuracy in the experiment by Lockhart *et al.* is greater than 0.95 [146], while Vo states the classification accuracy of sitting posture to be 0.60 only, which is very low [147]. A common method of posture classification is by using data from multiple accelerometers such as light weight thigh worn activePal accelerometers [148–150]. The classification accuracy of this accelerometer data are very high in almost all cases, except the standing/light activity in upright posture in the experiment performed by Bassett *et al.* [149]. Furthermore, electrocardiogram (ECG) is also used for posture classification in many experiments. In these experiments, signals were acquired using normal ECG monitor [151], or Holter monitor [27] or even downloaded data available in online repository [152].

Comparing the results of these existing methods for posture classification with the present DDP signal based method with an accuracy of 99.9% in binary and 86.6% in 3 level classifications, it can be said that the present approach performs creditably and is even better in some cases.

Table 6.13: Comparison of the existing methods for classifying sitting and supine posture

Serial	Authors & year	Experiment	Classification technique	Accuracy
1	Nicholas Foubert *et al.* (2012) [144]	Pressure sensor array	SVM, k-NN	0.94
2	Thurmon E. Lockhart *et al.* (2013) [146]	IMU signal	Wavelet based approach	0.968
3	David R. Bassett *et al.* (2014) [149]	2 accelerometers (activePal) data used	Coken kappa statistics	1.00
4	Nhat Nguyen Vo (2014) [147]	Accelerometer based sensor	ANN	Supine: 0.972 sitting: 0.608
5	Saeid Wahabi *et al.* (2015) [26]	ECG signal	SVM	Sitting: 0.98 and Supine: 0.94
6	Kate Lyden *et al.* (2016) [148]	thigh-worn, tri-axial activPAL3 accelerometer	their novel method	supine: 0.967, sitting: 0.929
7	Dai Sasakawa *et al.* (2018) [28]	Height and a Doppler radar cross section (RCS)	k-NN	Sitting 0.965, supine 1.00
8	Nindynar Rikatsih (2018) [153]	Movement data of UCI Machine Learning Repository	k-NN	0.995
9	Angel D. Ruiz1 *et al.* (2019) [152]	Electrocardiography and respiratory flow	linear SVM	0.995
10	Yutaka Yoshida *et al.* (2019) [27]	Holter electrocardiographic (ECG) recorder with built-in accelerometer	RF	Supine: 0.98, Sitting: 0.717
11	Present study	RF classification using mean, SD and normalized variance	binary RF	Supine: 1.00, Sitting: 0.997

Table 6.13 – continued from previous page

Serial	Authors & year	Experiment	Classification technique	Accuracy
12	Present study	RF classification using mean, SD, normalized variance, lateralization coefficient	3 level RF	Supine: 0.912, Sitting: 0.861 Standing: 0.824

6.5 Effective duration of rest estimation

It has been observed in Figure 5.14(d) of Section 5.2.3 that during a prolonged period of rest in the DS1 dataset, the average band power starts from a high value and continuously decreases till a certain value and then increases again. This feature is absent in the mean or the SD or the kurtosis of the signals (Figure 5.14(a)-(c)). Thus it can be said that the restfulness of a human being causes definitive changes in their spectral domain features, but not so in their statistical features.

In the present study, this observation in the spectral characteristics has been used to estimate the effective duration of rest of supine subjects in the DS1, DS2 and DS4 datasets. The effect of prolonged sitting has also been studied in analogous manner using the DS3 dataset.

However, for a detailed investigation of this aspect, all the statistical, spectral as well as other features listed in Section 6.1.4 has been estimated for all of these datasets and the earlier findings in Section 5.2.3 have been compared. Accordingly, the results and findings for those features in which the effect of rest is discernible have been provided in the following subsection. A comparison with other existing methods for estimation rest are given thereafter.

6.5.1 Result and findings

It was seen in Section 5.3.6 that the peak frequency PKF is a constant at dc and hence is not considered as a distinguishing parameter. On the other hand, the characteristics of the central frequency components MNF and MDF are almost identical, while the P_{MNF}, P_{MDF}, Band power and P_{PKF} form another almost identical set. Hence, only the central frequency MNF and the power at this central frequency P_{MNF} have been studied for this application.

DS1

The effect of restfulness on different states were observed for these spectral features in DS1. In order to do so, these characteristics were studied for the supine states Sup 1 to Sup 8 in $A1$ (Section 6.1.3) and the corresponding box plots have been shown in Figure 6.4(a) and Figure 6.4(b) respectively.

It is observed that the median values as well as the IQR of the MNF in Figure 6.4(a) increase up to a maxima at some interim state and then decrease till the Sup 8 state. The median value is maximum at Sup 3, whereas the IQR is maximum in Sup 4. It is observed from Figure 6.4(b) that the characteristics of P_{MNF} are almost the reverse of the MNF in Figure 6.4(a).

that is to say that in this case, the median value decreases with time upto Sup 3 and increases again till Sup 8. Along with that, the upper adjacent and lower adjacent levels also decrease upto Sup 3 and then increase upto Sup 8.

In order to validate the reversal of the two characteristics of P_{MNF} and MNF, the first moment SM1 has been observed. The box plots of SM1, as shown in Figure 6.4(c), are observed to be almost constant in nature. The SM1 can be thought of as the gain bandwidth product (GBP) where, P_{MNF} is the gain and MNF is the central frequency band. It is thus inferred that while the frequency bandwidth increases with restfulness, the power gets distributed over the larger bandwidth and so the system maintains a constant GBP by virtue of the reversal of the two characteristics.

Box plots of the spectral entropy of all the states are shown in Figure 6.5(a). The characteristics of median and IQR of the spectral entropy are similar to that of MNF in Figure 6.4(a), *i.e.* it increases upto a certain state and then decreases till the end. In this case, the maximum of the median, IQR and the overall range are all maximum at Sup 3. Thus it can be interpreted that the power spectral distribution increases till Sup 3 both in median sense as well as the in the range of values as evident from the IQR.

This is further validated in terms of the histogram of the occurrence of the maximum entropy in a set shown in Figure 6.5(b). It can be seen that most frequent occurrence of maximum entropy is the Sup 3 state, which is 4 to 6 minutes in the supine posture. This result has been stated in Table 6.14. As mentioned earlier, an interesting observation from Figure 6.4 and Figure 6.5 is that after this short duration, the system starts becoming active in some sense, thus leading to a decrease of system entropy and related changes in the associated features.

DS2

The same study has been conducted for the LH and RH acquired data in the DS2 datasets also where signals were acquired continuously for 10 minutes. Similar box plots have been plotted for both LH and RH for MNF, P_{MNF} and spectral entropy in Figure 6.6. Comparing Figure 6.6 with Figure 6.4, it can be seen that the same patterns are also observed for DS2. In Figure 6.6(a) and Figure 6.6(b), the median, IQR and the overall range of MNF is seen to be highest in Sup 3 for both LH and RH data. This is expectedly referred in the P_{MNF} plots in Figure 6.6(c) and Figure 6.6(d) where the median, upper and the lower adjacent levels are minimum in Sup 3 but the span of the IQR is maximum. It can also be seen from the spectral entropy plots in Figure 6.6(e) and Figure 6.6(f) that the maximum of median, IQR as well as

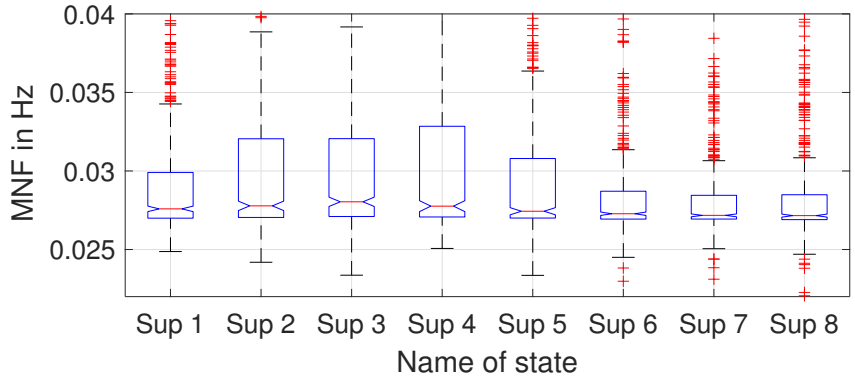

(a)

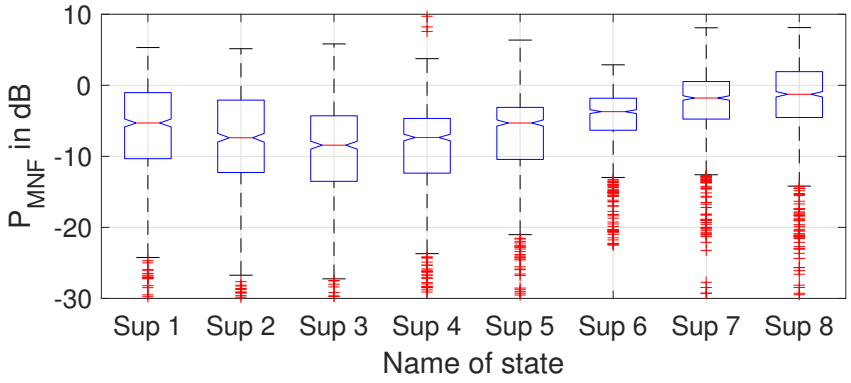

(b)

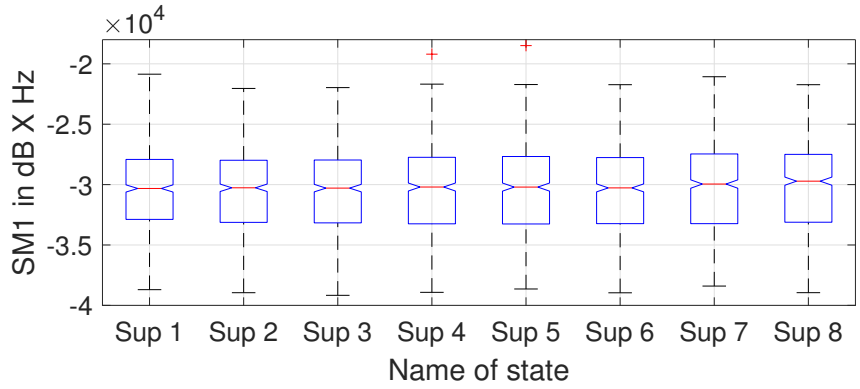

(c)

Figure 6.4: Box plots of (a) Mean frequency (MNF), (b) power at mean frequency P_{MNF} and (c) first moment (SM1) for the states Sup 1 to Sup 8 in DS1

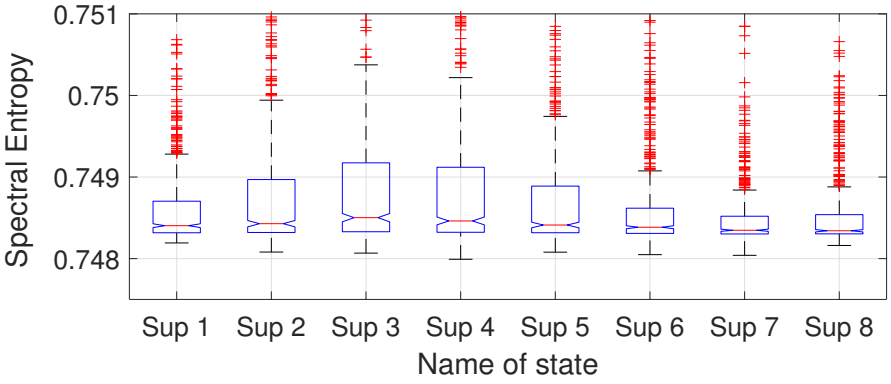

(a)

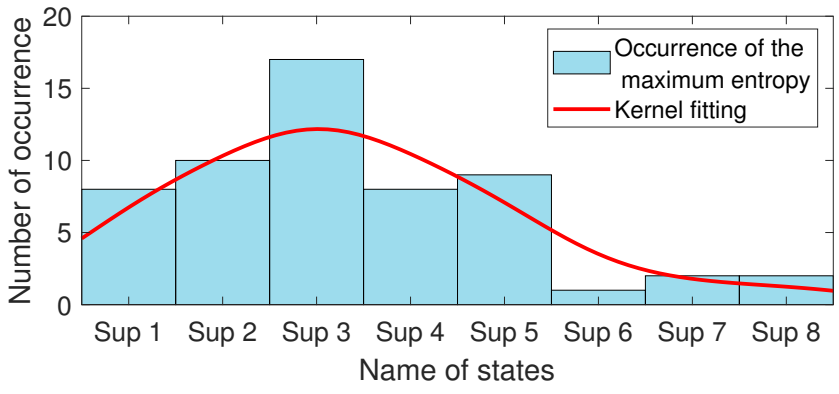

(b)

Figure 6.5: (a) Box plots of the entropy of the signal in 10 subsets and (b) Histogram of the occurrence of maximum entropy in DS1.

span occurs at the Sup 3. Furthermore, in all 6 plots, the respective changes from start to maximum/minimum to end transitions are continuous as in case of the DS1 data.

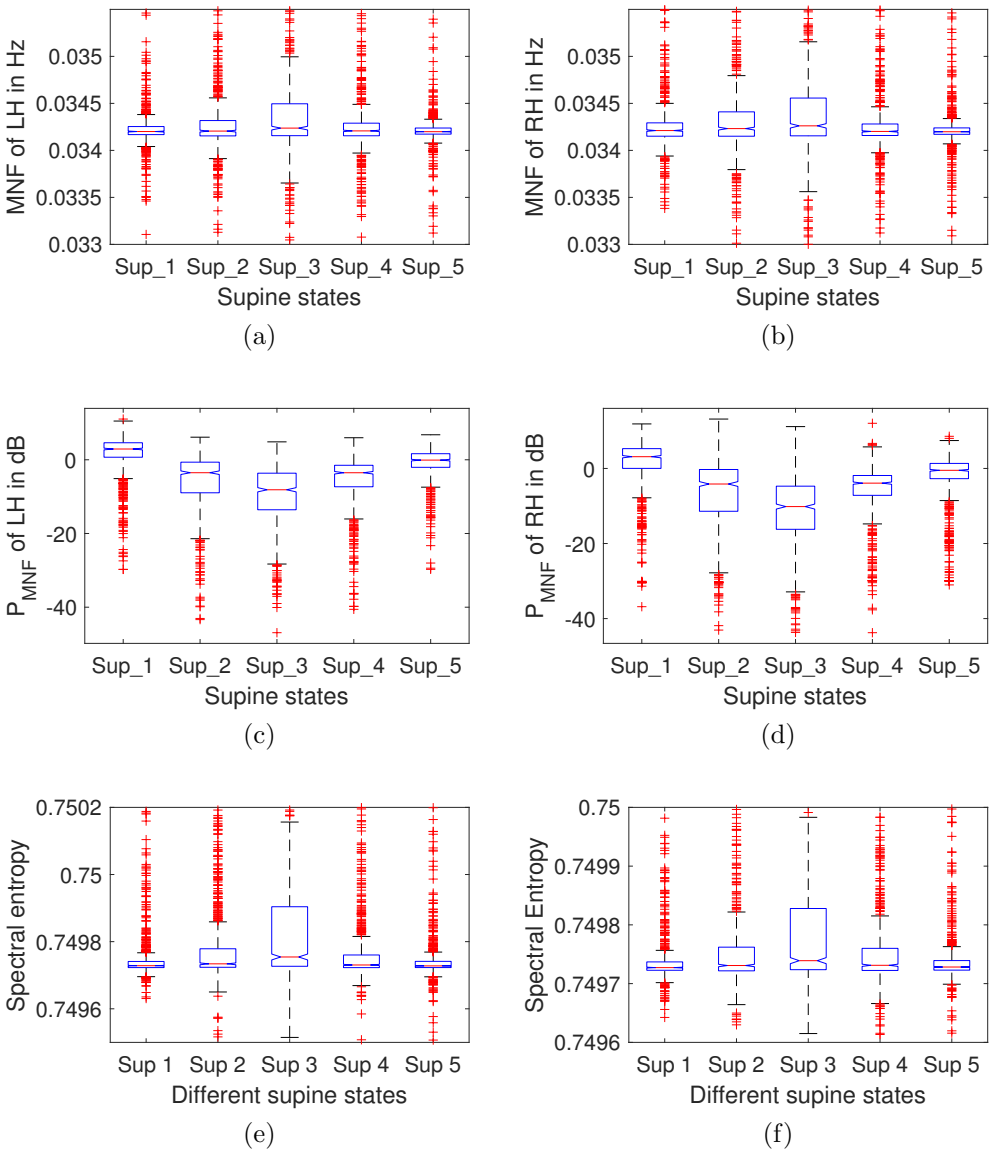

Figure 6.6: Box plots of (a) MNF_{LH}, (b) MNF_{RH}, (c)$PMNF_{LH}$, (d)$PMNF_{RH}$, (e)E_{LH} and (f)E_{RH} of the 5 supine states in DS2

DS4

The effective rest duration was also studied from the acquired LH, RH, LL and RL data in DS4 datasets. The same unimodal character (maximum at Sup 3) is observed in the MNF characteristics and occurs between 4 to 6 minutes, as evident from Figure 6.4. In Sup 3, the median value, range and span of the IQR of MNF are maximum. Exactly this feature can be observed in MNF plot of all the 4 classes of acquired signals in Figure 6.7. As expected, the characteristics are reversed in P_{MNF}, where the minimum of median, IQR upper and lower adjacent levels and maximum of the span of IQR occur at Sup 3 in all 4 respective plots of Figure 6.8.

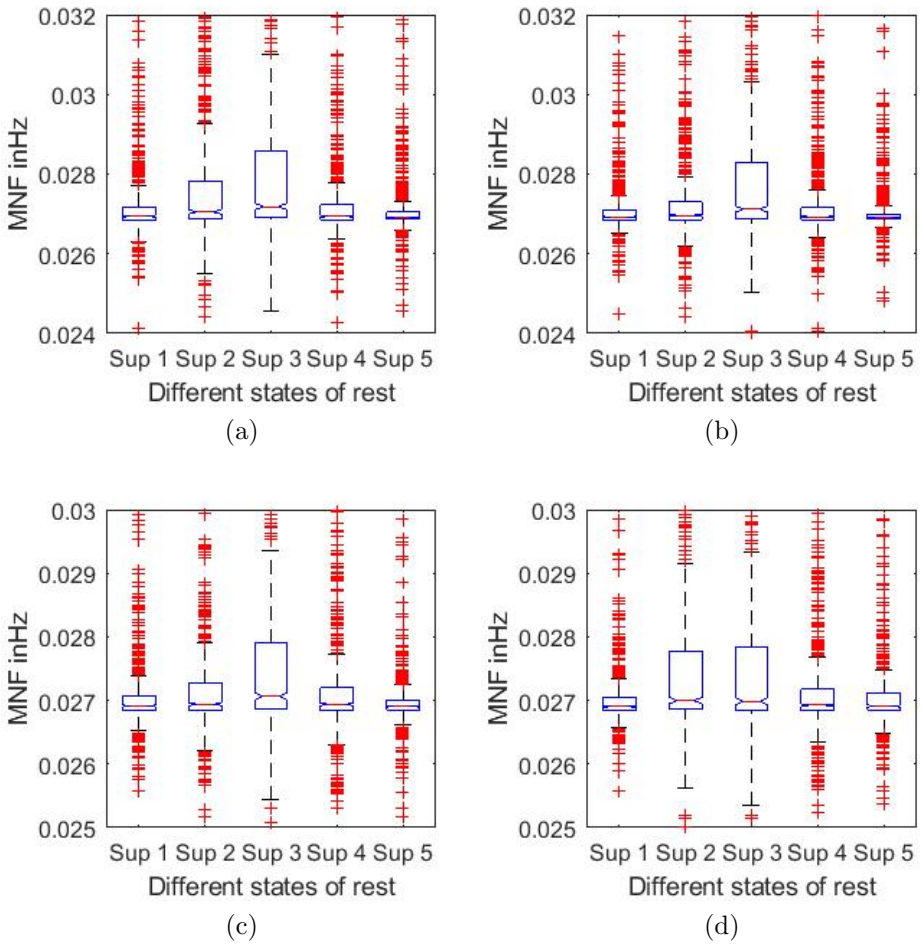

Figure 6.7: Mean frequency (MNF) of (a) LH, (b) RH, (c) LL and (d) RL of the 10 minutes 4 channel data in DS4

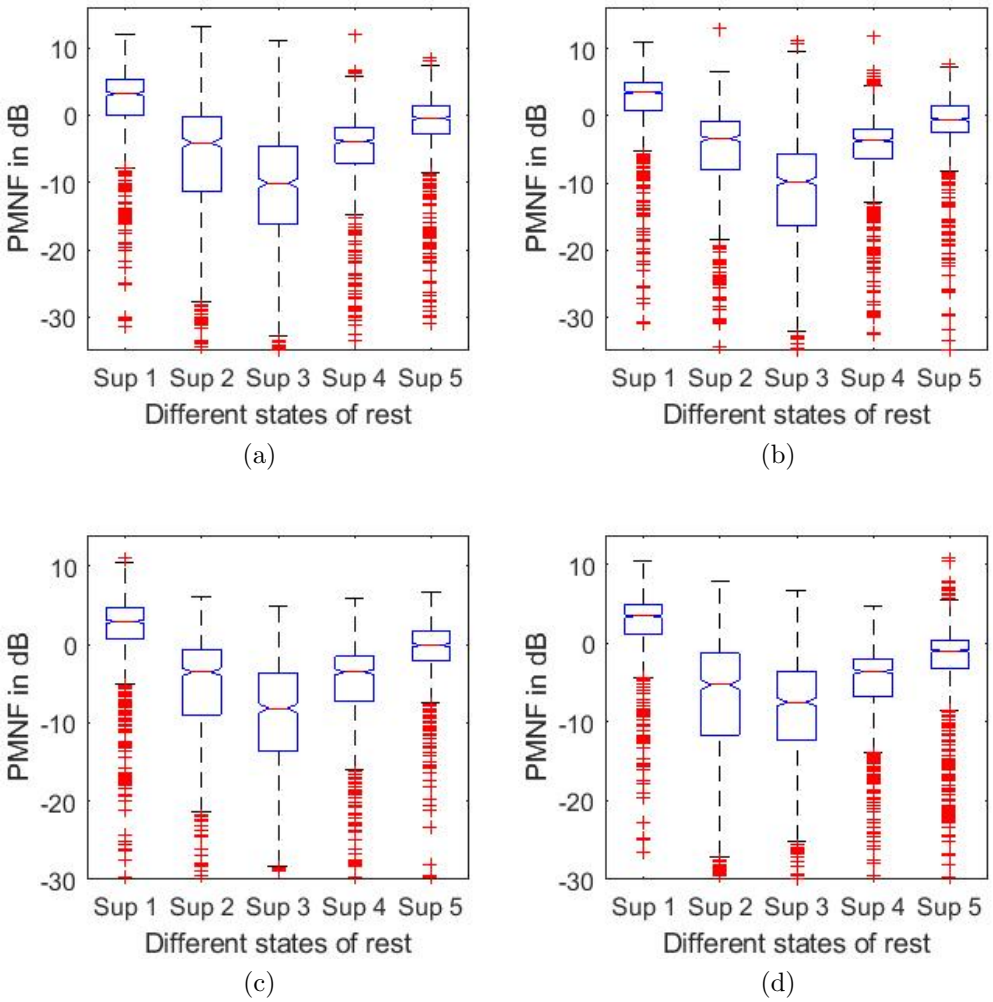

Figure 6.8: Power at mean frequency (PMNF) of (a) LH, (b) RH, (c) LL and (d) RL of the 10 minutes 4 channel data in DS4

As in the case of DS1 (Figure 6.5), in these cases also, the maximum spectral entropy occurs at Sup 3 for all 4 classes of data as seen in Figure 6.9. The spectral entropy is initially very low in Sup 1. Then it increases upto Sup 3 and further decreases again continuously till the end.

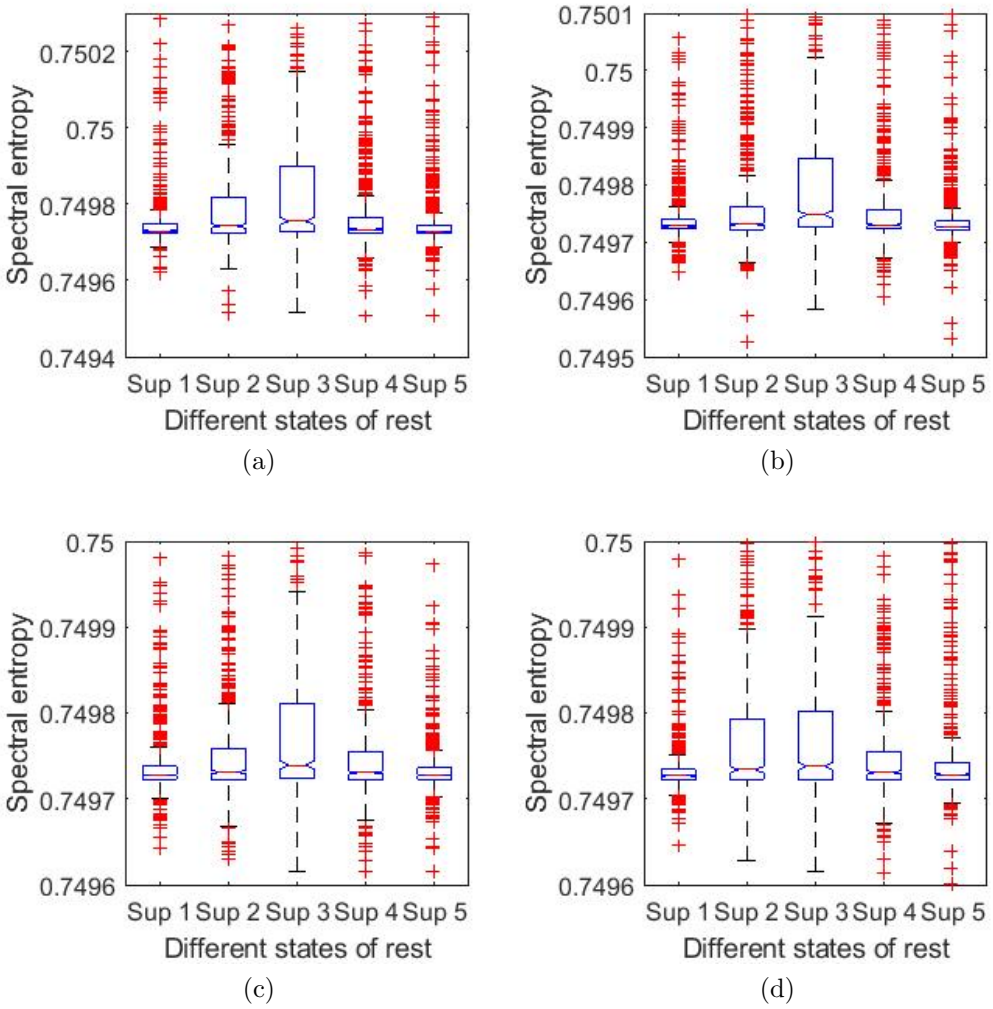

Figure 6.9: Spectral entropy of (a) LH, (b) RH, (c) LL and (d) RL of the 10 minutes 4 channel data in DS4

In order to compare the effect of rest on the acquired and the derived signals, the box plots of the mean values of all 4 acquired and 4 derived signals have been shown in Figure 6.10. It is observed that for the 4 acquired signals, the median keeps on increasing from Sup 1 to Sup 5 while the IQRs decrease till Sup 3 and then increase again. However, the mean of all 4

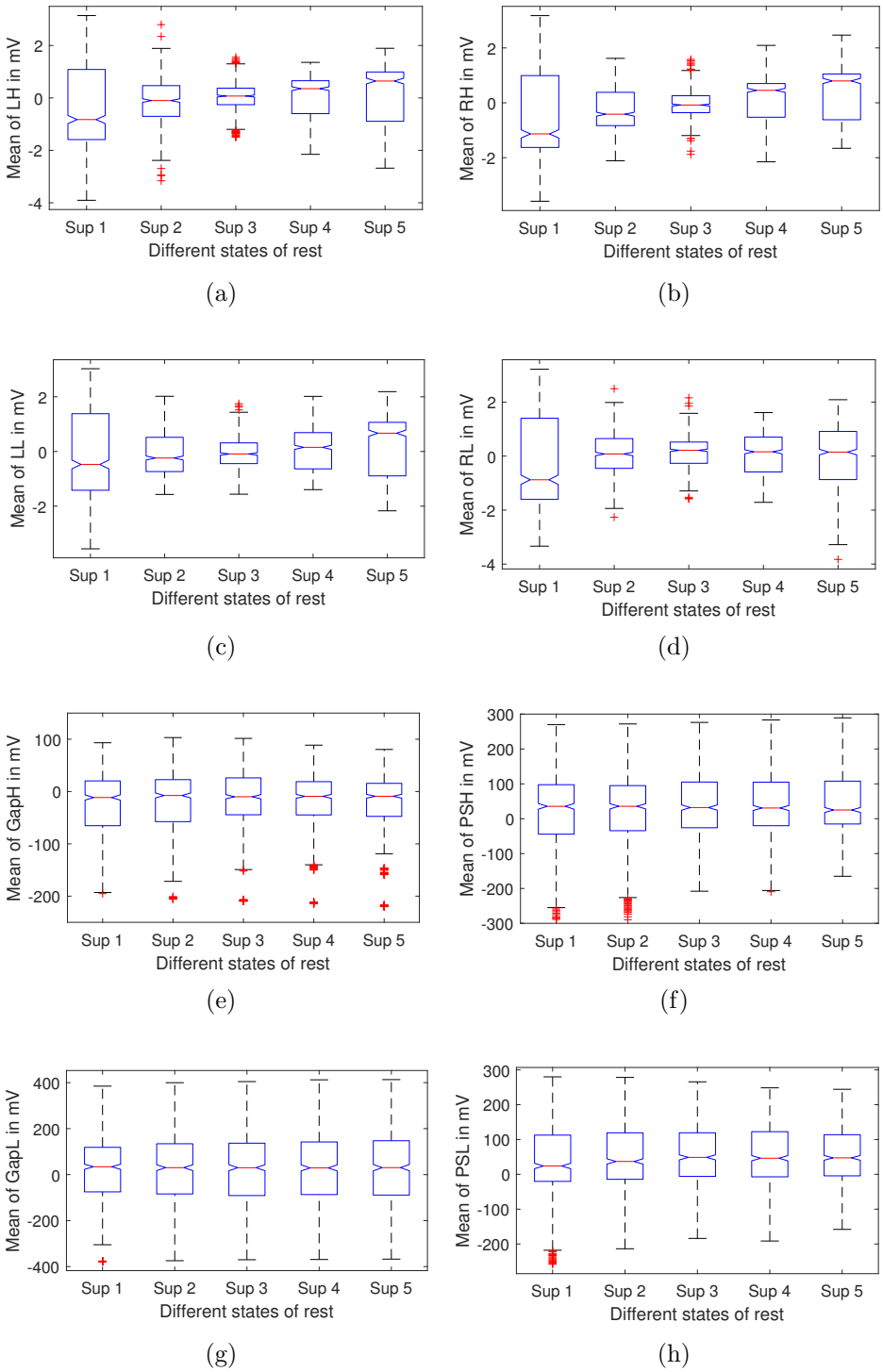

Figure 6.10: Box plots of mean values of (a) LH, (b) RH, (c) LL, (d) RL, (e) GH, (f) PSH, (g) GL and (h) PSL of the 10 minutes 4 channel data in DS4

derived signals have similar, almost constant characteristics both in terms of the median and the IQR in all the states.

Thus while the statistical mean also shows a definite change in characteristics with increasing duration of rest, the derived bilateral difference and common mode signals exhibit a constancy irrespective of the duration of rest.

In the next stage, the box plots of the SD of all 8 acquired and derived signals have been shown in Figure 6.11. It is observed that unlike the two distinctly separate characteristics exhibited for the mean, the SDs are constantly decreasing, both in terms of the median and the IQR, from Sup 1 to Sup 5 in all the acquired as well as the derived signals. However, the rate of decrease slowly reduces from Sup 1 till Sup 5. This phenomena may be indicative of the habituation of the system to this restful posture or to the reduction of orthostatic hypotension as the system relaxes from the sitting posture to the supine posture [126].

DS3

In the DS3 experiment, the duration of rest of the subjects pertained to the prolonged sitting posture after they returned from a walk. Also, after every 2 minutes, the acquisition was stopped and the BP and PR of the subjects were measured.

The box plots for the MNF, P_{MNF} as well as the spectral entropy for both LH and RH signals are plotted in Figure 6.12. The results for MNF for LH and RH show decreasing trends in the median as well as the IQR from Sit 2 till Sit 4. The PMNF of RH also shows a reversed trend in both these aspects, as expected. However, this is not valid for the PMNF of the LH signal and further, the results for the spectral entropy are inconclusive with notches extending beyond the ends of the box in both signals, presumably due to small sample size [154].

6.5.2 Comparison with existing methods

Rest in terms of *short nap* has been a topic of research in several studies as tabulated in Table 6.14. In most of these studies, sophisticated standard techniques like ECG and EEG have been used for sleepiness or alertness detection, while in some cases EOG has also been used to track slow eye movement that occurs due to fatigue or drowsiness along with EMG. Self reporting or performing definite tasks have been used in almost all cases to check change in efficiency and the output is measured using any standard scale.

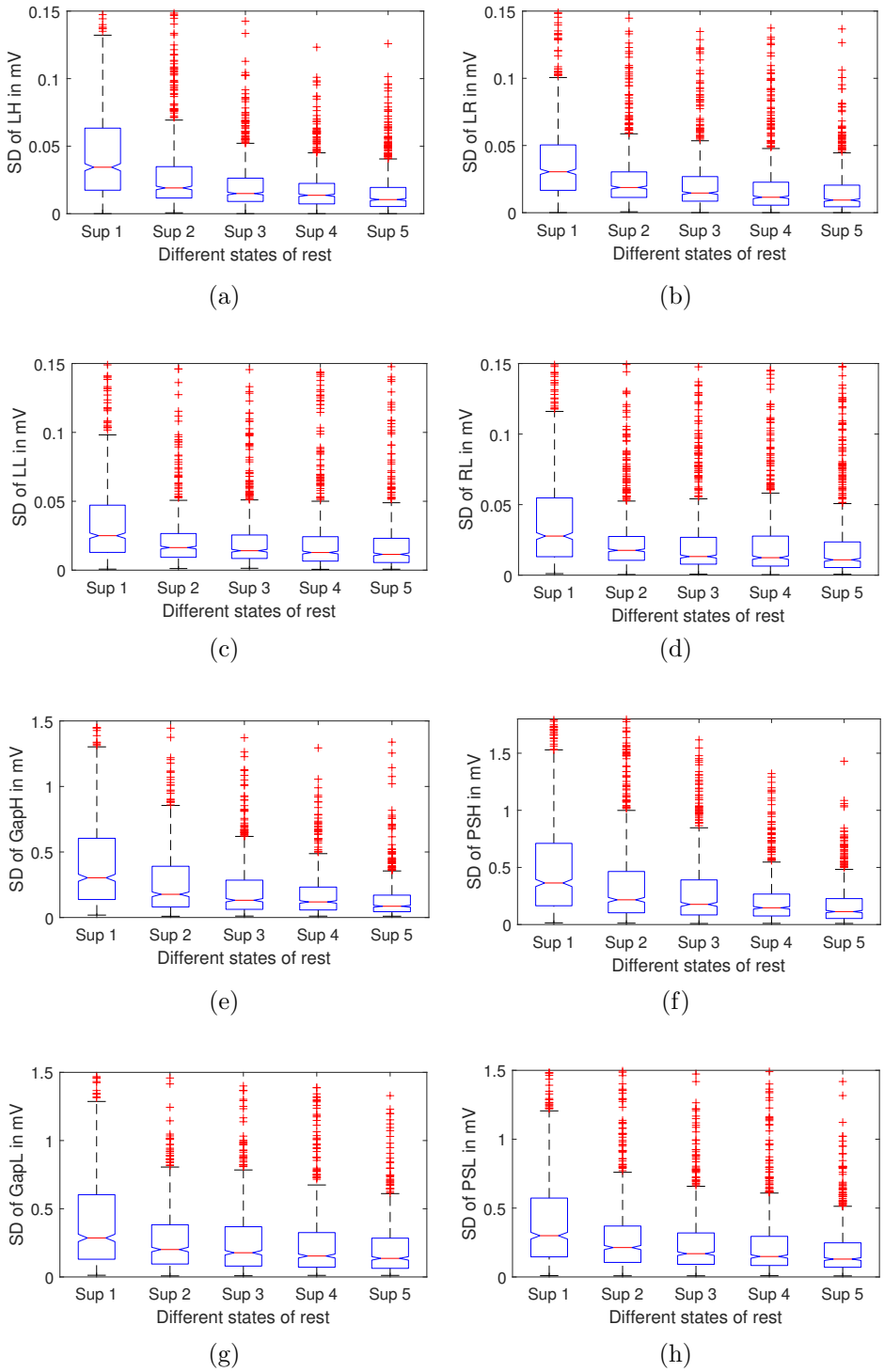

Figure 6.11: Box plots of SD values of (a) LH, (b) RH, (c) LL, (d) RL, (e) GH, (f) PSH, (g) GL and (h) PSL of the 10 minutes 4 channel data in DS4

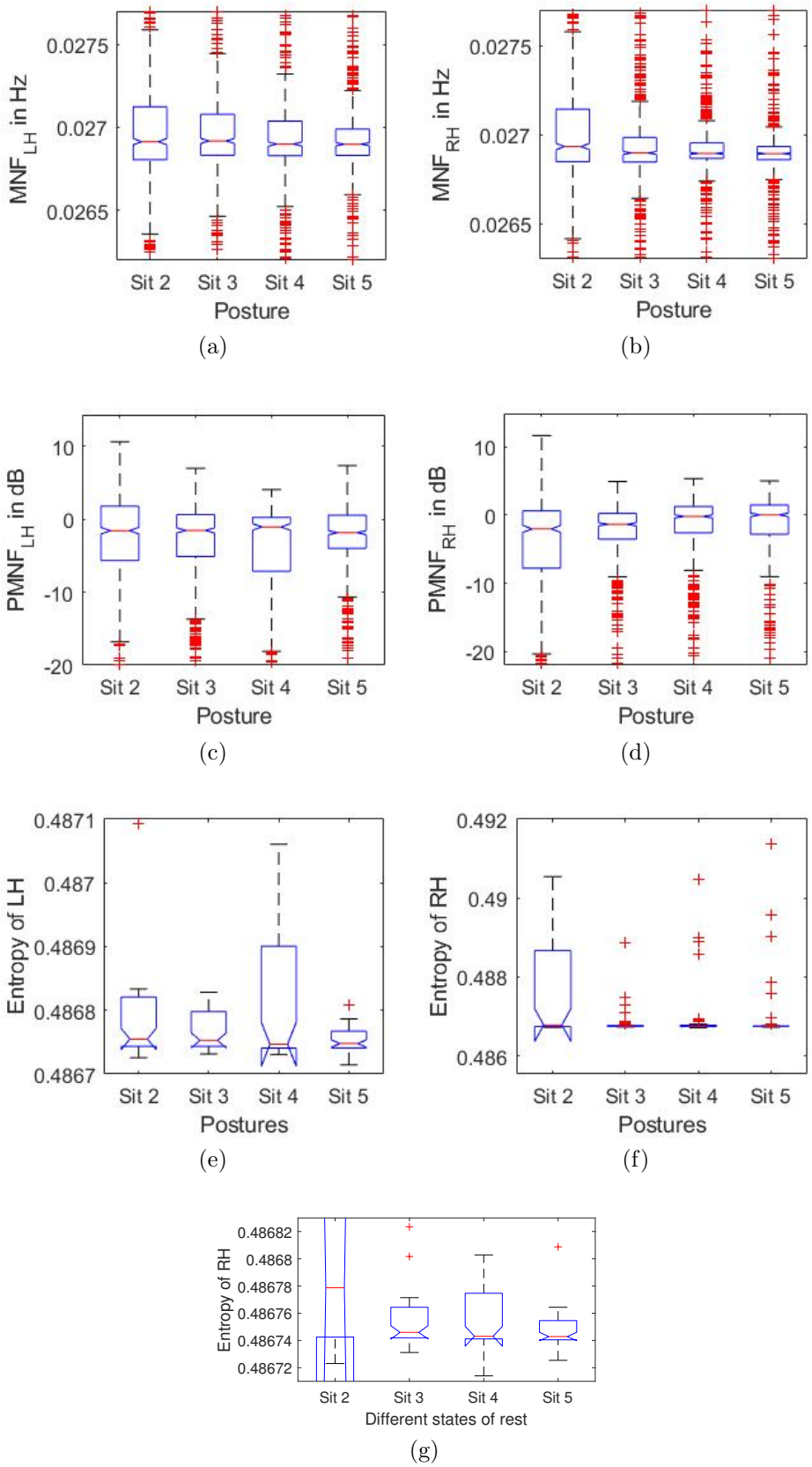

Figure 6.12: Box plots of (a) MNF_{LH}, (c)$PMNF_{LH}$, (e) $Entropy_{LH}$, (b) MNF_{RH}, (d)$PMNF_{RH}$, (f) $Entropy_{RH}$ and (g) zoomed plot of $Entropy_{RH}$ in the prolonged sitting phase in DS3 after the walk.

The outcomes of these experiments in terms of the duration that provides subsequent enhancement in subject efficiency vary between 7.3 minutes to 20 minutes, but most of these studies converge to an effective duration of around 10 minutes.

In the present case, the objective is to determine a physiologically determinable effective duration of rest while the subject was in daytime no-nap supine condition in a controlled environment. Hence, the subjects were not disturbed during the experiment and neither was any self reporting done by them. It has already been established in Section 6.5.1 that the effect of restfulness is obtained almost singularly from the maximum entropy of the acquired DDP signals. The results across all the three protocols of DS1, DS2 and DS4 experiments are identical. In all cases, the value of the effective duration of rest is obtained from the maxima of the median as well as the IQR of the maximum entropy parameter as 4 to 6 minutes.

Table 6.14: Estimation of effective duration of rest

Serial	Authors & year	Experiment	Measurement	Outcome
1	Mats Gillberg *et al.* (1996) [34]	Effect of short nap at day time	Self reported sleepiness/alertness, ECG and EEG	19.8 minutes
2	J. A. Horne *et al.* (1996) [35]	Effect of nap, coffee and placebo on drivers sleepiness/alertness	Self reported sleepiness, ECG indicates alertness	10.8 minutes
3	Masaya Takahashi *et al.* (2000) [29]	Effect of 15 minute nap after a short night sleep	Polygraph monitoring for sleep, Visual analog scale and ECG for subjective sleepiness and logical reasoning test for alertness	10.2 minutes
4	Amber J. Tietzel *et al.* (2001) [30]	Estimation of effective duration of short term rest after noctural sleep restriction	ECG and EOG measurement	10 minutes
5	Amber J. Tietzel *et al.* (2002) [31]	Estimation of effective duration of short term and ultra short rest after noctural sleep restriction	EEG and EOG measurement, different tests	10 minutes
6	Mitsuo Hayashi *et al.* (2005) [155]	Corrective power of short day time nap	Subjective mood, visual detection and symbol-digit substitution tasks, and slow eye movements	9.1 minutes

Table 6.14 – continued from previous page

Serial	Authors & year	Experiment	Measurement	Outcome
7	Mitsuo Hayashi *et al.* (1999) [32]	Effect of 20 minute nap and no nap at noon	EEG, mood, performance, and self-ratings of performance level	20 minutes
8	Mitsuo Hayashi *et al.* (1999) [33]	Effect of 20 minute afternoon nap on mood, performance and cardiac activity	EEG, mood, performance, and self-ratings of performance level	20 minutes
9	Mitsuo Hayashi *et al.* (2003) [36]	Effect of short daytime nap with caffeine, bright light and face washing on day time sleepiness	event related potentials (ERP) and EEG power spectra	15 minutes
10	Masaya Takahashi *et al.* (1998) [156]	Effect of post lunch short nap on alertness, performance, and autonomic balance	event-related potential, subjective sleepiness and ECG	7.3 minutes
11	Amber Brooks *et al.* (2006) [157]	Comparison of different length of afternoon nap	ECG, EMG, EOG	10 minutes
12	Nasser Al-Busaidi (2018) [158]	Subjective and objective effects of post lunch short nap	EEG,EOG and work place questionnaire	10 minutes
13	Cassie J. Hilditch (2016) [159]	10 or 30 minutes nap, which one associated with sleep inertia	The Samn-Perelli Fatigue Scale for fatigue measurement, polysomnography (PSG), EEG, EMG, EOG	10 minutes

Table 6.14 – continued from previous page

Serial	Authors & year	Experiment	Measurement	Outcome
14	Mohamed Romdhani (2020) [160]	Effects of nap after sleep loss on reaction time, mood, and biochemical response in athletes	Anaerobic sprint test, reaction time, Hooper index, Epworth Sleepiness Scale, biomarkers and antioxidant status.	20 minutes
15	Present method	Spectral entropy and other relevant features of DDP signals	Maximum entropy calculation	4 - 6 minutes

6.6 Discussions

Three different human condition monitoring applications are presented in this Chapter. These are hypertensive and normotensive subject classification, different posture classification and estimation of the effective duration of rest. The data acquisition experiments have been detailed in Chapter 4. The data used in each of these applications has been listed at the outset of this Chapter also.

In all cases, the acquired datasets have been preprocessed in a definite manner. At first data cleaning has been done to remove anomalies or to address missing data, this has been followed by z-normalization of the data. Thereafter, the datasets have been suitably quantized to enable the classification and interpretation. All the unilateral as well as the bilateral parameters presented in Chapter 5 have been listed in Section 6.1.4 for use as features in these applications. In the first two applications, the attribute selection and classification have been done in WEKA version 3.9.4 using the RF classifier.

Hypertensive and normotensive subject classification was done using DS2 where DDP signals were collected from two hands continuously for 10 minutes. After using attribute selection filter on the total set of features, only 5 parameters were selected, of which 4 are bilateral parameters. However, the most preferred attribute for differentiating hypertension is the standard deviation (indicating the random variations) of the left hand, which is physically located closer to the heart than the right hand. It is interesting to note that with increased duration of rest, the variations in the signal slopes of the derived signals of the hands, that is the bilateral difference signal GapH and the common mode signal PSH, are different for normal and hypertensive subjects. The lateralization coefficient of the mean is also helpful in this classification.

RF classification was used for this experiment with 10FCV and LOOCV. 10FCV tests were also done using SVM and k-NN classifiers. The best result provides an accuracy of 0.80 using LOOCV for RF classifier. It is known that methods based on ECG can differentiate these classes with accuracies well above 90%. In comparison, the classification accuracy of the DDP signals based method at 80.60% is significantly low. Yet, the minimal subject discomfort during its acquisition using the simple 10 minutes rest protocol and the simplicity of the protocol that allows even nominally skilled health workers to handle this procedure can be useful for primary monitoring and screening purposes.

In the next application, different postures were classified using parameters of DDP signals. While classifying sitting and supine postures from left hand

data only of the DS1 experiment, the accuracy achieved is 0.99 from just 3 parameters, specifically the mean, the SD and the normalized variance. The result has been cross-validated using 10FCV, LOOCV and LOSOCV.

While classifying sitting, supine and standing postures using LH and RH signals of the DS3 dataset, the accuracy achieved is 0.866 using 7 parameters only, of which 6 are the mean, the SD and the normalized variance of both hand signals and the remaining is the lateralization coefficient of the mean.

It can thus be said that the effect of posture change is mainly detected in the two most standard statistical features of the signals, namely their mean and SD or variance, and their combination, namely the lateralization coefficient of the mean. Furthermore, these affect the slow changing tonic as well as the fast changing phasic components of the DDP signals through the combination of the mean and its lateralization coefficient and the combination of SD and normalized variance of the signals respectively.

From the RF classifier results for 10FCV, LOOCV and LOSOCV, it is evident that the sitting and supine postures can be classified with an accuracy higher than 90% using these DDP signal features and this result is free from significant subjective bias. This is comparable to that achieved using several of the existing more complex methods.

In terms of the physiology of rest, it can be said that since the natural order of a system is disorder, and hence higher entropy [161], so an indicator of relaxation or relief from the stressors would be the increase of the spectral entropy, as also the maximum spectral entropy. Spectral entropy is the measure of system randomness. It is known from [162] that in a system with high entropy, the power spectrum is distributed over a wider range of frequencies.

It has been observed from the small IQRs of the MNF and PMNF box plots in the initial Sup states in case of DS1, DS2 and DS4 experiments that the power is initially concentrated near the central frequencies. Thereafter, it can be said that as the body becomes restful, the system bandwidth increases and its total power gets distributed over a larger frequency range causing the IQR of the MNF and PMNF box plots to spread but in reversed manner, while GBP in the box-plots of SM1 remain constant till typically the Sup 3 state. Thereafter this effect is reversed to some extent, indicative of a return from the maximal restful condition physiologically achieved. This duration for the 3^{rd} supine state from the start (Sup 3), that is 4 to 6 minutes in the supine posture, has thus been termed the effective duration of rest in this study.

This obtained result differs significantly from the other results of effective duration of rest. A probable cause is that those results are based on short nap, while in the present study, restfulness has been studied in terms of physiological changes and determined in no-nap condition.

In the DS3 experiment, the subjects assumed restful sitting posture after returning from a walk. So this provided a scope to explore whether a prolonged duration of sitting is comparable to that in a supine posture in the physiological sense. However, it is to be noted that since the acquisition was stopped after every 2 minutes in order to measure the BP and PR, so the restfulness of the subjects was in a sense disturbed and its effect is likely to be limited. As expected, some of the characteristics, particularly the mean frequency, exhibited the effect of rest but it was difficult to determine an effective duration of rest in this scenario.

CHAPTER 7

Conclusions and Scope for future work

The conclusions from all the studies conducted are summarized in this chapter, followed by a discussion of the scope for future work.

7.1 Conclusions

Differential dermal potential or DDP signal is the potential difference between two adjacent active sites on the skin surface without any electrical stimuli, typically the intermediate phalanges of the index and middle fingers of hands and feet. This signal has initially been acquired using the RISH Multi 18S multimeter based data acquisition system (DAS), *i.e.* RISH Multi 18S multimeter and RISH Multi SI232 assembly. This DAS is capable of acquiring low voltage signals (in order of 10μV) from multiple locations simultaneously with moderate speed, good accuracy and acceptable precision. It also has optical isolation to provide electrical safety. However, its major limitations are the lack of compatibility of its computer interface software Rishcom 100 with Windows 7 onwards updated OS platforms and its lack of portability, specially when the number of channels are more.

In view of this, two other advanced acquisition systems (Advantech USB-4704 and Keysight LXI) have been tested but these did not perform as expected. Advantech USB-4704 lacks the required accuracy as well as precision, while the Keysight LXI lacks in portability and consumes much power. It is also not able to acquire data with required sampling speed in high resolution.

The limitations of the RISH Multi 18S based system and the unsuitability of the other two systems tested led to the calibration and testing of a dedicated 4-channel data acquisition system that was designed and developed indigenously by Somen Biswas, a co-author in [1], in the same research laboratory in which the present study is done.

A standard protocol has been developed in this work for balancing and calibrating the 4-channel DAS. At first, a preliminary static calibration of

the 4-channel DAS is performed to estimate its nominal performance. It is typically found that all 4 channels are linear but not identical. To balance all 4 channels as well as to increase the relative accuracy, three tuning methods have been tested. These are: i) inverse slope multiplication, ii) spline fitting and iii) addition of error curve. The third method has been adopted due to its comparatively low standard deviation (SD) value in the operating voltage range. The DAS, thus updated, is calibrated again. It typically shows very good accuracy with very low static error as well as improved precision and sensitivity. Although the RMSE increases marginally after tuning but all 4 channels are balanced and hence, interchangeable. The common mode interference voltage (CMIV) of this balanced DAS is also observed to be very low. Finally, a comparison of the calibration results of the RISH Multi 18S and the balanced and standardized 4-channel DAS show that both these systems exhibit comparable performances. Thus, while both these systems have been used in the present work, the preferred system is the 4-channel DAS due to its enhanced portability and updated interfacing abilities.

In order to fulfill the multiple objectives of this present study, four (4) specific experiments have been designed and conducted to acquire 4 different datasets for 6 applications in total. All 4 experiments have certain common general conditions pertaining to subject selection, material and methods and experimental conditions maintained. The experiments thus start with a common preliminary protocol, followed by different data acquisition sequences.

The data sets collected from these experiments are labelled henceforth as DS1, DS2, DS3 and DS4, while the terms LH, RH, LL and RL denote left hand, right hand, left leg and right leg respectively. The description of all 4 experiments and all 6 applications are given hereafter.

Experiments : DS1: DDP signals are acquired from only LH for 20 minutes which include 2 minutes in sitting posture, then 2 minutes during change in posture from sitting to supine and last 16 minutes in supine posture

DS2: DDP signals are acquired from LH and RH of supine subjects for 10 minutes

DS3: DDP signals are acquired from LH, RH of subjects for a specific set sequence: supine for 4 minutes, then sitting and then standing for 2 minutes each. This is followed by a no recording 1 minute activity session. Then subject sits again and DDP signals are acquired till a specified condition is met.

DS4: DDP signals acquired continuously from LH, RH, LL and RL of supine subjects for 10 minutes

Applications : Application1: Validation of the DDP signal by comparing it with standard recommended endosomatic EDA signals (golden reference) using DS1 dataset

Application2: Study unilateral characteristics of DDP signals using DS2, DS3 and DS4 datasets

Application3: Study bilateral characteristics of DDP signals using DS4 dataset

Application4: Classification of hypertensive and normotensive subjects using LH and RH of DS2

Application5: Classification of different postures using LH of DS1 and both LH and RH data of DS3

Application6: Determination of the effective duration of rest in supine posture from LH of DS1, both hands data (LH and RH) of DS2 and all 4 channel data (LH, RH, LL and RL) of DS4 datasets and in sitting posture from both hands data (LH and RH) of DS3 dataset

In Application1, the DDP signals have been validated by establishing the physiological basis and comparison with 2 standard endosomatic EDA signals as well as their difference signal. Since this signal is recorded in the DC mode, hence it is inferred from the standard RC model of the skin that this signal primarily records the differential information communicated by the nerve endings or the capillaries in the dermis and hypodermis, rather than the sweat gland activity recorded in usual EDA signals. The autocorrelation functions (ACF) of these differential signals confirmed that these signals are non-random signals originating from inherent time-varying processes. Furthermore, two distinct patterns of the ACF have been identified that are correlated with 2 classes of underlying signals. The cross-correlation studies however established that these two signals differ significantly in the information contained at sub-millivolt levels. The next study showed that both these signals are stable and have low settling times, typically within 2 minutes, thus validating their usability in real-time applications.

Two statistical features of these signals, namely average mean and kurtosis, determined over the total duration of the experiment are found to be similar for the differential and difference signals, but these differ from those of the two reference signals. It is further found that these characteristics of the differential signal can be used to differentiate the sitting posture and change in posture from the supine posture.

The standard deviation and kurtosis as well as the 2 spectral characteristics, namely power spectral density (PSD) and average band power, of all 4

types of signals are similar. Furthermore, the standard deviation and kurtosis show measurable and consistent differences during the change in posture while 2 of the spectral characteristics, namely power spectral density (PSD) and average band power, are affected by the extended rest of the subjects.

Application2 involves the unilateral characterization of these signals. This has been done by clubbing together all the LH, RH, LL and RL signals from the DS2, DS3 and DS4 datasets into these four classes. Then all the datasets of durations longer than 2 minutes were sub-divided into multiple numbers of 2 minutes subsets. Thereafter the basic characteristics of these 4 classes of acquired signals were studied, followed by a study of their mean values and then the study of the (mean subtracted) debiased signals.

As was evident in the earlier study of hand signals by Bhattacharya [5], in this case also, 90% of all the acquired signals lie typically within ±200mV and are mostly positive or negative with very few transitive signals. But in this study, the analysis of the trends of signals show a marginal dominance of the constant signals (*i.e.* with variations within ±4mV) with the remaining signals being equitably distributed among the increasing and decreasing trends.

A comparative study of the overall characteristics of the signal mean, also referred as the bias, of all 4 signals and those of the original signals establish that they are almost identical. This reiterates the finding in Bhattacharya [5] that the mean, or bias, is representative of the acquired signal.

In case of the debiased signals, it is found that these lie within ±6mV in more than 95% cases, though the overall range is relatively high. Furthermore, from the zero crossing instant value (ZCI) and the slope of the fit (m), it is found that in more than 90% cases, signals cross 0mV axis within 800^{th} to 1600^{th} instant, *i.e.* within 40s to 80s, which is the middle of the whole epoch of 2 minutes. Slope of these signals are also very low (in the order of 10^{-2}) mV/instant). These findings are also in accordance with those in Bhattacharya [5].

In this study, a detailed spectral characterization of these signals has been performed. It is found that the characteristics of the power spectral density of these 4 classes of signals are similar and the maximum or peak frequency PKF occurs very close to the origin. Furthermore, the mean frequency MNF and median frequency MDF show similar characteristics with marginally higher magnitude in case of MDF. The overall range of MNF is 2.16×10^{-3} to 2.3×10^{-3}, whereas the overall range of MDF is 2.87×10^{-3} and 2.82×10^{-3} in this analysis. The respective power at these frequencies P_{MNF} and P_{MDF} are also similar to each other but that for the peak frequency P_{PKF} is little higher in magnitude. 3 moment parameters SM1, SM2 and SM3 have also been studied. SM1 can actually be considered as the gain-bandwidth

product (GBP). It is found that SM1 of all 4 parameters are very close to each other as if a constant GBP is maintained in the system. As the frequency components are very small and very similar to each other, SM1, SM2 and SM3 are similar in characteristics but with different values. Finally, the spectral entropy of the acquired signals have been studied. It is seen that LH has the maximum entropy, followed by RL, LL and RH and the difference is in the order of 10^{-4}. Their median values are almost similar for all 4 cases.

Application3 pertaining to the relational aspects of these 4 signals have been studied using the DS4 dataset and this establishes the prevalence of bilateral interrelations over all other combinations. A subsequent study of the bilateral characteristics of the hand and feet signals show that converging, diverging and parallel trends of pair of signals are almost equally prevalent, while cross-over appears in only very few number of cases. Furthermore, bilateral derived signals GapH, PSH, GapL and PSL, proposed by A. Bhattacharya [5] have also been studied. These are found to lie typically within ±400mV, which is higher than that of the acquired signals. Two lateralisation coefficients LC1 and LC2 have also been characterized statistically.

The interdependence of both the hand signals and both the feet signals have been further studied by plotting the bilateral parameters in two different axes and dividing the 4 quadrants into 8 sub regions. Some patterns are observed in μ_{LH} vs. μ_{RH}, μ_{LL} vs. μ_{RL}, ZCI_{LH} vs. ZCI_{RH} and ZCI_{LL} vs. ZCI_{RL} plots but no clear pattern is evident in the m_{LH} vs. m_{RH} or the m_{LL} vs. m_{RL} plots.

On the basis of the detailed characterizations, two bias parameters have been proposed in this study, namely differential bias μ_{diff} and common mode bias μ_{cb}, to quantify the hemispheric dominance between the bias of acquired signals. Typical ranges of these parameters have been determined. The Q-Q plot and chi-square test for normality for both these parameters establish their normality.

Furthermore, 4 ratio parameters have also been proposed in this study. These are the two ratios of the ZCIs, namely ZCI_{ratioH} and ZCI_{ratioL}, and the two ratios of the slopes, namely m_{ratioH} and m_{ratioL}. Another parameter, termed debias ratio (DR_k), has been proposed to represent the instantaneous behaviours of the debiased pair of signals. Its typical range is within ±14 for 95% cases. In view of the findings from the DR, another new parameter termed as log SD ratio ξ_{sd}, which is representative of a particular signal pair, is proposed for hands as well as for feet signals. It is found that the ratio of the SD of LH (or LL) and RH (or RL) signal pairs lie approximately within 0.10 to 10 times following a log-normal distribution and there is no significant hemispheric dominance in this parameter for the overall data collected for this population. All these proposed parameters have been statistically

characterized.

Finally, three different human condition monitoring applications are presented in detail. Application4 pertains to hypertensive and normotensive subject classification, Application5 to different posture classification and Application6 to the estimation of the effective duration of rest. In all cases, firstly data cleaning of the acquired datasets has been done to remove anomalies or to address missing data, followed by the z-normalization of the individual long datasets. After that, all the long datasets have been subdivided into 2 minute subsets, which have been further quantized into small sets of 10s to make them ready for use in these applications. In Application4 and Application5, the attribute selection and classification have been done in WEKA version 3.9.4 using the random forest (RF) classifier using all the unilateral as well as the bilateral parameters studied in Application2 and Application3 along with two additional derived features, namely normalized variance and normalized kurtosis. However, based on the preliminary observations in Application1, mainly spectral characteristics have been studied for the assessment of rest duration in Application6.

In Application4, DS3 data has been used for classification of hypertensive and normotensive subjects. Attribute selection filter selected only 5 attributes among all, of which 4 are bilateral parameters. However, the most preferred attribute for differentiating hypertension is the SD of the left hand. It is to be noted that while the SD is indicative of the random variations in the signal, the LH signal is from a location that is physically closer to the heart than the RH signal.

Study using RF classifier confirmed that both accuracy and F1 score are more than 0.75. 3 cross-validation (CV) experiments, *i.e.* 10 fold CV (10FCV), leave one out CV (LOOCV) and leave one subject out (LOSOCV) have been performed. Additionally, the RF results have been compared with those of k-nearest neighbour (kNN) and support vector machine (SVM). The results confirm that the best performance is achieved using the RF classifier. Although these results are significantly low in comparison to existing methods based on ECG, which can differentiate these classes with accuracies well above 90%, yet the minimal subject discomfort during its acquisition using the simple 10 minutes rest protocol and the simplicity of the protocol that allows even nominally skilled health workers to handle this procedure can be useful for primary monitoring and screening purposes.

In the first part of Application5, sitting and supine postures have been classified using the relevant 2 minute subsets of the LH signals in the DS1 datasets. This binary classification result shows that 10FCV in RF method can classify sitting posture with accuracy of 1.0, and supine posture with accuracy of 0.997 respectively using mean, SD and normalized variance. The

LOOCV and LOSOCV tests performed for cross-validation also support the 10FCV result. In the second part, a 3-level classification of supine, sitting and standing postures have been done using the relevant subsets of the DS3 datasets in a similar manner as in the earlier case. It is found that the same parameters as selected in the binary classification, only that this time they are from both hands, have majorly contributed in this application too. Along with that, 1 bilateral parameter, that of the laterization coefficient of the mean, also contributed to achieve the classification accuracy of more than 0.8.

In Application6, the *effective* duration of rest of supine subjects has been estimated using all three datasets DS1, DS2 and DS4. In terms of the physiology of rest, it can be said that since the natural order of a system is disorder, and hence higher entropy [161], or system randomness, is an indicator of relaxation or relief from the stressors. It is further known from [162] that in a system with high entropy, the power spectrum is distributed over a wider range of frequencies.

Accordingly, in all these cases, the system entropy shows a pronounced increase till the 3rd supine state lasting from 4 to 6 minutes, followed by a slight decrease as the human system gets into a state of prolonged rest. This is substantiated by analogous characteristics of the MNF and P_{MNF}. Thus, it is inferred that if a subject maintains a supine posture typically for 4 to 6 minutes, it provides effective rest to the system.

This obtained result differs significantly from the other results of effective duration of rest. A probable cause is that those results are based on short nap, while in the present study, restfulness has been studied in terms of physiological changes and determined in no-nap condition.

As part of this application, the same was tested for the prolonged sitting posture of the subjects in DS3. However, possibly since the acquisition was stopped after every 2 minutes to measure the blood pressure and pulse rate, the restfulness of the subjects was disturbed to some extent. The analysis also supports this finding since some of the characteristics, particularly the MNF, exhibited the effect of rest but it was difficult to determine an effective duration of rest in this scenario.

One interesting aspect noticeable from Application5 and Application6 is that the effect of posture change from one static posture to another is mainly detected in the time-domain statistical features of the signals, while the effect of rest is most discernible in the frequency domain or spectral features. Furthermore, posture change affects the slow changing tonic as well as the fast changing phasic components of the DDP signals through the combination of the mean and its lateralization coefficient and the combination of SD and normalized variance of the signals respectively.

Thus the differential dermal potentials have been established as valid signals with independent information content. These can be acquired reliably using suitable, yet simple data acquisition systems in well designed, yet simple experimental protocols. It is further validated that their various statistical, spectral, linear regression and other parameters are useful in screening, classification as well as monitoring of inherent or changing or static human conditions.

7.2 Scope for future work

For the present work, 4 channel DAS could be calibrated for a maximum resolution of 10μV although it has been designed for 1μV resolution. It needs to be calibrated for 1μV resolution with a suitable calibrator. The drift of this device has been studied for 2 minutes only. In order to use it for other long term uses, it is needed to study the drift of the DAS for longer periods. It is also possible to alter the sampling rate of the DAS to 50samples/s. In order to use that feature, detailed calibration and preliminary study will be needed.

In the study of the ACF of the DDP signals, two distinct patterns have been observed which are shown to result from two types of signal patterns. The reason behind these two patterns in the ACF characteristics and their implications, if any, in terms of the human system dynamics could be investigated in future.

The DDP signal has been modelled as a simple linear model in this study and has accordingly been represented in terms of its mean value, ZCI and the slope m. But from the study, it is seen that the signals are not exactly linear in characteristics. There is thus a scope to determine a method to determine the exact order of the signals and a suitable model to fit it and/or to develop some other complex mathematical model to represent these signals.

In this study, the 3-level classification of the sitting, standing and supine postures have been done using the hand data. It can be seen in future whether these postures can be classified using feet data also. Some other postures can also be tested. The effect of transition between postures on these signals can also be investigated with possible use in detecting human dynamics or flaws thereof.

The effective duration of rest of supine subjects has been estimated using these signals. It remains to be studied whether a similar physiological effect and/or an associated duration can be detected for a prolonged sitting posture. It is also to be seen whether these DDP signals can be used for sleep study and/or differentiating the different stages of sleep.

DDP signals were used for 3 condition monitoring experiments in this whole study. These results can be used as a baseline for further studies on human condition detection using electrical or non-electrical stimuli. It can also be tested whether this signal can be used for other human condition or abnormality assessment purposes.

Stretch receptor electrical activity [163], the electro-tonicity of the sub-surface muscles [164] and similar studies are topics of emergent research. It will be useful to investigate the utility of the DDP signals in these applications.

APPENDIX A

Appendix

A.1 Consent form

Note to the subjects:

You are being asked to take part in the research project described below. There are no known risks associated with this research. If you do not take part in the study, there will be no penalty. If you choose to take part, you have the right to stop at any time. However, we encourage you to talk to the research group so that we know why you are leaving the project. If there are any new findings during the study that may affect you, you will be told about them. Your part in this study is confidential. None of the information will identify you by name. All records will be maintained in codes so that identity is not disclosed. The collected data and information may be used and transferred to other research studied in the Research Laboratory. Your personal information will be suitably anonymised and/or masked to prevent tracing or identifying your identity. If you decide to enrol in this project, your involvement will be required in 2 or 3 phases for the experimental portion only and this may last for about 10-12 weeks in a phase. The results of this research study may be presented at meetings or in publications; however, your identity will not be disclosed in those presentations.

ABOUT THE RESEARCH TOPIC:

Topic: "*Study and characterization of the relational aspects of human biopotentials externally acquired from multiple locations*"

Biopotential based systems like Electrocardiogram (ECG), Electroencephalogram (EEG) and Electrodermal activity (EDA) based sensors are used abundantly to characterize several infirmities or diseases in humans since the biopotentials in different parts of the human body change under various physical, mental as well as social stressors. In a recent study, biopotentials have been acquired bilaterally from human subjects using a low cost,

passive, non-invasive EDA based system. A preliminary investigation of these potentials has indicated the existence of inter-relations between these bilateral signals. The aim of the present research is to perform a detailed study of the relational aspect of these and other biopotentials acquired externally from human subjects and to derive some definitive indices. The scope of research includes a feasibility study of using these indices in an expert system to classify the overall condition of the human health inclusive of physical, mental, social and spiritual wellbeing.

The bilateral biopotentials will be acquired using two systems. The first system comprises of 4 sets of multimeters (Make: RISH Multi 18S) with compatible adapters (Make: RISH Multi SI232) for online simultaneous recording of a maximum of 4 channels of data to the PC. The second system has been built indigenously in this laboratory, which can acquire potentials simultaneously from 4 locations and send to the PC. Both systems transmit data to the PC via optically isolated transmitter-receiver module to ensure safety to the human body from electrical hazards.

I, Mr./Mrs./Dr./Ms. ---------- resident of ---------- do hereby give consent voluntarily to record my endosomatic skin potential and other data pertaining to the research work being conducted by Mr. Arindam Sarkar under the guidance of Prof. Ratna Ghosh and Prof. Bhaswati Goswami in Instrumentation and Electronics Engineering Department, Jadavpur University. I have no objection to publication of my case study details without my name in any journal or any other reviews. I am signing this consent form voluntarily, out of free will, without any pressure and in my full senses.

Date: Full Signature:

Place:

Consent form explained/witnessed by: ----------

Date: Full Signature:

Place:

A.2 Overall Questionnaire

	SUBJECT CODE : S_ _ _				
	Full name	পুরো নাম			
	Sex (Male/Female)	লিঙ্গ(ছেলে/মেয়ে)			
	Age (years)	বয়স(বছর)			
	Please Answer the following - (write Y for yes and N for no):	***নিম্নলিখিতপ্রশ্নগুলির (হ্যাঁ বা না দিয়ে) উত্তর দিন***	*Do you take any medicine prescribed by doctor?*	*Do you take any medicine on your own?*	*Remarks, if any.*
1.	Do you have any disease from the following list (any history of Chronic illness)? (Y/N)	আপনার নিচের লেখা ব্যাধিগুলি থেকে, এক বা একের বেশী কোনো ব্যাধি (দীর্ঘস্থায়ী অথবা দুরারোগ্য) আছে? (হ্যা বা না)	কোনো রোগ থাকলে, হ্যা বা না দিযে উত্তর দিন	*আপনি কি ডাক্তারের বলা কোনো ওষুধ খান?*	*আপনি কি নিয়মিত নিজে থেকে কোনো ওষুধ খান?*
	High Blood Pressure/ Hyper tension	উচ্চ রক্তচাপ			
	Diabetes	মধুমেহ			
	Kidney problem	কিডনির সমস্যা			
	High Cholesterol	কোলেস্টেরল বেশী			
	Chronic Constipation	দীর্ঘস্থায়ীকোষ্ট-কাঠিন্য			
	Chronic Cardiac problem	দীর্ঘস্থায়ী হার্টের সমস্যা			
	Chronic Indigestion	দীর্ঘস্থায়ী বদহজমের সমস্যা			
	Any other Chronic illness	আর অন্য কোনো দীর্ঘস্থায়ী ব্যাধি			
	Prone to cold infection	সর্দি-কাশীর ধাত			
	Asthma	হাঁপানি			
	Headache	মাথা ব্যাথা			
	Migraine	মাইগ্রেন			
	Prostrate problem	প্রস্ট্রেট সমস্যা			
	Jaundice	ন্যাবা/পাণ্ডুরোগ			
	Dengue	ডেঙ্গু			
	Chicken pox	চিকেন-পক্স			
	Menstrual problem	মাসিকের সমস্যা			
	Others (mention)	অন্য কোনো সমস্যা (থাকলে জানান)			
	Mumps	ম্যাম্পস্			
	Toncil	টনসিল			

	Answer these questions in Yes/No	***নিচের প্রশ্নগুলির হ্যা বা না তে উত্তর দাও***	***Yes (Y)***	***No (N)***
2	Do you have any dominant or recurrent pain?	আপনার কোনো দীর্ঘস্থায়ী বা রোজকার বেথা আছে?		
	If yes (Y), please specify region.	হ্যা হলে কোথায়?		
3	Have you had surgery before?	আপনার কোনো অস্ত্রপচার হয়েছে?		
	If yes (Y), please specify	হ্যা হলে কোথায়?		
4	For females only: Any Hormone replacement (HR) therapy done?	মহিলাদের জন্য: আপনার কোনো হরমোনের চিকিত্সা হিয়েছে?		
5	Are you a consumer of alcohol?	আপনি কি মদ্যপান করেন?		
	if yes (Y) then, daily/weekly/monthly/occasional? is it more than 2 pegsor less?	হ্যা হলে, কিরোজ/সপ্তাহে/মাসে/মাঝে মধ্যে? ২ পেগের বেশি না কম?		
6	Do you smoke?	আপনি কি ধুমপান করেন?		
	if yes (Y), then what (cigarette/ biri/ cigar) ?	হ্যা হলে (সিগারেট/বিড়ি/সিগার)?		
	Is it more than 10 nos. daily or less?	দিনে ১০টার বেশি না কম?		
7	Do you take drugs?	আপনি কি মাদক সেবন করেন?		
	if yes (Y), then daily/weekly/monthly/occasional ?	হ্যা হলে, রোজ/সপ্তাহে/মাসে/মাঝে মধ্যে?		
8	Do you take Jardapaan?	আপনি কি জর্দা পান খান?		
9	Do you take Jarda masala / pan parag/ chutki /gutkha?	আপনি কি জর্দা মশল্া/পান পরাগ/চুটকি/গুটখা খান?		
	If yes (Y), please tell what?, How much?	হ্যা হলে কোনটি? কতটা?		
10	Are you left handed?	আপনি কি বাম হাতে কাজ করেন?	`	
	Measured Physical parameters -	**শারীরিকপরিমাপ**		
	Weight in kg.	ওজন কিলোগ্রামে		
	Height in meters	উচ্চতা মিটারে		
	BMI (Body mass Index) in metric	BMI সংখ্যায়		
	Waist measure in cm.	কোমর সেন্টিমিটারে		
	Hip measure in cm.	নিতম্বসেন্টিমিটারে		
	WHR (Waist to Hip Ratio)	কোমর ও নিতম্বের অনুপাত		

A.3 Daily Questionnaire set 1

Questions	DDMMYYYY	DDMMYYYY
Have you taken any drug from the list provided in table below within 24 hours?		
Please specify medicines or treatment that you are undergoing as on date, if different from that stated in comprehensive questionnaire.		
Has subject taken any anticholinergic drug knowingly or unknowingly? (If NO, then proceed for daily questionnaire 2, followed by acquisition of data, else exclude the subject for today)		

Strong or moderate AC effect: Amitriptyline (Elavil), Atropine, Benztropine (Cogentin), Chlorpheniramine (Actifed, Allergy & Congestion Relief, Chlor-Trimeton, Codeprex, Efidac-24 Chlorpheniramine, etc), Chlorpromazine (Thorazine), Clomipramine (Anafranil), Clozapine (Clozaril), Cyclobenzaprine (Amrix, Fexmid, Flexeril), Cyproheptadine (Periactin), Desipramine (Norpramin), Dexchlorpheniramine, Dicyclomine (Bentyl), Diphenhydramine (Advil PM, Aleve PM, Bayer PM, Benadryl, Excedrin PM, Nytol, Simply Sleep, Sominex, Tylenol PM, Unisom, etc.), Doxepin (Adapin, Silenor, Sinequan), Fesoterodine (Toviaz), Hydroxyzine (Atarax, Vistaril), Hyoscyamine (Anaspaz, Levbid, Levsin, Levsinex, NuLev), Imipramine (Tofranil), Meclizine (Antivert, Bonine), Nortriptyline (Pamelor), Orphenadrine (Norflex), Oxybutynin (Ditropan, Oxytrol), Paroxetine (Brisdelle, Paxil), Perphenazine (Trilafon), Prochlorperazine (Compazine), Promethazine (Phenergan), Protriptyline (Vivactil), Pseudoephedrine Cl/Triprolidine, HCl (Aprodine), Scopolamine (TransdermScop), Thioridazine (Mellaril), Tolterodine (Detrol), Trifluoperazine (Stelazine), Trimipramine (Surmontil)

Lesser AC effect: Alprazolam (Xanax), Fluphenazine (Prolixin), Amantadine (Symmetrel), Baclofen Carisoprodol (Soma), Cetirizine (Zyrtec), Cimetidine (Tagamet), Clorazepate (Tranxene), Codeine, Colchicine, Digoxin (Lanoxicaps, Lanoxin), Diphenoxylate (Lomotil), Furosemide (Lasix), Hydrochlorothiazide (Esidrix, Dyazide, HydroDIURIL, Maxzide & literally scores of other medications for high blood pressure), Loperamide (Imodium), Loratadine (Alavert, Claritin), Maprotiline, Nifedipine (Adalat, Procardia), Ranitidine (Zantac), Thiothixene (Navane), Tizanidine (Zanaflex)

A.4 Daily Questionnaire set 2

Questions	DDMMYYYY	DDMMYYYY
Are you stressed? Provide rating in scale of 0-5		
If yes, is the stress a) work related, b) emotional or c) any other? Please specify		
Have you taken any psychotic or antidepressant drug within 1 week?		
If yes, then provide the reason, list of medicine and time of taking medicine.		
Do you have any specific pain? Provide rating in scale of 0-5		
If yes, is the pain short term or long term?		
Is the pain in a) left half or b) right half of body or c) overall or d) not localized? If a) or b), please specify location.		
Do you have fever? Provide rating in scale of 0-5		
Do you have cough or cold? Provide rating in scale of 0-5		
Do you have any headache? Provide rating in scale of 0-5		
If yes, is the headache in a) left half or b) right half or c) overall or d) not localized? If a) or b), please specify location.		
Have you taken any cigarettes or any other intoxicating substance or caffeine containing drink within 72 hours?		

A.5 Daily Questionnaire set 3

Question	DDMMYYYY		DDMMYYYY	
Clothing of the subject (Light, Moderate, Heavy)				
Body temperature				
Bias voltages measured for 4 electrodes with respect to 1 reference electrode.	**Tag**	**Volt**	**Tag**	**Volt**
	Rish_IL		Rish_IL	
	Rish_ML		Rish_ML	
	Rish_IR		Rish_IR	
	Rish_MR		Rish_MR	

Bibliography

[1] A. Sarkar, S. Biswas, G. Datwal, S. Debnath, B. Goswami, and R. Ghosh, "Design and calibration of a multi-channel low voltage data acquisition system," in *2018 IEEE Applied Signal Processing Conference (ASPCON)*, 2018, pp. 119–123.

[2] P. H. Venables and M. J. Christie, "Electrodermal activity," *Techniques in psychophysiology*, vol. 54, no. 3, 1980.

[3] W. Boucsein, *Electrodermal activity*. Springer Science & Business Media, 2012.

[4] *RISH Multi 18S*, Rishabh Instruments Pvt. Ltd. [Online]. Available: http://rishabh.co.in/uploads/product/15030919_RISH_multi_18S_manual_with_back_new.pdf

[5] A. Bhattacharya, "Study and characterization of non-organ specific biopotential signals acquired from the human system," phdthesis, IEE, JU, Kolkata, India, Dec. 2019.

[6] Y. Yamamoto and T. Yamamoto, "Dispersion and correlation of the parameters for skin impedance," *Medical and Biological Engineering and Computing*, vol. 16, no. 5, pp. 592–594, 1978.

[7] "Hand anatomy," Online. [Online]. Available: https://eorthopod.com/hand-anatomy/

[8] J. D. Bronzino, *Biomedical Engineering Handbook*, 2nd ed. Springer Science & Business Media, 2000, vol. 1, ch. 2.

[9] A. L. Goldberger and E. Gold-berger, "Clinical electrocardiography, a simplified approach," *Critical Care Medicine*, vol. 9, no. 12, pp. 891–892, 1981.

[10] E. H. Houssein, M. Kilany, and A. E. Hassanien, "Ecg signals classification: a review," *International Journal of Intelligent Engineering Informatics*, vol. 5, no. 4, pp. 376–396, 2017.

[11] M. Zijlmans, D. Flanagan, and J. Gotman, "Heart rate changes and ecg abnormalities during epileptic seizures: prevalence and definition of an objective clinical sign," *Epilepsia*, vol. 43, no. 8, pp. 847–854, 2002.

[12] E. Niedermeyer and F. L. da Silva, *Electroencephalography: basic principles, clinical applications, and related fields*. Lippincott Williams & Wilkins, 2005.

[13] S. Noachtar and J. Rémi, "The role of eeg in epilepsy: a critical review," *Epilepsy & Behavior*, vol. 15, no. 1, pp. 22–33, 2009.

[14] M. M. Siddiqui, S. Rahman, S. H. Saeed, and A. Banodia, "Eeg signals play major role to diagnose sleep disorder," *International Journal of Electronics and Computer Science Engineering (IJECSE)*, vol. 2, no. 2, pp. 503–505, 2013.

[15] L. C. Jameson and T. B. Sloan, "Using eeg to monitor anesthesia drug effects during surgery," *Journal of clinical monitoring and computing*, vol. 20, no. 6, pp. 445–472, 2006.

[16] W. Szurhaj, M.-D. Lamblin, A. Kaminska, and H. Sediri, "Eeg guidelines in the diagnosis of brain death," *Neurophysiologie Clinique/Clinical Neurophysiology*, vol. 45, no. 1, pp. 97–104, 2015.

[17] M. R. Nuwer, S. E. Jordan, and S. S. Ahn, "Evaluation of stroke using eeg frequency analysis and topographic mapping," *Neurology*, vol. 37, no. 7, pp. 1153–1153, 1987.

[18] M. Cifrek, V. Medved, S. Tonković, and S. Ostojić, "Surface emg based muscle fatigue evaluation in biomechanics," *Clinical biomechanics*, vol. 24, no. 4, pp. 327–340, 2009.

[19] J. Taborri, J. Keogh, A. Kos, A. Santuz, A. Umek, C. Urbanczyk, E. van der Kruk, and S. Rossi, "Sport biomechanics applications using inertial, force, and emg sensors: A literature overview," *Applied bionics and biomechanics*, vol. 2020, 2020.

[20] C.-T. Lin, J.-T. King, P. Bharadwaj, C.-H. Chen, A. Gupta, W. Ding, and M. Prasad, "Eog-based eye movement classification and application on hci baseball game," *IEEE Access*, vol. 7, pp. 96 166–96 176, 2019.

[21] L. Y. Deng, C.-L. Hsu, T.-C. Lin, J.-S. Tuan, and S.-M. Chang, "Eog-based human–computer interface system development," *Expert Systems with Applications*, vol. 37, no. 4, pp. 3337–3343, 2010.

[22] A. Avolio and G. Parati, "Reflecting on posture," *Journal of hypertension*, vol. 29, no. 4, pp. 655–657, 2011.

[23] K. Peterson, E. T. Ozawa, G. M. Pantalos, and M. K. Sharp, "Numerical simulation of the influence of gravity and posture on cardiac performance," *Annals of biomedical engineering*, vol. 30, no. 2, pp. 247–259, 2002.

[24] P. Van Leeuwen and H. C. Kümmell, "Effects of posture on cardiac time intervals," *American journal of noninvasive cardiology*, vol. 5, pp. 125–128, 1991.

[25] S. S. Thomas, V. Nathan, C. Zong, K. Soundarapandian, X. Shi, and R. Jafari, "Biowatch: A noninvasive wrist-based blood pressure monitor that incorporates training techniques for posture and subject variability," *IEEE journal of biomedical and health informatics*, vol. 20, no. 5, pp. 1291–1300, 2015.

[26] S. Wahabi, S. Pouryayevali, and D. Hatzinakos, "Posture-invariant ecg recognition with posture detection," in *2015 IEEE International Conference on Acoustics, Speech and Signal Processing (ICASSP)*. IEEE, 2015, pp. 1812–1816.

[27] Y. Yoshida, E. Yuda, K. Yamamoto, Y. Miura, and J. Hayano, "Machine-learning estimation of body posture and physical activity by wearable acceleration and heartbeat sensors," *Int. J.(SIPIJ)*, vol. 10, pp. 1–9, 2019.

[28] D. Sasakawa, N. Honma, T. Nakayama, and S. Iizuka, "Human posture identification using a mimo array," *Electronics*, vol. 7, no. 3, p. 37, 2018.

[29] M. T. DMSc and H. A. DMSc, "Maintenance of alertness and performance by a brief nap after lunch under prior sleep deficit," *Sleep*, vol. 23, no. 6, p. 813, 2000.

[30] A. J. Tietzel and L. C. Lack, "The short-term benefits of brief and long naps following nocturnal sleep restriction," *Sleep*, vol. 24, no. 3, pp. 293–300, 2001.

[31] ——, "The recuperative value of brief and ultra-brief naps on alertness and cognitive performance," *Journal of sleep research*, vol. 11, no. 3, pp. 213–218, 2002.

[32] M. Hayashi, S. Ito, and T. Hori, "The effects of a 20-min nap at noon on sleepiness, performance and eeg activity," *International Journal of Psychophysiology*, vol. 32, no. 2, pp. 173–180, 1999.

[33] M. Hayashi, M. Watanabe, and T. Hori, "The effects of a 20 min nap in the mid-afternoon on mood, performance and eeg activity," *Clinical Neurophysiology*, vol. 110, no. 2, pp. 272–279, 1999.

[34] M. Gillberg, G. Kecklund, J. Axelsson, and T. Åkerstedt, "The effects of a short daytime nap after restricted night sleep," *Sleep*, vol. 19, no. 7, pp. 570–575, 1996.

[35] J. A. Horne and L. A. Reyner, "Counteracting driver sleepiness: effects of napping, caffeine, and placebo," *Psychophysiology*, vol. 33, no. 3, pp. 306–309, 1996.

[36] M. Hayashi, A. Masuda, and T. Hori, "The alerting effects of caffeine, bright light and face washing after a short daytime nap," *Clinical Neurophysiology*, vol. 114, no. 12, pp. 2268–2278, 2003.

[37] Y. Liang, Z. Chen, R. Ward, and M. Elgendi, "Hypertension assessment via ecg and ppg signals: An evaluation using mimic database," *Diagnostics*, vol. 8, no. 3, p. 65, 2018.

[38] J. S. Rajput, M. Sharma, and U. R. Acharya, "Hypertension diagnosis index for discrimination of high-risk hypertension ecg signals using optimal orthogonal wavelet filter bank," *International journal of environmental research and public health*, vol. 16, no. 21, p. 4068, 2019.

[39] P.-Y. Courand, S. Jenck, G. Bricca, H. Milon, and P. Lantelme, "R wave in avl lead: an outstanding ecg index in hypertension," *Journal of hypertension*, vol. 32, no. 6, pp. 1317–1325, 2014.

[40] J. S. Rajput, M. Sharma, R. San Tan, and U. R. Acharya, "Automated detection of severity of hypertension ecg signals using an optimal bi-orthogonal wavelet filter bank," *Computers in Biology and Medicine*, vol. 123, p. 103924, 2020.

[41] M. Simjanoska, M. Gjoreski, A. M. Bogdanova, B. Koteska, M. Gams, and J. F. Tasic, "Ecg-derived blood pressure classification using complexity analysis-based machine learning." in *HEALTHINF*, 2018, pp. 282–292.

[42] T. Seidler, K. Hellenkamp, B. Unsoeld, S. Mushemi-Blake, A. Shah, G. Hasenfuss, and A. Leha, "A machine learning approach for the prediction of pulmonary hypertension," *Journal of the American College of Cardiology*, vol. 73, no. 9S1, pp. 1589–1589, 2019.

[43] M. Poddar, A. C. Birajdar, J. Virmani *et al.*, "Automated classification of hypertension and coronary artery disease patients by pnn, knn, and svm classifiers using hrv analysis," in *Machine learning in Bio-signal analysis and diagnostic imaging*. Elsevier, 2019, pp. 99–125.

[44] W. Prokasy, *Electrodermal activity in psychological research*. Elsevier, 2012.

[45] P. Venables and M. Christie, "Mechanisms, instrumentation, recording techniques, and quantification of responses," *Electrodermal activity in psychological research*, 2012.

[46] Society for Psychophysiological Research Ad Hoc Committee on Electrodermal Measures, W. Boucsein, D. C. Fowles, S. Grimnes, G. Ben-Shakhar, W. T. Roth, M. E. Dawson, and D. L. Filion, "Publication recommendations for electrodermal measurements," *Psychophysiology*, vol. 49, no. 8, pp. 1017–1034, 2012.

[47] M. J. Christie and P. H. Venables, "Site, state, and subject characteristics of palmar skin potential levels," *Psychophysiology*, vol. 9, no. 6, pp. 645–649, 1972.

[48] A. S. Scerbo, L. W. Freedman, A. Raine, M. E. Dawson, and P. H. Venables, "A major effect of recording site on measurement of electrodermal activity," *Psychophysiology*, vol. 29, no. 2, pp. 241–246, 1992.

[49] R. Edelberg, "Electrical properties of the skin," *Methods in psychophysiology*, pp. 1–53, 1967.

[50] W. Rickles Jr and J. Day, "Electrodermal activity in non-palmer skin sites," *Psychophysiology*, vol. 4, no. 4, pp. 421–435, 1968.

[51] P. Venables and E. Sayer, "On the measurement of the level of skin potential," *British Journal of Psychology*, vol. 54, no. 3, p. 251, 1963.

[52] P. H. Venables and I. Martin, *A manual of psychophysiological methods*. Amsterdam: North-Holland Publishing Company; New York: Wiley, 1967.

[53] P. Venables and M. Christie, "Electrodermal activity. in 1. martin & venables ph (eds.), techniques in psychophysiology (pp. 3–67)," 1980.

[54] R. Zangroniz, A. Martinez Rodrigo, J. M. Pastor García, M. López Bonal, and A. Fernández-Caballero, "Electrodermal activity sensor for classification of calm/distress condition," *Sensors*, vol. 17, p. 2324, 10 2017.

[55] K. P. Stoller and B. E. Taff, "Method and apparatus for detecting body illness, dysfunction, disease and/or pathology," Dec. 10 1985, uS Patent 4,557,271.

[56] M.-Z. Poh, N. C. Swenson, and R. W. Picard, "A wearable sensor for unobtrusive, long-term assessment of electrodermal activity," *IEEE transactions on Biomedical engineering*, vol. 57, no. 5, pp. 1243–1252, 2010.

[57] M. J. Christie and P. H. Venables, "Characteristics of palmar skin potential and conductance in relaxed human subjects," *Psychophysiology*, vol. 8, no. 4, pp. 525–532, 1971.

[58] D. Lykken, R. Rose, B. Luther, and M. Maley, "Correcting psychophysiological measures for individual differences in range." *Psychological Bulletin*, vol. 66, no. 6, p. 481, 1966.

[59] T. Forbes, "Problems in Measurement of Electrodermal Phenomena," *Psychophysiology*, vol. 1, no. 1, pp. 26–30, 1964.

[60] W. W. Grings and A. M. Schell, "Magnitude of electrodermal response to a standard stimulus as a function of intensity and proximity of a prior stimulus." *Journal of Comparative and Physiological Psychology*, vol. 67, no. 1, p. 77, 1969.

[61] S. Fisher, "Body image and asymmetry of body reactivity." *The Journal of Abnormal and Social Psychology*, vol. 57, no. 3, p. 292, 1958.

[62] P. A. Obrist, "Skin resistance levels and galvanic skin response: Unilateral differences," *Science*, vol. 139, no. 3551, pp. 227–228, 1963.

[63] D. T. Lykken, W. G. Iacono, K. Haroian, and T. Bouchard Jr, "Habituation of the skin conductance response to strong stimuli: A twin study," *Psychophysiology*, vol. 25, no. 1, pp. 4–15, 1988.

[64] M. Fredrikson, "Orienting and defensive reactions to phobic and conditioned fear stimuli in phobics and normals," *Psychophysiology*, vol. 18, no. 4, pp. 456–465, 1981.

[65] E. Duffy, "The concept of energy mobilization." *Psychological Review*, vol. 58, no. 1, p. 30, 1951.

[66] R. W. Picard, S. Fedor, and Y. Ayzenberg, "Multiple arousal theory and daily-life electrodermal activity asymmetry," *Emotion Review*, vol. 8, no. 1, pp. 62–75, 2016.

[67] M. E. Dawson, A. M. Schell, and D. L. Filion, *Handbook Of Psychophysiology*, 3rd ed. Cambridge University Press, 2007, ch. The electrodermal system., pp. 159–181.

[68] E. Binboga, S. Guven, F. Çatıkkaş, O. Bayazıt, and S. Tok, "Psychophysiological responses to competition and the big five personality traits," *Journal of human kinetics*, vol. 33, pp. 187–194, 2012.

[69] L. Silvert, S. Delplanque, H. Bouwalerh, C. Verpoort, and H. Sequeira, "Autonomic responding to aversive words without conscious valence discrimination," *International Journal of Psychophysiology*, vol. 53, no. 2, pp. 135–145, 2004.

[70] M. Page and R. C. A. Robson, "Galvanic skin responses from asking stressful questions," *British Journal of Nursing*, vol. 16, no. 10, pp. 622–627, 2007.

[71] M. Lader and L. Wing, "Habituation of the psycho-galvanic reflex in patients with anxiety states and in normal subjects," *Journal of neurology, neurosurgery, and psychiatry*, vol. 27, no. 3, p. 210, 1964.

[72] M. H. Lader and L. Wing, *Physiological measures, sedative drugs, and morbid anxiety.* Oxford UP, 1966, vol. 14.

[73] J. Kritikos, G. Tzannetos, C. Zoitaki, S. Poulopoulou, and D. Koutsouris, "Anxiety detection from electrodermal activity sensor with movement & interaction during virtual reality simulation," in *2019 9th International IEEE/EMBS Conference on Neural Engineering (NER).* IEEE, 2019, pp. 571–576.

[74] M. Sarchiapone, C. Gramaglia, M. Iosue, V. Carli, L. Mandelli, A. Serretti, D. Marangon, and P. Zeppegno, "The association between electrodermal activity (eda), depression and suicidal behaviour: A systematic review and narrative synthesis," *BMC psychiatry*, vol. 18, no. 1, p. 22, 2018.

[75] W. G. Iacono, D. T. Lykken, L. J. Peloquin, A. E. Lumry, R. H. Valentine, and V. B. Tuason, "Electrodermal activity in euthymic unipolar and bipolar affective disorders: A possible marker for depression," *Archives of General Psychiatry*, vol. 40, no. 5, pp. 557–565, 1983.

[76] W. G. Iacono, L. J. Peloquin, D. T. Lykken, K. P. Haroian, R. H. Valentine, and V. B. Tuason, "Electrodermal activity in euthymic patients with affective disorders: One-year retest stability and the effects of stimulus intensity and significance." *Journal of Abnormal Psychology*, vol. 93, no. 3, p. 304, 1984.

[77] J. Wendt, M. Lotze, A. I. Weike, N. Hosten, and A. O. Hamm, "Brain activation and defensive response mobilization during sustained exposure to phobia-related and other affective pictures in spider phobia," *Psychophysiology*, vol. 45, no. 2, pp. 205–215, 2008.

[78] M. C. Corballis and I. L. Beale, "Bilateral symmetry and behavior," *Psychological Review*, vol. 77, no. 5, pp. 451–464, 1970.

[79] K. Amunts, L. Jäncke, H. Mohlberg, H. Steinmetz, and K. Zilles, "Interhemispheric asymmetry of the human motor cortex related to handedness and gender," *Neuropsychologia*, vol. 38, no. 3, pp. 304–312, 2000.

[80] C. D. Good, I. Johnsrude, J. Ashburner, R. N. Henson, K. J. Friston, and R. S. Frackowiak, "Cerebral asymmetry and the effects of sex and handedness on brain structure: a voxel-based morphometric analysis of 465 normal adult human brains," *Neuroimage*, vol. 14, no. 3, pp. 685–700, 2001.

[81] K. Hugdahl, "Bilateral electrodermal asymmetry: past hopes and future prospects," *International journal of neuroscience*, vol. 39, no. 1-2, pp. 33–44, 1988.

[82] D. N. O'Connell and M. T. Orne, "Endosomatic electrodermal correlates of hypnotic depth and susceptibility," *Journal of psychiatric research*, vol. 6, no. 1, pp. 1–12, 1968.

[83] A. Affanni, "Wearable instrument to measure simultaneously cardiac and electrodermal activities," in *2016 IEEE International Symposium on Medical Measurements and Applications (MeMeA)*. IEEE, 2016, pp. 1–5.

[84] A. Affanni, A. Piras, R. Rinaldo, and P. Zontone, "Dual channel electrodermal activity sensor for motion artifact removal in car drivers' stress detection," in *2019 IEEE Sensors Applications Symposium (SAS)*. IEEE, 2019, pp. 1–6.

[85] A. Affanni, R. Bernardini, A. Piras, R. Rinaldo, and P. Zontone, "Driver's stress detection using skin potential response signals," *Measurement*, vol. 122, 03 2018.

[86] A. Bhattacharya, D. Basu, B. Goswami, and R. Ghosh, "Measuring human biopotentials to ascertain parameters for health," in *Communication and Industrial Application (ICCIA), 2011 International Conference on*. IEEE, 2011, pp. 1–4.

[87] *RISH Multi SI 232*, Rishabh Instruments Pvt. Ltd. [Online]. Available: http://rishabh.co.in/uploads/product/SI_232_MANUAL_10-2011_NEW-1.pdf

[88] A. Bhattacharya, D. Basu, B. Goswami, and R. Ghosh, "A reliable signal conditioning circuit to acquire human biopotentials." *International Journal on Smart Sensing & Intelligent Systems*, vol. 6, no. 3, 2013.

[89] K. Kasos, S. Zimonyi, B. Gonye, F. Köteles, E. Kasos, E. Kotyuk, K. Varga, A. Veres, and A. Szekely, "Obimon: An open-source device enabling group measurement of electrodermal activity," *Psychophysiology*, vol. 56, no. 8, p. e13374, 2019.

[90] D. Van Der Mee, M. Gevonden, J. Westerink, and E. De Geus, "Validity of electrodermal activity-based measures of sympathetic nervous system activity from a wrist-worn device," *International Journal of Psychophysiology*, vol. 168, pp. 52–64, 2021.

[91] M. Díaz-Boladeras, X. Llanas, M. Musté, E. Pérez, C. Pérez, A. Barco, and A. Català, "Validation of a nonintrusive wearable device for distress estimation during robotic roller assisted gait," in *International Work-Conference on Artificial Neural Networks*. Springer, 2021, pp. 570–582.

[92] S. Nandy, B. Goswami, and R. Ghosh, "Deriving a linear model for passively acquired bio-potentials using sample acf," in *2018 IEEE Applied Signal Processing Conference (ASPCON)*. IEEE, 2018, pp. 64–68.

[93] R. Trivers, B. Fink, M. Russell, K. McCarty, B. James, and B. G. Palestis, "Lower body symmetry and running performance in elite jamaican track and field athletes," *PloS one*, vol. 9, no. 11, p. e113106, 2014.

[94] J. Manning and L. Pickup, "Symmetry and performance in middle distance runners," *International Journal of Sports Medicine*, vol. 19, no. 03, pp. 205–209, 1998.

[95] V. Serdyuk, *Scoliosis and Spinal Pain Syndrome: New understanding of their origin and ways of successful treatment*, 1st ed. Byword Books Private Limited, 2014.

[96] M. J. van Putten, J. M. Peters, S. M. Mulder, J. A. de Haas, C. M. Bruijninckx, and D. L. Tavy, "A brain symmetry index (bsi) for online eeg monitoring in carotid endarterectomy," *Clinical neurophysiology*, vol. 115, no. 5, pp. 1189–1194, 2004.

[97] M. Yan, Z. Hou, and Y. Gao, "A bilateral brain symmetry index for analysis of eeg signal in stroke patients," in *Biomedical Engineering and Informatics (BMEI), 2011 4th International Conference on*, vol. 1. IEEE, 2011, pp. 8–11.

[98] C. Piazza, M. Miyakoshi, Z. Akalin-Acar, C. Cantiani, G. Reni, A. M. Bianchi, and S. Makeig, "An automated function for identifying eeg independent components representing bilateral source activity," in *XIV Mediterranean conference on medical and biological engineering and computing 2016*. Springer, 2016, pp. 105–109.

[99] J. Ziegler, H. Gattringer, and A. Mueller, "Classification of gait phases based on bilateral emg data using support vector machines," in *2018 7th IEEE International Conference on Biomedical Robotics and Biomechatronics (Biorob)*. IEEE, 2018, pp. 978–983.

[100] J. R. Cram and J. C. Steger, "Emg scanning in the diagnosis of chronic pain," *Biofeedback and self-regulation*, vol. 8, no. 2, pp. 229–241, 1983.

[101] T. W. Boonstra, B. C. van Wijk, P. Praamstra, and A. Daffertshofer, "Corticomuscular and bilateral emg coherence reflect distinct aspects

of neural synchronization," *Neuroscience letters*, vol. 463, no. 1, pp. 17–21, 2009.

[102] H. Yoon, S. H. Hwang, J.-W. Choi, Y. J. Lee, D.-U. Jeong, and K. S. Park, "Slow-wave sleep estimation for healthy subjects and osa patients using r–r intervals," *IEEE journal of biomedical and health informatics*, vol. 22, no. 1, pp. 119–128, 2017.

[103] C. A. Mangina and J. H. Beuzeron-Mangina, "Direct electrical stimulation of specific human brain structures and bilateral electrodermal activity," *International Journal of Psychophysiology*, vol. 22, no. 1-2, pp. 1–8, 1996.

[104] G. Brand, J. Millot, M. Saffaux, and N. Morand-Villeneuve, "Lateralization in human nasal chemoreception: differences in bilateral electrodermal responses related to olfactory and trigeminal stimuli," *Behavioural brain research*, vol. 133, no. 2, pp. 205–210, 2002.

[105] J. S. Gross and J. A. Stern, "An investigation of bilateral asymmetries in electrodermal activity," *The Pavlovian journal of biological science: official journal of the Pavlovian*, vol. 15, no. 2, pp. 74–81, 1980.

[106] P. Bob, M. Susta, K. Glaslova, J. Pavlat, and J. Raboch, "Lateralized electrodermal dysfunction and complexity in patients with schizophrenia and depression." *Neuro endocrinology letters*, vol. 28, no. 1, pp. 11–15, 2007.

[107] K. L. Subotnik, A. M. Schell, M. S. Chilingar, M. E. Dawson, J. Ventura, K. A. Kelly, G. S. Hellemann, and K. H. Nuechterlein, "The interaction of electrodermal activity and expressed emotion in predicting symptoms in recent-onset schizophrenia," *Psychophysiology*, vol. 49, no. 8, pp. 1035–1038, 2012.

[108] M. S. Myslobodsky and J. Rattok, "Bilateral electrodermal activity in waking man," *Acta Psychologica*, vol. 41, no. 4, pp. 273–282, 1977.

[109] D. C. Fowles, M. J. Christie, R. Edelberg, W. W. Grings, D. T. Lykken, and P. H. Venables, "Publication recommendations for electrodermal measurements," *Psychophysiology*, vol. 18, no. 3, pp. 232–239, 1981.

[110] R. Wyatt and B. Tursky, "Skin potential levels in right-and left-handed males," *Psychophysiology*, vol. 6, no. 2, pp. 133–137, 1969.

[111] A. Pigorini, A. G. Casali, S. Casarotto, F. Ferrarelli, G. Baselli, M. Mariotti, M. Massimini, and M. Rosanova, "Time–frequency spectral analysis of tms-evoked eeg oscillations by means of hilbert–huang transform," *Journal of neuroscience methods*, vol. 198, no. 2, pp. 236–245, 2011.

[112] D. Jaiswal, M. Moulick, D. Chatterjee, R. Ranjan, R. K. Ramakrishnan, A. Pal, and R. Ghosh, "Assessment of cognitive load from bio-potentials measured using wearable endosomatic device," in *Proceedings of the 6th ACM Workshop on Wearable Systems and Applications*, ser. WearSys '20. New York, NY, USA: Association for Computing Machinery, 2020, p. 13–18. [Online]. Available: https://doi.org/10.1145/3396870.3400012

[113] A. Sarkar, A. Bhattacharya, R. Ghosh, and B. Goswami, "A comparative study of biopotentials acquired from left and right hands of human subjects," in *Advanced Computational and Communication Paradigms*. Springer, 2018, pp. 110–117.

[114] J. G. Webster and H. Eren, *Measurement, instrumentation, and sensors handbook: spatial, mechanical, thermal, and radiation measurement*. CRC press, 2017.

[115] E. A. Lipman, "Electrical safety information," Tech. Rep., Aug. 2007. [Online]. Available: http://web.physics.ucsb.edu/~phys13CH/electrical_safety.pdf

[116] A. K. Ghosh, *Introduction to measurements and instrumentation*. PHI Learning Pvt. Ltd., 2012.

[117] D. Murty, *Transducers and instrumentation*. PHI Learning Pvt. Ltd., 2010.

[118] E. W. Weisstein, "Accuracy," *from MathWorld–a Wolfram Web Resource. http://mathworld. com/Accuracy/html*, 2008.

[119] B. B. Winter and J. G. Webster, "Reduction of interference due to common mode voltage in biopotential amplifiers," *IEEE Transactions on Biomedical Engineering*, no. 1, pp. 58–62, 1983.

[120] T. Degen and H. Jackel, "Enhancing interference rejection of preamplified electrodes by automated gain adaption," *IEEE transactions on biomedical engineering*, vol. 51, no. 11, pp. 2031–2039, 2004.

[121] D. Noble, "The role of stochasticity in biological communication processes," *Progress in Biophysics and Molecular Biology*, vol. 162, pp. 122–128, 2021.

[122] A. Faller and M. Schuenke, *Color atlas of human body*, 1st ed. Thieme, 2004, ch. The Skin and Its Appendages, p. 663.

[123] ——, *Color atlas of human body*, 1st ed. Thieme, 2004, ch. The Autonomic Nervous System, p. 606.

[124] Y.-J. Wang, C.-H. Chen, C.-Y. Sue, W.-H. Lu, and Y.-H. Chiou, "Estimation of blood pressure in the radial artery using strain-based pulse wave and photoplethysmography sensors," *Micromachines*, vol. 9, no. 11, p. 556, 2018.

[125] G. E. Box, G. M. Jenkins, G. C. Reinsel, and G. M. Ljung, *Time series analysis: forecasting and control*. John Wiley & Sons, 2015.

[126] J. G. Bradley and K. A. Davis, "Orthostatic hypotension," *American family physician*, vol. 68, no. 12, pp. 2393–2398, 2003.

[127] A. Phinyomark, P. Phukpattaranont, and C. Limsakul, "Feature reduction and selection for emg signal classification," *Expert systems with applications*, vol. 39, no. 8, pp. 7420–7431, 2012.

[128] S. Du and M. Vuskovic, "Temporal vs. spectral approach to feature extraction from prehensile emg signals," in *Proceedings of the 2004 IEEE International Conference on Information Reuse and Integration, 2004. IRI 2004.* IEEE, 2004, pp. 344–350.

[129] M. A. Oskoei and H. Hu, "Support vector machine-based classification scheme for myoelectric control applied to upper limb," *IEEE transactions on biomedical engineering*, vol. 55, no. 8, pp. 1956–1965, 2008.

[130] *Application Note 118: EMG Frequency Signal Analysis*, Biopac Systems, Inc, Goleta, CA, May 2021. [Online]. Available: http://www.biopac.com/Manuals/app_pdf/app118.pdf

[131] M. Borowska, "Entropy-based algorithms in the analysis of biomedical signals," *Studies in Logic, Grammar and Rhetoric*, vol. 43, no. 1, pp. 21–32, 2015.

[132] M. S. Myslobodsky and J. Rattok, "Asymmetry of electrodermal activity in man," *Bulletin of the Psychonomic Society*, vol. 6, no. 5, pp. 501–502, 1975.

[133] G. Schulter and I. Papousek, "Bilateral electrodermal activity: relationships to state and trait characteristics of hemisphere asymmetry," *International Journal of Psychophysiology*, vol. 31, no. 1, pp. 1–12, 1998.

[134] G. Holmes, A. Donkin, and I. H. Witten, "Weka: A machine learning workbench," in *Proceedings of ANZIIS'94-Australian New Zealnd Intelligent Information Systems Conference*. IEEE, 1994, pp. 357–361.

[135] B. Çığşar and D. Ünal, "Comparison of data mining classification algorithms determining the default risk," *Scientific Programming*, vol. 2019, 2019.

[136] L. Breiman, "Random forests," *Machine learning*, vol. 45, no. 1, pp. 5–32, 2001.

[137] A. Who, "global brief on hypertension," *World Health Organization*, 2013.

[138] "Cardiovascular diseases (cvds)," *World Health Organization*, 11 June 2021. [Online]. Available: https://www.who.int/news-room/fact-sheets/detail/cardiovascular-diseases-(cvds)

[139] WHO, "Hypertension in india - who," *World Health Organization*, 2021. [Online]. Available: https://www.who.int/india/health-topics/hypertension

[140] H. Ni, Y. Wang, G. Xu, Z. Shao, W. Zhang, and X. Zhou, "Multiscale fine-grained heart rate variability analysis for recognizing the severity of hypertension," *Computational and mathematical methods in medicine*, vol. 2019, 2019.

[141] G. Kovacs, A. Avian, V. Foris, M. Tscherner, X. Kqiku, P. Douschan, G. Bachmaier, A. Olschewski, M. Matucci-Cerinic, and H. Olschewski, "Use of ecg and other simple non-invasive tools to assess pulmonary hypertension," *PloS one*, vol. 11, no. 12, p. e0168706, 2016.

[142] D. Chicco and G. Jurman, "The advantages of the matthews correlation coefficient (mcc) over f1 score and accuracy in binary classification evaluation," *BMC genomics*, vol. 21, no. 1, pp. 1–13, 2020.

[143] S. Raschka, "An overview of general performance metrics of binary classifier systems," *arXiv preprint arXiv:1410.5330*, 2014.

[144] N. Foubert, A. M. McKee, R. A. Goubran, and F. Knoefel, "Lying and sitting posture recognition and transition detection using a pressure sensor array," in *2012 IEEE International Symposium on Medical Measurements and Applications Proceedings*. IEEE, 2012, pp. 1–6.

[145] H. Jeong and W. Park, "Developing and evaluating a mixed sensor smart chair system for real-time posture classification: Combining pressure and distance sensors," *IEEE Journal of Biomedical and Health Informatics*, vol. 25, no. 5, pp. 1805–1813, 2020.

[146] T. E. Lockhart, R. Soangra, J. Zhang, and X. Wu, "Wavelet based automated postural event detection and activity classification with single imu (tempo)," *Biomedical sciences instrumentation*, vol. 49, p. 224, 2013.

[147] N. N. Vo and H. Yu, "A wearable posture detection device for inpatient healthcare," *Journal of Medical Devices-Transaction of The ASME*, vol. 8, no. 3, 2014.

[148] K. Lyden, D. John, P. Dall, M. H. Granat *et al.*, "Differentiating sitting and lying using a thigh-worn accelerometer," *Med Sci Sports Exerc*, vol. 48, no. 4, pp. 742–747, 2016.

[149] D. R. Bassett Jr, D. John, S. A. Conger, B. C. Rider, R. M. Passmore, and J. M. Clark, "Detection of lying down, sitting, standing, and stepping using two activpal monitors." *Medicine and science in sports and exercise*, vol. 46, no. 10, pp. 2025–2029, 2014.

[150] F. Foerster, M. Smeja, and J. Fahrenberg, "Detection of posture and motion by accelerometry: a validation study in ambulatory monitoring," *Computers in human behavior*, vol. 15, no. 5, pp. 571–583, 1999.

[151] S. Wahabi, *Variability in ECG biometrics: state of the art and subspace methods*. University of Toronto (Canada), 2015.

[152] A. D. Ruiz, J. S. Mejía, J. M. López, and B. F. Giraldo, "Characterization of cardiac and respiratory system of healthy subjects in supine and sitting position," in *Iberian Conference on Pattern Recognition and Image Analysis*. Springer, 2019, pp. 367–377.

[153] N. Rikatsih and A. A. Supianto, "Classification of posture reconstruction with univariate time series data type," in *2018 International Conference on Sustainable Information Engineering and Technology (SIET)*. IEEE, 2018, pp. 322–325.

[154] "boxplot," online, 2022. [Online]. Available: https://in.mathworks.com/help/stats/boxplot.html#namevaluepairarguments

[155] M. Hayashi, N. Motoyoshi, and T. Hori, "Recuperative power of a short daytime nap with or without stage 2 sleep," *Sleep*, vol. 28, no. 7, pp. 829–836, 2005.

[156] M. Takahashi, H. Fukuda, and H. Arito, "Brief naps during post-lunch rest: effects on alertness, performance, and autonomic balance," *European journal of applied physiology and occupational physiology*, vol. 78, no. 2, pp. 93–98, 1998.

[157] A. Brooks and L. Lack, "A brief afternoon nap following nocturnal sleep restriction: which nap duration is most recuperative?" *Sleep*, vol. 29, no. 6, pp. 831–840, 2006.

[158] N. Al-Busaidi, S. Morrison, B. Hadley, A. McAlister, and M. Brown, "Subjective benefit versus sleep inertia after short post lunch nap," *INTERNATIONAL JOURNAL OF ADVANCED MEDICINE*, vol. 2, no. 4, pp. 6–10, 2018.

[159] C. J. Hilditch, S. A. Centofanti, J. Dorrian, and S. Banks, "A 30-minute, but not a 10-minute nighttime nap is associated with sleep inertia," *Sleep*, vol. 39, no. 3, pp. 675–685, 2016.

[160] M. Romdhani, N. Souissi, Y. Chaabouni, K. Mahdouani, T. Driss, K. Chamari, and O. Hammouda, "Improved physical performance and decreased muscular and oxidative damage with postlunch napping after partial sleep deprivation in athletes," *International journal of sports physiology and performance*, vol. 15, no. 6, pp. 874–883, 2020.

[161] R. Arnheim, *Entropy and art: An essay on disorder and order*. Univ of California Press, 1974.

[162] İ. Eşer, L. Khorshid, Ü. Yapucu Güneş, and Y. Demir, "The effect of different body positions on blood pressure," *Journal of Clinical Nursing*, vol. 16, no. 1, pp. 137–140, 2007.

[163] P. Mougkogiannis and A. Adamatzky, "Low frequency electrical waves in ensembles of proteinoid microspheres," *Scientific Reports*, vol. 13, no. 1, p. 1992, 2023.

[164] E. Pannese, *Neurocytology: fine structure of neurons, nerve processes, and neuroglial cells*. Springer, 2015.